1-1-2011

Effects of Aging and Crystal Attributes on Particle Size Distributions in Breakage Experiments in Stirred Vessels

Sheena Magtoya Reeves

EFFECTS OF AGING AND CRYSTAL ATTRIBUTES ON PARTICLE SIZE DISTRIBUTIONS IN BREAKAGE EXPERIMENTS IN STIRRED VESSELS

By

Sheena Magtoya Reeves

A Dissertation
Submitted to the Faculty of
Mississippi State University
in Partial Fulfillment of the Requirements
for the Degree of Doctorate of Philosophy
in Chemical Engineering
in the Dave C. Swalm School of Chemical Engineering

Mississippi State, Mississippi

April 2011

EFFECTS OF AGING AND CRYSTAL ATTRIBUTES ON PARTICLE SIZE DISTRIBUTIONS IN BREAKAGE EXPERIMENTS IN STIRRED VESSELS

By

Sheena Magtoya Reeves

Approved:

Priscilla J. Hill Associate Professor Dave C. Swalm School of Chemical Engineering (Director of Dissertation and Advisor)	Rebecca Toghiani Associate Professor Dave C. Swalm School of Chemical Engineering (Committee Member)
Keisha B. Walters Assistant Professor Dave C. Swalm School of Chemical Engineering (Committee Member)	Judy Schneider Associate Professor Department of Mechanical Engineering (Committee Member)
Rafael Hernandez Associate Professor Dave C. Swalm School of Chemical Engineering (Graduate Coordinator)	Sarah A. Rajala Professor Department of Electrical Engineering and Dean of Bagley College of Engineering

Name: Sheena Magtoya Reeves

Date of Degree: April 29, 2011

Institution: Mississippi State University

Major Field: Chemical Engineering

Major Professor: Dr. Priscilla J. Hill

Title of Study: EFFECTS OF AGING AND CRYSTAL ATTRIBUTES ON PARTICLE SIZE DISTRIBUTIONS IN BREAKAGE EXPERIMENTS IN STIRRED VESSELS

Pages in Study: 208

Candidate for Degree of Doctorate of Philosophy

Particle breakage can be significant in stirred vessels such as crystallizers. During crystallization, particle breakage can occur due to particle contact with other particles, the impeller, the suspension fluid, and/or the vessel. Such breakage produces fines and can cause filter plugging downstream. Although research has been conducted with respect to particle breakage, a comprehensive study is still needed to quantify the breakage occurring in stirred vessels. The overall goal of this research is to model the particle breakage occurring in a stirred vessel by analyzing the particle size and shape distributions that result from breakage. Breakage experiments are based on collision influences that affect the two dominant collisions types, crystal-to-crystal and crystal-to-impeller collisions. Results showed that the quantity of fines produced are affected by the solids concentration or magma density and suspension fluid utilized. Additionally, aqueous saturated solutions produced particle size distributions that differ from those obtained using a nonsolvent. Similar particle size distributions for two different materials (NaCl and KCl) are achieved in the same nonsolvent (acetonitrile) by adjusting the agitation rate using the Zwietering correlation to account for property differences;

moreover, the same agitation rate adjustment produced similar distributions for KCl in acetone and acetonitrile which were both nonsolvents. However, modifications to the Zwietering correlation, such as changing the significance of the initial particle size, are proposed before this method of adjustment is deemed accurate. Number-based population modeling of particle breakage is achieved within 1-5% error for NaCl at each agitation rate investigated. Breakage modeling using a discretized population balance equation with Austin's equation for attrition and the power law form of the product function for fragmentation is a viable approach; however, more work is needed to increase the accuracy of this model.

DEDICATION

I would like to dedicate this dissertation to my parents, Gregory and Wanda Reeves, Sr., my sister, Nickole, and my brothers, Gregory Jr. and Christopher. Thank you Ma and Pops for encouraging me throughout this process. Your Baby Girl loves you dearly and appreciates your love, support, and prayers.

ACKNOWLEDGEMENTS

I would like to acknowledge my committee members for their guidance in this process. First, I thank my advisor Dr. Priscilla Hill for providing me with an opportunity to perform both undergraduate and graduate research while attending this great university. I also thank my committee members, Dr. Judy Schneider, Dr. Rebecca Toghiani, and Dr. Keisha Walters for much needed insight and guidance throughout this entire process and for being willing to serve on my committee with your extremely busy schedules. I sincerely appreciate your questions and comments. I would like to thank my officemates, Jaclyn Hall, Adebola Coker, and Devkant Gandhi for plenty laughs, conversions, and other lifelong memories over the years. I also thank Stephen Castellane for being a wonderful undergraduate worker and always finishing anything I assigned.

I would like to thank my all friends and family members in Chicago, Mississippi, New Orleans, and across the world for supporting me. Special thanks goes to Word of Faith Christian Center and the Generation 6:20 KIDS for being my family away from home for so many years and providing me what a million laughs and memories. Special thanks goes to all of these special individuals who have impacted my research in some way - the faculty and staff of the Dave C. Swalm School of Engineering, NSF, Dr. Adrienne Minerick and NOBCChE, Drs. Lakeisha and Byron Williams, Dr. Tommy Stevenson, Dr. Tonya Stone, Dr. William Person, the AGEM staff (Ms. Shylnn Morris, Ms. LaTonya Hardin), and my fellow AGEM scholars.

This material is based upon work supported by the National Science Foundation under Grant No. (CTS 0448740). Any opinions, findings, and conclusions or recommendations expressed in this material are those of the author and do not necessarily reflect the views of the National Science Foundation.

Lastly, I would like to thank my God for granting me the grace to finish this task. Faith has definitely been a part of my success. I will never take my experience lightly. I am truly "…confident of this very thing, that He which hath begun a good work in you will perform it [or see it to completion] until the day of Jesus Christ." (Philippians 1:6 KJV)

TABLE OF CONTENTS

Page

DEDICATION ii

ACKNOWLEDGEMENTS iii

LIST OF TABLES ix

LIST OF FIGURES xii

NOMENCLATURE xvii

CHAPTER

I. INTRODUCTION 1

1.1 References 3

II. LITERATURE REVIEW 4

2.1 Particle Size and Shape Characterization and Representation 5
2.1.1 Particle Size and Shape 5
2.1.2 Shape Factors 5
2.1.3 Particle Size and Mass Analysis 8
2.1.3.1 Optical Microscopy 10
2.1.3.2 Sieving 12
2.1.4 Particle Size Distribution 13
2.2 Crystallization 16
2.2.1 Growth and Nucleation 20
2.2.2 Separation Techniques 21
2.2.2.1 Filtration 21
2.2.2.2 Centrifugal Sedimentation 22
2.2.3 Particle Suspension in Agitated Vessels 22
2.3 Particle Breakage in a Stirred Vessel 29
2.3.1 Collisions and Contact Nucleation 31
2.3.2 Impact Energy 34
2.3.2.1 Rittinger's Law 34
2.3.2.2 Kick's Law 35
2.3.2.3 Bond's (Work) Law 35

2.3.2.4 Collision Based Equations 35
2.3.3 Previous Breakage Research in a Stirred Vessel 36
2.3.3.1 Analysis Techniques 40
2.3.3.2 Collisions and Breakage 40
2.3.3.3 Particle Size and Shape 41
2.4 Population Balance Equation (PBE) 41
2.4.1 Discretizing the Differential Equation 45
2.4.2 Power Law Form of Product Function 47
2.5 References 48

III. RESEARCH OBJECTIVES 53

IV. BREAKAGE CHARACTERIZATION OF NACL CRYSTALS SUSPENDED IN A STIRRED VESSEL 54

4.1 Introduction 54
4.2 Methodology 57
4.2.1 Crystal Growth and Processing 57
4.2.2 Aqueous Saturated Solution 59
4.2.3 Breakage Procedure 59
4.2.3.1 Magma Density Investigation 61
4.2.3.2 Agitation Rate Investigation 61
4.2.3.3 Initial Particle Size Investigation 62
4.2.4 Filtration and Separation Procedure 69
4.2.5 Analytical Procedure 72
4.3 Results 73
4.3.1 Technique and Reproducibility 73
4.3.2 Magma Density (MD) 75
4.3.3 Agitation Rate 81
4.3.3.1 Adjusted Agitation Rates 96
4.3.4 Initial Particle Size 99
4.3.4.1 Fragmentation vs. Attrition 99
4.4 Conclusions 111
4.5 References 114

V. QUANTIFICATION OF NaCl, KCl, AND POTASH ALUM CRYSTALS IN NONSOLVENTS FROM BREAKAGE IN A STIRRED VESSEL 116

5.1 Introduction 116
5.2 Methodology 119
5.3 Results 122
5.3.1 Mass, Number, and Shape Analysis 122
5.4 Effect of Crystal and Suspension Fluid Properties 122
5.4.1 Fluid Properties 127
5.4.2 Initial Crystal Size 131

5.4.3 Crystal Size and Other Characteristics 133
5.5 Modeling Particle Breakage 137
5.6 Conclusions 149
5.7 References 151

VI. RESEARCH CONCLUSIONS 153

6.1 References 159

APPENDIX

A MATERIAL PROPERTIES 160

A.1 Suspension Fluid Properties 161
A.2 Solid Properties 162

B VESSEL PROPERTIES 164

B.1 Vessel Dimensions and Schematic 165

C SUSPENSION CALCULATIONS 167

C.1 Suspension Calculations 168
C.1.1 System Constants 168
C.1.2 Just Suspended NaCl Mesh 40 Particles Calculation 169
C.1.3 Adjusted Agitation Rate Calculations 170
C.1.3.1 Mesh 40 KCL Particles in Acetonitrile 170
C.1.3.2 Mesh 60 KCl Particles in Acetonitrile 172
C.1.3.3 Mesh 30 Potash Alum Particles in Acetone 173
C.1.3.4 For Mesh 20 Potash Alum Particles in Acetone 175
C.1.3.5 Mesh 40 KCl Particles in Acetone 176
C.1.3.6 Mesh 60 KCl Particles in Acetone 177

D IMAGE ACQUISITON AND ANALYSIS PROCEDURE 178

D.1 Image Acquisition 179
D.2 Image-Pro Plus Analysis Directions 180

E ADDITIONAL PARTICLE SIZE DISTRIBUTIONS 182

E.1 Initial Particle Size Investigation PSDs 183

F PARTICLE BREAKAGE IMAGES 187

F.1 NaCl Breakage 188

G STATISTICAL DATA 197

G.1 NaCl Confidence Intervals 198
G.2 KCl and Potash Alum Confidence Intervals 199
G.3 Confidence Intervals of Comparisons 200

H SAMPLE ANALYSIS PROCEDURE 201

I SIMULTANEOUS DIFFERENTIAL SCANNING CALORIMETER AND THERMO GRAVIMETRIC ANALYSIS (SDT) RESULTS 206

LIST OF TABLES

TABLE		Page
2.1	Particle Analysis Techniques (Allen, 1997)	10
2.2	Crystal Systems and Bravais Lattices	19
2.3	Crystal Collision Types and Secondary Nucleation Effect	33
2.4	Crystal Breakage in the Literature	38
2.5	Operating Conditions of Literature Breakage Research	39
4.1	Experimental Plan for Magma Density Investigation	62
4.2	Experimental Plan for Agitation Rate Investigation	63
4.3	Experimental Plan for Initial Particle Size	64
4.4	Minimum Stirrer Speed Needed for Particle Suspension	66
4.5	Example of Broken Particle Analysis Technique	71
4.6	Mass Fraction of NaCl Reproducibility Runs	75
4.7	Mass Fractions of NaCl Agitation Investigation	76
4.8	ACTL Agitation Rate Mass Fractions of NaCl Crystals	82
4.9	SS Agitation Rate Mass Fractions of NaCl Crystals	83
4.10	Adjusted Agitation Rates of NaCl Crystals	97
4.11	Initial Particle Size Mass Fractions of Broken NaCl Crystals at 1500 rpm	104
5.1	Crystal Habit and Hardness of Select Crystals	117
5.2	Reynold's Number Calculation for ACTL, SS, ACTE	120
5.3	Adjusted Agitation Rate Using Reynold's Number	120

5.4 Adjusted Agitation Rates Based on NaCl at 1500 rpm Using Zwietering's Correlation 121

5.5 Agitation Rates and Mass Fractions of Adjusted NaCl, KCl, and Potash Alum 123

5.6 Adjusted Agitation Rate Using Zwietering's Correlation for Acetone Trial 128

5.7 KCl Mass Fractions in ACTL and ACTE 131

5.8 Breakage Function Parameters for NaCl, KCl, and Potash Alum 143

5.9 Attrition and Fragmentation Rate of Breakage Table for NaCl Crystal Breakage Agitation Experiments in Acetonitrile 147

5.10 Number Fraction Error Deviation Table for NaCl Crystal Breakage Agitation Experiments in Acetonitrile 148

5.11 Number Fraction Error Deviation Table for Mesh 40 NaCl in ACTL, KCl in ACTE, and Potash Alum in ACTE 149

6.1 Crystal Breakage in the Literature with this Work 154

6.2 Operating Conditions of Literature Breakage Research with this Work 155

A.1 Properties of Suspension Fluids 161

A.2 Kinematic Viscosity Table 161

A.3 Density Measurements of Suspension Fluids 162

A.4 Properties of Crystals 162

A.5 Solubility Table of Crystals (T = 20°C) 163

G.1 Aqueous Saturated Solution Confidence Intervals 198

G.2 Acetonitrile NaCl Confidence Intervals 199

G.3 KCl Confidence Intervals 199

G.4 Potash Alum Confidence Intervals 200

G.5 Comparison of Materials Confidence Intervals 200

H.1 Sample Raw Data of Crystals From Image Pro Analysis 202

H.2 Number of Particles per Major Axis L_i Range and Aspect Ratio Chart of Particles in Each Sample Range 203

H.3 Major Axis L_i and Number Fraction n_i of Particle in each Sample Range..... 204

LIST OF FIGURES

FIGURE		Page
2.1	Particle Size Range of Select Industrial Particles (Goldman, 1984)	6
2.2	Schematic of an Agitation Vessel	26
4.1	PSDs of Unbroken NaCl Crystals of Various Size Ranges	67
4.2	PSDs of Unbroken Laboratory Grown Mesh 6 and 10 NaCl Crystals	68
4.3	PSDs of Commercial Unbroken Mesh 30, 40, and 60 NaCl Crystals	69
4.4	Variation of PSD with sample size	74
4.5	PSD of NaCl Crystal Breakage for 30 Minutes at 1500 rpm in ACTL based on Changes to the Magma Density	77
4.6	PSD of NaCl Crystal Breakage for 30 Minutes at 1500 rpm in SS Based on Change in Magma Density	78
4.7	Average Aspect Ratio of NaCl Child Particles Based on Change in Magma Density	79
4.8	Average Roundness of NaCl Child Particles Based on Change in Magma Density	80
4.9	Average Major Axis of NaCl Child Particles Based on Change in Magma Density	81
4.10	PSD of NaCl Crystal Breakage for 30 Minutes in ACTL Based on Change in Agitation Rate	85
4.11	PSD of NaCl Crystal Breakage for 60 Minutes in ACTL Based on Change in Agitation Rate	86
4.12	PSD of NaCl Crystal Breakage for 30 Minutes in SS Based on Change in Agitation Rate	87

4.13 PSD of NaCl Crystal Breakage for 60 Minutes in SS Based on Change in Agitation Rate 88

4.14 Average Aspect Ratio of NaCl Child Particles Based on Change in Agitation Rate 89

4.15 Average Roundness of NaCl Child Particles Based on Change in Agitation Rate 90

4.16 Average Major Axis of NaCl Child Particles Based on Change in Agitation Rate 91

4.17 Average Major Axis of NaCl Child Particles based on Change in Agitation Rate for 30 Minutes 92

4.18 Average Major Axis of NaCl Child Particles Based on Change in Agitation Rate for 60 Minutes 93

4.19 Average Major Axis of NaCl Child Particles Based on Change in Agitation Rate in ACTL 94

4.20 Average Major Axis of NaCl Child Particles Based on Change in Agitation Rate in SS 95

4.21 PSD of NaCl Crystal Breakage Based on Adjusted Agitation Rates of SS and ACTL for 30 and 60 Minutes 98

4.22 Unbroken Laboratory Grown Mesh 6 NaCl Crystal 100

4.23 Broken Laboratory Grown Mesh 6 NaCl Crystals 101

4.24 Unbroken Mesh 40 Commercial NaCl Crystal 102

4.25 Broken Commercial Mesh 40 NaCl Crystal 103

4.26 Average Aspect Ratio of NaCl Child Particles Based on Change in Initial Particle Range 105

4.27 Average Roundness of NaCl Child Particles Based on Change in Initial Particle Range 106

4.28 Average Major Axis of NaCl Child Particles Based on Change in Initial Particle Range 107

4.29 PSD of Mesh 6 and 10 NaCl Fines (<300 microns) Agitated for 30 and 60 Minutes at 1500 rpm 108

4.30 PSD of Mesh 30 NaCl Crystal Breakage in ACTL for 30 and 60 Minutes at 1500 rpm 109

4.31 PSD of Mesh 40 NaCl Crystal Breakage in ACTL for 30 and 60 Minutes at 1500 rpm 110

4.32 PSD of Mesh 60 NaCl Crystal Breakage in ACTL for 30 and 60 Minutes at 1500 rpm 111

5.1 PSD for KCl Crystal Breakage in ACTL for 30 and 60 minutes at 1600 rpm 124

5.2 PSD for KCl Crystal Breakage in ACTL for 30 and 60 Minutes at 1780 rpm 125

5.3 PSD for Potash Alum Crystal Breakage in Acetone for 30 and 60 Minutes at 1560 rpm 126

5.4 PSD for Potash Alum Crystal Breakage in Acetone for 30 and 60 Minutes at 1680 rpm 127

5.5 PSD of Mesh 40 KCl Crystal Breakage in ACTL and ACTE for 30 and 60 Minutes 129

5.6 PSD of Mesh 60 KCl Crystal Breakage in ACTL and ACTE for 30 and 60 Minutes 130

5.7 PSD of Mesh 40 Potash Alum Crystals Agitated in Acetone for 30 and 60 Minutes at 1640 rpm 132

5.8 PSD of Mesh 40 KCl and Potash Alum Crystals Agitated in Acetone for 30 and 60 Minutes 134

5.9 Comparison of Octahedral and Cubic Crystal Habits 135

5.10 Sieve Diameters of Cubic Crystal (gray marks represent sieve diameters) 136

5.11 Sieve Diameters of Octahedral Crystal (gray marks represent sieve diameters) 136

5.12 Simulation of Austin Attrition Function with $\beta = 3.5$, $\gamma = 2.8$, and $\phi = 0.36$ 138

5.13 Simulation of Power Law Form of the Product Function with $p = 5$ and $m = 2$ 139

5.14 Modeling of Mesh 40 NaCl Crystal Breakage Agitated in Acetonitrile for 30 and 60 Minutes 141

5.15 Modeling of Mesh 40 Potash Alum Crystal Breakage Agitated in Acetone for 30 and 60 Minutes 142

5.16 Modeling of Mesh 40 KCl Crystal Breakage Agitated in Acetone for 30 and 60 Minutes 143

5.17 Modeling Results for NaCl Crystal Breakage in Acetonitrile at 1000 rpm for 30 and 60 Minutes 144

5.18 Modeling Results for NaCl Crystal Breakage in Acetonitrile at 1500 rpm for 30 and 60 Minutes 145

5.19 Modeling Results for NaCl Crystal Breakage in Acetonitrile at 2000 rpm for 30 and 60 Minutes 146

5.20 Attrition and Fragmentation Breakage Rates for NaCl Crystal Breakage Agitation Rate Investigation 147

B.1 Schematic of Breakage System 166

E.1 Mesh 6 NaCl Crystal Breakage Results 183

E.2 Mesh 6 NaCl Crystal Breakage Results <1000 Microns without Adjustments 184

E.3 Mesh 10 NaCl Crystal Breakage Results 185

E.4 Mesh 10 NaCl Crystal Breakage <600 microns without Adjustment 186

F.1 Unbroken Mesh 40 NaCl Crystals 188

F.2 SS Broken NaCl Crystals 189

F.3 ACTL Broken NaCl Crystals 190

F.4 Mesh 40 KCl Crystal Breakage 191

F.5 Mesh 60 KCl Crystal Breakage 192

F.6 Unbroken Mesh 20 Potash Alum Crystals 193

F.7 Mesh 20 Potash Alum Crystal Breakage 194

F.8 Unbroken Mesh 30 Potash Alum Crystals 195

F.9 Mesh 30 Potash Alum Crystal Breakage 196

H.1 Graph of Number Fraction and Major Axis for Particles in the Sample 205

I.1 Simultaneous Differential Scanning Calorimeter and Thermo Gravimetric Analyzer (SDT) or DSC-TGA Results of Commercial Sodium Chloride Crystals 207

I.3 Simultaneous Differential Scanning Calorimeter and Thermo Gravimetric Analyzer (SDT) or DSC-TGA Results of a Mesh 10 Laboratory Grown Sodium Chloride Crystal 208

NOMENCLATURE

Symbols

ACTE	Acetone
ACTL	Acetonitrile
CI	Confidence Interval
KCl	Potassium Chloride
MD	Magma Density, g/100 mL
NaCl	Sodium Chloride
PA	Potassium Aluminum Sulfate
PBE	Population Balance Equation
PSD	Particle Size Distribution
rpm, rps	Revolutions per minute (second)
SDT	Simultaneous Differential Scanning Calorimeter and Thermo Gravimetric Analyzer
SE	Standard Deviation or Error
SS	Saturated Solution
TDS	Total Dissolved Solids

Nomenclature

a	Value used for Zwietering parameter, S, dimensionless
A	Surface Area, m^2
a, b, c	Lattice Symmetry Lengths in Chapter 2

b_{ij}	Discretized number-based breakage function, no./no.
b(v,w)	Number-based breakage function, no./no./mm^3
C	Distance between impeller and vessel bottom, m
C_D	Drag Coefficient, dimensionless
C_K	Kick's Constant, m^3/kg
C_R	Rittinger's Constant, m^4/kg
D	Impeller Diameter, m
d, d_p, D	Particle Diameter, m
E	Energy, J
g, g_c	Gravitational constant, 9.81 m/s^2
H	Hardness, N/m^2
H	Height of fluid in vessel, m
H_v	Vicker's Hardness, N/m^2
k	Efficiency Factor, dimensionless
K_c	Fracture Toughness, $N/m^{3/2}$
L, L_i	Length, m
m	power law exponent, dimensionless
M, M_T	Mass, total mass, kg
M_i	Mass in increment i, kg
N, N_T	Number or total number of particles, dimensionless
n(v)	Number density or population density, no./mm^3/m^3
n_{fi}	Number fraction of particles in increment i, dimensionless
N_i	Number of particles in increment i, dimensionless
N_{js}	Just Suspended Agitation Rate, rps

p	Number of child particles produced when parent particle is broken
S	Zwietering's Constant, dimensionless
S	Surface, Surface Area, m^2
S_c	Breakage constant, $\mu m^{-3\alpha}/min$
S_d	Standard Deviation, dimensionless
S_i, S_j	Discretized volume-based specific rate of breakage, min^{-1}
S(v), S(w)	Number-based specific rate of breakage, min^{-1}
t	Time, min
T	Vessel Diameter, m
U	Axial Velocity, m/s
v, *v*	Impact Velocity, m/s
v, w	particle volume, μm^3
V	Volume, mL or L
V_t	Terminal Velocity, m/s
W	Work input to system, N m
Wi	Bond's Work Index, kWh/sh. ton
W_{pl}	Work of a Given Particle, J
x_i	Mass fraction of increment i, dimensionless
x_c, x_p	Child particle, parent-sized particle mass fraction, dimensionless
z	Arbitrary length, m
z	Total error, dimensionless
z_i	Model error of increment i, dimensionless

Subscripts

c	Child particle
F	Feed
i, j	Size intervals
p	Parent particle
p	Particle property
P	Product
T	Total number, dimensionless
v	Vicker's

Greek Letters

α	Exponential factor in specific rate of breakage, dimensionless
α, β, γ	Lattice symmetry angles in Chapter 2
β	Constant in breakage function, dimensionless
β_j	Birth probability function, dimensionless
γ	Constant in breakage function, dimensionless
Γ	Fracture resistance, J/m^2
δ_j	Death probability function, dimensionless
θ_w	Sphericity, dimensionless
μ	Shear modulus, N/m^2
μ	Viscosity, cP
ν	Kinematic viscosity, m^2/s
ξ	Fraction of particle loss due to impact, dimensionless

ρ	Density, kg/m^3
$\Delta\rho$	Change in density $(\rho_s-\rho_L)/\rho_L$, kg/m^3
ρ_L	Denisty of liquid/mother liquor, kg/m^3
ρ_s	Density of solid/crystal, kg/m^3
ϕ	Shape factor, aspect ratio, dimensionless
ϕ	Constant in breakage function, dimensionless
ϕ_R	Roundness shape factor, dimensionless
ϕ_S	Surface shape factor, dimensionless
ϕ_V	Volume shape factor, dimensionless
χ	Particle Loading, $\frac{g\ solid}{g\ liquid} \times 100$, dimensionless

CHAPTER I

INTRODUCTION

Solids handling is considered to be more difficult than the handling of liquids and gases (Rhodes, 2008). Due to the difference in the chemical and physical properties of solid particulates, the attributes of size and morphology are important in particle processing although they do not pertain to gases and liquids. The properties of particles often affect the operating conditions in industry as well as the final product size distribution. Solids handling is one industrial concern since several problems can exist. One particular problem in the area of particle handling is particle breakage. Solids processing commonly occurs in industrial units such as crushers, grinders, agitated vessels, crystallizers, and even fluidized beds. However, during the production or growth of these solids, particle breakage can occur altering the desired particle size distribution or plugging filters downstream during crystallization (Allen, 1997). The chemical manufacturing industry often desires solid particles consistent in both size and shape, especially in the area of pharmaceuticals where correct drug dosage is essential (Cadle, 1965). This research aims to describe the breakage that occurs during agitation of slurries in a stirred vessel. Multiple factors can cause particle breakage; however, an in depth knowledge of the physical and mechanical properties of these systems must be acquired to accurately represent the breakage seen in industry (Ramkrishna, 2000; Mullin, 2001). Using discretized population balance equations that describe the system, a breakage function based on experimental results is determined for agitated systems under set

conditions (Ramkrishna, 2000; Kumar, 1997; Austin, 1971). Although some previous work has been conducted in this area, an extensive study on parameters influencing particle breakage in an agitated vessel is needed to obtain substantial and accurate breakage equation parameters for the modeling procedure. This work looks to provide a comprehensive study of particle breakage in an agitated vessel based on the dominant causes of collisions. From this work, modeling of the breakage function that describes particle breakage will occur.

In Chapter 2, further background information is provided along with a literature review on particle analysis and characterization techniques, crystallization, and population balance equations. Chapter 3 provides details on the research objective. Chapter 4 discusses the effects of agitating NaCl crystals in a nonsolvent or in a saturated solution while varying magma density, agitation rate, and initial particle size. Chapter 5 presents the breakage of NaCl, KCl, and potassium aluminum sulfate dodecahydrate (potash alum) crystals in nonsolvents and presents modeling for each crystal type along with the modeling of the NaCl agitation rate investigation. Final conclusions and further discussion are presented in Chapter 6.

1.1 References

Allen, T. (1997). *Particle Size Measurement Volume 1: Powder Sampling and Particle Size Measurement 5th Ed.*, Chapman & Hall, London.

Austin, L. (1971). Introduction to the mathematical description of grinding as a rate process. *Powder Tech. Vol. 5*, 1-17.

Cadle, R.C. (1965). *Particle Size: Theory and Industrial Applications*, Reinhold Publishing Corporation, New York.

Kumar, S. and D. Ramkrishna (1997). On the solution of population balance equations by discretization - III. Nucleation, growth and aggregation of particles. *Chem. Eng. Sci. Vol. 52(24)*, 4659-4679.

Mullin, J. W. (2001). *Crystallization 4th Ed*., Butterworth-Heinemann, Boston.

Ramkrishna, D. (2000). *Population Balances: Theory and Applications to Particulate Systems in Engineering*, Academic Press, San Diego.

Rhodes, M. (2008). *Introduction to Particle Technology, 2nd Ed.*, Wiley & Sons, London.

CHAPTER II

LITERATURE REVIEW

From the creation of Egyptian bricks to the start of the Industrial Revolution, particle science and technology has led to the development of materials such as nanoparticles and carbon nanotubes (Ennis, 1994; Allen, 1997). However, particle technology remains a fertile area of research due to many phenomena remaining unexplained (Rhodes, 2008). During the last decade, more emphasis has been placed on the importance of the particle size distribution (PSD) in industrial processes since product quality is economically important. For example, DuPont, a major chemical processing company, manufactures products in which 62% by volume are comprised of powders, crystalline solids, granules, slurries, dispersions, pastes, and other solid-liquid mixtures (Ennis, 1994). Particles are often present naturally as the main or a by-product or added to engineering systems (Ramkrishna, 2000). In industry, companies often utilize solids to manufacture a product or preserve a product (Conti, 1980). Several factors can influence the production of a particle; therefore, the characterization of solid particles is an important aspect in all areas involving particle technology (Svarovsky, 2000). To design better particulate processes, it is first necessary to understand 1) particle attributes and characterization techniques, 2) particle formation processes such as crystallization, and 3) factors affecting particle mechanisms such as breakage. Here, the focus is on particle breakage in stirred vessels.

2.1 Particle Size and Shape Characterization and Representation

2.1.1 Particle Size and Shape

In industrial operations, it is necessary to know the shape and size distributions of the solid particulates produced (Davey, 2000). An individual solid particle can be represented or characterized by its size, shape, or even density (McCabe, 2001). Here, it is noted that a particle's shape and size refer to separate characteristics of the particle. The size of a particle refers to a measurement such as length or diameter, while the shape describes the outline or geometry of the particle. Solid particle shapes include needles, plates, cubes, spheres, or other more complex shapes. A solid particle not only varies in shape, but also in size. Figure 2.1 shows the average particle size range of some solids in microns (Goldman, 1984).

In the case of fillers for paper and paint, particles can range from the nanometer to micrometer (micron) range, while solution grown crystals, such as NaCl, are produced in the micron to millimeter range. Particle shape is significant because particles that grow as needles or dendrites are more likely to break and form secondary nuclei (Davey, 2000). The measurement and evaluation of particle shape is indeed important in particle characterization.

2.1.2 Shape Factors

When considering the analysis of particulate solids, accurate values of particle length, width, and thickness are needed to present a valid calculation of particle volume. Since exact values of these parameters for irregularly shaped particles are impossible, the usage of shape factors to describe particles arose (Mullin, 2001). Shape factors are useful in relating the morphology of a crystal to system operating conditions (Allen, 1997).

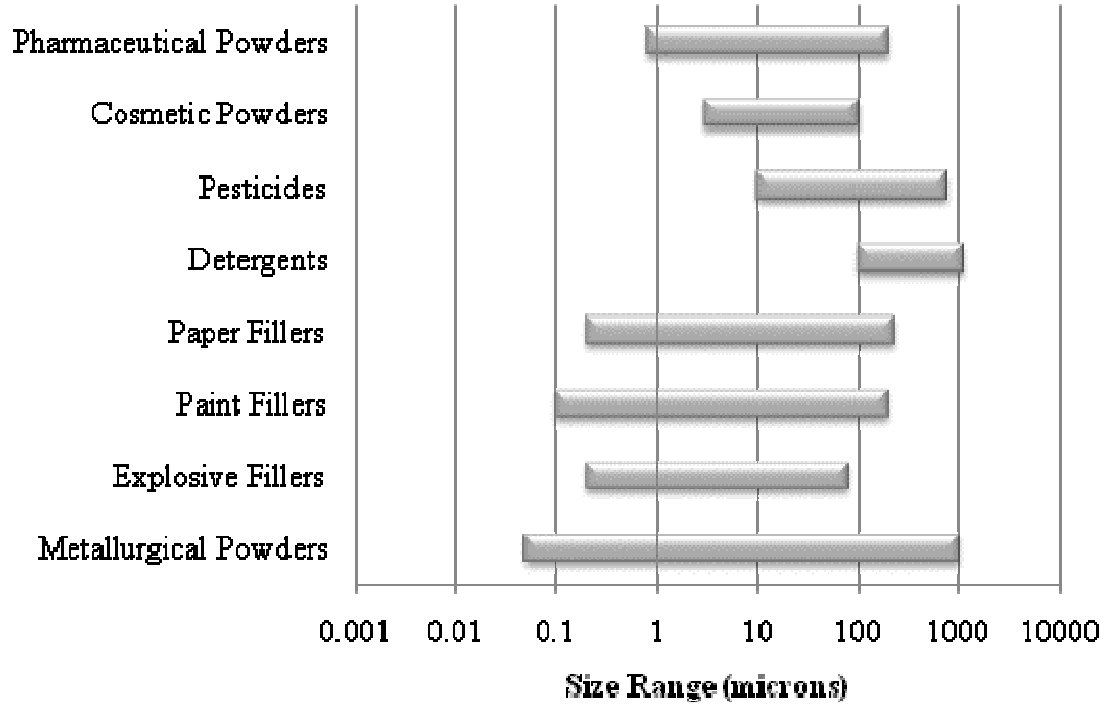

Figure 2.1 Particle Size Range of Select Industrial Particles (Goldman, 1984)

Qualitative analysis of particle morphology includes classifications such as acicularity (needle-shaped) versus roundness (circular). Quantitative analysis utilizes particle parameters, such as diameter, to obtain descriptive information regarding the shape of the particle (Allen, 1997). Shape factors are usually based on relationships between the dimensions of a particle or one single dimension and the particle's volume or surface area. The latter relationships are designated in the literature by Allen (1997) and Mullin (2001) as a volume shape factor

$$\phi_v = \frac{L^3}{v} \tag{2.1}$$

and a surface shape factor

$$\phi_s = \frac{L^2}{v} \tag{2.2}$$

where ϕ_v denotes the volume shape factor; $\phi_{s,}$ the surface shape factor; L , a length parameter of the particle such as diameter in the case of a sphere; and v, the volume of the particle. For example, in the case of a cube with sides of z length, the equations reduce to $\phi_v = \frac{z^3}{z \times z \times z} = 1$ and $\phi_s = \frac{z^2}{z \times z \times z} = \frac{1}{z}$. In this case, it is noted that $\phi_v \neq \phi_s$ unless the length z equals 1.

Volume and surface shape factors are often tedious to manually measure especially in the case of particles smaller than 500 μm. This perception is due to the large quantity of particles (several thousand) that make up a normal particulate sampling (Mullin, 2001) and due to the irregular shapes of the particles. Therefore, other shape factors were developed to characterize particle shape which involved measuring a projection of a sample of particles, namely sphericity and roundness. Since two dimensional microscopes are often available, these factors are often based on a 2D image of a particle. Sphericity describes the resemblance of a particle to a sphere based on diameter. Roundness, or circularity, also describes the spherical nature of a particle (Mullin, 2001; Allen, 1997); however, the equation for roundness includes the perimeter of the particle which serves as a representation of the morphological boundary of the particle's surface (Mazzarotta, 1996). Common equations for sphericity (Wadell, 1934) and roundness (Allen, 1997) are provided below.

$$Sphericity, \theta_w = \frac{surface\ area\ of\ a\ sphere\ having\ the\ same\ volume\ as\ the\ particle}{surface\ area\ of\ the\ particle} \tag{2.3}$$

$$Roundness, \phi_R = \frac{(perimeter\ of\ a\ particle)^2}{4\pi(cross-sectional\ area\ or\ projection\ area)} \tag{2.4}$$

It should be noted that for a sphere both the values of roundness and sphericity are equal to one.

Another set of shape factors are aspect ratios. The most common calculations for the dimensionless aspect ratio noted in the literature (Allen, 1997) are the elongation ratio (width/length) and flakiness ratio (length/height). A more recent calculation (Hill, 2004) uses

$$Aspect\ Ratio = \frac{Major\ Axis}{Minor\ Axis} \tag{2.5}$$

as a representation of shape factor. This equation considers the orientation of the particle on a microscope slide when deciding the axes. Most imaging software calculates length and width using normal, fixed x, y coordinates. Thus, the values of length and width will change with respect to the orientation of the material. Major and minor axis measurements remain constant despite orientation.

2.1.3 Particle Size and Mass Analysis

Particle distributions are represented in industry using either particle sizes or mass (weight) as in the use of number fractions and weight fractions. Solid particle characterization is normally based on the particle size and its distribution (Svarovsky, 2000). A particle size distribution can be presented in analytical form such as a continuous function or as a set of discretized data (Svarovsky, 2000). Since crystallization models are based on the number of particles in the system, number-based particle size analysis is favored over mass analysis. For a comparison between mass analysis and number-based size analysis, consider a single 10 μm particle having a cubic

volume of 1,000 μm^3. This single particle possesses the same volume and mass as one thousand 1-μm particles (Allen, 1997). In mass analysis, the single particle and the thousand particles are of equal mass fraction while the number fractions are quite different. Mass balances and solubility data provide information regarding crystal yield; however, the particle or crystal size distribution cannot be determined by these values (Davey, 2000). Both mass and enthalpy balances give no clarity on the PSD of the product from a crystallizer (McCabe, 2001).

In most cases involving particle size analysis, a continuous distribution is not used. Instead, researchers and statisticians utilize discrete analysis (Kumar, 1997; Goldman, 1984). A discrete measurement describes the measurement of a finite number of observations over a finite interval whereas a continuous measurement refers to an infinite number of observed measurements (Goldman, 1984). Sizing techniques which represent data as continuous are sometimes cumulative (Goldman, 1984). That is, each value in the graph is the summation of that point and the previous points until completion is reached. Continuous population balance equations (PBEs) are difficult to solve using analytical techniques (Kumar, 1997). Furthermore, it is hard to determine the shape of the actual distribution (Goldman, 1984) because analysis of every particle in a sample is laborious and time consuming. Therefore, small representative population samples are chosen based on a predetermined method (Allen, 1997). Particle size is presented by displaying percentages or fractions based on particle size ranges (Svarovsky, 2000). Mathematically, several types of distributions exist.

Normal or Gaussian distributions and log-normal distributions are continuous distributions used to describe most industrial distributions (Rhodes, 2008, Svarovsky, 2000). For powders and particle suspensions, PSDs are unlikely to fit Gaussian

distributions because PSDs are skewed, and the bell-shaped curve of the normal distribution will produce negative particle sizes (Svarovsky, 2000), a result not applicable. Log-normal distributions are the most widely used type of distribution function (Svarovsky, 2000). However, the use of discretized population balance equations to describe particle behavior has risen over the last decade (Evans, 1997; Svarovsky, 2000; Kumar, 1997). Four common particle analysis techniques are listed in Table 2.1. Each technique is based on either mass or number and has a unique analysis range. Selected techniques are discussed further in the following subsections.

Table 2.1 Particle Analysis Techniques (Allen, 1997)

Analysis type	**Basis of analysis**	**Analysis Range**
Sieving (woven wire)	mass	37-4000 microns
Centrifugal Sedimentation	mass	0.01-10 microns
Optical Microscopy	number	0.8-150 microns
Electron Microscopy	number	0.001-5 microns

2.1.3.1 Optical Microscopy

For solids such as cubes or spheres, the particle shape and size can easily be measured; on the other hand, a more enhanced method is needed to analyzed irregularly shaped crystals (McCabe, 2001). Particle size analysis is usually accomplished by laser diffraction, sieving, light scattering, or electron microscopy depending on particle size (Allen, 1997; Davey, 2000). Another commonly used technique in particle size analysis is optical microscopy. This technique provides a method whereby particle observation and parameter measurement can occur. Optical microscopy is especially useful in

analyzing particle morphology, or a particle's shape and texture (Allen, 1997). Differences in the light reflected from the light source usually represent damage to or impurities in particles.

Microscope calibration is an important step in ensuring the accuracy of the particle size and shape values obtained using optical microscopy. The theoretical lower limit (based on wavelength) for particle analysis using optical microscopy is approximately 0.2μm (Allen, 1997). A glass slide provides stable conditions for orienting a particle, which maximizes the two dimensional projected area of the actual particle (Allen, 1997). Analysis through optical microscopy can result in the knowledge of the sizes and shapes of a vast number of particles; however, these data must further be analyzed to determine its relevance or insignificance (Cadle, 1965). Various types of automated microscopy exist; however, image analysis systems are unable to disseminate artifacts in particle streams as well as a human operator. The automated systems are also unable to adjust focus during measurements in the field of view (Allen, 1997). This error can lead to false characterizations in particulate systems which embody a wide range of particle sizes.

Another type of measurement in particle analysis is chord length. A chord length is a random length of a particle based on its orientation with respect to a detection source or, in the case of optical microscopy, the actual microscope; however, chord lengths are only valid if the same particle size distribution can be achieved after changing the analysis or detection direction for randomly oriented particles (Allen, 1997).Thus, manually operated optical microscopy is one of the best tools in which the analysis of particle size and morphology can occur.

2.1.3.2 Sieving

The use of screens or sieves provides one method of particle separation by mass. Standard screens measure particles between 38μm and 76mm (McCabe, 2001). Although particles are three dimensional, sieving is a function of only two particle dimensions (Allen, 1997). Testing sieves are comprised of woven wire screens that have been standardized based on mesh and dimensions. For example, the Tyler standard screen series are based on the opening of the 200-mesh screen which is set at 0.074mm or 74μm (McCabe, 2001). All other sieves are based on the set value of the 200-mesh sieve. The next sieve in the series has an opening area that is exactly twice the area of the 200-mesh sieve. Doubling the area correlates to a ratio of $\sqrt{2}$ or 1.41 between sieve diameters. In addition, intermediate screens are also produced with a ratio of $\sqrt[4]{2}$ or 1.189 (McCabe, 2001).

In screen or sieve analysis, the sieves are usually stacked together, one on top of the other, with the largest opening on the top. The smallest mesh is placed on the bottom of the stack; a bottom recovery tray is placed below the smallest mesh to recover particles smaller than the smallest mesh size. The sample is placed on the top sieve allowing only the smaller particles movement through the sieves. The stack is then placed on a mechanical shaker for a definite time to allow further separation of the particles. After separation, the particles remaining on each individual sieve are weighed and recorded for further analysis (McCabe, 2001). The summation of the masses of each sieve yields

$$M_T = \sum_i M_i \tag{2.6}$$

where M_T is the total mass recovered, and M_i is the mass recovered in each increment *i*. The first increment would fall between the bottom pan and the smallest mesh size. Mass fractions can be determined for each sieve or increment using

$$x_i = \frac{M_i}{M_T} \tag{2.7}$$

where x_i is the mass fraction of a single increment. Moreover,

$$\sum_i \frac{M_i}{M_T} = \sum_i x_i = 1 \tag{2.8}$$

for all mass fractions of a given sample. The mass or weight fractions retrieved from sieving can further represent the population of particles as a weight distribution based on sieve apertures.

2.1.4 Particle Size Distribution

The distribution of particles in a given system is usually denoted as a particle size distribution. Researchers often mistakenly refer to distributions developed using weight fractions as size distributions (Goldman, 1984); however, this terminology is invalid as the distributions are weight distributions. In terms of crystallization, most particle size distributions are presented in the form of number or population density (McCabe, 2001; Allen, 1997; Mullin, 2001). A single crystal is often represented by an average size, or bin, in terms of particle size distributions (Davey, 2000). This size is based on a characteristic of the crystal such as area, diameter, or length. Four types of particle size distributions are used to describe a system or systems (Svarovsky, 2000)

1. number (N)
2. length (L)
3. surface area (S)
4. mass or volume (M or V)

where the length, surface area, and volume distributions weight the number PSD by the length, surface area, and volume of each particle respectively. Here mass (M) and volume (V) of a particle are related by the particle's density (ρ): ρV=M.

As discussed in Section 2.1.3.2, the total mass in a system is denoted by

$$M = \sum M_i \tag{2.9}$$

where M = the total mass and M_i = partial masses or the mass found in each increment observed. Similarly, for the number-based PSD,

$$N = \sum N_i \tag{2.10}$$

where N = the total number of particles and N_i represents the number of particles in the *i*th interval (Goldman, 1984). For a group of crystals suspended in a fluid, the crystal size is represented by a characteristic length, L, and the volume is represented by V. The number of crystals of size L or less in the fluid is denoted by N(L) (McCabe, 2001; Allen, 1997; Myerson, 2002). Let N be the total number of particles measured. The frequency or number fraction of particles relative to any interval is equal to N_i/N as shown in Eq. (2.14) (Goldman, 1984). If the diameter, d, is the length measured, analysis can be performed based on changes to the diameter or the number of diameters in the system. Other analysis measurements in particle number studies include the average (mean), $\bar{d}$, variance, s_d^2, and standard deviation, s_d . From Goldman (1984), if d_i is the diameter of particles in *i,* then

$$\text{Mean: } \bar{d} = \sum \frac{d_i}{N} \tag{2.11}$$

$$\text{Variance: } s_d^2 = \frac{\sum(d_i - \bar{d})^2}{(N-1)} \tag{2.12}$$

$$\text{Standard Deviation: } s_d = \sqrt{s_d^2}. \tag{2.13}$$

From these measurements, the change in particle diameter is approximated.

PSDs are usually presented as a histogram with a continuous curve, like a dashed line, to approximate the distribution (Allen, 1997). The area of height under each point corresponds to a frequency or number fraction of particles in between two points (Cadle, 1965). The number fractions are based on size increments which are a function of the average particle size in the increment. The equation for number fraction, n_f, for the *i*th interval is

$$n_{f_i} = \frac{N_i}{N}. \tag{2.14}$$

Statisticians suggest the use of 10 to 20 classes or bins for mass-based analysis (Cadle, 1965) while in powder technology using 20-25 size intervals was deemed appropriate for PSDs (Goldman, 1984). In the classification of data, identical sized class intervals are not required; however, some correlation between each class interval must exist (Cadle, 1965) as in the case of sieve screens (McCabe, 2001).

A second method of presenting size distribution data is called cumulative analysis. In this method, each increment is added consecutively starting with the increment containing the smallest particles. The cumulative sums are plotted versus the maximum particle size in each increment (McCabe, 2001). This method reveals and accounts for any loss of material due to experimentation.

To predict the PSD of a physical, chemical, or mechanical process, the PSD of the final product is compared to the original, or unaltered, material (Goldman, 1984). To determine the reliability of the systems, distribution measurements of the same sample

are repeated. This is known as reproducibility testing (Goldman, 1984). Reproducibility should be within 2% at the mean (Davies, 1984). These steps produce the acceptability of any particle analysis work.

2.2 Crystallization

Several substances are crystalline which means having atoms which are arranged in a repeating, three dimensional pattern (Myerson, 1999; Mullin 2001). Hair, wood, and even some polymers are partially crystalline (Myerson, 1999). Crystallization is a method where crystalline material are form in industry. Crystallization is often used as a means of solid product purification or as a separation technique in the solid/liquid industry (Myerson, 1999). The two major industrial crystallization techniques are suspension crystallization and the solidification of melts (Davey, 2000; Mullin, 2001). Suspension or solution crystallization often involves non-agitated or agitated vessels where the crystal growth rate from solution is slow. A solution containing the crystalline material is either cooled or evaporated to produce a supersaturated solution to cause the crystalline material to come out of solution (Davey, 2000). This method allows the formation of pure crystals (Mullin, 2001). Melt crystallization occurs from the melt without the presence of a solvent (Gilbert, 1991). For example, the crystalline material is heated above its melting point and is then sprayed in millimeter sized drops on a cool surface where crystallization occurs. Alternatively, the drops are sprayed in a tower and cool as they fall through the tower forming full crystals prior to reaching the bottom of the tower (Davey, 2000). Both solution and melt crystallization are common in batch crystallization production (Davey, 2000). Suspension crystallization is used to control the yields and produce desirable physical characteristics of particulate materials (Davey, 2000).

The magma of a vessel describes the two phase mixture of a suspension fluid or mother liquor and the crystals in a vessel (McCabe, 2001). The magma density is a solids concentration expressed as the ratio between the mass of the crystals and the volume of the mother liquor. Magma density is usually defined as

$$Magma\ Density = \frac{grams\ of\ crystals}{100\ mL\ of\ mother\ liquor}. \quad (2.15)$$

The influence of a solid particle's shape and size is seen throughout crystallization processes. Crystallization is defined as the reverse of dissolving or the growth of a particle in a saturated solution based on solubility information (McDonough, 1992). Although yields and high purity are important, the physical appearance (shape and size) is also significant in solid crystallization (McCabe, 2001). In order to market a final crystalline product, crystals are usually required to maintain some degree of uniformity in size and shape (McCabe, 2001). For example, the size of particles in aerosol cans will determine whether the particles will remain in the can, spray evenly, or produce clumps of particles when sprayed. The shape of the particles will also decide the fate of the particles since oddly shaped particles tend to clog spray nozzles (Cadle, 1965).

The morphology or shape of a crystal is based on the packing symmetry of the crystal lattice (Davey, 2000). However, some chemical species are known to crystallize into more than one distinct crystal structure or habit, which is known as polymorphism. Various polymorphs of a substance possess differences in physical properties such as solubility (Myerson, 1999). In the case of carbon, the element can crystallize as the cubic diamond crystal or the hexagonal graphite crystal (Myerson, 1999). Diamond is a much stiffer material than graphite, yet both materials are formed from the same element.

Crystallization systems often contain both small and large particles. Thermodynamically, the surface energy per unit area of a small particle and a large

particle have different values at the same temperature (McCabe, 2001). The smaller particles contain a significantly larger amount of surface energy per unit area and can ultimately alter the equilibrium of a system. When small particles, or fines, and large particles are simultaneously present in supersaturated solutions, equilibrium becomes more complex. In a supersaturated solution, small crystals (size depends on characteristics of the system) can be in equilibrium; however, this equilibrium is unstable in the presence of larger crystals. This instability is due to Ostwald ripening, which is the dissolution of a small crystal (usually less than 1 μm) during the simultaneous growth of a larger crystal (McCabe, 2001). Ostwald ripening is usually prevented by particle suspension in a nonsolvent. The ability to decrease the effect of Ostwald ripening is important during the particle growth process.

When crystals form, they usually appear as polyhedrons with characteristic sharp corners and edges with flat sides or faces (McCabe, 2001). These characteristics will vary based on crystal structure and growth conditions with the main difference being seen on the interfacial angles of the crystals (McCabe, 2001). Seven crystal systems or classes are known to produce 14 Bravais lattices which are listed in Table 2.2. Crystals are characterized into one of the 14 lattices based on the symmetry between the crystal's edges (a, b, c) and the angles between the faces of the crystal (α, β, γ). These parameters are established during the growth of the crystal.

Table 2.2 Crystal Systems and Bravais Lattices

Lattice Systems	**Crystal Systems**	**Bravais Lattice**	**Symmetry**	**Angle**
Cubic	Cubic	Simple Cubic Body-centered Cubic Face-centered Cubic	a=b=c	α=β=γ=90°
Tetragonal	Tetragonal	Simple Tetragonal Body-centered Tetragonal	a=b≠c	α=β=γ=90°
Hexagonal	Hexagonal	Hexagonal	a=b≠c	α=β=90°, γ=120°
Rhombohedral	Trigonal	Simple Rhombohedral	a=b=c	α=β=γ≠90°
Orthorhombic	Orthorhombic	Simple Orthorhombic Body-centered Orthorhombic Face-centered Orthorhombic Base-centered Orthorhombic	a≠b≠c	α=β=γ=90°
Monoclinic	Monoclinic	Simple Monoclinic Base-centered Monoclinic	a≠b≠c	α=γ=90°≠β
Triclinic	Triclinic	Simple Triclinic	a≠b≠c	α≠β≠γ≠90°

Note: Sources (McCabe, 2001; Mullin, 2001; Brandon, 2008)

2.2.1 Growth and Nucleation

Crystallization from a solution requires two steps – growth and nucleation. Crystal growth describes the growth or enlargement of an existing crystal to a larger sized crystal. Nucleation describes the birth or beginning of a new crystal (Myerson, 1999). A common problem during crystal growth is secondary nucleation. Primary nucleation occurs spontaneously either when no crystalline material is present (homogeneous) or in the presence of foreign material such as dust particles (heterogeneous). Secondary nucleation occurs when an existing crystal in the mother liquor or magma is damaged producing smaller particles or nuclei (Mullin, 2001; McCabe, 2001). Often, these smaller particles (less than 1μm) experience Ostwald ripening or agglomerate with other particles. The newly formed nuclei usually break away from the larger crystals due to high velocities or shear stresses in the boundary layer. This is known as fluid-shear nucleation (McCabe, 2001). The effects of secondary nucleation are discussed further in Section 2.3.1.

In addition to product purity, the average size and size distribution of the product, the shape of the product crystals, and the properties of the final dry product crystals are important attributes to control during crystallization operations (Myerson, 1999). Primarily, the crystal size and shape distribution have a strong effect on the ability to filter the crystals. Secondarily, the distribution affects the degree of particle suspension in a crystallizer or vessel. Filtration and suspension are both discussed further in detail in the following sections.

2.2.2 Separation Techniques

2.2.2.1 Filtration

Filtration is an important step in removing solids suspended in solutions. Filtration describes the separation of solid material from a liquid source by forcing the liquid to travel through a porous medium upon which the solids are retained (Dahlstrom, 1997; Dickey, 1961). This separation is driven by the pressure difference established between the two sides of the porous medium used (Dickey, 1961). Vacuum filtration is often utilized in solid/liquid separations, especially in regards to the crystallization of solid particulates because it is faster than gravity filtration. Vacuum filtration creates separation by producing suction, or negative pressure, below the filter medium (Dickey, 1961). The suction causes the liquid to push through the medium capturing any suspended particles larger than the pore size or retention size of the filtration medium. In crystallization, this type of filtration is used because it reduces particle growth and nucleation during filtering by reducing the filtering time. This approach is especially useful for laboratory scale batch experiments.

Filters have 3 main categories: cake filters, clarifying filters, and crossflow filters. For laboratory experiments of particle breakage, cake filtering is the optimum option. Cake filters, as the name implies, separate large amounts of solids from liquids in the form of a cake or sludge (McCabe, 2001). Based on the selection of porous medium, some small solid particles are trapped in the medium during filtration; however, this entrapment causes the immobilization of the remaining solids through the filter (McCabe, 2001; Dickey, 1961). Some criteria for selecting a filter media (McCabe, 2001; Dickey, 1961) include: 1) the ability of the medium to retain the solids and produce a relatively clear filtrate; 2) the chemical and physical resistance of the medium to withstand the

filtration process; and 3) the ability of the filter to discharge cleanly and completely from the medium.

2.2.2.2 Centrifugal Sedimentation

Centrifugal sedimentation is another method of solid and liquid separation. This separation occurs because of a density difference that exists between the solid material and the liquid source (Svarovsky, 2000). Centrifugal forces cause the particles to maneuver radially through the liquid medium. Centrifugal sedimentation is commonly used to remove finer particles from liquid sources (Svarovsky 2000). In a bowl type centrifuge, samples are inserted into an imperforated bowl and rotated at high speeds (~5000 rpm). During rotation, the liquid escapes through the holes in the bowl while the separated solid particles remain in the bowl. The particles are usually recovered by manual discharge especially in batch operations (Svarovsky, 2000). In other cases, once the initial solid-liquid separation is complete, the liquid is removed and the containment filter is placed upside down in the centrifuge. After repeating the centrifuge process, solid particles are then captured in a collection lid. Since vacuum filtration particle capture is limited by the pore size of the filter medium, this method of separation is important in determining whether or not any particles remain in solutions after undergoing filtration.

2.2.3 Particle Suspension in Agitated Vessels

Of the chemicals produced in the world, over 50% are produced using a stirred vessel including suspending solids in crystallizers (Hemrajani, 2004). Fluid mechanics and particle mechanics represent the basis for all solid-liquid mixing systems (Uhl, 1966). The two phased mixing usually occurs in impeller-stirred tanks or vessels. Some common solid-liquid systems that utilize impeller-stirred tanks include crystallization, paper pulp

slurries, sugar crystal slurries, paint pigment, and clay slurries (Gray, 1986; Hemrajani, 2004). Here, it is noted that agitation and mixing do not depict the same concepts. Mixing depicts the random distribution of two phases that occurs during the stirring process. On the other hand, agitation refers to the movement of material in some vessel (McCabe, 2001).

Crystals must be kept suspended because the crystals that settle to the bottom of the vessel are likely to agglomerate (Davey, 2000). Solid dispersion through the mother liquid is accomplished by increasing the stirrer speed above that needed for suspension (Lyons, 1967). Therefore, correlations have been developed to predict complete suspension of particles. Particle suspension is categorized in three main types (McCabe, 2001; Mersmann, 2001):

1. Incomplete or nearly complete suspension. In this case, most particles are suspended in the magma while some particles remain in contact with the bottom of the vessel. This suspension is undesirable for mixing or particle breakage.
2. Complete (off-bottom) suspension. No particles contact the bottom of the vessel for more than 1 or 2 seconds. This condition is ideal; however, a concentration gradient will exist with the top of the mother liquor clearer or less concentrated than the remaining suspension fluid.
3. Homogeneous or uniform suspension. Clear liquid no longer resides at the top of the vessel. The particle size distribution of the contents is constant throughout the entire vessel; however, concentration gradients may still exist in the vessel. Moreover, a uniform PSD of a vessel containing a wide size distribution is highly uncommon due to several interrupting factors in the vessel (contact and collisions).

Particle suspension depends on several factors including the properties of the solid and mother liquor, the geometry and type of crystallizer or stirred vessel, the impeller characteristics, and the operating conditions of the vessel (Lyons, 1967; Mersmann, 2001; McCabe, 2001). One of the most important aspects of any vessel is the selection of the impeller (e.g. rotor, propeller, and stirrer). The impeller serves two purposes: mixing of the solid/liquid system and suspending of the particles in the vessel (Mersmann, 2001). A propeller, a type of impeller, is used to maneuver the fluid in the system at a rate greater than the solids in that system. The pattern created by the impeller is designed to return all fluid and materials back to the impeller (Lyons, 1967). An impeller is usually needed for suspension because most solid particles have densities that are greater than the density of the liquid or mother liquor. Four or six 45° pitched blades are typically used in the agitation of solid-liquid mixtures (Gray, 1986). Axial flow impellers are most suitable for solid suspensions (Hemrajani, 2004).

To achieve complete particle suspension, the tip speed of the impeller must be greater than the settling velocity, or the gravitational pull, of the solids (McCabe, 2001). Some properties of solid-liquid systems that can further affect particulate suspension include (Lyons, 1967):

- Particle properties (density, size, size range, shape, hardness)
- Solids concentration (loading, magma density)
- Liquid or mother liquor properties (density, viscosity)

Furthermore, particles suspended in stirred tanks are also subjected to several forces (Gray, 1986; McCabe, 2001). Four particular forces are listed below:

- Gravitational force – due to the density difference between the liquid and particle.

- Inertial force - due to movement caused by the rotation of the axis of the impeller.
- Viscous and inertial force - due to drag of liquid on a particle's surface caused by the movement of the particle with respect to the movement of the liquid in the system.
- Frictional force - occurs between the surfaces of colliding particles.

Gravitational forces move the particles toward the bottom of the vessel. Drag forces move particles in the same direction of the liquid movement. The liquid moves radially away from the impeller due to centrifugal force (Gray, 1986).

Agitated vessels are often comprised of rounded tank bottoms, impellers, shafts, inlet/outlet streams, and wells for thermometers or other measuring devices. Figure 2.2 details the layout of a typical batch agitation vessel with the parts labeled a - f. The layout of an agitation vessel will affect the degree of particle suspension. For example, a 2 inch marine propeller with 3 blades and a 0.5 inch axial impeller with 4 blades will produce different flows as well as have different impacts on particle suspension.

Particle suspension is a crucial aspect of crystallization and almost all industrial processes involving slurries in agitated vessels (McCabe, 2001). One important part of mixing operations (such as dissolution or crystallization) is the movement of materials around the surface of particles (Uhl, 1966). Adequate particle suspension is important in crystallization and the production of uniform particles (Mersmann, 2001). If particles remain at the bottom of the vessel during stirring, no upward liquid velocities exist that are capable of moving particles (Gray, 1986). When particle density is greater than that of the liquid, the particle will be more prone to sink to the bottom of the vessel. This is

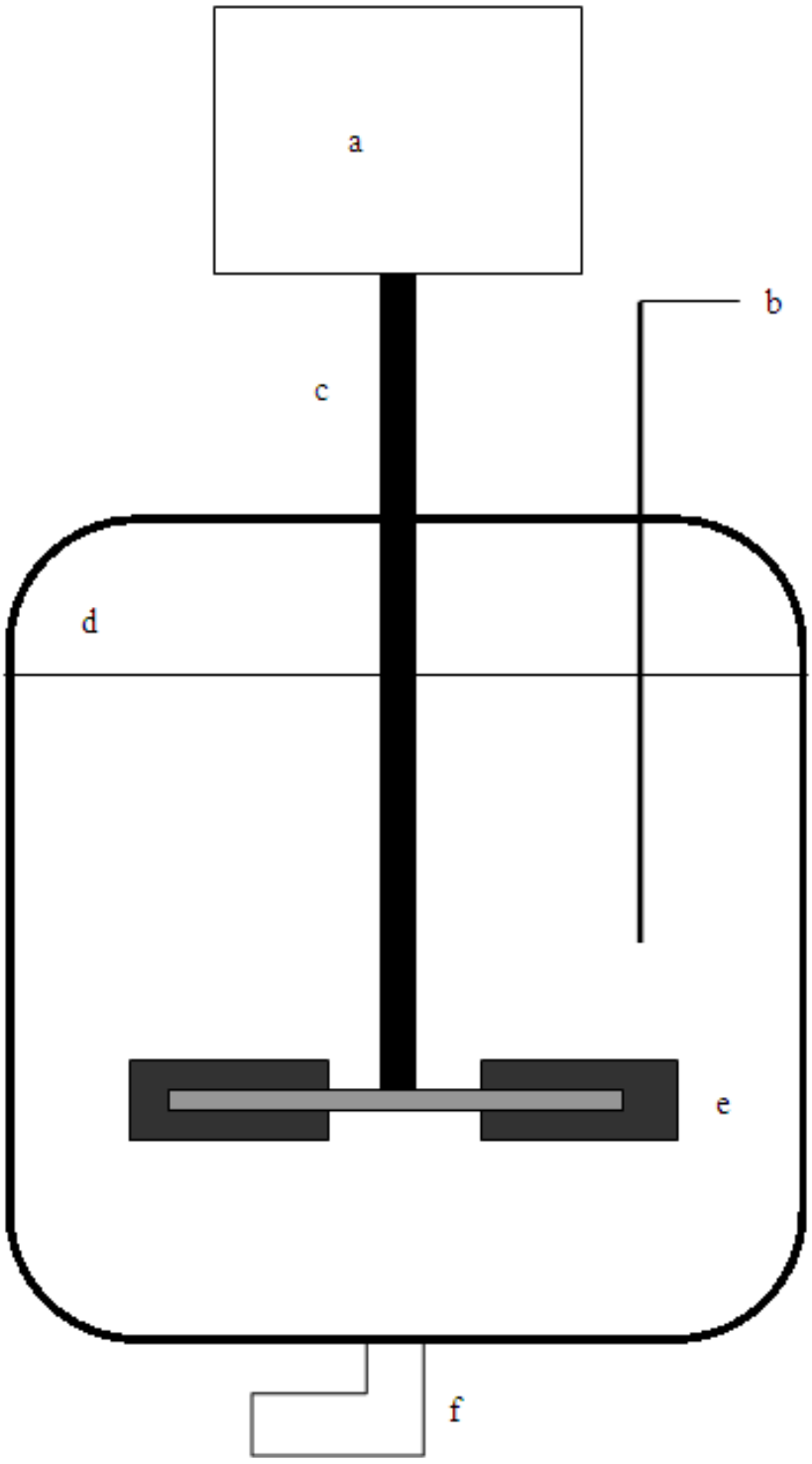

Figure 2.2 Schematic of an Agitation Vessel

Notes: a) the motor, b) measuring device such as thermocouple, c) the impeller shaft, d) the magma surface, e) the impeller, and f) the drainage valve.

known as particle settling in industry (Gray, 1986). To prevent settling, the terminal or settling velocity must be exceeded. The free or terminal settling velocity (McDonough, 1992) is given by

$$V_t = \left(\frac{2g_c M_p(\rho_p - \rho)}{\rho \rho_p A_p C_D}\right)^{1/2} \tag{2.16}$$

where g_c is the gravitational constant, M_p is the mass of the particle, ρ_p is the density of the particle, A_p is the projected area of the particle, ρ is the density of the liquid, and C_D is the drag coefficient (which is a function of Reynolds number). As the particle settling velocity increases, the power requirement for the system also increases. For a spherical particle (Atiemo-Obeng, 2004; McDonough, 1992),

$$V_t = \left(\frac{4g_c d_p(\rho_p - \rho)}{3\rho C_D}\right)^{1/2} \tag{2.17}$$

where d_p is the particle diameter. An increase in the diameter of a particle produces an increase in the speed needed to keep the particle suspended (Gray, 1986).

Agitation in a stirred vessel is a common process in industry but challenging to simulate (Marshall, 2004). Computation fluid dynamics (CFD) is often used to model a stirred tank (Marshall, 2004). In stirred vessels, two fluid motion phenomena are noted - convection and diffusion. Convection describes the rotation of fluid in space while diffusion is related to the presence of velocity or concentration gradients in the vessel (McCabe, 2001; Marshall, 2004). Turbulence often occurs in solids suspensions; therefore, the interaction between turbulent and mixing processes should be taken into consideration (Kresta, 2004). Turbulence can also occur due to solid particulates going against the flow (Kresta, 2004). Turbulence is commonly measured by the Reynolds (Re) number. In a pipe, the Reynolds number (Marshall, 2004) is

$$Re = \frac{\rho U d}{\mu} \tag{2.18}$$

where ρ is the fluid density, U is the axial velocity, d is the pipe diameter, and μ is the dynamic viscosity. For a stirred vessel, the Reynolds number is

$$Re = \frac{\rho N D^2}{\mu} \tag{2.19}$$

where N is the impeller speed in revolutions per second (rps) and D is the diameter of the impeller (Marshall, 2004). In a tank where mixing is occurring, transition from laminar to turbulent flow occurs at a Reynolds number between 50 - 5000 based on the power number of the impeller (Marshall, 2004; Hemrajani, 2004). Creeping flow is defined by $Re \leq 10$, while fully turbulent systems are given by $Re \geq 10^4$(Hemrajani, 2004). At low Re, viscosity forces are dominant while inertial forces dominate the system at high Re (Kresta, 2004).

Solids suspensions in stirred tanks are usually designed using the off-bottom or just suspended impeller speed, N_{js} (Marshall, 2004). Turbulent fluctuations caused by agitation at the bottom of the vessel are considered an important mechanism in determining off-bottom suspension (Kresta, 2004). However, most just suspended correlations neglect or pay little attention to the effect of fluid flow patterns on particle distributions (Marshall, 2004). One correlation for particle suspension was developed by Zwietering (1958). Zwietering sought to determine the conditions for complete solid particle suspension without regard to quantitative analysis of particle distribution over the height of a vessel (Zwietering, 1958). Zwietering utilized visual observations of approximately 1000 experiments to determine the minimal propeller speed for particle suspension. No samples were taken from any experiment; thus, the resulting particle size distributions were not provided. Zwietering based calculations on five different impellers

in six tanks with tanks ranging from 6 inches to 2 feet in diameter (Zwietering, 1958). From these experiments, Equation 2.20 was derived to determine the minimum stirrer speed, N_{js}, needed for particle suspension.

$$N_{js} = S\frac{\nu^{0.1} d_p^{0.2}\left(\frac{g*\Delta\rho}{\rho_L}\right)^{0.45} X^{0.13}}{D^{0.85}} \tag{2.20}$$

where

$$S = f\left(\frac{T}{D}; \frac{T}{C}: \text{impeller type}\right) \tag{2.21}$$

In Equations 2.20 and 2.21, ν is the kinematic viscosity, $\Delta\rho = \rho_s - \rho_L$ (solid density minus fluid density), ρ_L is the suspension fluid density, g is the gravitational constant (usually g_c), d_p is the particle diameter, *X* is the particle loading which equals $100 * \frac{weight\ of\ solid}{weight\ of\ the\ liquid}$, D is the diameter of the impeller, and S is a dimensionless constant describing the geometry of the vessel where T is the diameter of the tank or vessel and C is the off bottom clearance or distance between the impeller and the bottom of the vessel. Values for the constant S have been determined based on impeller type (propeller, turbine, flat, angled), impeller diameter, vessel geometry (flat bottom, round bottom), vessel diameter, and C (Atiemo-Obeng, 2004). When N_{js} is met, particles are not uniformly distributed throughout the vessel (Kresta, 2004). Despite numerous attempts to enhance the viability of Zwietering's correlation, results remain significantly unchanged (Kresta, 2004).

2.3 Particle Breakage in a Stirred Vessel

The presence of excess, small particles in a system may cause unnecessary filter plugging and ultimately, may alter the final results. Small particles are often the result of particle breakage in industrial equipment. Particle breakage is evident in fluidized beds

and slurry transportation lines (Conti, 1980) and is a common result of slurry agitation in a vessel (Mersmann, 2001). Particle breakage occurs when an area of the particle is subjected to a stress that is greater than the ability of the particle to resist that stress, which is called the particle's fracture strength (Mazzarotta, 1992).That is, the energy applied to the particle exceeds the energy required to keep damage, such as cracks or breakage, from occurring to the particle. Particle breakage can be attributed to two phenomena – attrition and fragmentation.

Attrition is caused by the wearing or grinding down that occurs from contact between the suspended crystals and the reactor wall, impeller, other crystals, and other mobile and stationary parts of equipment (Bravi, 2003). Attrition results in one large child particle approximately the size of the parent particle and many child particles that are orders of magnitude smaller. Attrition produces small particles often called fines. Fines not only clog filters; they also bind to other particles forming clumps that may be observed or misinterpreted as larger particles in some analytical equipment. Attrition is the erosion of smaller pieces of a material whereas fragmentation describes the separating or splitting of a particle into smaller portions (Mazzarotta, 1996; Bemrose, 1987). Fragmentation occurs when a large section (a chunk or a chip) of a particle is separated from the original parent crystal and the child particle sizes are of the same order of magnitude as the parent particle size (Bemrose, 1987; Mazzarotta, 1996). Fragments of the parent crystals exhibit much larger particle sizes than those resulting from attrition and cause a different resulting geometry to the parent crystal compared to attrition. Attrition is thought to cause particles to become more rounded; whereas, fragmentation produces particles of an irregular nature. It is also suggested that attrition is more

probable as a result of crystallization procedures when compared to fragmentation due to the material used (Nienow, 1978; Bravi, 2003).

Although particle breakage produces small particles, it also changes the morphology of the original, parent crystals and alters the particle size distribution (Mazzarotta, 1996). Therefore, particle breakage must be controlled in industrial systems. To measure breakage effects accurately, it is necessary to prevent other mechanisms such as growth from occurring.

Researchers perform crystallization in nonsolvents because the use of a nonsolvent ensures that breakage is the only mechanism occurring in an experiment instead of dissolution or growth (Conti, 1980; Bravi, 2003). With the breakage mechanism isolated, changes in the size and morphology are only due to breakage. Previous research has presented only a qualitative analysis of changing morphology due to crystal breakage. In more recent years, the focus has switched to quantitative analysis of crystal morphology as well (Mazzarotta, 1996). Quantitative analysis has included particle collisions within the breakage system.

2.3.1 Collisions and Contact Nucleation

Particle size reduction can be undesirable in processes such as particle growth and nucleation (Mazzarotta, 1992). One result of particle contact with the walls of the vessel, the stirrer or propeller, or other particles in the vessel is contact nucleation. This type of secondary nucleation is the most significant nucleation mechanism in crystallizers (Davey, 2000; McCabe, 2001). Contact nucleation can occur at low supersaturation, which is the condition used for optimum growth of good quality crystals (McCabe, 2001).

Particle breakage in a stirred vessel may result from several methods or collision influences within a crystallization system. The various types of crystal collision that occur in a stirred vessel and their effect on secondary nucleation is presented in Table 2.3. Collision types include crystal-to-crystal, crystal-to-impeller, crystal-to-vessel, or crystal-to-fluid (Garside, 1985; Shamlou, 1990).The effect of each type of collision varies with respect to the system under observation.

The type of bonding in a material plays a role in where and how a particle may break based on bond strengths. Molecular motion is confined to an oscillation about a fixed position (Mullin, 2001). In a stirred vessel, the greatest impact velocity usually occurs when a suspended particle collides with the impeller, or stirrer (Gahn, 1999a); therefore, most attrition occurs as a result of collisions between the suspended crystal and the impeller. Impact can occur on the face, edge, or corner of a crystal with corner contact being the most probable (Gahn, 1999a). Solids will often fracture when a deforming force is applied (Mullin, 2001); therefore, repeated contact with its surroundings will yield a more rounded, reduced-sized crystal (Gahn, 1997; Gahn, 1999a). Since particles are expected to become more spherical (Mazzarotta, 1996), a value for roundness is usually analyzed in attrition experiments. Fluid-dynamic breeding occurs as a result of parent crystals interacting with the movement of the suspension fluid. This breeding produces kinetic energy based on the turbulence occurring on the agitated crystals (Shamlou, 1990). Secondary nucleation also plays an important role in determining the particle size distribution (Shamlou, 1990).

Table 2.3 Crystal Collision Types and Secondary Nucleation Effect

Collision Type	**Effect in Secondary Nucleation Production**
Crystal-to-Crystal *(Shamlou, 1990)*	Rate of generation is proportional to the rate of collision between the crystals and the collision energy.
Crystal-to-Impeller *(Shamlou, 1990)*	Rate of generation is proportional to the impact energy, impact frequency, and the number of initial parent crystals.
Crystal-to-Crystallizer *(Shamlou, 1990, Evans, 1974)*	Coated and uncoated crystallizer walls produced a negligible effect on the overall rate of nucleation.
Crystal to Fluid (Fluid-induced Breeding) *(Shamlou, 1990)*	Rate of generation is a function of the number of parent crystals undergoing attrition, the frequency of crystal disruption, and the number of nuclei attrited per disruption.

Weaker particles are expected to fracture or have more gross fragmentation when compared to stronger, more durable particles. To cause attrition or fragmentation of a particle, sufficient energy to cause breakage must be supplied by the system. This energy must surpass the surface strength of the crystals under investigation. The ability of this energy to transfer between the crystals and the suspension fluid while agitated determines if breakage will occur. There exist several probable mechanisms that affect the breakage process. Some mechanisms have great influence on the results while others only have a minor significance (Shamlou, 1990).

2.3.2 Impact Energy

When considering a system where collisions occur, a force exists whereby the structure of one or both materials can no longer withstand the force caused by the collision which causes damage in the form of cracks or breakage (Gahn 1997). In some particle technology processes, the energy required to cause damage to particles is calculated using one of three equations: Rittinger's Law, Kick's Law, or Bond's Law (Kanda, 2006). All three laws are based on the grinding process instead of a collision process as the case of an agitated vessel.

2.3.2.1 Rittinger's Law

$$\frac{E}{M} = C_R\left(S_p - S_f\right) \tag{2.22}$$

For Rittinger's equation, E/M is the energy per mass, C_R is a constant based on material properties, and S_p and S_f are product and feed average surface areas. Rittinger's law assumes that the energy consumed is proportional to the amount of freshly produced surface (Kanda, 2006).

2.3.2.2 Kick's Law

$$\frac{E}{M} = C_k \ln\left(\frac{x_f}{x_p}\right) \tag{2.23}$$

In Kick's equation, C_k is Kick's constant, which is calculated for different materials and x_f and x_p are the feed particle size and product particle size. Kick's law assumes that the energy is related to the ratio between the feed and product particle sizes (Kanda, 2006).

2.3.2.3 Bond's (Work) Law

$$W = W_i\left(\frac{10}{\sqrt{P}} - \frac{10}{\sqrt{F}}\right) \tag{2.24}$$

The work input to the system, W, is related to Bond's work index, W_i, is dependent upon the material. The particle size of the product and feed in microns are represented by P and F, respectively. Bond's Work index is defined as the energy required to the unit mass of a particle of infinite size to a size where 80% passes through a 100 micron sieve (Snow, 1997).

2.3.2.4 Collision Based Equations

Gahn and Mersmann (1997, 1999a) developed an equation based on the hardness of a particle and the speed of the propeller to determine the amount of impact or the impact energy needed to cause damage to a single particle. The model was developed for collisions between particles and a hard surface based on the abrasion volume. In agitated vessels, the impeller and the wall of the reactor serve as hard surfaces. Single particle impact tests were conducted using seven different materials allowing each to fall through a pressurized tube. Crystal size varied from 400-2000 μm. (Gahn, 1997). In each experiment, fifty crystals were examined with each crystal weighed before and after impact testing. Each experiment was repeated six times. The model provided a

relationship between particle size and the mass of fragments produced by abrasion or breakage (Gahn, 1997). The model utilizes several characteristics of a particle including the Vickers' hardness (H_v), the shear modulus (μ), the fracture resistance (Γ), the efficiency factor (K), and the plastic deformation work for a given particle (W_{pl}). Later, the authors extended the model to include both growth and breakage occurring simultaneously (Gahn, 1999b). The models readily and quantitatively address the particle size but neglect the particle shape.

Other research on impact attrition modeling was conducted by Ghadiri and Zhang theoretically (Ghadiri, 2002) and experimentally (Zhang, 2002). The model was developed based on fracture mechanics and physical properties such as hardness (H), fracture toughness (K_c), the characteristic particle length (l), particle density (ρ), and the impact velocity (v). The developed expression modeled the volume fraction of a particle lost due to impact, ξ, based on an attrition propensity parameter and an experimentally determined (Zhang, 2002) constant, α. This constant was measured for three crystalline materials: NaCl, KCl, and MgO. Impact was made between a single crystal and a hard flat surface using compressed air and a sapphire surface (Zhang, 2002). Each test used 20-25 particles with each test conducted ten times. Results showed that the amount of breakage occurring was a factor of the material properties, the impact velocity, and the initial particle size (Zhang, 2002).

2.3.3 Previous Breakage Research in a Stirred Vessel

Although the studies of Gahn and Mersmann (1997, 1999a, 1999b) and Ghadiri and Zhang (2002) produced vital information regarding the impact energy needed to fracture a particle, the effects of other collision types were not investigated. Furthermore,

impact tests were only for single particles and were not conducted in a stirred vessel. Other parameters must be considered when modeling particle breakage.

Table 2.4 highlights previous particle breakage research conducted in a stirred vessel while Table 2.5 gives the operating conditions for each investigation. Particles ranged from 100 - 1800 microns in size with most researchers using laboratory grown crystals. Variations in operating conditions included agitation rate (Nienow, 1978; Offermann, 1982; Shamlou, 1990), suspension density (Nienow, 1978; Offermann, 1982; Mazzarotta, 1992; Chianese, 1993; Synowiec, 1993), and residence time (Nienow, 1978; Conti, 1980; Shamlou, 1990; Mazzarotta, 1992; Mazzarotta, 1996). Bravi et al. (2003) studied the effect of breakage on multiple crystals while only one study (Offermann, 1982) investigated the effect of using a saturated solution versus a nonsolvent on particle breakage in a stirred vessel.

Table 2.4 Crystal Breakage in the Literature

Source	Crystals Examined	Crystal Habit	Size Range, microns	Laboratory Grown
Nienow and Conti, 1978	Copper Sulfate	Octahedral*	1200-1800	Yes
	Nickel Ammonium Sulfate	Monoclinic*		
Conti and Nienow, 1980	Nickel Ammonium Sulfate Hexahydrate	Monoclinic*	~1060	Yes
Offermann and Ulrich, 1982	Sodium Chloride	Cubic*	300-400	NR
Shamlou et. al, 1990	Potassium Sulfate	Orthorhombic*	Varied (600-1000)	Yes
Mazzarotta, 1992	Potassium Sulfate	Orthorhombic*	500-600, 1000-1180	Yes
Chianese et. al, 1993	Potassium Sulfate	Orthorhombic*	1000-1180	Yes
Synowiec et. al, 1993	Potassium Sulfate	Orthorhombic*	Varied (100-1000)	Yes
	Potassium Aluminum Sulfate	Octahedral*		
Mazzarotta, 1996	Sucrose	Monoclinic*	1180-1400	No
Bravi et al., 2003	Citric Acid	Monoclinic	500-600	No
	Pentaerythritol	Tetragonal	500-600	
	Potassium Chloride	Cubic	250-300	
	Potassium Sulfate	Orthorhombic	355-425	
	Sodium Chloride	Cubic	355-425	
	Sodium Perborate	Dendritic	425-500	
	Sodium Sulphate	Monoclinic	710-850	
	Sucrose	Monoclinic	355-425	

NOTE: * Obtained from Mullin, 2001. NR = Not recorded.

Table 2.5 Operating Conditions of Literature Breakage Research

Source	Agitation Rate, rpm	Suspension Density, kg/m3	Fluid	Time
Nienow and Conti, 1978	Varied (500-900)	Varied (88.5-265.5)	saturated solution (50/50 wt % water/methanol), nonsolvent (acetone)	Varied (0-24 hr.)
Conti and Nienow, 1980	420	88.5	saturated solution	Varied (0-48 hr.)
Offermann and Ulrich, 1982	Varied (0-1600)	Varied (0-510)	nonsolvent (acetone), aqueous saturated solution	5 sec.
Shamlou et. al, 1990	Varied (0-2000)	363	methanol (low solubility)	Varied (0-60 min.)
Mazzarotta, 1992	950, 1100	Varied (13.33-30.00)	saturated hydroalcoholic solution	Varied (0.5-10 hr.)
Chianese et. al, 1993	650	Varied (5-60)	saturated (methanol-water) solution, saturated water	2 hr.
Synowiec et. al, 1993	NR	Varied (0-88)	saturated ethanol solution	2 hr.
Mazzarotta, 1996	1100	100	nonsolvent (xylene)	Varied (0-8 hr.)
Bravi et al., 2003	700* 600 800 1000 900 800 700 700	100	nonsolvent (xylene)	1 hr.

NOTE: * Agitation rates in this study are adjusted for off bottom clearance for each individual crystal presented in Table 2.4.

2.3.3.1 Analysis Techniques

Various analysis techniques have been utilized for particle breakage research. In most cases (Chianese, 1993; Mazzarotta, 1992; Mazzarotta, 1996; Bravi, 2003), researchers used mass distributions based on sieving results. Particle counters were also used. Conti and Nienow (1980) utilized a Zeiss TGZ-3 particle counter to count approximately 1000 particles into 5 size ranges from 0 - 22.4μm in 3.6μm intervals. Offermann and Ulrich (1982) used a Coulter Counter TA II with a 100 micron orifice based on predetermined volumes.

Mazzarotta et. al (1996) captured four images of particles from each sieve to determine the distribution. Bravi et. al (2003) used sieving to determine the size distribution and optical microscopy for morphology determination. The morphology of the crystals was determined by analyzing 10-20 crystals from each sieve. The morphological parameters selected were roundness and β (width/length) as an aspect ratio measurement. Alternatively, crystal samples were also collected during agitation at various times (Shamlou, 1990; Synowiec, 1993) and analyzed. This process is questionable since removing crystals during the breakage process alters the dynamics of the overall system (i.e. suspension density) and may not present a representative sample if the system is not well-mixed.

2.3.3.2 Collisions and Breakage

Originally, Nienow and Conti (1978) determined that crystal-to-impeller and crystal-to-vessel collisions were more dominant for low solids concentration (<100 kg/m^3); however, at high solids concentration (300 kg/m^3), particle-to-particle collisions were considered more dominant. Later, crystal-to-impeller and crystal-to-fluid collisions

were attributed as the main causes of particle breakage (Shamlou, 1990; Synowiec, 1993), and crystal-to-crystal collisions were determined to have no significant effect on particle breakage (Synowiec, 1993).

Particle breakage was found to be more common at the beginning of the agitation run (Conti 1980). Attrition or erosion was the most dominant breakage source (Nienow, 1978; Shamlou, 1990; Mazzarotta, 1992) with no substantial gross fragmentation although both attrition and fragmentation were found to occur (Mazzarotta, 1992; Synowiec, 1993). Neglecting fragmentation in modeling was discouraged (Mazzarotta, 1992). More work is needed to determine the effect of each individual mechanism on particle breakage in a stirred vessel.

2.3.3.3 Particle Size and Shape

In an early study, particles became more rounded with time (Conti, 1980). Mazzarotta (1996) found that sugar crystals became less spherical for original-sized crystals in the first 10 minutes; however, after 10 minutes, the crystals became more spherical. Increases in the initial particle size produces an increase in the number of fragments produced when the agitation rate is greater than about 630 rpm (Offermann, 1982). The particle size of fragments produced from breakage decreased with time (Conti, 1980) until a residence time of 60 minutes (Shamlou, 1990). The fragments produced were irregularly shaped (Chianese, 1993).

2.4 Population Balance Equation (PBE)

Mathematical modeling of solid particle behavior is one area of rapid development in particle technology (Rhodes, 2008). Population balances serve as a representation of characteristic behaviors of the population (Ramkrishna, 2000) and are

often based on surroundings or mechanics. Earlier population density equations date back to the work of Randolph and Larson (1962) and Hulbert and Katz (1964). Chemical engineers utilize population balances in several areas such as solid-liquid and gas-solid dispersions. Population balances also play a crucial role in the analysis and design of nanoparticles (Ramkrishna, 2000). Population balances usually represent a distribution of a particle population. Four different methods are utilized to express the size distribution of aggregated particles based on size:

- Cumulative weight distribution
- Weight percent distribution
- Cumulative number of particles
- Population (or number) density

The cumulative weight distribution is mostly associated with sieve analysis; however, population density has the greatest significance in controlling the size distribution (Randolph, 1962). The population density is based on the number of particles, the mass density is based on the mass of the particles, and the volume density is based on the volume of the particles (Ramkrishna, 2000). The number density is the derivative of the number of particles per slurry volume with respect to length or particle volume. Since particles with size $v + \delta v$ are either created or destroyed in most systems (as the case of particle breakage or aggregation), the population balance equation (PBE) must take into account all mechanisms whereby which particles appear or disappear from a given size range. The creation of new particles in a size range is referred to as a *birth* process. Likewise, the removal of existing system particles from a size range is called a *death* process (Ramkrishna, 2000). In the death process, a single particle undergoes breakage to the extent that the original particle form no longer exists. However, the

presence of the newly formed smaller particles from the death process represents the birth process in other size ranges (Ramkrishna, 2000). Other processes resulting from particle motion such as particle breakage should also be accounted for in PBEs. The modeling of PBEs must address each mechanism to accurately represent the system (Ramkrishna, 2000).

The variables representing particle properties are either discrete or continuous. Sieve analysis is one depiction of discrete measurements where discrete size intervals are used. Brownian motion, which can be measured as the motion of a small particle (e.g. pollen) in space over time, is an example of a measurement with a continuous variable (Ramkrishna, 2000). In crystallization, the particle size distribution is usually modeled using PBEs based on the size of the crystal. The changes in the size of the crystal reveal whether particle growth or reduction has occurred based on comparison with the initial size of the crystal (Ramkrishna, 2000). In a crystallization system, a particle's state or condition is based on any changes occurring within the system and the birth and death processes.

PBE modeling of the birth and death terms must be specific to the system under investigation (Ramkrishna, 2000). For example, during the crystallization process, the breakage of existing particles can add to the birth of new particles and must be accounted for in the PBE for the system. A generic PBE for breakage is presented in Eq. (2.25).

$$\frac{d}{dt}n(z,t:v) = [Input] - [Output] + [Particle\ Birth] - [Particle\ Death] \quad (2.25)$$

where n is the number density, t is time, z is the position, and v is the volume of the particle.

The quantity of particles in a system at a given time is a result of the number of particles flowing into a system and the number of new particles formed in the system minus the particles flowing out of the system and any particles destroyed in the system. Here it is noted that particle growth also occurs in crystallization systems; however, only breakage is considered here as shown in the following equation.

$$\frac{dn(v,t)}{dt} = \left(\frac{dn}{dt}\right)_{breakage} \tag{2.26}$$

Early solutions to the PBE were first developed by Hulbert and Katz (1964) and by Randolph and Larson (1962). Their proposed solution was the method of moments (Mesbah, 2009). From Mullin (2001), the population density is defined as

$$\frac{dN}{dL} = n. \tag{2.27}$$

where n is the number density, L is length, and N is the total number of particles per unit volume. The zeroth moment is then described by

$$N = \int_0^L n\, dL \tag{2.28}$$

and the first moment, cumulative length, is

$$\mathcal{L} = \int_0^L nL\, dL \tag{2.29}$$

however, this measurement was not very useful which led to the evaluation of the second and third moments in Equations 2.30 and 2.31.

$$A = \beta \int_0^L nL^2 dL \tag{2.30}$$

$$M = \alpha\rho_c \int_0^L nL^3 dL \tag{2.31}$$

In these equations, α represents the volume shape factor and β is the surface shape factor. The crystal density is represented by ρ_c. The second moment is directly proportional to

the surface area, A, while the third moment is proportional to the total mass, M. In general the *j*th moment is represented by

$$m_j = \int_0^L nL^j dL \tag{2.32}$$

These moments can be used to describe the size distribution of particles. Of these moments, the zeroth and third moments are the most widely used for PBEs.

Several authors have developed relationships to describe particle breakage with population balance equations (Mazzarotta, 1996; Conti, 1980; Nienow, 1978); however, most attrition models neglect the changing morphology of the crystal as a result of breakage (Hill, 1995; Briesen, 2009). Briesen (2009) proposed that the shape of a particle should not be ignored when developing a breakage model. Briesen reports that the effect of shape change can be modeled based on the selection of a shape modification function. The modeling of the breakage function, the discretizing of differential equations and the solving of PBEs are important in determining the effect of particle size and shape changes and are discussed further in the following sections.

2.4.1 Discretizing the Differential Equation

Discretization techniques have been proven as powerful and computationally efficient alternatives to partial integral differential PBEs (Kumar, 1997; Ramkrishna, 2000; Hill, 1995). In the discretized method, a continuous size range is divided into discrete size ranges, or bins. The information gathered is used to determine a set of macroscopic balance equations for the population of the bins (Kumar, 1997).

Austin (1976) described the grinding of a particle in discrete form based on two specifications: 1) the specific rate of breakage based on particle size and 2) the quantity and distribution of daughter or child particles produced when the particles break. For a

range of particle sizes represented by size interval *j*, the rate of breakage at time *t* is equal to $S_j w_j(t)W$ where $w_j(t)$represents the weight fraction of particles of size *j* in the total particle weight, *W* with S_j being the specific rate of breakage of size *j* particles. Here, size *j* is larger than size *i*. This relationship results in a rate-mass balance (Austin, 1976) for a batch grinder of

$$\frac{dw_i(t)}{t} = -S_i w_i(t) + \sum_{\substack{j=1 \\ i>1}}^{i-1}\left(B_{i,j} - B_{i+1,j}\right)S_j w_j(t) \tag{2.33}$$

where t represents the time of grinding. $B_{i,j}$ is the weight fraction of fragments of size *i* and smaller that were formed when particles in interval *j* were broken. The cumulative breakage distribution function $B_{i,j}$ (Austin, 1976) is represented as

$$B_{i,j} = \phi\left(\frac{x_i}{x_j}\right)^{\gamma} + (1-\phi)\left(\frac{x_i}{x_j}\right)^{\beta}, \quad (0 \le \phi \le 1) \tag{2.34}$$

where values of γ and β vary and depend on the material used. Therefore, breakage can be designed based on the values of β, γ, and □ in terms of parent particle size, x_j, and child particle size, x_i.

A new method for discretizing the breakage equation was introduced by Hill and Ng (1995). When considering only particle breakage, the number based breakage equation can be represented as

$$\frac{dn(v)}{dt} = \int_v^{\infty} b(v,w)S(w)n(w)dw - S(v)n(v) \tag{2.35}$$

in a continuous form and as

$$\frac{d}{dt}N_i(t) = \sum_{j=i+1}^{\infty} b_{ij}S_j N_j(t) - S_i N_i(t) \tag{2.36}$$

in a simple discrete form. Hill included β_j and δ_i to represent the birth and death term probability functions in the breakage equation as shown by

$$\frac{d}{dt}N_i = \sum_{j=i+1}^{\infty} \beta_j b_{ij} S_j N_j - \delta_i S_i N_i \tag{2.37}$$

The equation was developed as a means to simultaneously predict the evolution of the total number of particles and conserve mass.

2.4.2 Power Law Form of Product Function

Another method of representing the breakage function was presented by Hill (2004). The equation used a power law form of the product function to describe the breakage function

$$b'_v(v,w) = \frac{pv^m(w-v)^{m+(m+1)(p-2)}[m+(m+1)(p-1)]!}{w^{pm+p-1}m![m+(m+1)(p-2)]!} \tag{2.38}$$

where the terms m and p are adjustable constants. The equation guarantees mass conservation and allows the user to set the number of child particles, p.

Although models have been developed, experimental data are needed to validate the proposed model. Specifically, an investigation of the operating conditions and parameters should thoroughly be investigated to determine how each parameter will affect the breakage occurring in a stirred vessel. From these results, models should be developed that correlate all mechanisms present within the system.

2.5 References

Allen, T. (1997). *Particle Size Measurement Volume 1: Powder Sampling and Particle Size Measurement 5th Ed.*, Chapman & Hall, London.

Atiemo-Obeng, V. A., Penney, W.R., and P. Armenante (2004). Solid-liquid Mixing. In Paul, E. D., Atiemo-Obeng, V. A., and S. M. Kresta (Eds.). *Introduction of the Handbook of Industrial Mixing*, Wiley & Sons, New Jersey, 543-582.

Austin, L., Shoji, K., Bhatia, V., Jindal, V., and K. Savage (1976). Some Results on the Description of Size Reduction as a Rate Process in Various Mills. *Ind. Eng. Chem., Process Des. Dev., Vol. 15(1)*, 187-196.

Bemrose, C. R. and J. Bridgewater (1987). A Review of Attrition and Attrition Test Methods. *Powder Tech. Vol. 49*, 97.

Brandon, D., and W.D. Kaplan (2008). *Microstructural Characterization of Materials. 2nd Ed.*, Wiley & Sons, West Sussex.

Bravi, M., Di Cave, S., Mazzarotta, B., and N. Verdone (2003). Relating the attrition behavior of crystals in a stirred vessel to their mechanical properties. *Chem. Eng. J. Vol. 94*, 223-229.

Briesen, H. (2009). Two-dimensional population balance modeling for shape dependent crystal attrition. *Chem. Eng. Sci. Vol.64(4)*, 661-672.

Cadle, R.C. (1965). *Particle Size: Theory and Industrial Applications*, Reinhold Publishing Corporation, New York.

Chianese, A., Di Berardino, F., and A.G. Jones (1993). On the Effect of Secondary Nucleation on the Crystal Size Distribution from a Seeded Batch Crystallizer. *Chem. Eng. Sci. Vol. 48(3)*, 551-560.

Conti, R. and A.W. Nienow (1980). Particle abrasion at high solids concentration in stirred vessels-II. *Chem. Eng. Sci. Vol. 35*, 543-547.

Dahlstrom, D.A., Bennett, R.C., Emmett, Jr., R.C., Harriott, P., Laros, T., Leung, W., McCleary, C., Miller, S.A., Morey, B., Oldshue, J.Y., Priday, G., Silverblatt, C.E., Slotee, J.S., Smith, J.C., and D.B. Todd (1997). Liquid-Solid Operations and Equipment. In Perry, R.H. and D.W. Green. *Perry's Chemical Engineers' Handbook 7th Ed.*, McGraw-Hill, New York, 18.1-18.125.

Davey, R. and J. Garside (2000). *From Molecules to Crystallizers: An Introduction to Crystallization*, Oxford Science Publications, Oxford.

Davies, R. (1984). Particle Size Measurement: Experimental Techniques. In M.E. Fayed and L. Otten (Eds.). *Handbook of Powder Science and Technology*, Van Nostrand Reinhold, New York, 31-68.

Dickey, G.D. (1961), *Filtration*, Reinhold Publishing Corporation, New York.

Ennis, B. J., Green, J., & R. Davies (1994). Particle Technology: The Legacy of Neglect in the U.S. *Chem. Engng. Progress Vol. 90(4)*, 32-43.

Evans, L.B., Joseph, B., and W.D. Seider (1997), System Structures for Process Simulation, *AIChE J. Vol. 23*, 658.

Evans, T. W., Margolis, G. and A. F. Sarofim (1974). Mechanisms of secondary nucleation in agitated crystallizers. *AIChE J*. Vol. 20, 950-958.

Gahn, C. and A. Mersmann (1997). Theoretical Prediction and Experimental Determination of Attrition Rates. *Chem. Eng. Res. Design Vol. 75(2)*, 125-131.

Gahn, C., and A. Mersmann (1999a). Brittle fracture in crystallization processes Part A. Attrition and abrasion of brittle solids. *Chem. Eng. Sci. Vol.54,* 1273-1282.

Gahn, C., and A. Mersmann (1999b). Brittle fracture in crystallization processes Part B. Growth of fragments and scale-up of suspension crystallizers. *Chem. Eng. Sci. Vol. 54,* 1283-1292.

Garside, J. (1985). Industrial Crystallization from Solution. *Chem. Eng. Sci. Vol. 40(1)*, 3-26.

Ghadiri, M. and A. Zhang (2002). Impact attrition of particulate solids. Part 1: A theoretical model of chipping. *Chem. Eng. Sci. Vol. 57*, 3659-3669.

Gilbert, S. (1991). Melt Crystallization: Process Analysis and Optimatization. *AIChE J. Vol. 37(8)*, 1205-1218.

Goldman, A.S. and H.D. Lewis (1984). Particle Size Analysis: Theory and Statistical Methods. In M.E. Fayed and L. Otten (Eds.). *Handbook of Powder Science and Technology*, Van Nostrand Reinhold, New York, 1-30.

Gray, J.B. and J.Y. Oldshue (1986). Agitation of Particulate Solid-Liquid Mixtures. In V.W. Uhl and J.B. Gray (Eds.). *Mixing: Theory and Practice. Vol. III*, Academic Press, Orlando, 1-59.

Hemrajani, R.R. and G.B. Tatterson (2004). Mechanically Stirred Vessels. In E.L. Paul, V.A. Atiemo-Obeng, and S.M. Kresta. *Handbook of Industrial Mixing: Science and Practice*, Wiley and Sons, 345-390.

Hill, P.J. and K.M. Ng (1995). New Discretization Procedure for the Breakage Equation. *AIChE J. Vol. 41(5)*, 1204-1216.

Hill, P. (2004). Statistics of Multiple Particle Breakage Accounting for Particle Shape. *AIChE J. Vol. 50 (5)*, 937-952.

Hulbert, H.M and S.L. Katz. (1964). Some Problems in Particle Technology: A Statistical Mechanical Formulation. *Chem. Eng. Sci. Vol. 19*, 555-574.

Kanda, Y. and N. Kotake. (2006). Communition Energy and Evaluation in Fine Grinding. In A.D. Salman, M. Ghadiri, and M.J. Hounslow Eds. *Handbook of Powder Technology, Vol. 12: Particle Breakage*, 529-550.

Kresta, S.M. and R.S. Bradley (2004). Turbulence in Mixing Applications. In E.L. Paul, V.A. Atiemo-Obeng, and S.M. Kresta. *Handbook of Industrial Mixing: Science and Practice*, Wiley and Sons, 19-88.

Kumar, S. and D. Ramkrishna (1997). On the solution of population balance equations by discretization - III. Nucleation, growth and aggregation of particles. *Chem. Eng. Sci. Vol. 52(24)*, 4659-4679.

Lyons, E.J. (1967). Suspension of Solids. In V.W. Uhl and J.B. Gray (Eds.). *Mixing: Theory and Practice. Vol. II*, Academic Press, San Diego, 225-261.

Marshall, E.M. and A. Bakker (2004). Computational Fluid Mixing. In E.L. Paul, V.A. Atiemo-Obeng, and S.M. Kresta (Eds). *Handbook of Industrial Mixing: Science and Practice*, Wiley and Sons, 257-343.

Mazzarotta, B. (1992). Abrasion and Breakage Phenomena in Agitated Crystal Suspensions. *Chem. Eng. Sci. Vol. 47(12)*, 3105-3111.

Mazzarotta, B., Di Cave, S., and G. Bonifazi (1996). Influence of Time on Crystal Attrition in a Stirred Vessel. *AIChE J. Vol. 42 (12)*, 3354-3558.

McCabe, W.L., Smith, J.C., and P. Harriet (2001). *Unit Operations of Chemical Engineering*, McGraw-Hill, New York.

McDonough, R.J. (1992). *Mixing for the Process Industries*, Van Nostrand Reinhold, New York.

Mersmann, A. (2001). *Crystallization Technology Handbook 2nd Ed*., Marcel Dekker, Inc., New York.

Mesbah, A., Kramer, H.J.M., Huesman, A.E.M., and P.M.J. Van den Hof (2009). A control oriented study on the numerical solution of the population balance equation for crystallization processes. *Chem. Eng. Sci. Vol. 64*, 4262-4277.

Mullin, J. W. (2001). *Crystallization 4th Ed*., Butterworth-Heinemann, Boston.

Myerson, A.S. (1999). Crystallization Basics. In A.S. Myerson (Ed.), *Molecular Modeling Applications in Crystallization*, Cambridge University Press, Cambridge, 55-105.

Myerson, A.S. (2002). *Handbook of Industrial Technology 2nd Ed*., Butterworth Heinemann, Boston.

Nienow, A. W., and R. Conti (1978). Particle abrasion at high solids concentration in stirred vessels. *Chem. Eng. Sci. Vol. 33*, 1077-1086.

Offermann, H. and J. Ulrich (1982). On the Mechanical Attrition of Crystals. In S.J. Jancic and E.J. de Jong (Eds.). *Industrial Crystallization 81*, North-Holland, New York, 313-314.

Ramkrishna, D. (2000). *Population Balances: Theory and Applications to Particulate Systems in Engineering*, Academic Press, San Diego.

Randolph, A.D., and M.A. Larson (1962). Transient and Steady State Size Distributions in Continuous Mixed Suspension Crystallizers, *AIChE J. Vol. 8(5)*, 639-645.

Rhodes, M. (2008). *Introduction to Particle Technology, 2nd Ed.*, Wiley & Sons, London.

Shamlou, P.A., Jones, A. G., and K. Djamarani (1990). Hydrodynamics of Secondary Nucleation in Suspension Crystallization. *Chem. Eng. Sci. Vol. 45(5)*, 1405-1416.

Snow, R.H., Allen, T., Ennis, B.J., and J.D. Lister (1997). Size Reduction and Size Enlargement. In Perry, R.H. and D.W. Green. *Perry's Chemical Engineers' Handbook 7th Ed.*, McGraw-Hill, New York, 20.1-20.89.

Svarovsky, L. (2000). *Solid-Liquid Separation 4th Ed.*, Butterworth Heinemann, Oxford.

Synowiec, P., Jones, A.G., and P. Ayazi Shamlou (1993). Crystal Break-Up in Dilute Turbently Agitated Suspensions. *Chem. Eng. Sci. Vol. 48(20)*, 3485-3495.

Wadell, H. (1934). Some New Sedimentation Formulas. *Physics Vol. 5(10)*, 281-291.

Uhl, V.W. and J.B. Gray (1966). Introduction. In V.W. Uhl and J.B. Gray (Eds.) *Mixing: Theory and Practice Vol. I.*, Academic Press, Orlando, 1-5.

Zhang, A. and M. Ghadiri (2002). Impact attrition of particulate solids. Part 2: Experimental work. *Chem. Eng. Sci. Vol. 57*, 3671-3686.

Zwietering, T. N. (1958). Suspending Solid Particles in Liquids by Agitators. *Chem. Eng. Sci. Vol.8*, 244-253.

CHAPTER III

RESEARCH OBJECTIVES

The objective of this work is to quantitatively model the breakage that occurs in a stirred vessel using discretized population balance equations. The first step is to determine the effect of aging using an aqueous saturated solution versus a nonsolvent for breakage experiments. This is essential to determining if other mechanisms have a significant effect on breakage results from saturated solution experiments. Secondly, it will be determined if fragmentation, attrition, or both types of breakage occur as a result of suspending particles in an agitated vessel. Next, particles of various crystalline materials will be investigated to determine if PSD breakage characteristics remain constant for particles having differences in crystal geometries. Lastly, particle size distributions will be modeled using populations balance equations.

CHAPTER IV

BREAKAGE CHARACTERIZATION OF NACL CRYSTALS SUSPENDED IN A STIRRED VESSEL

4.1 Introduction

The study of solid particulates is needed to provide fundamental information for the design of manufacturing processes and equipment. One important design parameter is the particle size distribution (PSD). Both the initial size and shape of a particle can influence the PSD, especially in agitated or stirred vessels. When particles are suspended in an agitated vessel, collisions are possible. Collision causes stress to the particle (Shamlou, 1990) which results in fractures that ultimately cause the particle to break. Particle breakage changes the PSD of solid particles in stirred vessels such as crystallizers where uniform product PSD is required (Mullin, 2001). However, it is highly unlikely that two crystals of the same material, identical in external shape and size are produced of a given substance (Mullin, 2001). Because differences in size and shape exist, the analysis of single crystal breakage is not sufficient for particle breakage research. Instead, sets of particles should be investigated from particle breakage experiments.

To reduce the effect of breakage, such as attrition and fragmentation, crystallization must be performed in a controlled environment. To determine the desired control parameters, research is needed to determine the effect of operating conditions on

particle breakage. Some researchers state that attrition occurs in stirred vessels but not fragmentation (Bravi, 2003; Nienow, 1978).

One study of particle breakage related the attrition resistance of crystals to their mechanical properties (Bravi, 2003). Other authors have studied the influence of certain operating conditions on particle breakage including the agitation time (Bravi, 2003; Conti, 1980; Nienow, 1978; Mazzarotta ,1992; Mazzarotta 1996). One particular study investigated the residence time effect on sugar crystals suspended in a stirred vessel (Mazzarotta, 1996). However, a complete analysis of operating conditions based on experiments on a single material is not available although the work is needed (Mazzarotta, 1992; Chianese, 1993); thus providing motivation for this research.

One concern in breakage experiments is the selection of suspension fluid. Crystallization processes do not occur in a nonsolvent but in saturated solutions; however, the effect of having crystals in a saturated solution may alter the final results (Offermann, 1982). Therefore, breakage experiments should be examined in both nonsolvents and saturated solutions. Some researchers (Offermann, 1982; Mazzarotta, 1996; Bravi, 2003) preferred using nonsolvents for breakage research to avoid particle dissolution, primary nucleation, and particle growth. Other authors (Synowiec, 1993; Mazzarotta, 1992; Chianese,1993) selected the use of a saturated solution that resembled cooling or suspension crystallization conditions. Only one study (Offermann, 1982) has simultaneously examined the effects of using a nonsolvent or saturated solution in a side-by-side study. Offermann (1982) determined that more fines, or nuclei, were produced in the nonsolvent than in the saturated solution. More studies are needed to determine if this relationship remains constant under various operating conditions.

To design experiments, the mechanics of the operating system must be considered. Various types of crystal collisions occur during agitation in a stirred vessel. Two important collisions are the crystal-to-impeller and the crystal-to-crystal collisions (Shamlou, 1990). Crystal-to-impeller collisions are influenced by three main factors.

1. Residence time, *t*. This factor corresponds to the period of time the impeller has to make contact with the particles. The more time allowed for breakage increases the probability of particle contact with the impeller blades.
2. Impeller speed, N. The agitation rate influences the frequency of collisions between the impeller and the crystals. As the rate increases, the number of collisions will increase.
3. Initial particle size, d_p. Theoretically, larger particles will be subjected to the impeller more than smaller particles due to the higher surface area presented by the larger particles.

Crystal-to-crystal collisions are influenced by two primary factors.

1. Initial particle count. An increase in the number of initial particles poses a potential for an increase in the number of crystal-to-crystal collisions. One method of monitoring this change is through the manipulation of the magma density (MD) which represents the mass of the crystals per 100 mL of magma.
2. Impeller-to-crystal collisions. Due to colliding with the moving impeller, a given crystal is no longer moving with the flow of the fluid, but the crystal is traveling at a speed relative to the collision speed and angle of the

impact between the impeller and crystal. This movement can potentially alter the homogeneity of the vessel if impact occurs.

To investigate the effects of crystal-to-impeller and crystal-to-crystal collisions, experiments are conducted for a set of initial particles sizes of NaCl crystals for different residence times, various agitation rates for different residence times, and a range of magma density values for a constant residence time and agitation rate. The goal is to quantify breakage of NaCl crystals in stirred vessels by investigating the initial (parent) particle size range and resulting broken (child) particle size range in terms of the particle size distribution, shape factors, attrition, and fragmentation. NaCl particles are used for this research because they are hard crystals (less prone to breakage), are cubic, and have been said to be more prone to attrition than fragmentation (Offermann, 1982). The focus of this chapter is to determine the significance of aging using a solvent vs. a nonsolvent as well as the effect of crystal-to-crystal and crystal-impeller collision influences on the production of particle breakage in the forms of attrition or fragmentation.

4.2 Methodology

4.2.1 Crystal Growth and Processing

NaCl crystals larger than the commercially available size (~300-600 microns) were initially sought for the breakage experiments 1) to enhance the attrition and fragmentation that occurred and 2) to compare the overall results to trends seen with smaller sizes. In theory, larger crystals will exhibit a behavior which is more adept to breakage than the ordinary, industrial produced size. Therefore, NaCl crystals were grown in the laboratory before the breakage procedure. To have the NaCl crystals form without a non-caking agent present, a commercial canning and pickling salt was used for

all experiments. A mixture of NaCl and deionized (DI) water, which was supplied from a Barnstead Nanopure Diamond Water Purifier (Thermo Fisher Scientific, Waltham, MA), was placed in a volumetric flask. The flask was placed on a hot plate to induce mixing. Agitation was caused by a 3 inch stir bar. According to literature sources, the best technique for growing NaCl crystals was the evaporation of solvent (Davey, 2000; Garside, 1985). This process was deemed appropriate because the solubility of NaCl in water is practically insensitive to temperature changes. The solution was transferred into glass dishes where the crystals were allowed to form through solvent evaporation during a time frame of 24 - 48 hours. A Whirlpool dehumidifier (Whirlpool, Benton Harbor, MI) was located adjacent to the dishes to remove any excess moisture evaporating from the dishes. The dehumidifier also eliminates the opportunity for vaporized solution to condense on the edges of the crystallization dishes causing unnecessary nucleation.

Once the crystals were fully developed, highly regular crystals were manually selected using forceps, and dried for 24 – 48 hours using a desiccator. The unbroken NaCl crystals were then sieved into Mesh 6 (3350-7500 microns) and Mesh 10 (2000-3350 microns) sieve trays using a shaker for five minutes. In addition to the larger grown crystals, smaller crystals from the commercial source were also used. For the commercial NaCl, the crystals were sieved using Mesh 30 (600-850 microns), Mesh 40 (425-600 microns), and Mesh 60 (250-425 microns) sieve trays during a five minute shaking period. The unbroken Mesh 6, Mesh 10, Mesh 30, Mesh 40, and Mesh 60 crystals were placed in separate, sealed plastic containers until needed for experimentation.

4.2.2 Aqueous Saturated Solution

Saturated solutions (SS) for breakage experiments were prepared using literature data for the solubility of NaCl in water at 20°C (Appendix A.4). A saturated solution was made by mixing a known mass of NaCl crystals into a predetermined quantity of deionized water based on solubility criteria. The solution was then heated above the saturation temperature to 50°C to ensure the complete dissolution of the NaCl crystals in the water. The density and the conductivity of the saturated solution were measured before and after experiments to check for changes in the solution concentration. Deionized water was utilized in the production of the saturated solution to minimize the presence of impurities from the normal water source. These impurities can have an unwanted effect on the morphology of the crystals and the solubility of the material in the solvent.

Conductivity testing was conducted with a Fisher Scientific Accumet® excel XL50 Dual Channel ph/Ion/Conductivity Meter. Conductivity and TDS (2 Cell Type, Cell K= 1.00/cm, Factor=0.60) measurements of the saturated solution were recorded before the experiment, after vacuum filtration, and after centrifuging. Values were recorded for select experiments for comparison. Density measurements were taken of selected experiments using an Anton Paar DMA 4500 Density Meter (Anton Paar, Ashland, VA; Repeatability, st.dev. Density, 0.00001 g/cm^3. Temp. 0.01°C). Approximately 1 mL of sample is inserted into the measuring cell of the meter. All density readings were recorded at 20°C.

4.2.3 Breakage Procedure

Breakage experiments were conducted using an assembly of a Fisher Scientific hotplate equipped with a thermocouple, a Fisher Scientific Digital Stirrer equipped with a

2 inch diameter impeller, and a stand (Thermo Fisher Scientific, Waltham, MA). The digital stirrer was attached to the pole of the stand while the hotplate was positioned on the base of the stand (see Appendix B for layout). A 1000 mL beaker, in which breakage occurred, was placed on the hotplate. A detachable strap was connected to the system to hold the beaker in place and to prevent movement from the motor vibrating.

One crystal size range, from those separated by the sieve trays, was chosen for the parent particles used in the breakage experiments. A magma density, grams of crystals per 100 mL of nonsolvent, was used for measurements. For experiments, acetonitrile (Fisher, 0.2 μm filtered HPLC grade) was the nonsolvent, and the magma density was held constant at 5g crystals/100 mL magma (denoted MD5) for all experiments except where otherwise stated. An analytical balance (Mettler Toledo PG5002-S DeltaRange, Switerland; Max 5100 g; Min. 0.5 g; e = 0.1g; d = 0.1g/0.01g or Mettler Toledo AB54-2, Switerland; Max 51g; Min. 10 mg; e = 1mg; d = 0.1mg) was used to measure 25g NaCl for suspension in 500 mL of suspension fluid. Initially, only the suspension fluid was placed in a 1 liter beaker. The beaker was placed on a hotplate where the temperature was monitored using an attached thermocouple. Once the beaker was strapped to the device stand, the 4-bladed impeller was lowered into the beaker [1.5 cm] from the bottom of the vessel. Off-the-bottom clearance calculations based on Zwietering correlation (Zwietering, 1958) are presented in Appendix C.1.2 for Mesh 40 particles. For all experiments, Parafilm M laboratory film (Pechiney Plastic Packing, Chicago, IL) was placed around the top of the beaker as close to the propeller as possible to prevent the solution from splashing out of the beaker over time.

Once the setup was complete, the temperature on the hotplate was set to a constant temperature of 20°C (room temperature 20 ± 2°C , and the stirrer speed was

selected based on the agitation rate needed for the experiment (± 5 rpm). Once the operating conditions were satisfied, the predetermined quantity of unbroken NaCl was added to the beaker and a timer started. The following sections discuss the investigations under consideration for particle breakage experimentation. Once the total allotted residence time was reached, the stirrer was immediately stopped, and the beaker was removed from the strap and transported to the filtration station.

4.2.3.1 Magma Density Investigation

An investigation of magma density will highlight particle breakage occurring from particle-to-particle and particle-to-impeller interactions in the vessel based on a common initial particle size. Since Mesh 40 NaCl crystals (425-600 μm) are more abundant from the source, this particle size range was chosen for this investigation. Five magma density values were chosen from 1-10 and are listed in Table 4.1. The corresponding total weight of crystals for each experiment and an approximate number of NaCl crystals in the vessel are also presented. The estimated number of particles was determined by measuring the weight of 600 NaCl particles (0.2 g). For each run, constant values for residence time (30 minutes) and agitation rate (1500 rpm) were utilized. Experiments were performed in acetonitrile and then repeated in aqueous saturated solution.

4.2.3.2 Agitation Rate Investigation

The influence of agitation rate was investigated in acetonitrile and in saturated solution for Mesh 40 NaCl crystals. Five agitation rates were chose for this investigation: 1000, 1250, 1500, 1750, and 2000 rpm. Each rate was examined at two residence times, 30 minutes and 60 minutes and were compared to an unbroken sample represented by

time equal to zero minutes in Table 4.2. Values for the agitation rate in terms of revolutions per second are also presented in Table 4.2. The magma density was held constant at 5g crystals/100 mL suspension fluid for each run.

Table 4.1 Experimental Plan for Magma Density Investigation

Run	Suspension Fluid	Magma Density	Grams per 500 mL suspension fluid	Approximate number of particles
1	*ACTL/SS*	1	5	15,000
2		2	10	30,000
3		5	25	75,000
4		7	35	105,000
5		10	50	150,000

4.2.3.3 Initial Particle Size Investigation

To determine breakage based on initial particle size, 3 residence times (unbroken or zero minutes, 30 minutes and 60 minutes) and five initial size ranges (Table 4.3) were chosen for analysis. Particle breakage occurred in acetonitrile at 1500 rpm for this investigation. Sieve diameters ranged from 250 μm to 3.35 mm. To avoid confusion, size ranges will be represented by the sieve diameter of the capture tray of each range. For example, Mesh 40 represents the particles captured on the 425 μm sieve diameter tray. For these experiments, Mesh 6 and 10 crystals were grown in the laboratory as described in Section 4.2 while Mesh 30, 40, and 60 crystals were sieved directly from the commercial source. Multiple residence times were used to determine the evolution of particle size and shape with respect to time.

Particle suspension is an important aspect of particle breakage in stirred vessels. Zwietering's correlation provides a vital equation in determining what agitation rate is needed to ensure no particle remains in contact with the bottom of the vessel for longer than 1-2 seconds so that each crystal is subject to the impeller blades (Zwietering, 1958; Allen, 1997; McCabe, 2001).

Table 4.2 Experimental Plan for Agitation Rate Investigation

Experiment	**Suspension Fluid**	**Rate, rpm**	**Rate, rps**	**Time, min**
1	***Acetonitrile/ Saturated Solution***	1000	16.67	0 30 60
2		1250	20.83	0 30 60
3		1500	25.00	0 30 60
4		1750	29.17	0 30 60
5		2000	33.33	0 30 60

NOTE: rpm is revolutions per minute and rps is revolutions per second

Table 4.3 Experimental Plan for Initial Particle Size

Run	Mesh #	Sieve Diameter (microns)	time (min)
1	***6***	3350	0
2			30
3			60
4	***10***	2000	0
5			30
6			60
7	***30***	600	0
8			30
9			60
10	***40***	425	0
11			30
12			60
13	***60***	250	0
14			30
15			60

Zwietering provided the following equation:

$$N_{js} = S\frac{v^{0.1}d_p^{0.2}\left(\frac{g*\Delta\rho}{\rho_L}\right)^{0.45}X^{0.13}}{D^{0.85}} \tag{4.1}$$

where ν is the kinematic viscosity, $\Delta\rho = \rho_s - \rho_L$ (solid density minus fluid density), ρ_L is the suspension fluid density, g is the gravitational constant, d_p is the particle diameter, X is the particle loading which equals $100 * \frac{mass\ of\ solid}{mass\ of\ liquid}$, and D is the diameter of the

impeller. The dimensionless constant S was also determined by Zwietering by graphing the ratio of the vessel diameter, T, to impeller diameter versus S based on the ratio of the clearance of the agitator from the bottom of the vessel, C, to the height of the liquid, H. Based on this research, Zwietering concluded that

$$S = (T/D)^a \tag{4.2}$$

with a = 0.82 for propeller agitators (Mullin 2001). Values for Zwitering's S parameter based on other impeller geometries are recorded in the literature (Atiemo-Obeng, 2004). For the laboratory setup (see Appendix B for equipment layout), T = 4 in. (~10.1 cm) and D = 2 in. (~5.0 cm). Table 4.4 shows the minimum stirrer speed needed to suspend the particles in the initial particle size investigation. Just-suspended agitation rates are based on an S constant of 5.2 based on the dimensionless relationships of D /T and C/T. The smallest particles, Mesh 60, require an agitation rate of at least 798 rpm (13.31 rps) to suspend the NaCl particles. The largest particles in this investigation require the stirrer speed to be at least 1342 rpm (22.36 rps). An agitation rate of 1500 rpm (25 rps) is greater than any just-suspended rate listed in Table 4.4 and is used in this investigation. A constant value for magma density, 5g/100 mL acetonitrile, was also used. In Figure 4.1, a graph of PSDs for the different initial particle size ranges is shown. In Figure 4.2, the laboratory grown Mesh 6 and 10 PSDs are shown as number fraction vs. major axis while Figure 4.3 depicts Mesh 30, 40, and 60 PSDs. Each distribution has a dominant major axis size (~60% of total particles) that is different than any other particle size range.

Table 4.4 Minimum Stirrer Speed Needed for Particle Suspension

Mesh	**d_p microns**	**d_p m**	**$d_p^{0.2}$**	**N_{js} rps**	**N_{js} rpm**
6	3350	0.00335	0.320	22.36	1342
10	2000	0.002	0.289	20.17	1210
30	600	0.0006	0.227	15.85	951
40	425	0.00043	0.212	14.79	888
60	250	0.00025	0.190	13.31	798

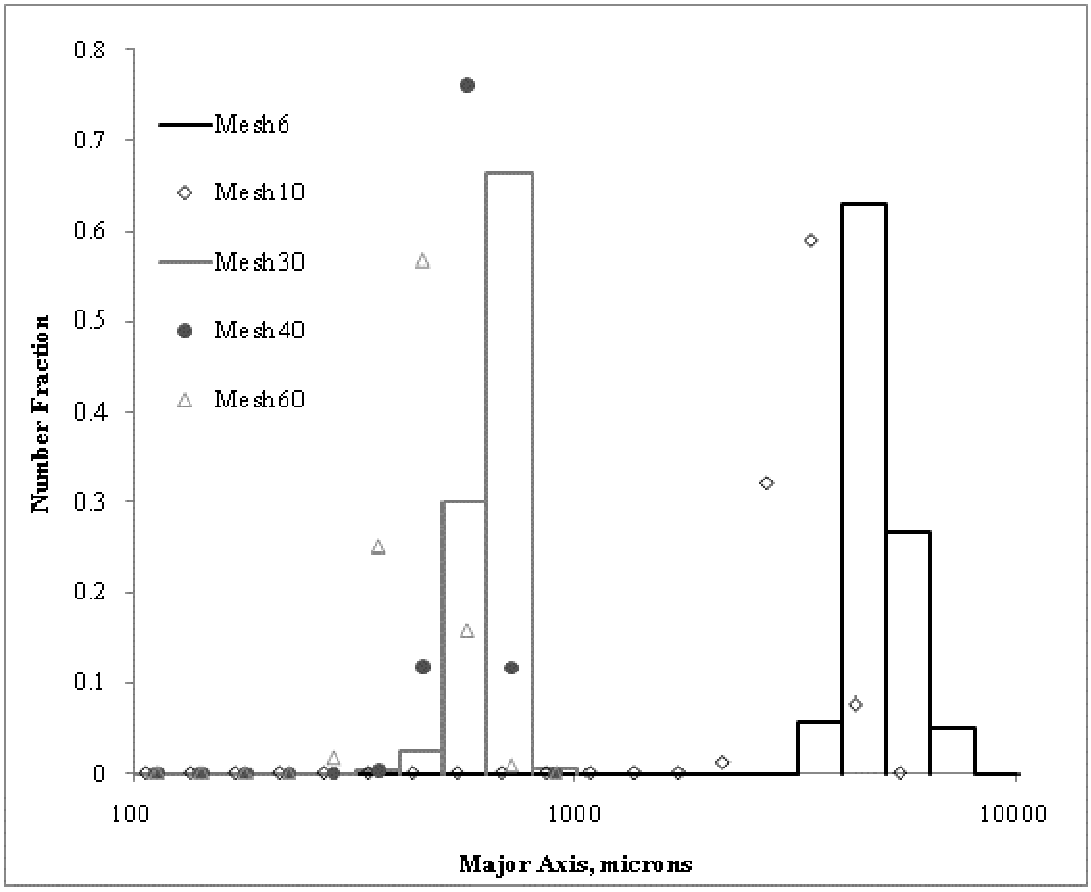

Figure 4.1 PSDs of Unbroken NaCl Crystals of Various Size Ranges

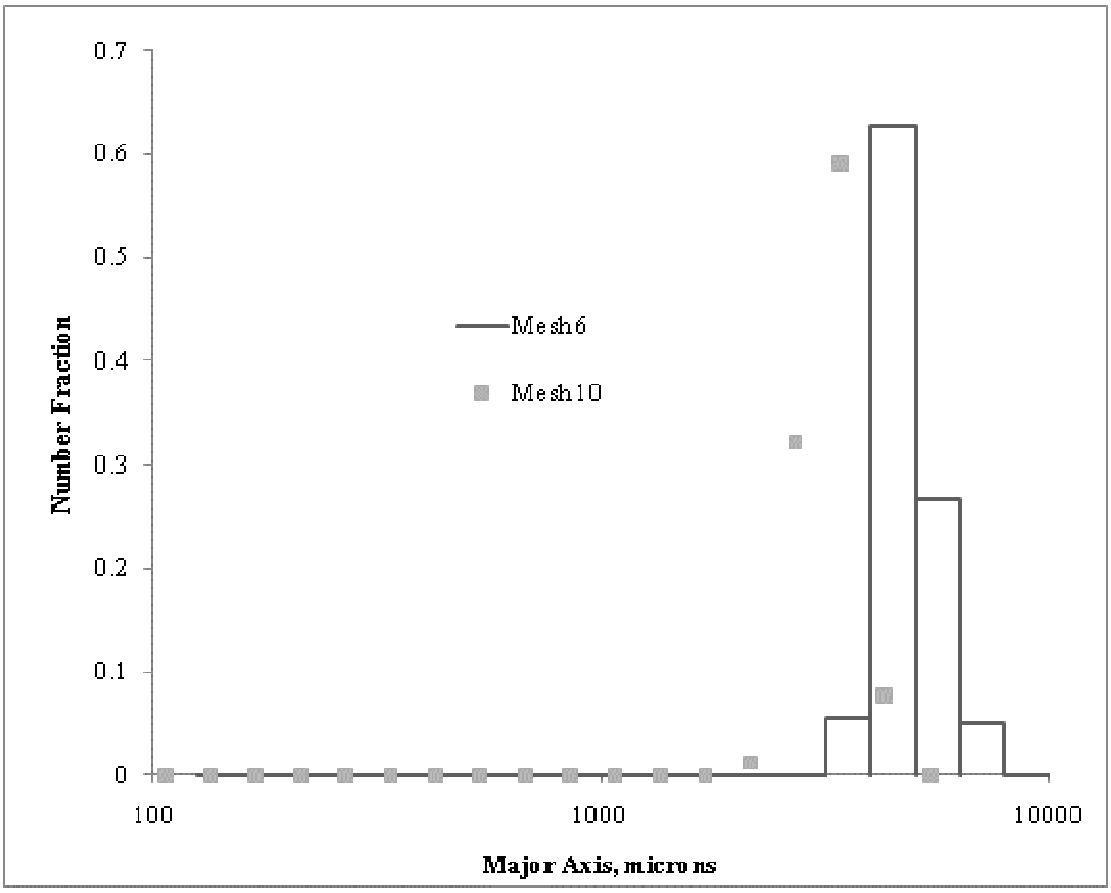

Figure 4.2 PSDs of Unbroken Laboratory Grown Mesh 6 and 10 NaCl Crystals

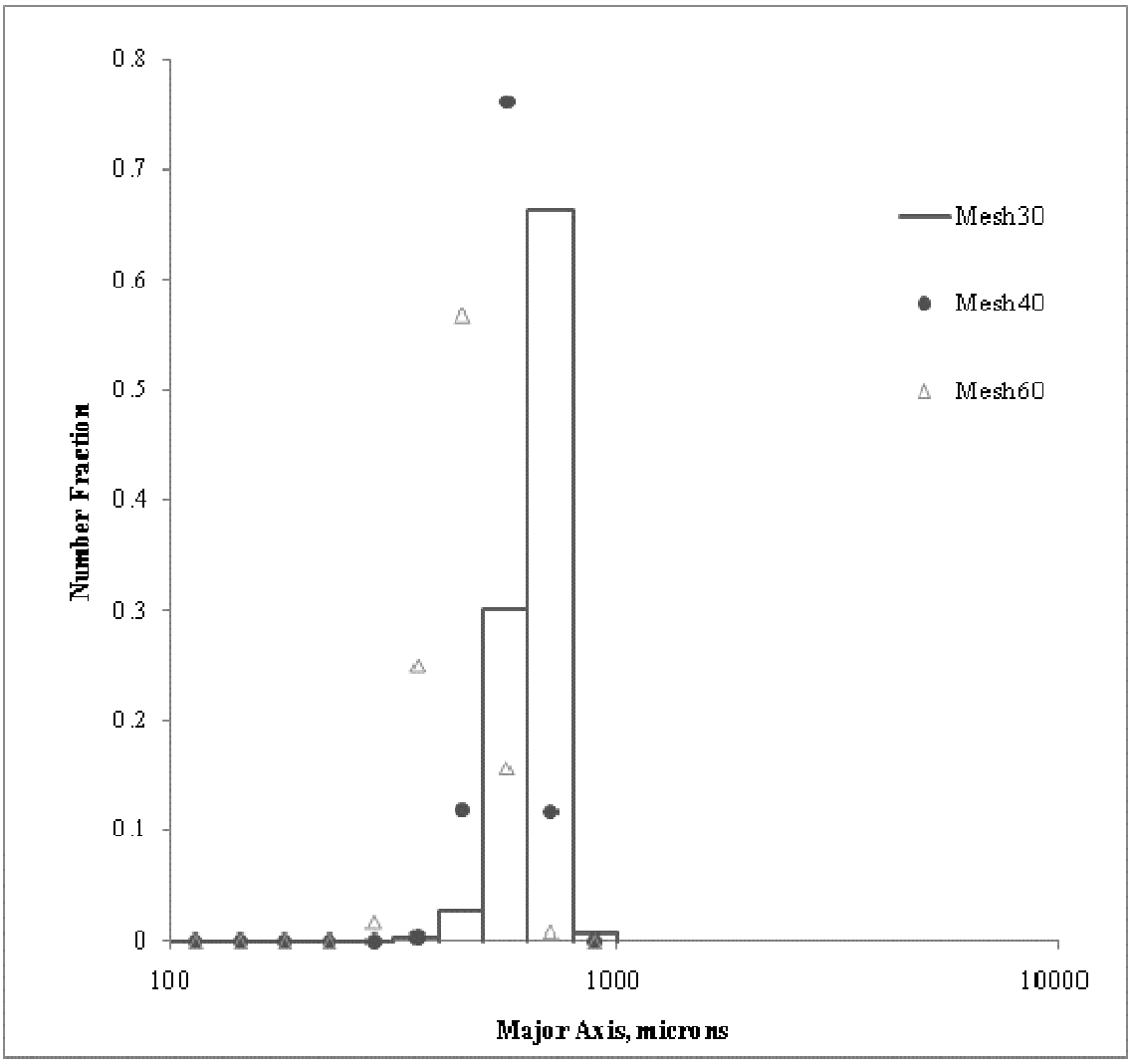

Figure 4.3 PSDs of Commercial Unbroken Mesh 30, 40, and 60 NaCl Crystals

4.2.4 Filtration and Separation Procedure

Filtration was performed immediately after stirring to prevent growth or nucleation from occurring after breakage. The resulting slurry was transferred to an awaiting flask with an attached funnel. All beaker contents were filtered using Whatman #50 filter paper (particle retention = 2.7 μm) in a Bückner funnel connected to the flask. A Dryfast® Vacuum Pump (Gardner Denver Welch Vacuum Technology, Shebogan, WI) was attached to the flask and provided vacuum filtration (absolute pressure 100

Torr.). After being subjected to vacuum pressure, the filtered particles were then transferred to a weigh boat and were placed in a desiccator for at least 10 minutes to remove any excess moisture before analysis.

For each mesh size, the broken particles were sieved using the initial particle/sieve size, a predetermined medium particle size tray, and the bottom recovery pan. Mesh 10 experiments, for example, were sieved using Meshes 10 and 30 and the bottom pan. For each experiment, the mass of parent-sized particles (retained by sieve of initial parent particle size range) was recorded as well as the mass of broken or child particles based on the weight of the particles in each size bin. The masses were converted to mass fractions for comparison. No particle size distribution based on mass recovery was conducted for this research. The resulting three particle size samples were then separated for the image analysis procedure.

The purpose of creating samples from three size ranges was to obtain a representative sample. If some form of separation, such as sieving, is not performed, an accurate representation of the sample is hindered since smaller particles tend to settle to the bottom of a sample based on void space between larger particles. Based on the weights of the 3 bins after particle breakage, corresponding mass fractions were chosen to evaluate the results. Table 4.5 gives an example of this concept. The mass fraction of the analyzed particles remained identical to the mass fraction of the unsieved broken particles. The resulting particle size distribution will be closer to the original versus choosing particles by random or choosing a constant number of particles from each bin. The mass of the particles analyzed was chosen for all experiments so that more than 600 particles were represented in each size interval according to literature specification (Allen, 1997; Cadle, 1965).

In some cases, further analysis of the SS was needed to determine if fines remained in solution after vacuum filtration. Centrifugal sedimentation was performed in a Sorvall Legend X1 Centrifuge (Thermo Scientific, Waltham, MA USA) equipped with four swinging buckets (Max speed = 5000 rpm). Centricon Plus-70 (Millipore Corporation, Billerica, MA) centrifugal filter devices were used (volume range: 15-70 mL; minimum final concentrate volume: 350 µL; diameter: 60 mm; length: 121 mm; material: polypropylene). The devices were equipped with Ultracel PL-100 kDa NMWL (nominal molecular weight limit ≈ 0.02 µm) membranes made of regenerated cellulose. The remaining solution (minus sample for density and conductivity measurements) was tested for fine particulate matter. The buckets were rotated at a speed of 4000 rpm for 5 minutes to remove the liquid from the solid. Buckets were allowed to reach the rotation speed prior to time beginning. After removing the liquid, the filter device was inverted, and the process was repeated to retrieve the solid product. Filters were measured and weight recorded prior to centrifuging.

Table 4.5 Example of Broken Particle Analysis Technique

Recovery Bin	Grams Recovered	**Mass Fraction of Recovery**	Amount Analyzed	**Mass Fraction of Analyzed Particles**
1	20	**0.80**	1.60	**0.80**
2	4	**0.16**	0.32	**0.16**
3	1	**0.04**	0.08	**0.04**

4.2.5 Analytical Procedure

Both the unbroken and broken NaCl crystals were evaluated using one of two microscope systems. The first system, a DINOlite digital microscope (ANMO Electronics, Hsinchu, China), possessed the largest field of view. Images were captured from this microscope using DINOlite Imaging Software and stored into name specific files for further analysis. The second microscope system consists of an Olympus BX51 polarizing light microscope (Olympus, Tokyo, Japan) with an Olympus Q-Color 5 camera mounted on top for image capturing. The Olympus microscope was connected to Image-Pro® Plus software (Media Cybernetics, Bethesda, MD, USA), which controlled image capturing and filing for this system. Particles larger than the field of view of the Olympus microscope were analyzed with the DINOlite microscope. Here, it is noted that both microscope systems were calibrated using a slide containing a 1 mm ruler with 0.01 mm markings and were tested routinely to check for commonality of results between the two microscopes. Both the parent particles and broken parent particles of the larger size ranges (Mesh 6 and 10) were analyzed using the DINOlite system. Smaller particles were characterized using the Olympus system - namely, the particles recovered in the bottom sieve pan.

All images were analyzed using Image Pro Plus 6.0 (Media Cybernetics, Inc., Silver Spring, MD, USA, 2006) software. Step-by-step directions are provided in Appendix D. Images were calibrated by observing a stage micrometer 1 mm in length with 0.01 mm markings with both microscope systems. Recorded measurements include the 2D projected area, aspect ratio (major axis divided by the minor axis), major axis, minor axis, perimeter, and roundness. All information was recorded and exported to a spreadsheet. Further characterization of information was conducted using an MS Excel

worksheet that sorted the data according to major axis and aspect ratio. Geometric size intervals were set based on a calculated length, L_i. For example, the initial size interval for Mesh 40 particles was from 0 - 12.5 µm with 12.5 µm equal to L_1. For every subsequent interval, the maximum length was determined by using Eq. 4.3. The equation represents the volume of the particle doubling with each increase in interval size.

$$L_{i+1} = 2^{1/3} \times L_i \tag{4.3}$$

The number fraction for each size interval was determined by dividing the number of crystals in a particular interval by the total number of crystals analyzed (see Appendix H for sample procedure). Further statistical analysis was conducted using Design Expert 8 software (Stat-Ease, Inc., Minneapolis, MN, USA, 2010) and provided information regarding the statistical significance of the degree of breakage observed.

4.3 Results

4.3.1 Technique and Reproducibility

To determine the minimum number of particles required for size analysis, particles from one sample were analyzed with progressively larger sample sizes until continuity was presented in the curve and until adding more particles did not change the distribution. Figure 4.4 presents the variation of the PSD with sample size. From the graph, analyzing over 600 particles is sufficient for this research which also represents the ideal number of particles investigated in powder technology (Davies, 1984).

Before beginning breakage experiments, a set of runs was conducted to test the reproducibility of results. For each run, 25g of NaCl was suspended in 500 mL of

acetonitrile or aqueous saturated solution (MD5) at an agitation rate of 1500 rpm. The agitation time used for this experiment was 30 minutes.

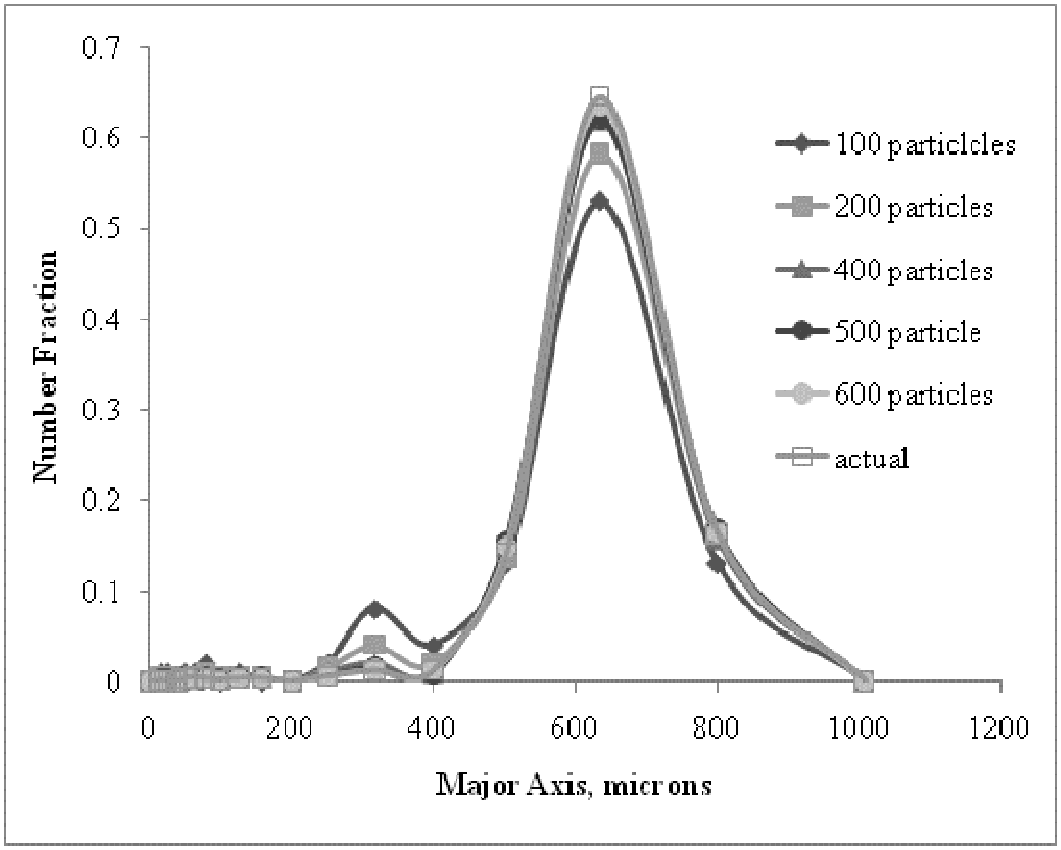

Figure 4.4 Variation of PSD with sample size

Table 4.6 shows the mass fraction of parent sized (x_p) and child (x_c) NaCl crystals. With respect to each suspension fluid, no significant difference existed in the mass fractions of each run. This finding shows good reproducibility. Results of each investigation are presented in forms of mass fractions (x_p, x_c), PSDs (number fraction vs. major axis), and shape factors of child particles in terms of average aspect ratio (major axis/minor axis), roundness, and length (major axis).

Table 4.6 Mass Fraction of NaCl Reproducibility Runs

Suspension Fluid	x_p	x_c
Acetonitrile	0.93	0.07
	0.93	0.07
	0.92	0.08
Aqueous Saturated Solution	0.96	0.04
	0.94	0.06
	0.96	0.04

4.3.2 Magma Density (MD)

Table 4.7 gives the mass fractions of the MD investigation. Increasing the MD in a saturated solution from 1- 10 produced an increase in the weight percentage of child particles from 5% to 10%. In ACTL, the weight percentage of recovered child particles increased from 13% to 24% which is more than double the fraction of child particles recovered in SS. This finding suggests that more breakage occurred in ACTL than in SS at the same agitation rate.

Figures 4.5 and 4.6 present the PSDs in ACTL and SS, respectively. Statistically, the breakage results produced in SS are significantly different than the PSD of ACTL MD breakage. Confidence intervals (CI) are presented in Appendix G. In each case, the most breakage in terms of number fraction occurred for the highest solids concentration of MD10. This finding indicates that increasing MD will also increase the effect of crystal-to-crystal and crystal-to-impeller collisions regardless of the use of a nonsolvent versus a saturated solution; however, the magnitude of the breakage and the PSD of the breakage will vary in the two suspension fluids.

Table 4.7 Mass Fractions of NaCl Agitation Investigation

Run	Suspension Fluid	Magma Density	x_p	x_c
1	***SS***	1	0.95	0.05
2		2	0.91	0.09
3		5	0.91	0.09
4		7	0.93	0.08
5		10	0.90	0.10
6	***ACTL***	1	0.88	0.13
7		2	0.85	0.15
8		5	0.75	0.25
9		7	0.82	0.18
10		10	0.76	0.24

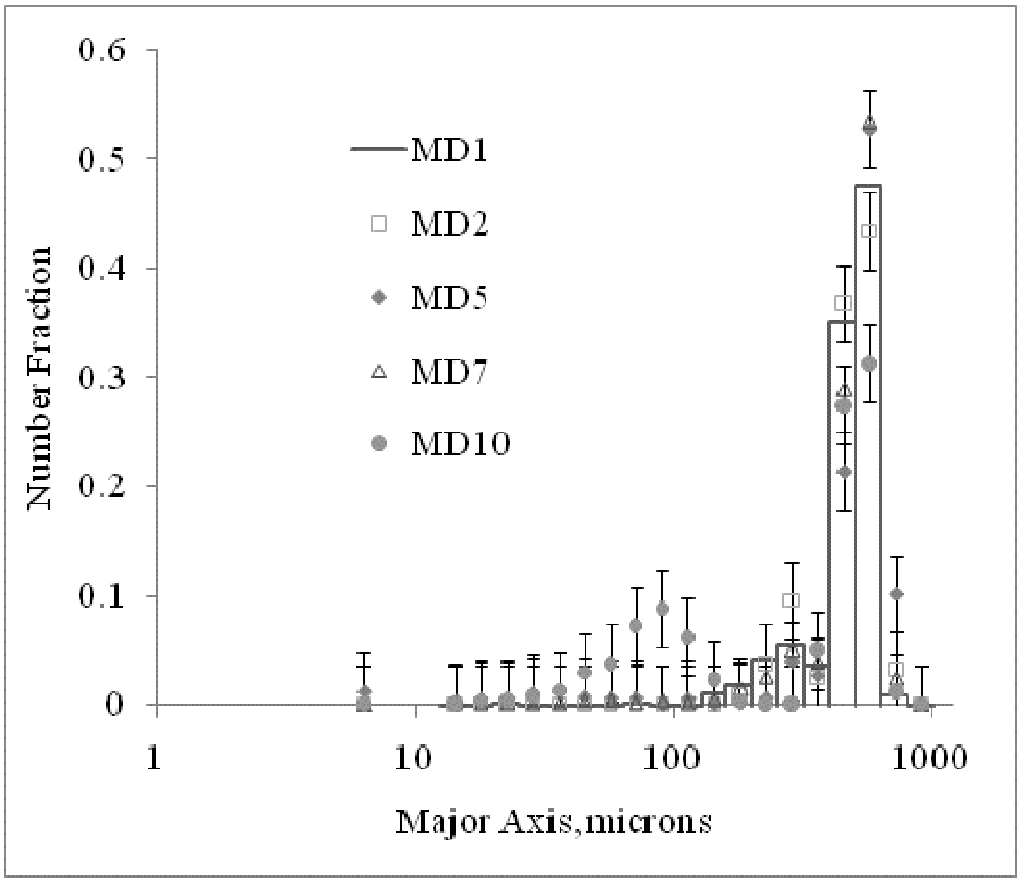

Figure 4.5 PSD of NaCl Crystal Breakage for 30 Minutes at 1500 rpm in ACTL based on Changes to the Magma Density

NOTE: Magma density is in g crystals/100 mL ACTL

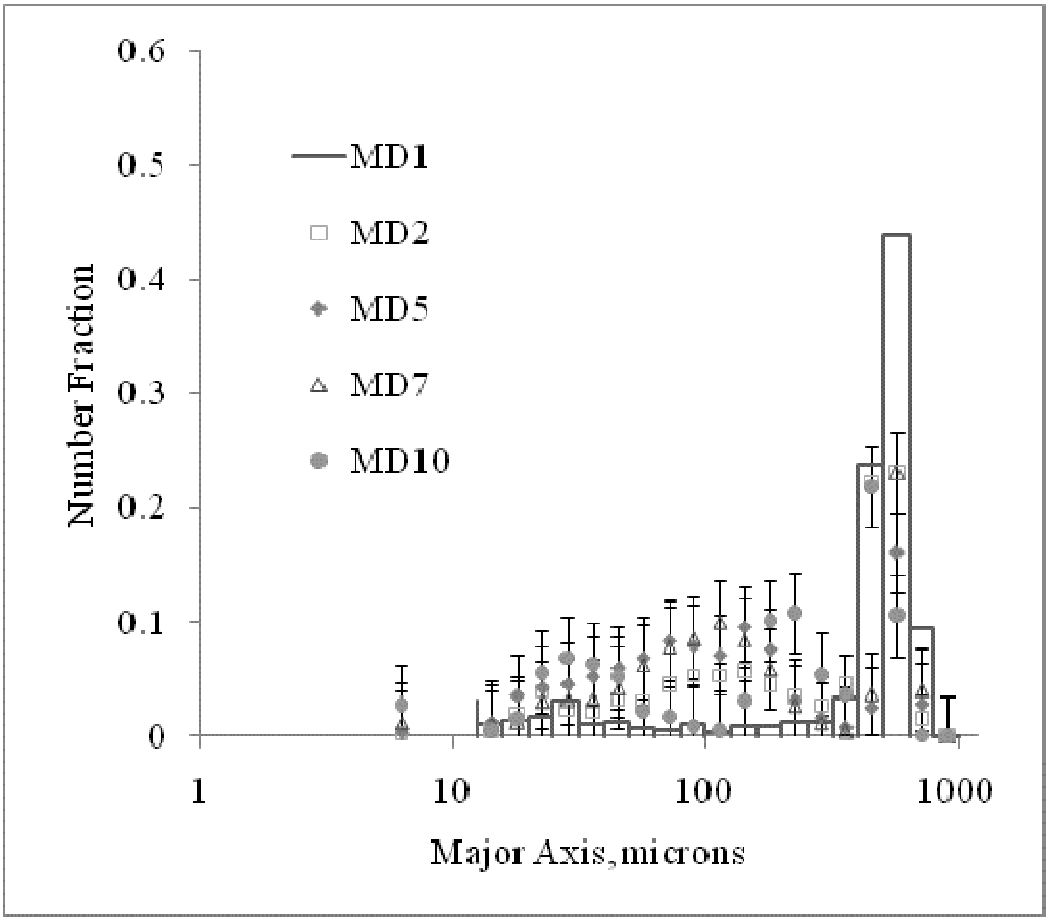

Figure 4.6 PSD of NaCl Crystal Breakage for 30 Minutes at 1500 rpm in SS Based on Change in Magma Density

Figures 4.7-4.9 depict the average shape factors of the MD investigation child particles. The curves shown in Figure 4.7-4.9 are shown to guide the eye to show trends. In terms of aspect ratio, values varied slightly in both ACTL and SS with MD10 being the only deviation. Overall, the SS child particles revealed higher aspect ratio values which indicates the child particles did not become more rounded (aspect ratio approaches 1) due to collisions. To further predict if the child particles were rounded, the average roundness value was also investigated. In Figure 4.8, the largest deviation in roundness values is seen for the SS child particles while the ACTL child particles remained around a constant value of 1.2. These values are again higher than those of a circle (roundness

equals to 1). The average major axis of the MD child particles is presented in Figure 4.9. The average size of the ACTL child particles is twice the size of the SS particles with MD10 being the deviation. Let us recall that the mass fraction of the ACTL child particles was twice as large as well as shown in Table 4.7. Since the child particles are twice as large, more mass is expected for ACTL than SS child particles.

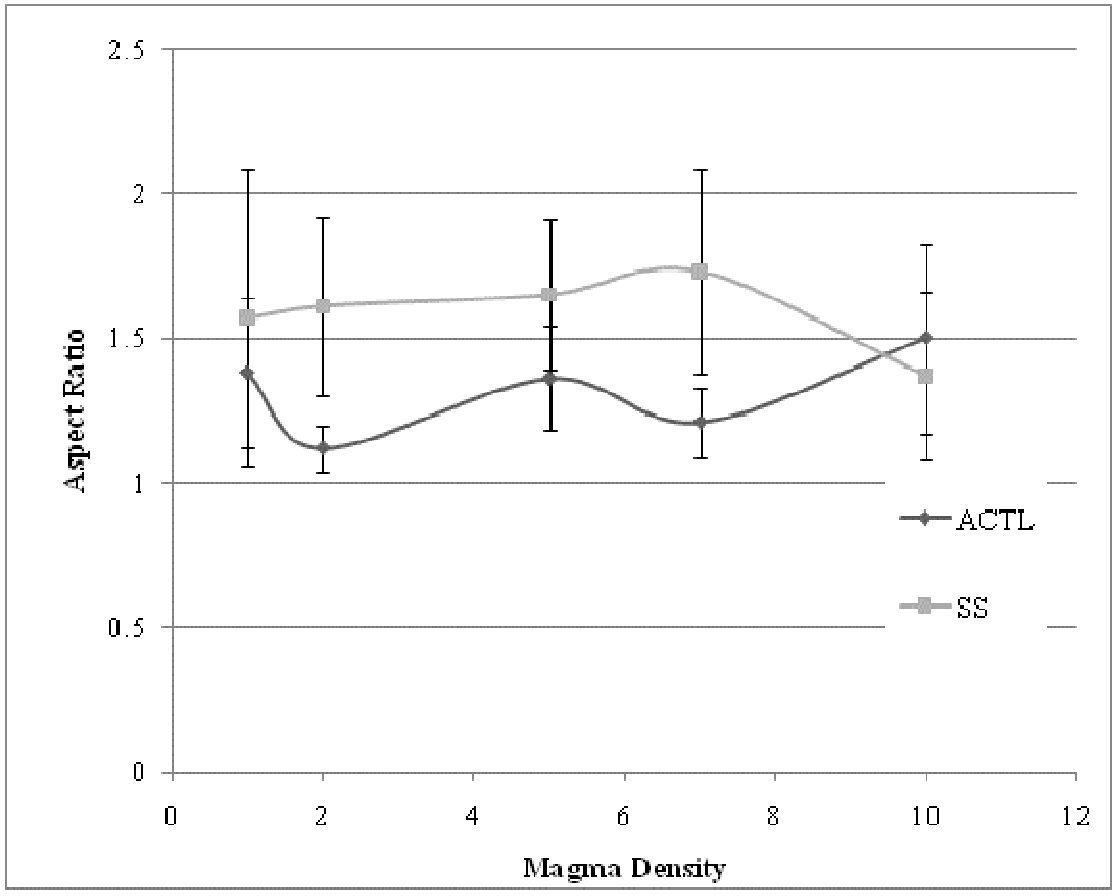

Figure 4.7 Average Aspect Ratio of NaCl Child Particles Based on Change in Magma Density

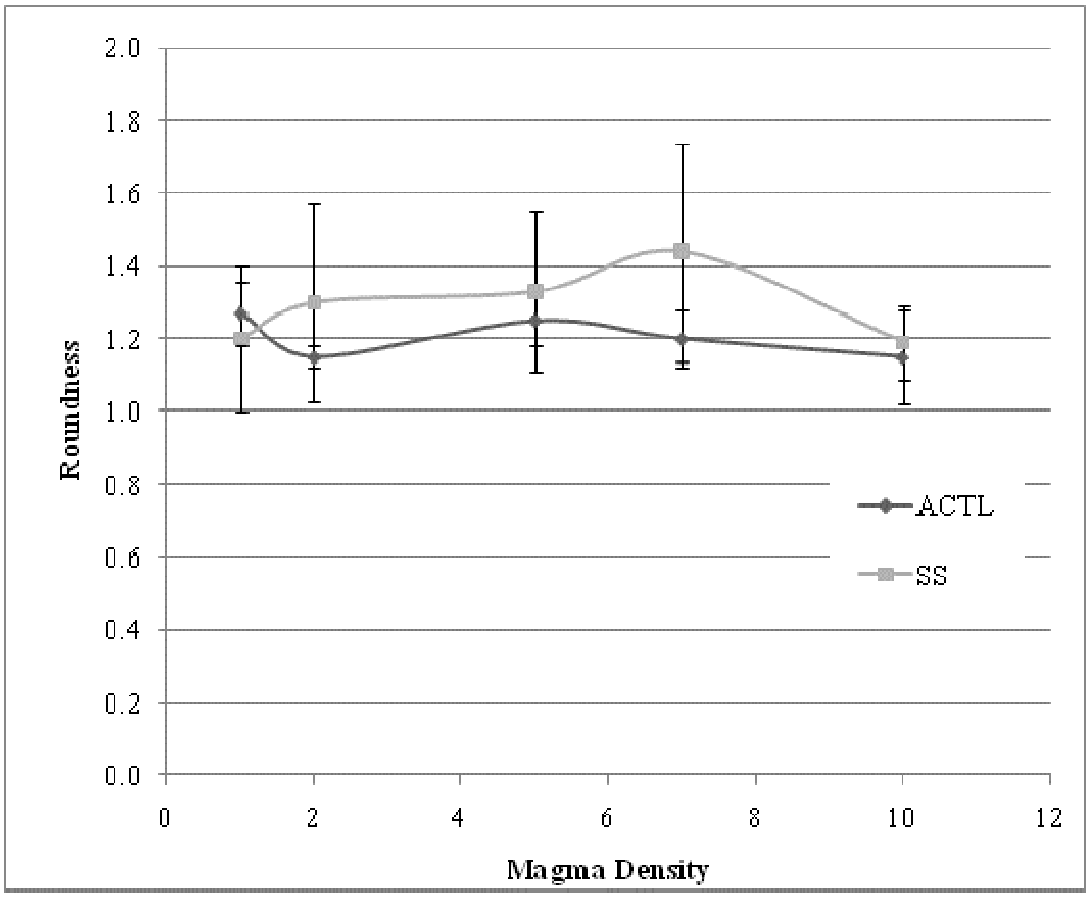

Figure 4.8 Average Roundness of NaCl Child Particles Based on Change in Magma Density

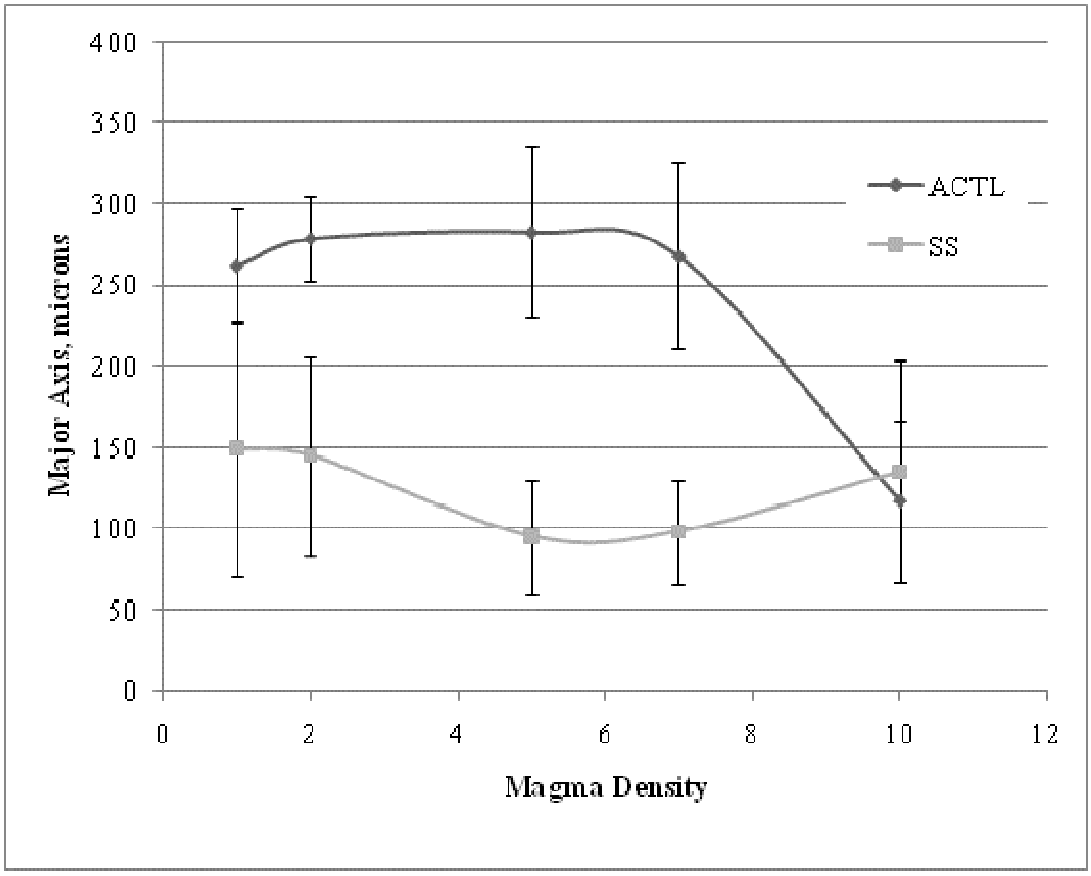

Figure 4.9 Average Major Axis of NaCl Child Particles Based on Change in Magma Density

Moreover, from the number fraction analysis, more breakage occurred in SS than in ACTL. For this reason, mass or weight analysis should not be the only analysis conducted in particle breakage experiments as was the case in previous research (Bravi, 2003). A more appropriate method has been presented in this research.

4.3.3 Agitation Rate

Table 4.8 and Table 4.9 give the mass fractions of the particles recovered during the agitation rate investigation in ACTL and SS (respectively) for 30 and 60 minutes. Comparing 30 and 60 minute runs in ACTL, no significant difference is recorded

Table 4.8 ACTL Agitation Rate Mass Fractions of NaCl Crystals

a.

Time (min)	RPM	x_p	x_c
30	1000	0.97	0.03
30	1250	0.96	0.04
30	1500	0.94	0.06
30	1750	0.94	0.06
30	2000	0.93	0.07

b.

Time (min)	RPM	x_p	x_c
60	1000	0.97	0.03
60	1250	0.93	0.07
60	1500	0.93	0.07
60	1750	0.94	0.06
60	2000	0.92	0.08

Table 4.9 SS Agitation Rate Mass Fractions of NaCl Crystals

a.

Time (min)	RPM	x_p	x_c
30	1000	0.99	0.01
30	1250	0.96	0.04
30	1500	0.95	0.05
30	1750	0.94	0.06
30	2000	0.92	0.08

b.

Time (min)	RPM	x_p	x_c
60	1000	0.996	0.004
60	1250	0.99	0.01
60	1500	0.90	0.10
60	1750	0.86	0.14
60	2000	0.84	0.16

although a slight increase in mass fraction is seen with an increase in agitation rate for each time. This indicates that most of the breakage occurred during the first 30 minutes of agitation. With the same comparison made in SS, the mass fraction of child particles recovered in Table 4.9 doubled with respect to time. This indicates that significant

breakage occurs after 30 minutes. Similar increases are also seen as the agitation rate is increased.

Figures 4.10 - 4.13 depict the agitation rate PSDs based on suspension fluid and time. Investigation of Figure 4.10 and Figure 4.11 reveals that varying the agitation rate from 1000 to 1750 rpm has no significant effect on NaCl PSDs for 30 and 60 minutes exists. The exception was for particles agitated for 60 minutes at 2000 rpm. In that particular run, several small peaks (under 0.1 fraction) are noticed for particles < 100 μm. These particles are usually attributed to attrition instead of fragmentation.

The presence of both fragmentation and attrition is also seen in the SS Agitation Rate PSDs in Figures 4.12 and 4.13; however, the child particles have a broader size distribution in SS than in ACTL. An increase in time and agitation rate individually and simultaneously produced more child particles especially in the form of attrition. This finding may also suggest that over time the fragments that initially existed were broken down and converted into the attrition size range. Between SS and ACTL, the slower rates (1000, 1250 rpm) investigated are not significantly different. However, a significant difference was found between SS and ACTL for the agitation rates greater than 1500 rpm with respect to agitation rate. This finding suggests that particle breakage in a SS will produce a PSD different than a nonsolvent.

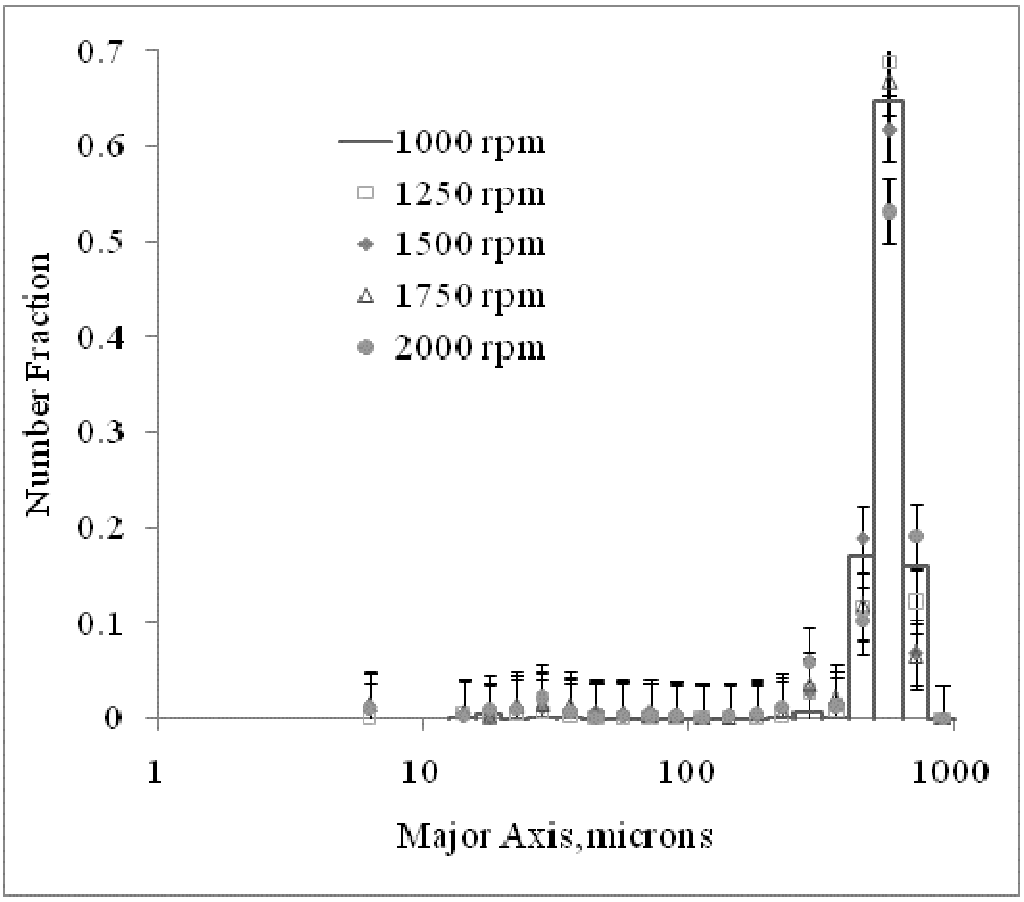

Figure 4.10 PSD of NaCl Crystal Breakage for 30 Minutes in ACTL Based on Change in Agitation Rate

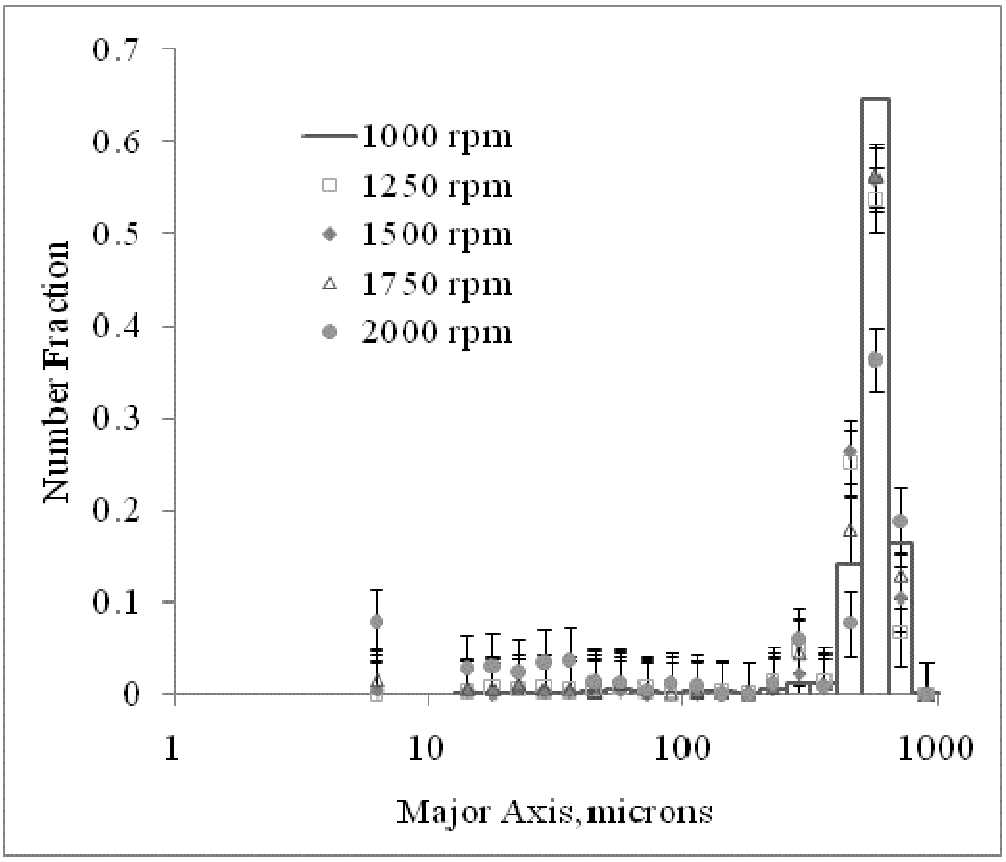

Figure 4.11 PSD of NaCl Crystal Breakage for 60 Minutes in ACTL Based on Change in Agitation Rate

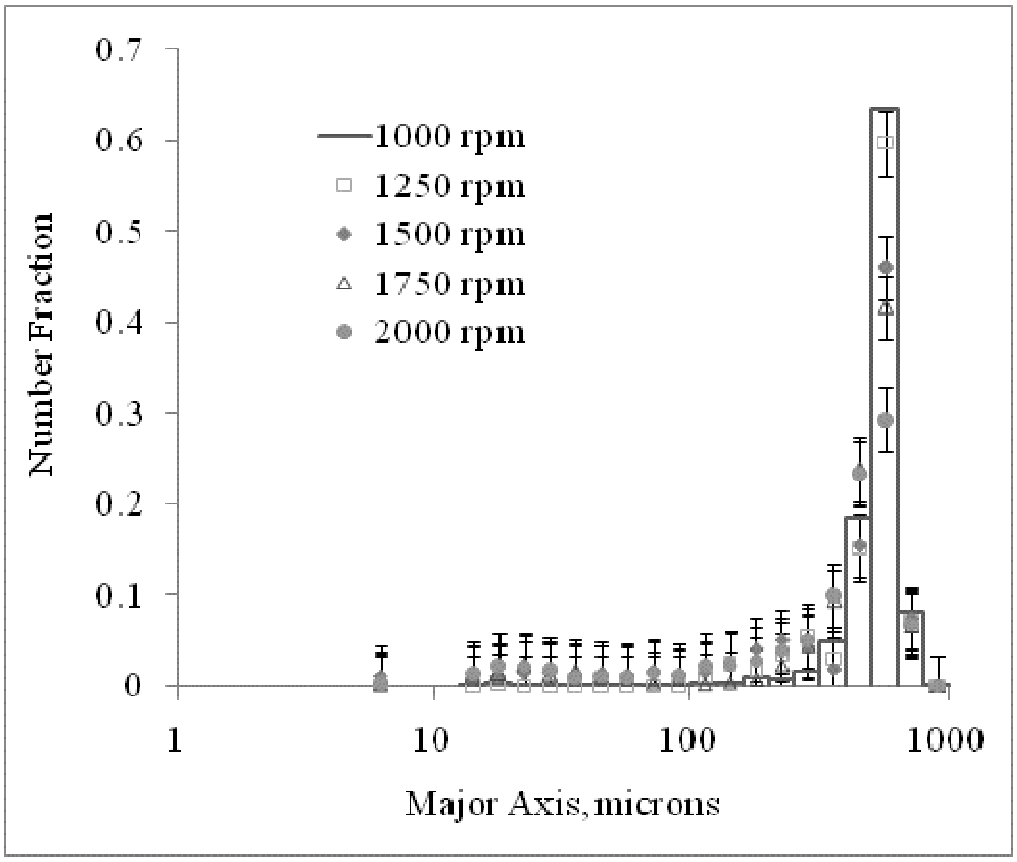

Figure 4.12 PSD of NaCl Crystal Breakage for 30 Minutes in SS Based on Change in Agitation Rate

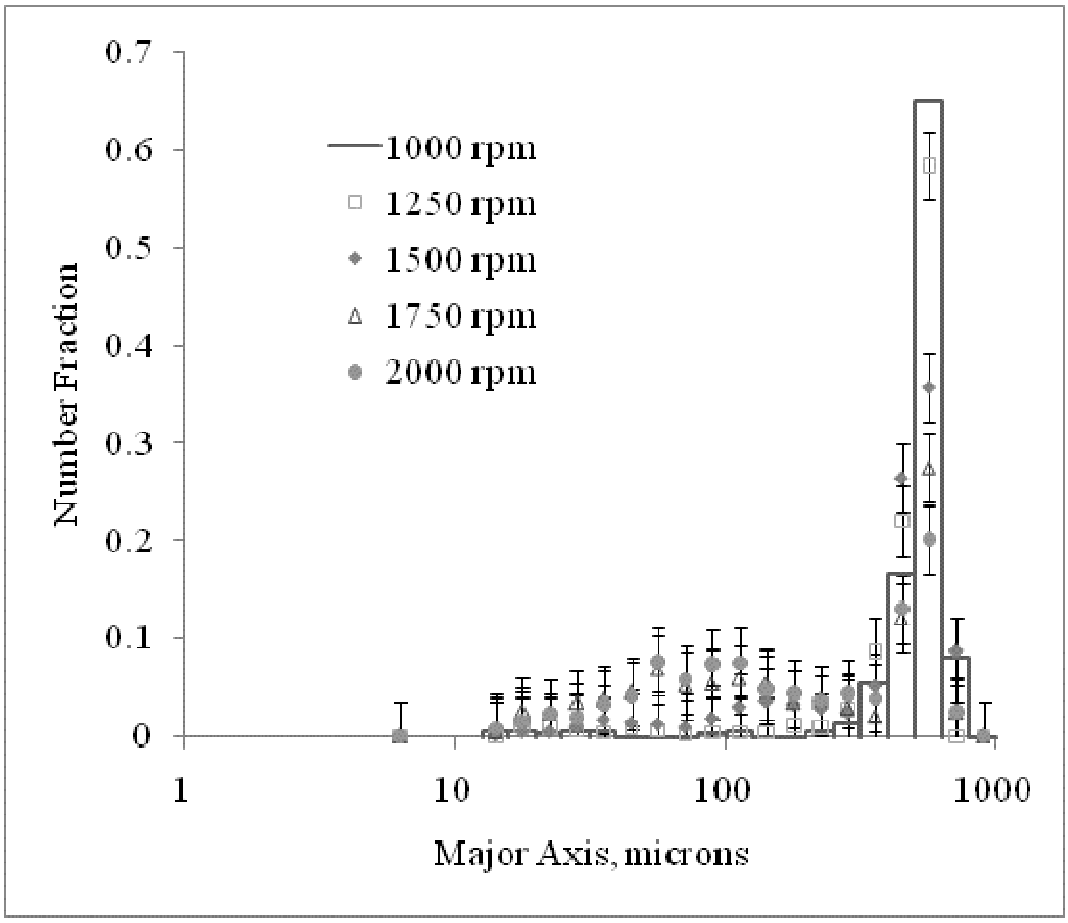

Figure 4.13 PSD of NaCl Crystal Breakage for 60 Minutes in SS Based on Change in Agitation Rate

In terms of shape factors, only a slight increase in aspect ratio with respect to agitation rate is noted with no significant differences in suspension fluid or residence time as shown in Figure 4.14. In Figure 4.15, roundness values were very similar for all experiments at 1000 rpm; however, deviation in roundness values increased as the agitation rate increased. This finding signifies that various particle shapes are produced due to particle agitation in a stirred vessel and not necessarily rounded particles. A comprehensive graph of the agitation rate effect on the child particles major axis is presented in Figure 4.16 with graphs based on time in Figures 4.17 and 4.18 and based on suspension fluid in Figures 4.19 and 4.20.

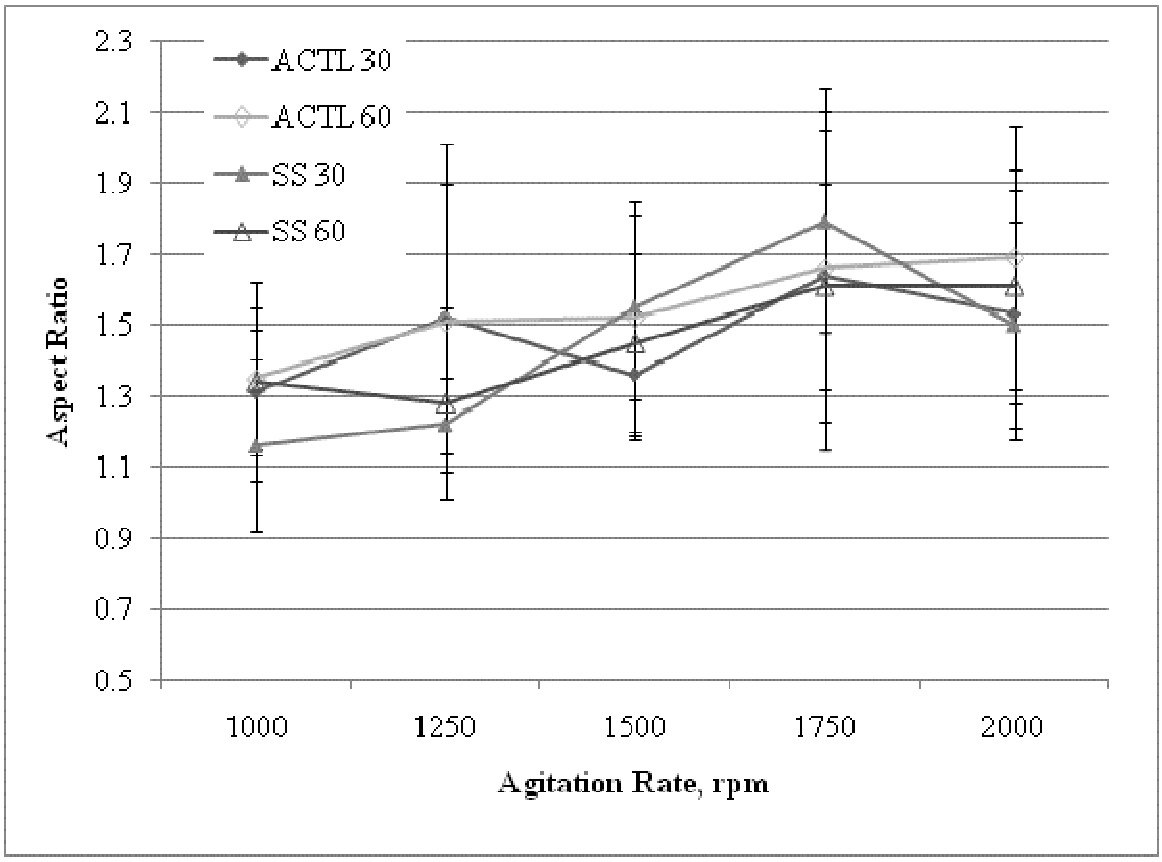

Figure 4.14 Average Aspect Ratio of NaCl Child Particles Based on Change in Agitation Rate

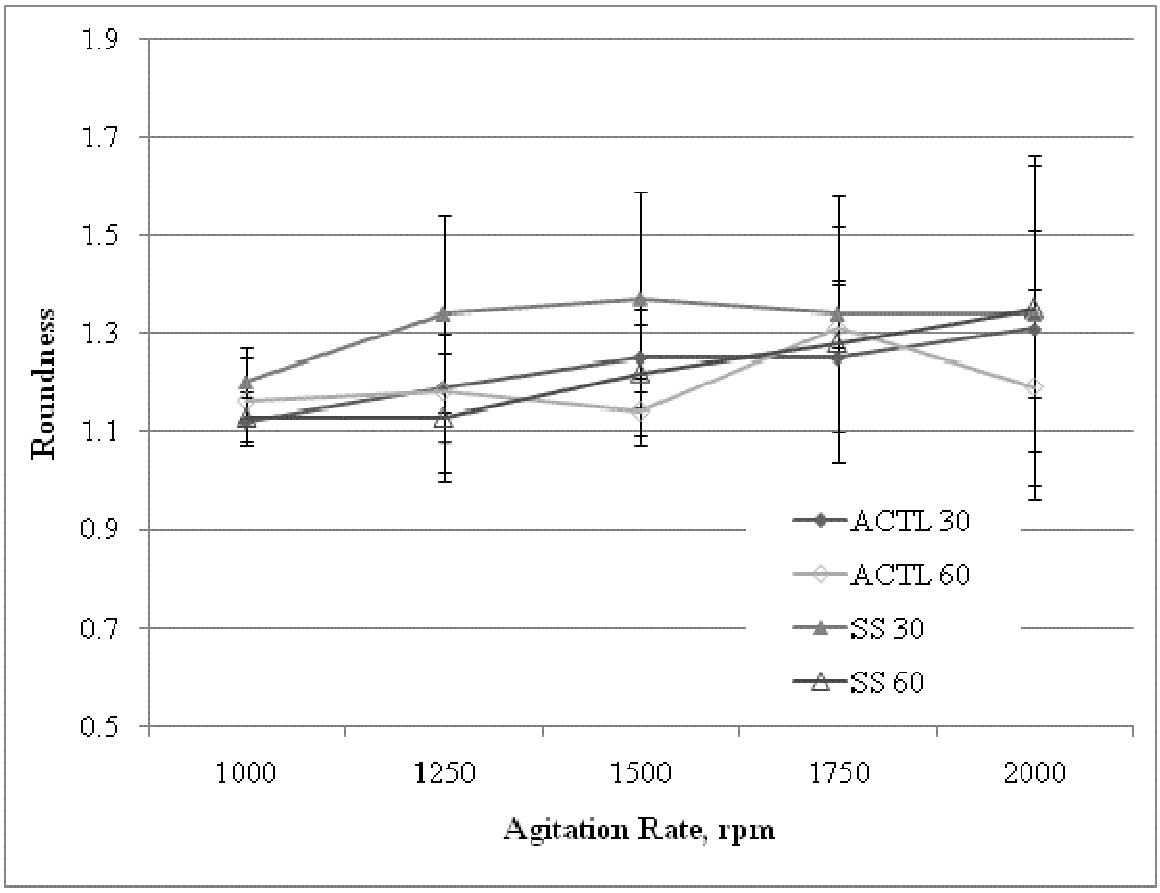

Figure 4.15 Average Roundness of NaCl Child Particles Based on Change in Agitation Rate

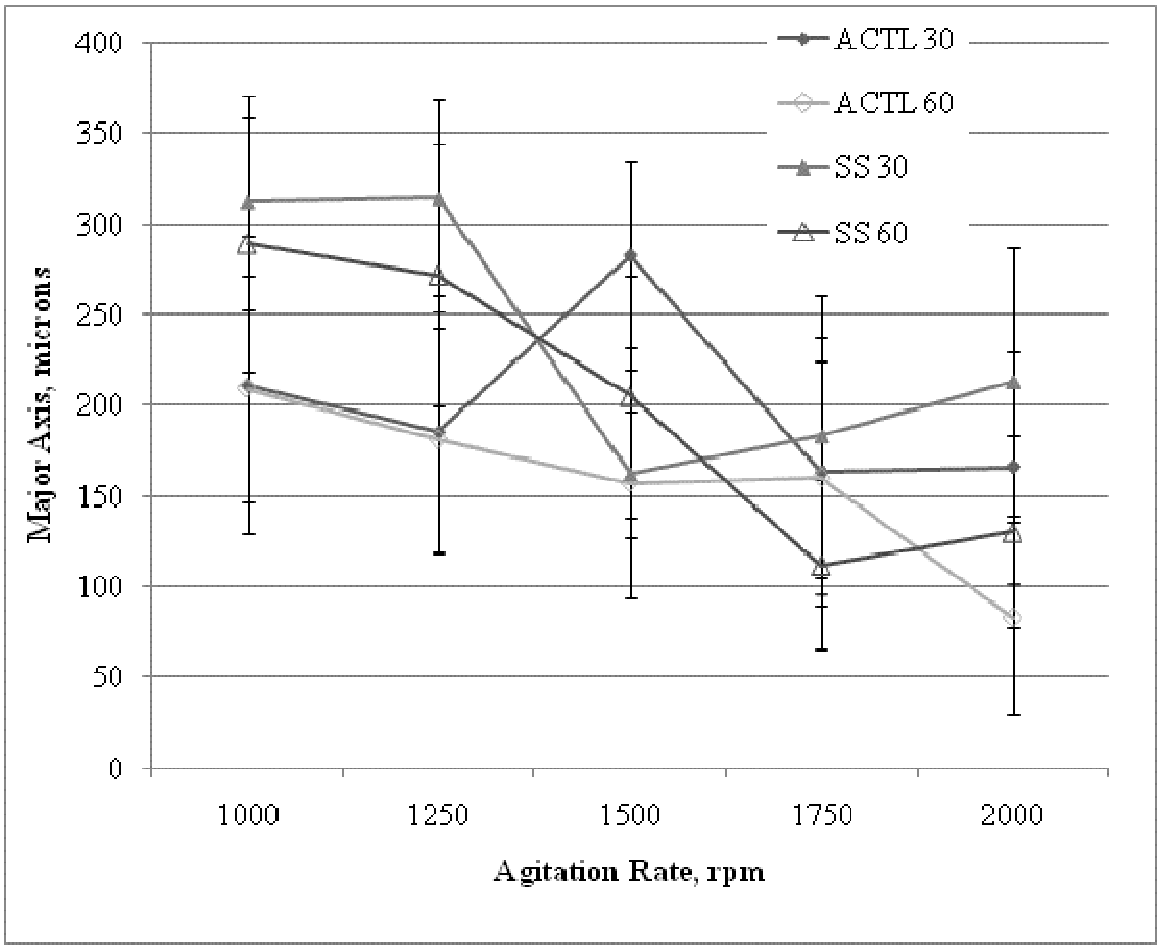

Figure 4.16 Average Major Axis of NaCl Child Particles Based on Change in Agitation Rate

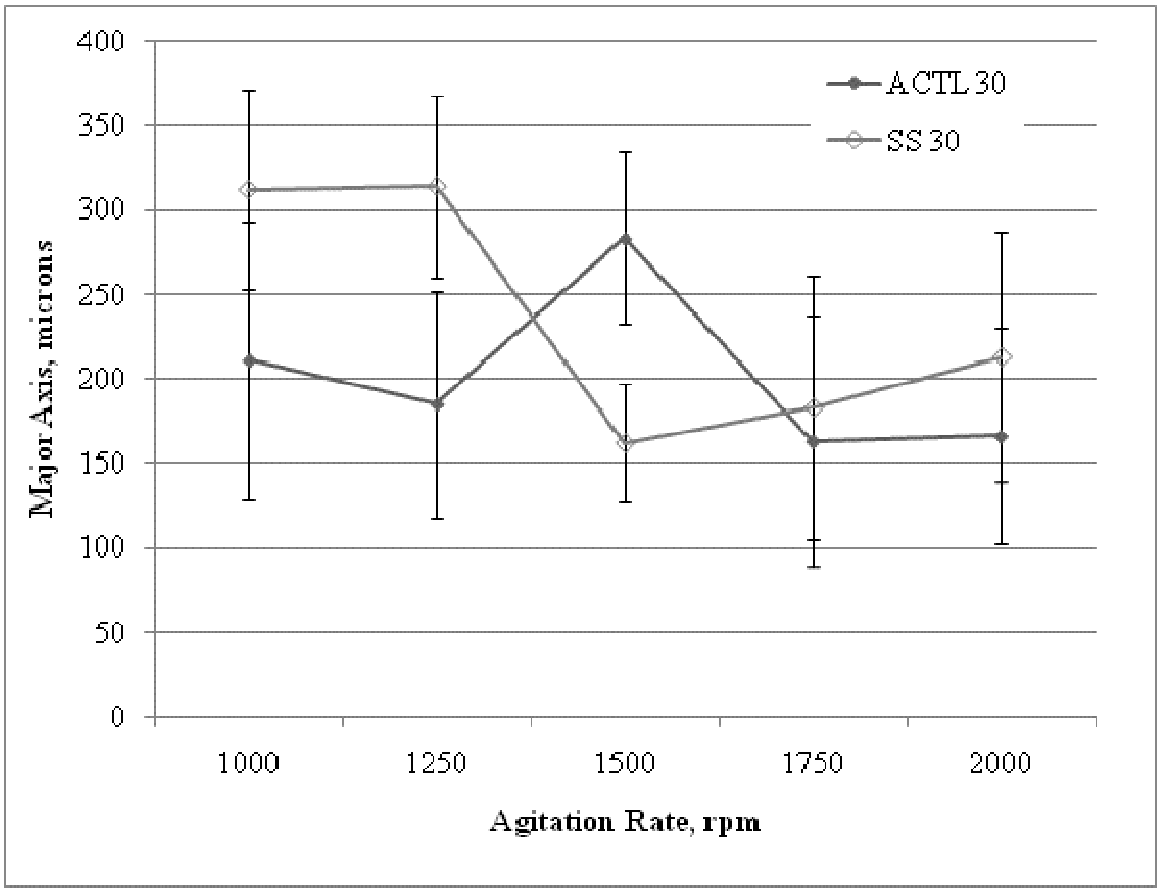

Figure 4.17 Average Major Axis of NaCl Child Particles based on Change in Agitation Rate for 30 Minutes

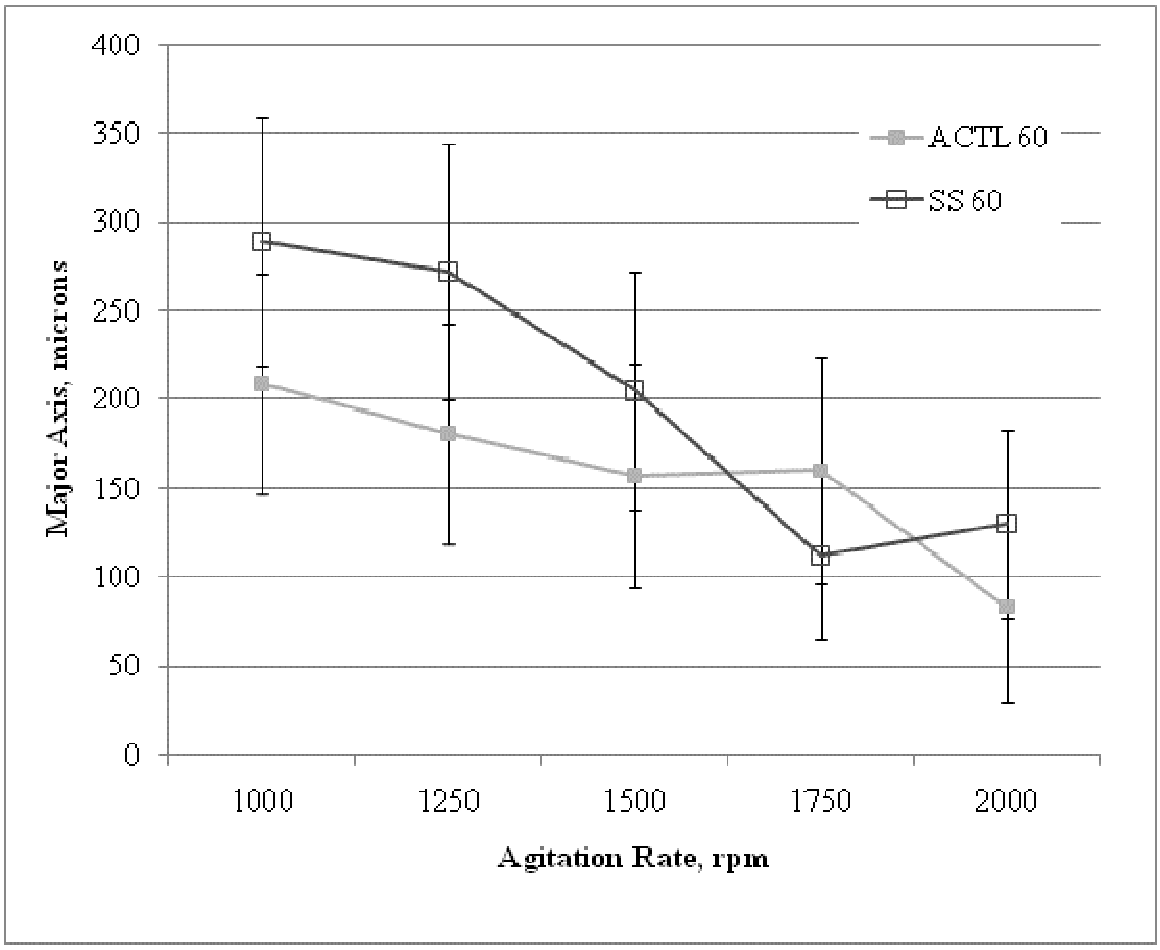

Figure 4.18 Average Major Axis of NaCl Child Particles Based on Change in Agitation Rate for 60 Minutes

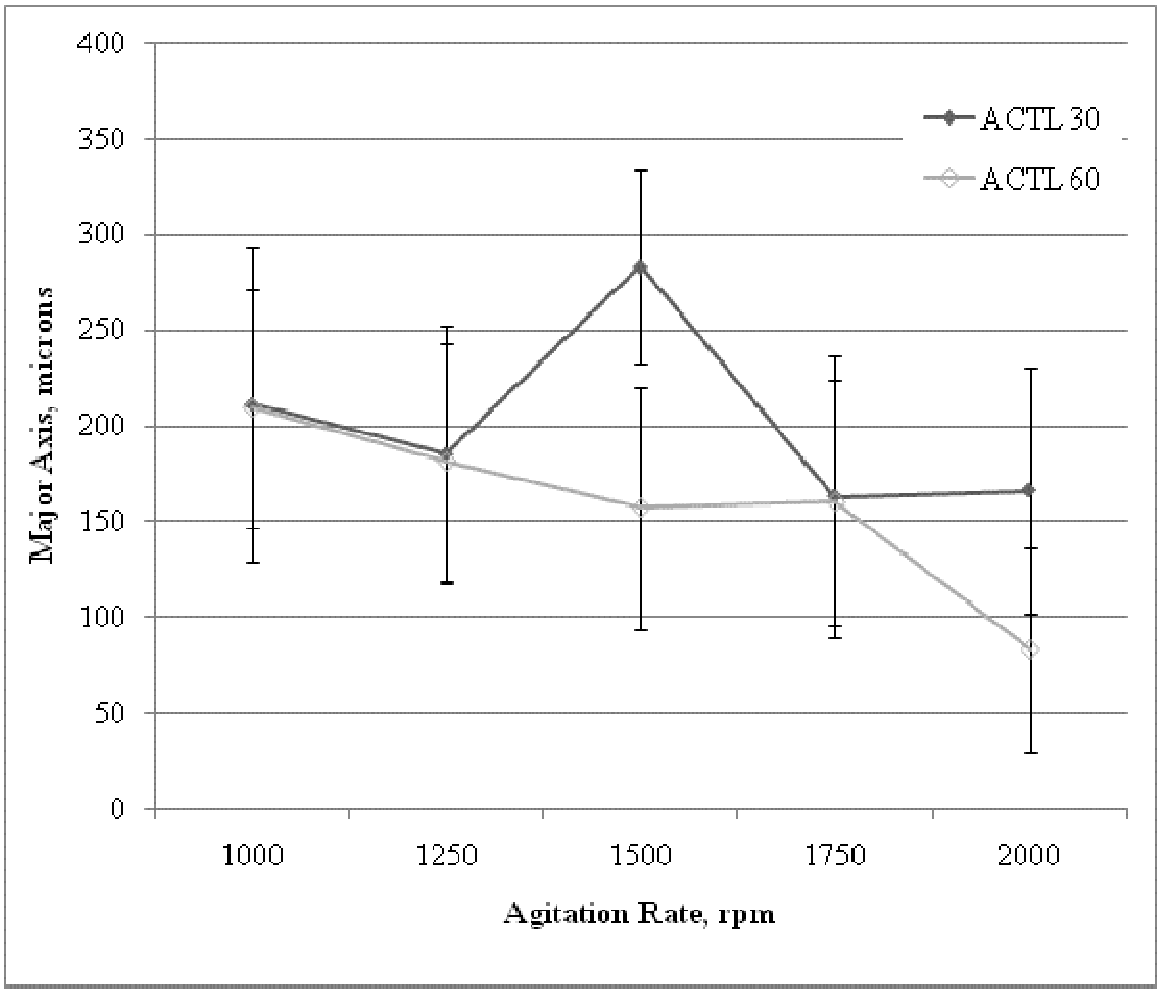

Figure 4.19 Average Major Axis of NaCl Child Particles Based on Change in Agitation Rate in ACTL

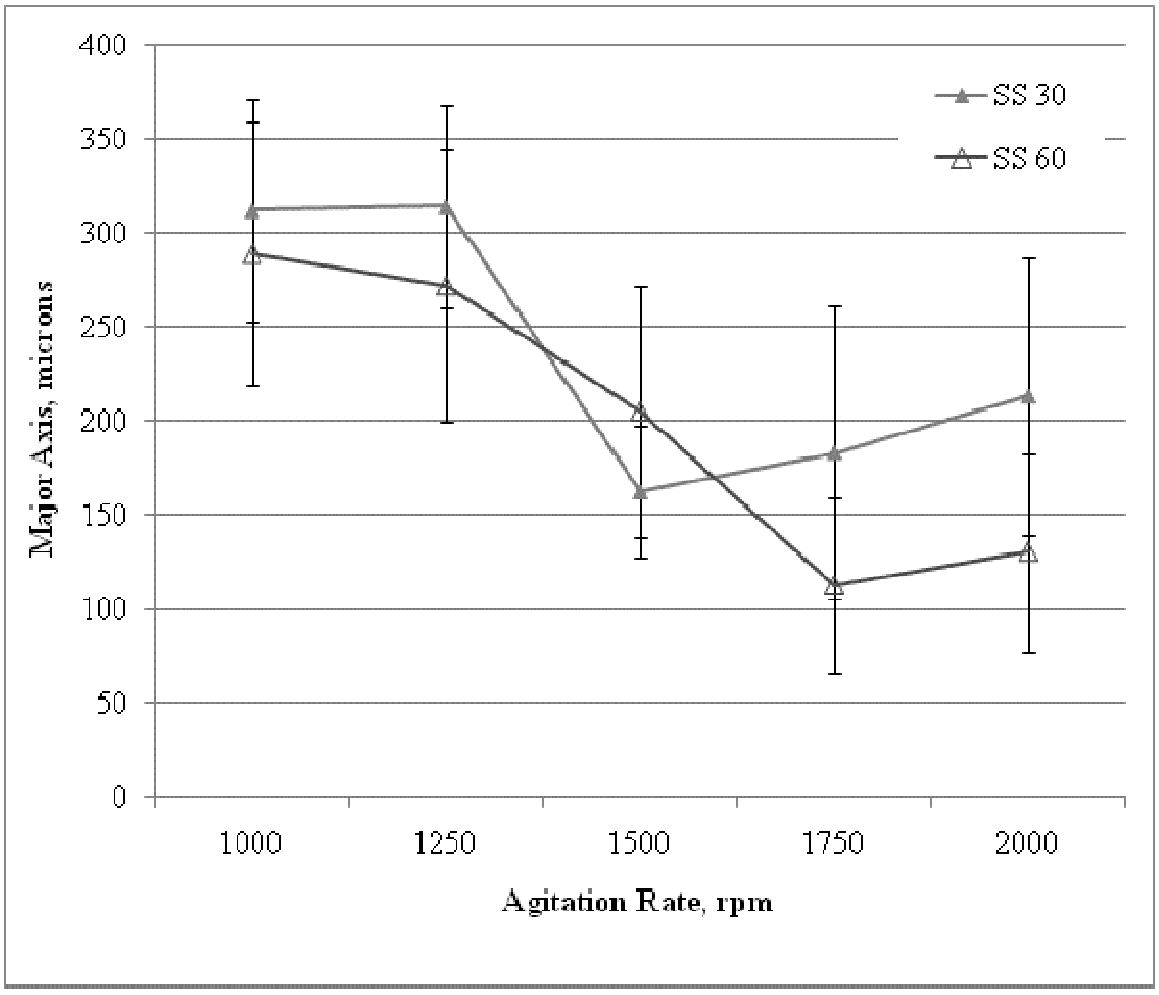

Figure 4.20 Average Major Axis of NaCl Child Particles Based on Change in Agitation Rate in SS

For the 30 minute comparison, the major axis overall decreased as expected with respect to agitation rate with 1500 rpm being the deviation in both suspension fluids. Likewise, a decrease in the size of the child particles produced was seen in the 60 minute experiment with 1750 rpm in SS as the exception. The particles in SS were slightly larger than in ACTL in both cases.

In Figure 4.19, the only difference seen in the average major axis with respect to agitation rate was seen at 1500 rpm where the particle decreased in size from ~275 microns to ~100 microns. Otherwise, similarly sized particles were produced at each time

in ACTL. For the SS runs, average particle sizes decreased after 1250 rpm, but the particles were similar for the remaining agitation rates with deviation increasing as the agitation rate increased. Findings are consistent in mass and number analysis in that no significant difference exists in ACTL for 30 and 60 minutes.

4.3.3.1 Adjusted Agitation Rates

Since the properties of acetonitrile and an aqueous NaCl saturated solution are different, it is considered that the difference seen in the PSDs are a result of the discrepancies in the material properties. To account for the properties of the liquids, the suspension correlation (Zwietering, 1958) becomes

$$N_{SS} = S\frac{v_{SS}^{0.1} d_p^{0.2}\left(\frac{g^*(\rho_{NaCl}-\rho_{SS})}{\rho_{SS}}\right)^{0.45} \chi_{SS}^{0.13}}{D^{0.85}} \tag{4.4}$$

for the saturated solution. For acetonitrile,

$$N_{ACTL} = S\frac{v_{ACTL}^{0.1} d_p^{0.2}\left(\frac{g^*(\rho_{NaCl}-\rho_{ACTL})}{\rho_{ACTL}}\right)^{0.45} \chi_{ACTL}^{0.13}}{D^{0.85}} \tag{4.5}$$

with S, d_p, g, and D representing constants in both equations. The resulting ratio between the agitation rates of NaCl particles suspended in a saturated solution to suspension in acetonitrile becomes

$$\frac{N_{SS}}{N_{ACTL}} = \frac{v_{SS}^{0.1}\left(\frac{\rho_{NaCl}-\rho_{SS}}{\rho_{SS}}\right)^{0.45} \chi_{SS}^{0.13}}{v_{ACTL}^{0.1}\left(\frac{\rho_{NaCl}-\rho_{ACTL}}{\rho_{ACTL}}\right)^{0.45} \chi_{ACTL}^{0.13}} \tag{4.6}$$

Or

$$N_{SS} = N_{ACTL}\frac{v_{SS}^{0.1}\left(\frac{\rho_{NaCl}-\rho_{SS}}{\rho_{SS}}\right)^{0.45} \chi_{SS}^{0.13}}{v_{ACTL}^{0.1}\left(\frac{\rho_{NaCl}-\rho_{ACTL}}{\rho_{ACTL}}\right)^{0.45} \chi_{ACTL}^{0.13}} \tag{4.7}$$

when solving for the adjusted saturated solution agitation rate. In the case of N_{ACTL}= 1500 rpm or 25 rps (material properties presented in Appendix A), the calculation of an equivalent agitation rate equals

$$N_{SS} = (25\ rps)\frac{\left(1.667\times10^{-6}\right)^{0.1}\left(\frac{2.165-1.20}{1.20}\right)^{0.45}(4.167)^{0.13}}{\left(4.866\times10^{-7}\right)^{0.1}\left(\frac{2.165-0.781}{0.781}\right)^{0.45}(6.353)^{0.13}} \tag{4.8}$$

$$N_{SS} = (25\ rps)\frac{(0.2644)(0.9066)(1.204)}{(0.2336)(1.294)(1.272)} \tag{4.9}$$

$$N_{SS} = (25\ rps)\frac{(0.2886)}{(0.3845)} = 25\ rps\ (0.751) \tag{4.10}$$

$$N_{SS} = \ 18.76 rps = 1{,}125\ rpm \tag{4.11}$$

Further examples of this calculation are provided in Appendix C. Table 4.10 gives the adjusted agitation rates for SS based on NaCl in acetonitrile. The equivalent of particle breakage in acetonitrile at 2000 rpm is equivalent to agitation at 1500 rpm in saturated solution. Figure 4.21 compares the PSD of these agitation rates in their

Table 4.10 Adjusted Agitation Rates of NaCl Crystals

Acetonitrile Rate, rpm	**SS Rate, rpm**
1000	750
1250	940
1500	1130
1750	1310
2000	1500

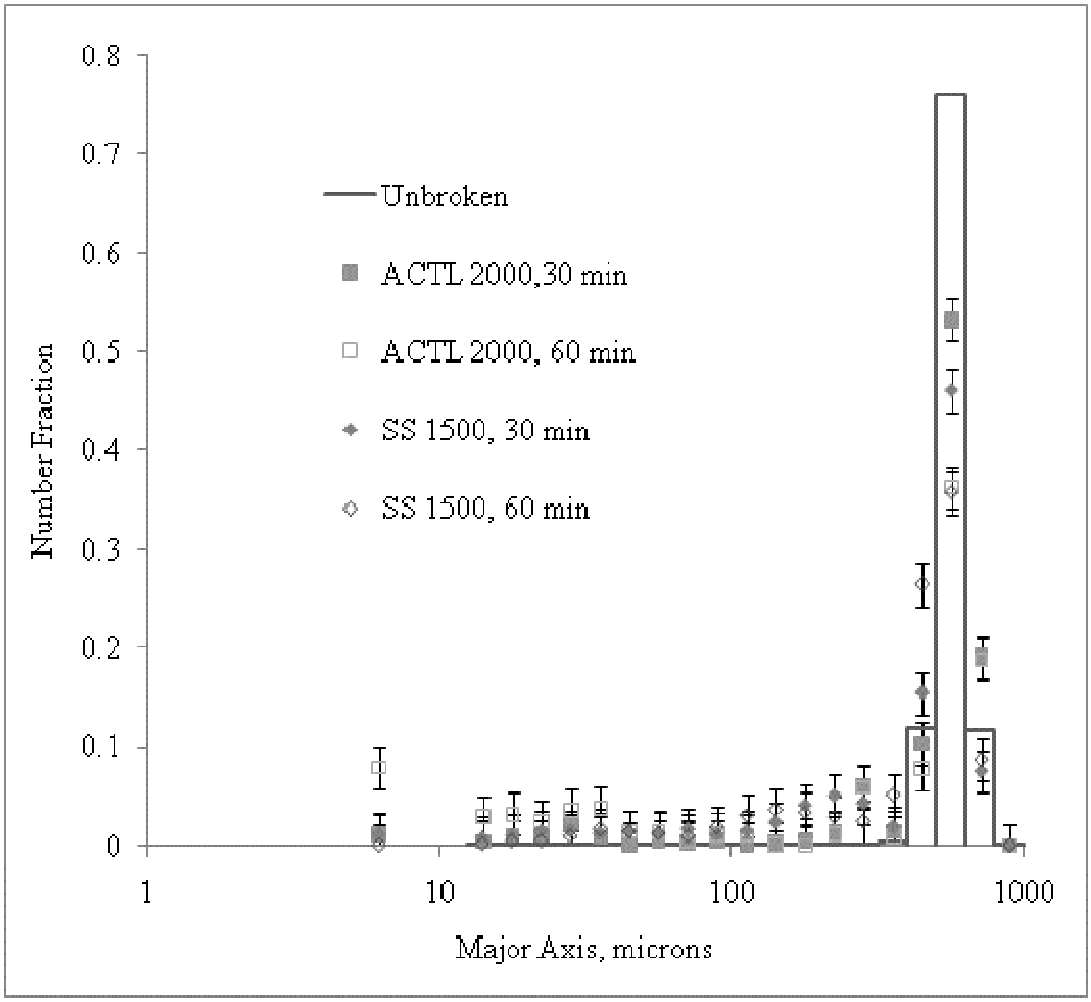

Figure 4.21 PSD of NaCl Crystal Breakage Based on Adjusted Agitation Rates of SS and ACTL for 30 and 60 Minutes

respective mother liquors based on residence time. Although the agitation rate has been adjusted based on a relationship developed by Zwietering's correlation, the PSD achieved in the nonsolvent is not equivalent to the PSD produced by breakage in aqueous saturated solution. This finding suggests that although using Zwietering's correlation as an adjustment factor accounts for some of the differences in solution properties, it is not a perfect adjustment. Furthermore, identical PSDs are not achieved in nonsolvents and solvents as suggested in the literature (Chianese, 1993). Therefore, it cannot be assumed

that breakage is the only mechanism occurring when particles are suspended in saturated solutions.

4.3.4 Initial Particle Size

4.3.4.1 Fragmentation vs. Attrition

Figure 4.22 depicts the image of an unbroken NaCl crystal, and Figure 4.23 shows an image of crystal fragments taken with the DINOlite microscope. From the image, the corners of the original salt crystals became rounded as predicted in the literature (Nienow, 1978; Briesen, 2009). However, attrition at the particle corners was not the only phenomena observed. The top of the image in Figure 4.23 shows a particle with damage as far as the center of the particle. Within the same image, fragments of various morphologies are seen, none of which are totally rounded. Since the particle in Figure 4.22 represents the largest particle size and is laboratory grown, a comparison is made with the smaller Mesh 40 sized particles in Figures 4.24 and 4.25. Once again, the corners of the particles (Figure 4.25) have been subjected to attrition at the corners with a decrease in size; however, more damage occurred for the larger particles.

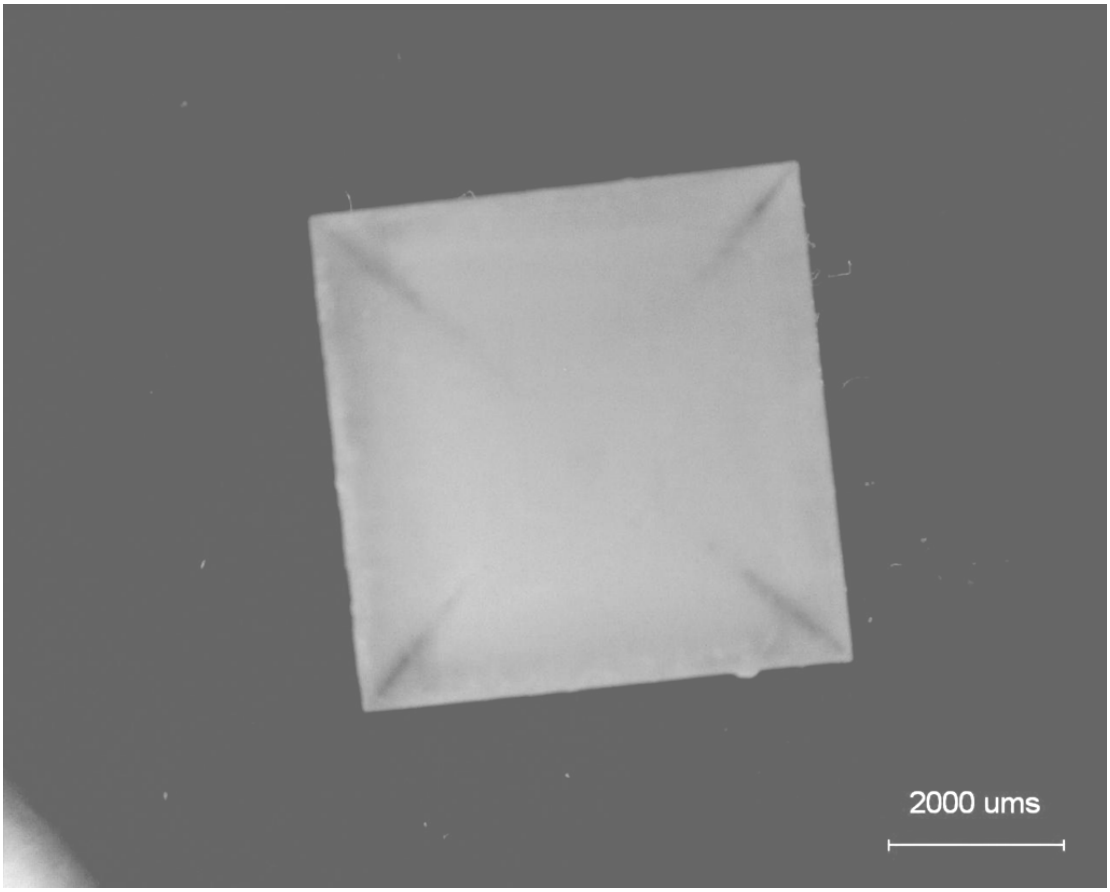

Figure 4.22 Unbroken Laboratory Grown Mesh 6 NaCl Crystal

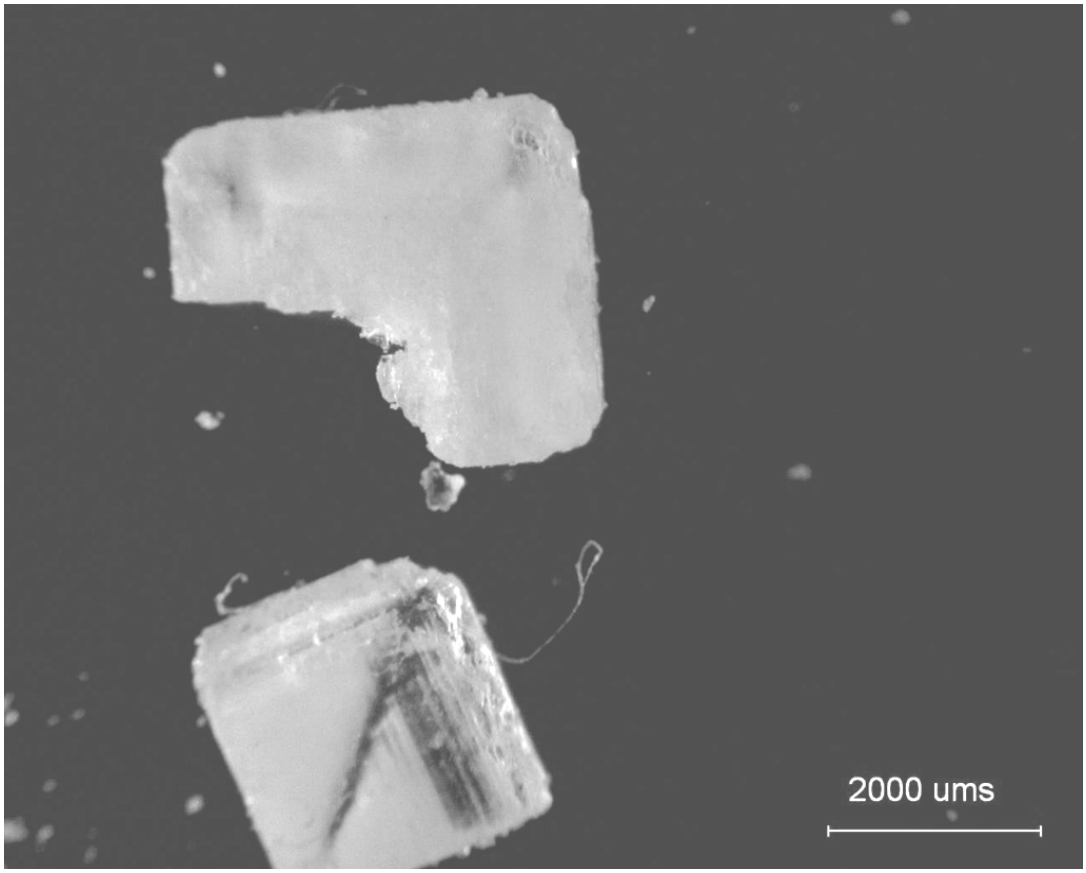

Figure 4.23 Broken Laboratory Grown Mesh 6 NaCl Crystals

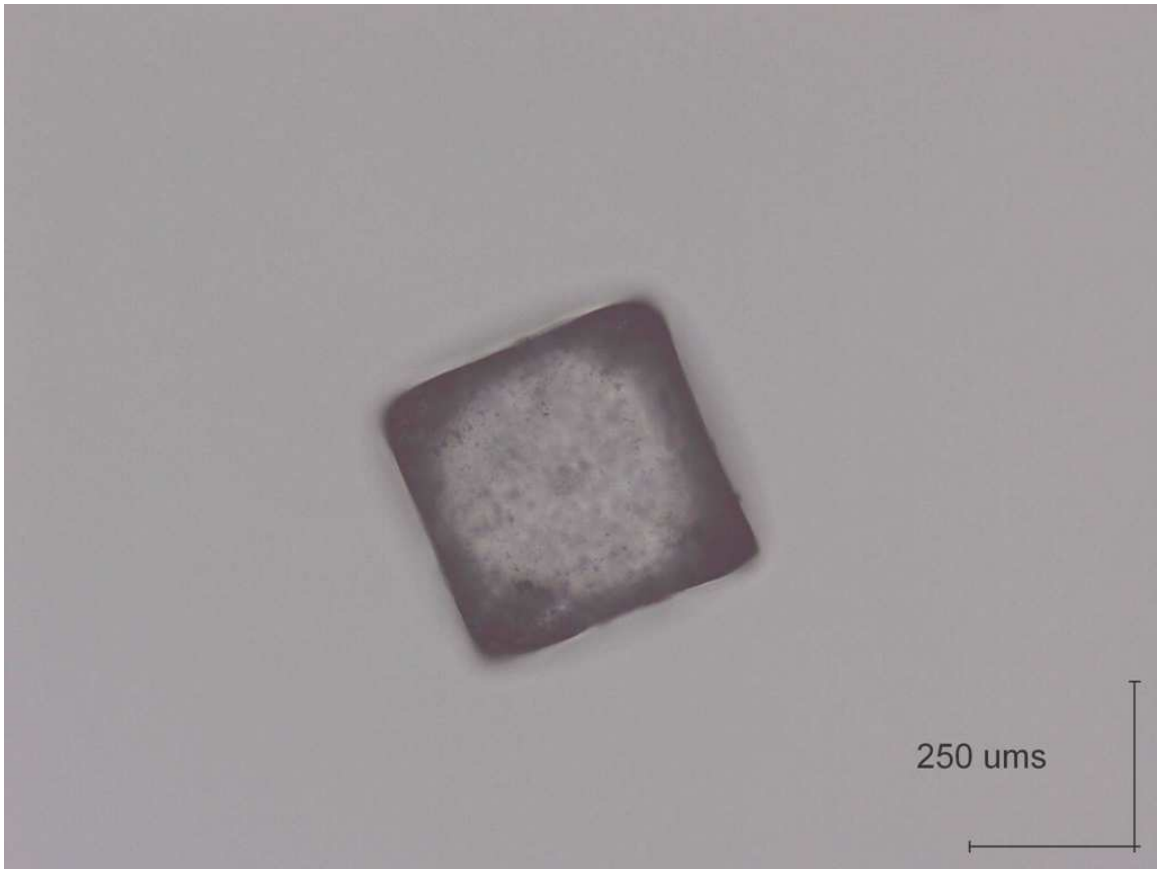

Figure 4.24 Unbroken Mesh 40 Commercial NaCl Crystal

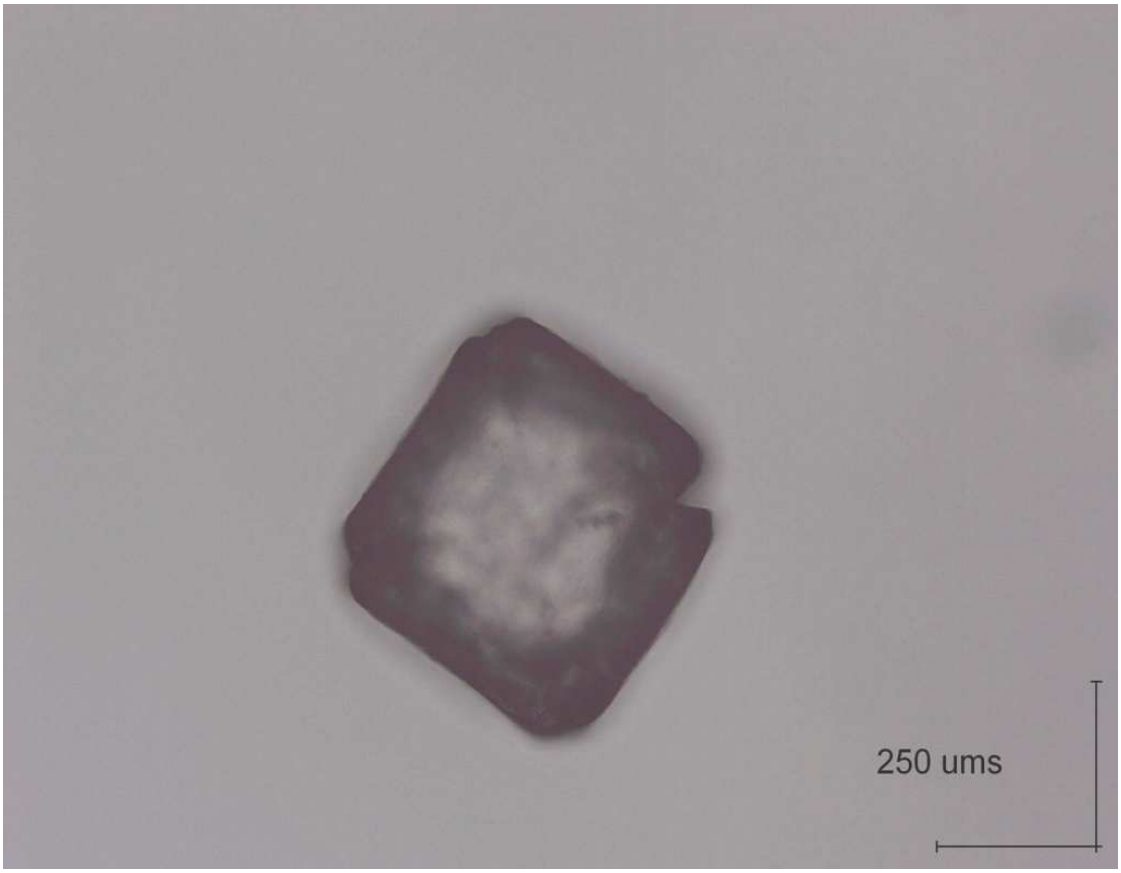

Figure 4.25 Broken Commercial Mesh 40 NaCl Crystal

Table 4.11 lists the mass fraction results of the initial particle size experiments for 30 and 60 minutes. More breakage (by weight) is seen in the 10 and 30 mesh particles. For the smallest size examined, only a slight amount of breakage occurred. For the remaining sizes, between 3 - 30 % of the recovered NaCl crystals were converted to child particles. Based on time, increases in the amount of child particles produced increased with Mesh 10 being the only exception. More breakage was expected with time since the particles are presented with more opportunities to collide with each other and the impeller.

Table 4.11 Initial Particle Size Mass Fractions of Broken NaCl Crystals at 1500 rpm

Mesh	**Time, min**	x_p	x_c
6	30	0.97	0.03
	60	0.89	0.11
10	30	0.86	0.14
	60	0.88	0.12
30	30	0.84	0.16
	60	0.69	0.31
40	30	0.94	0.06
	60	0.93	0.07
60	30	0.999	0.001
	60	0.993	0.007

In Figures 4.26 - 4.28, shape factor analysis of the effects of initial particle size on child particles is presented. In terms of aspect ratio, the largest deviation or error occurred with the smallest parent particles, Mesh 60 at 30 and 60 minutes. The average aspect ratio values were similar for the laboratory grown Mesh 6 and Mesh 10 crystals but varied for the other three size ranges. Roundness values shown in Figure 4.27 averaged around 1.3 in both time investigations. The least amount of deviation occurred for the Mesh 40 child particles. Lastly, the average major axis of the child particles is presented in Figure 4.28. As the particle size range decreased, the deviation or error from the average major axis decreased for 30 and 60 minutes from ~150 microns to 100 microns. The size of the child particles formed after 60 minutes is independent of the original parent particle size.

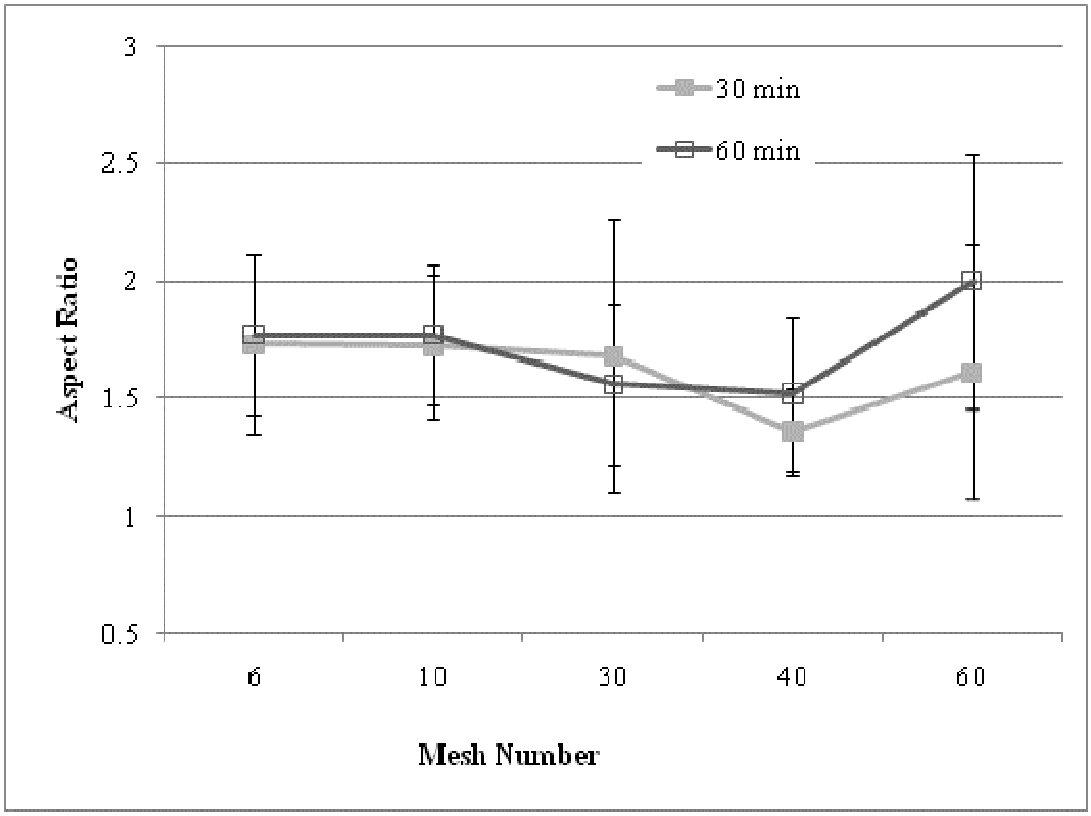

Figure 4.26 Average Aspect Ratio of NaCl Child Particles Based on Change in Initial Particle Range

NOTE: Initial Particle Size Range corresponds to the different mesh numbers.

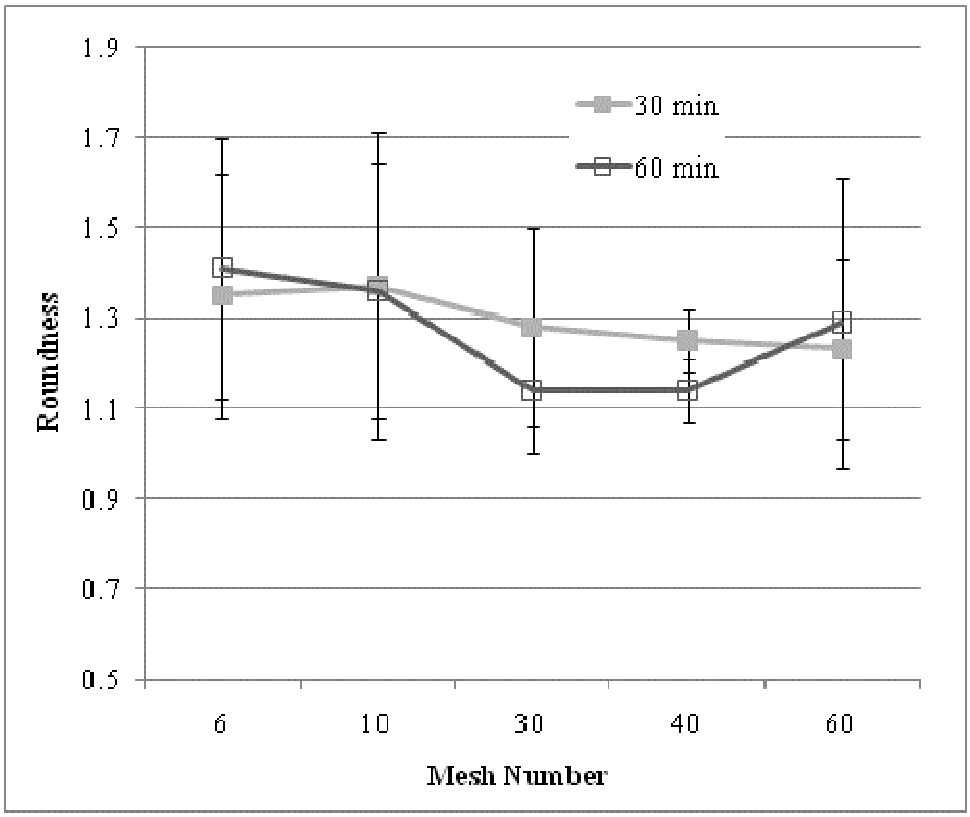

Figure 4.27 Average Roundness of NaCl Child Particles Based on Change in Initial Particle Range

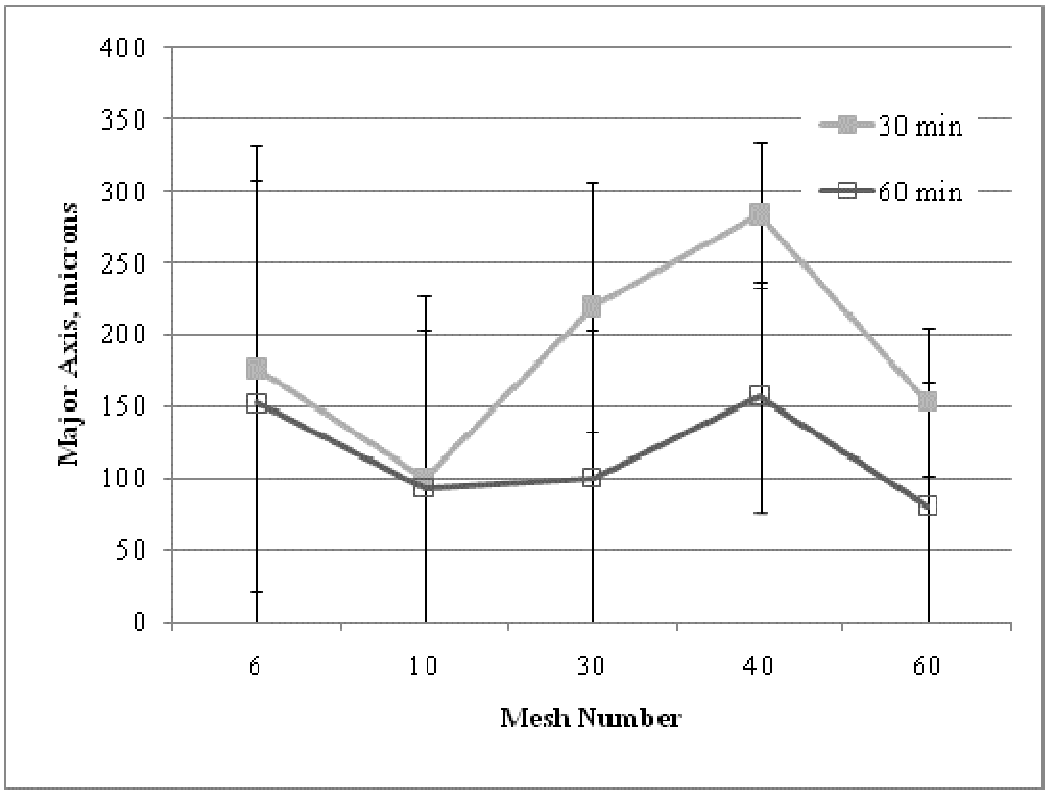

Figure 4.28 Average Major Axis of NaCl Child Particles Based on Change in Initial Particle Range

Figure 4.29 highlights child particles < 300 microns produced from the breakage experiments with Mesh 6 and 10 particles (full PSDs are in Appendix E). The lines shown for Mesh 6 particles at 30 minutes show the fines number fraction over the size range shown. Each point on the graph represents the midpoint of the size interval. For example, the number fraction at around 200 microns represents particles with major axes greater than around 175 microns but less than 225 microns. The number fraction is this graph represents the total number of particles in each interval divided by the total number of child particles produced with a major axis less than 300 microns. The open points represent the 30 minute runs while the closed points represent 60 minute runs. Finer

particles (0 - 50 microns) are produced by increasing time for both Mesh 6 and Mesh 10 particles.

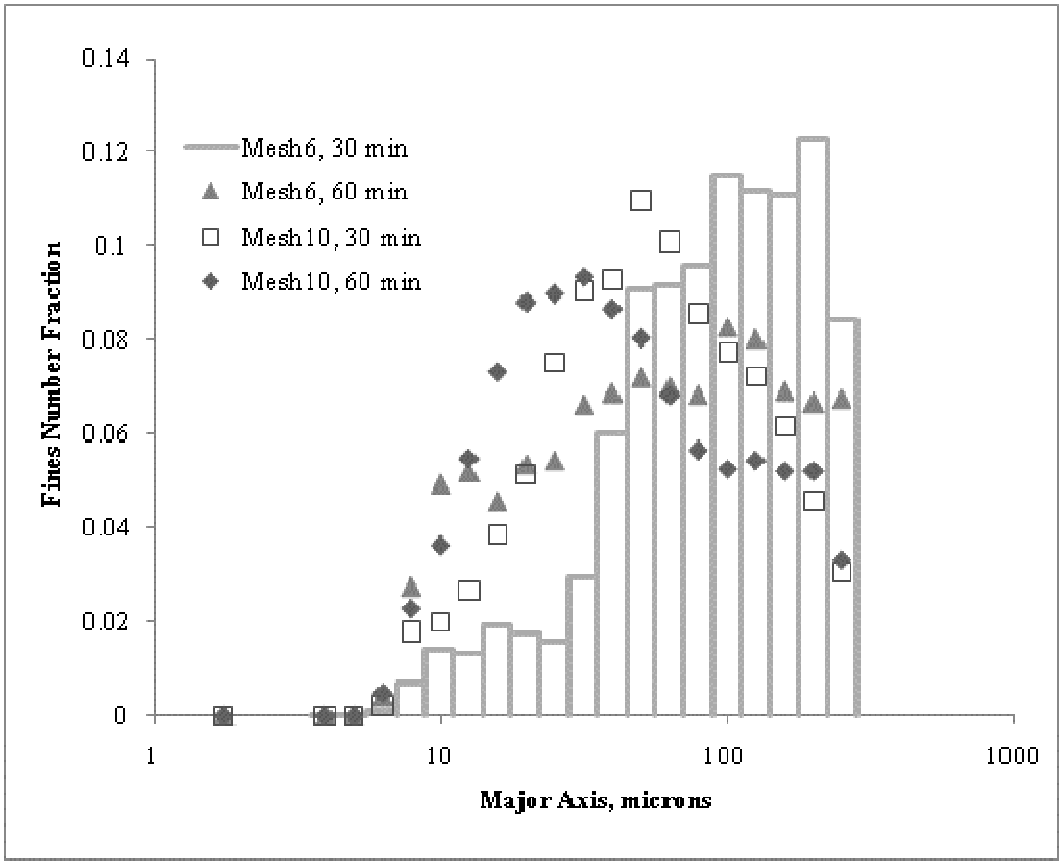

Figure 4.29 PSD of Mesh 6 and 10 NaCl Fines (<300 microns) Agitated for 30 and 60 Minutes at 1500 rpm

In Figures 4.30 - 4.32, the particle size distribution of unbroken and broken (30, 60 minute) particles for Mesh 30, 40, and 60 NaCl crystals are shown. In Figure 4.30, only a slight amount (number fraction of less than 0.10 for particles less than 12.5 μm) of attrition is seen when the Mesh 30 particles are agitated for 60 minutes with no significant change in 30 minutes. However, it is noted that the attrition results seen for 60 minutes altered the particles in the 400-625 μm range on the graph. The 625-800 μm

range remains consistent with the unbroken sample and 30 minute run implying that breakage mostly occurred to the smaller particles in the unbroken sample.

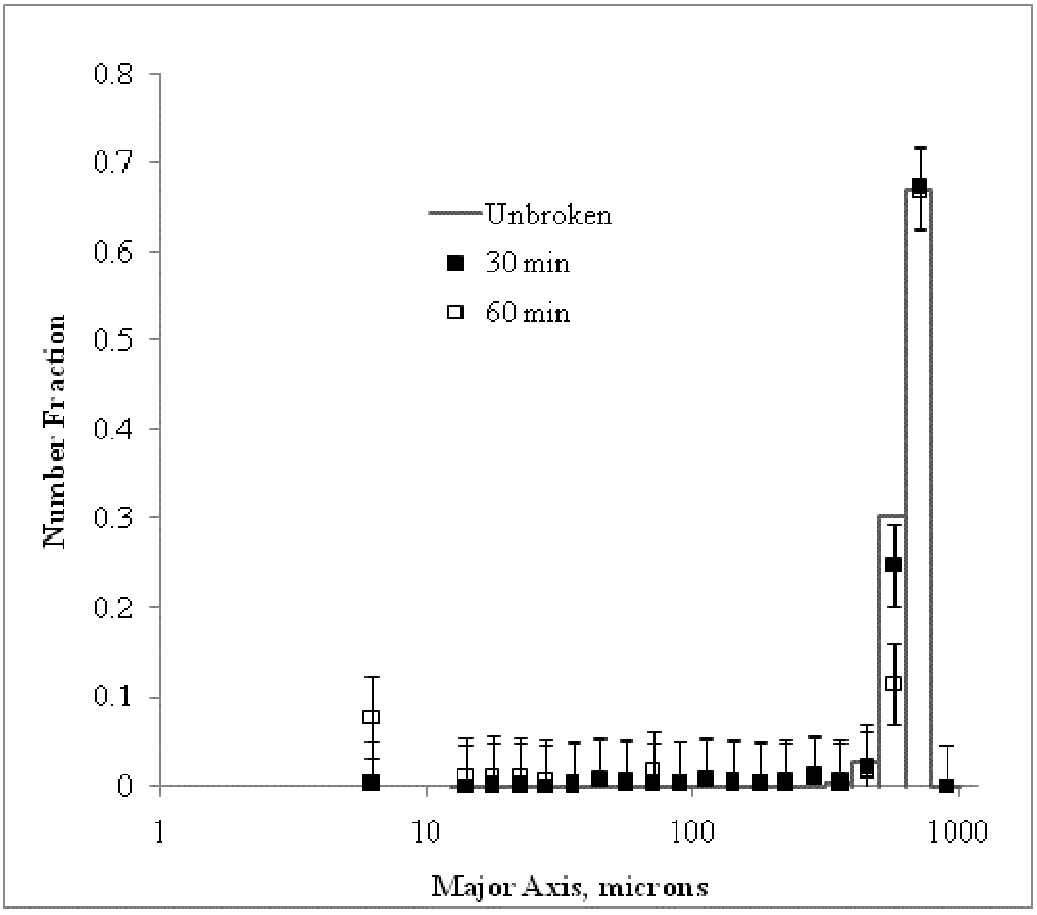

Figure 4.30 PSD of Mesh 30 NaCl Crystal Breakage in ACTL for 30 and 60 Minutes at 1500 rpm

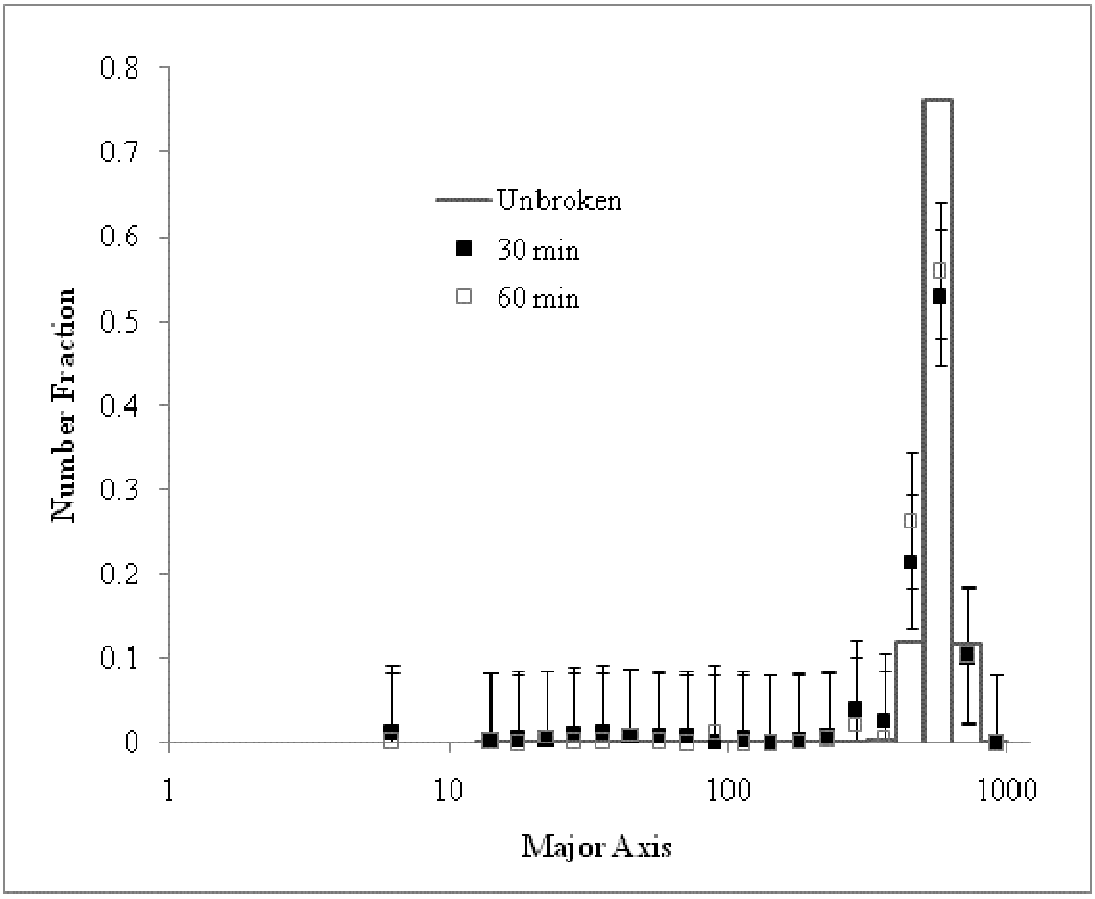

Figure 4.31 PSD of Mesh 40 NaCl Crystal Breakage in ACTL for 30 and 60 Minutes at 1500 rpm

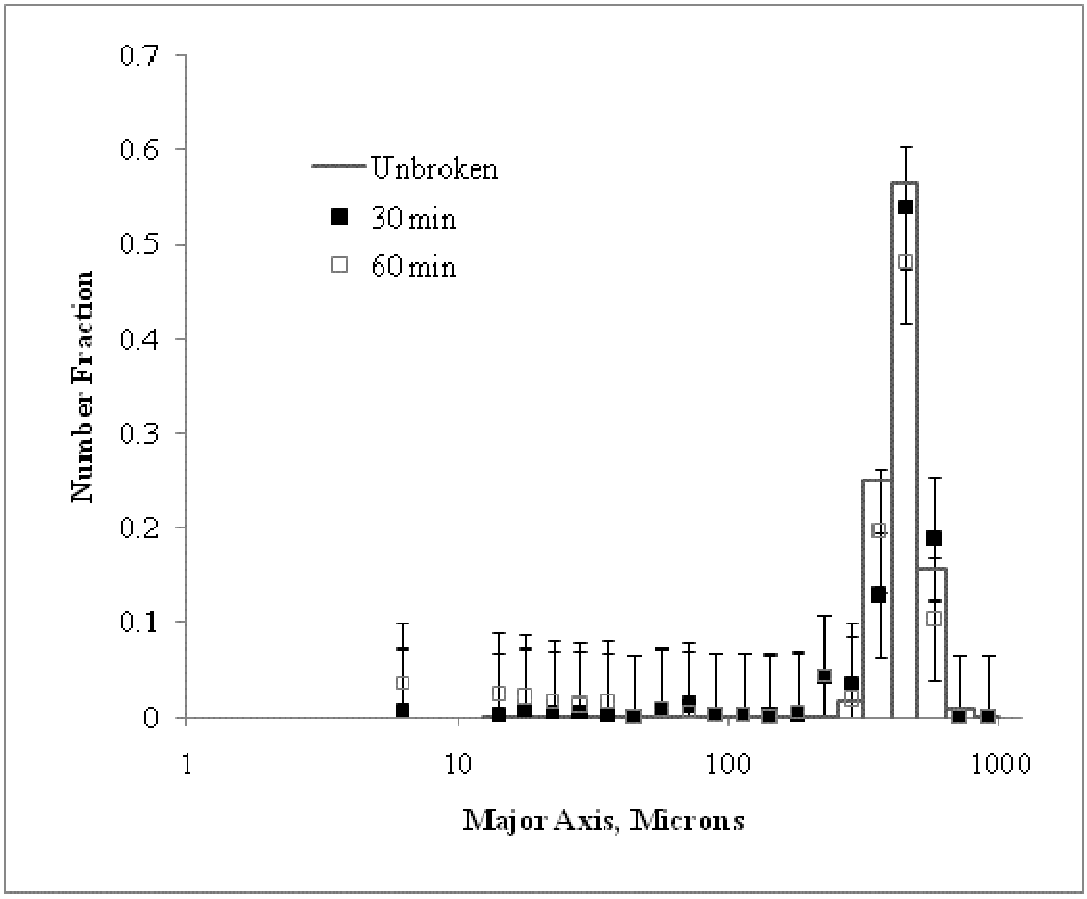

Figure 4.32 PSD of Mesh 60 NaCl Crystal Breakage in ACTL for 30 and 60 Minutes at 1500 rpm

Mesh 40 particles, smaller in size, showed significantly more breakage at the dominant peak of the unbroken sample in Figure 4.31 when compared to Mesh 30 breakage. However, no significant number fraction resulted for the child particles. For the Mesh 60 particles in Figure 4.32, the 30 and 60 minute runs produced both attrition and fragmentation. Both occurred at less than 5% by number but cumulatively were around 10% by number.

4.4 Conclusions

From breakage experiments in an aqueous saturated solution and a nonsolvent (acetonitrile), more fines were produced in aqueous saturated solution unlike what is

reported in the literature (Offermann, 1982). Both suspension fluids produced significantly different PSDs. Since more breakage occurred in saturated solution, other mechanisms (aging or nucleation) cannot be neglected in breakage experiments. Therefore, the optimal suspension fluid for particle breakage experiments is a nonsolvent.

To determine the magnitude of crystal-to-crystal and crystal-to-impeller collisions, experiments were designed to investigate three effects: initial particle size, agitation rate, and magma density. In the initial particle size investigation, images showed both fragmentation and attrition occurring as a result of particle suspension in a stirred vessel; however, attrition was more prominent as the initial particle size decreased. Increasing the magma density had the greatest effect on the amount of fines or child particles produced by weight and by number. An increase in time or agitation rate resulted in an increase in child particle production on a smaller scale than magma density; thus, it is concluded that crystal-to-crystal and crystal-to-impeller collisions dominate particle suspension systems. Mass-based particle analysis results are skewed because the larger particles weigh much more than the fines and can hide the true amount of fines produced; therefore, both number and mass analysis should be conducted for particle breakage investigations. Additionally, shape factor analysis reveals trends not seen in mass or number analysis.

Based on number, significant breakage occurred for Mesh 6 and 10 particles but was not seen with the smaller Mesh 30, 40, and 60 parent particles. From the number-based specific rate of breakage equation,

$$S(v) = S_c v^{\alpha} \tag{4.12}$$

where v is particle volume and α is a nonnegative number, it is expected that more breakage would occur at larger particle volumes (major axis) as demonstrated by these results.

Residence time had little to no effect in the initial particle size investigation, but it had a greater influence on the PSD in the agitation rate investigation. Agitation rate experiments produced both attrition and fragments based on PSD observations. The highest rate of 2000 rpm produced the most child particles in terms of number fraction which showed that agitation rate influences the PSD at higher agitation rates. Increasing the magma density will increase the crystal-to-crystal collision effects regardless of using a solvent or a nonsolvent but with difference particle size distributions. Child particles did not become more rounded in any of the three investigations based on aspect ratio and roundness values.

From the shape factors investigated, the major axis and aspect ratio were determined as the most appropriate factors in modeling particle breakage, especially in the initial particle size investigation. In terms of crystal-to-impeller collisions, residence time was the most influential on particle breakage when the agitation rate was increased; therefore, the combination of increasing residence and agitation rate has a greater influence on particle breakage when compared to each individual parameter. The initial particle size had a great influence on the number of child particle produced, but this result is hidden in mass analysis due to the difference in the weight of the various particle sizes. In terms of crystal-to-crystal collisions, increasing the magma density produced the most breakage seen in this investigation which agrees with Nienow and Conti (1978) and should not be ignored when designing equipment where particles are suspended in a stirred vessel.

4.5 References

Allen, T. (1997). *Particle Size Measurement Volume 1: Powder Sampling and Particle Size Measurement, 5th Ed.*, Chapman & Hall, London.

Atiemo-Obeng, V. A., Penney, W.R., and P. Armenante (2004). Solid-liquid Mixing. In Paul, E. D., Atiemo-Obeng, V. A., and S. M. Kresta (Eds.). *Introduction of the Handbook of Industrial Mixing*, Wiley & Sons, New Jersey, 543-582.

Bravi, M., Di Cave, S., Mazzarotta, B., and N. Verdone (2003). Relating the attrition behavior of crystals in a stirred vessel to their mechanical properties. *Chem. Eng. J. Vol. 94*, 223-229.

Briesen, H. (2009). Two-dimensional population balance modeling for shape dependent crystal attrition. *Chem. Eng. Sci. Vol. 64(4)*, 661-672.

Cadle, R.C. (1965). *Particle Size: Theory and Industrial Applications*, Reinhold Publishing Corporation, New York.

Chianese, A., Di Berardino, F., and A.G. Jones (1993). On the Effect of Secondary Nucleation on the Crystal Size Distribution from a Seeded Batch Crystallizer. *Chem. Eng. Sci. Vol. 48(3)*, 551-560.

Conti, R. and A.W. Nienow (1980). Particle abrasion at high solids concentration in stirred vessels-II. *Chem. Eng. Sci. Vol. 35*, 543-547.

Davey, R. and J. Garside (2000), *From Molecules to Crystallizers: An Introduction to Crystallization*, Oxford Science Publications, Oxford.

Davies, R. (1984). Particle Size Measurement: Experimental Techniques. In M.E. Fayed and L. Otten (Eds.). *Handbook of Powder Science and Technology*, Van Nostrand Reinhold, New York, 31-68.

Garside, J. (1985). Industrial Crystallization from Solution. *Chem. Eng. Sci. Vol. 40(1)*, 3-26.

Mazzarotta, B. (1992). Abrasion and Breakage Phenomena in Agitated Crystal Suspensions. *Chem. Eng. Sci. Vol. 47(12)*, 3105-3111.

Mazzarotta, B., Di Cave, S., and G. Bonifazi (1996). Influence of Time on Crystal Attrition in a Stirred Vessel. *AIChE J. Vol. 42 (12)*, 3354-3558.

McCabe, W.L., Smith, J.C., and P. Harriet (2001). *Unit Operations of Chemical Engineering*, McGraw-Hill, New York.

Mullin, J. W. (2001). *Crystallization 4th Ed*., Butterworth-Heinemann, Boston.

Nienow, A. W., and R. Conti (1978). Particle abrasion at high solids concentration in stirred vessels. *Chem. Eng. Sci. Vol. 33*, 1077-1086.

Offermann, H. and J. Ulrich (1982). On the Mechanical Attrition of Crystals. In S.J. Jancic and E.J. de Jong (Eds.). *Industrial Crystallization 81*, North-Holland, New York, 313-314.

Shamlou, P.A., Jones, A. G., and K. Djamarani (1990). Hydrodynamics of Secondary Nucleation in Suspension Crystallization. *Chem. Eng. Sci. Vol. 45(5)*, 1405-1416.

Synowiec, P., Jones, A.G., and P. Ayazi Shamlou (1993). Crystal Break-Up in Dilute Turbently Agitated Suspensions. *Chem. Eng. Sci. Vol. 48(20)*, 3485-3495.

Zwietering, T. N. (1958). Suspending Solid Particles in Liquids by Agitators. *Chem. Eng. Sci. Vol.8*, 244-253.

CHAPTER V

QUANTIFICATION OF NaCl, KCl, AND POTASH ALUM CRYSTALS IN NONSOLVENTS FROM BREAKAGE IN A STIRRED VESSEL

5.1 Introduction

Particle breakage occurs during crystallization for a variety of systems. Crystals may differ in morphology, structure or habit, or hardness. Crystal morphology is dependent upon the growth rate of each crystal face (Mullin, 2001). The growth of a crystal face is determined by environmental conditions, crystal geometry, and impurities in the system (Mullin, 2001). The resulting morphology of crystal growth is usually manipulated by the selection of the solvent or controlling the growth environment such as the crystallization temperature (Mullin, 2001).

A crystal is not only characterized by its morphology. Hardness is used to describe the abrasion or breakage resistance of a material and is often correlated with parameters such as stirrer diameter or stirrer tip speed used to process crystals (Ulrich, 1990). Vicker's hardness, in particular, is considered the first step in defining the abrasion resistance of industrial salts. In a Vicker's measurement, a pyramidal indentation of a known load is used to make an impression on the material (Tabor, 1956). The size of the indentation is used to determine a hardness number in kg_f/m^2 (Mullin, 2001). New ultra-microhardness devices allow the measurement of Vicker's hardness of small crystals (Ulrich, 1990).

Solid particulates have many functions and are produced for multiple purposes. Sodium chloride (NaCl) is most commonly known as table salt and for its use as a food ingredient while potassium chloride (KCl), referred to as the muriate of potash, is mainly used as an ingredient of fertilizer (Mullin, 2001; Potassium Chloride, 2008). Potash alum (potassium aluminum sulfate dodecahydrate) is used in water purification processes and as an ingredient in baking soda (Alum, 2008) In terms of crystal habit, both NaCl and KCl are considered cubic (Table 5.1) while potash alum is octahedral (Mullin, 2001). All three crystalline materials are water soluble with solubility values listed in Appendix A.5. NaCl, KCl, and potash alum are commonly produced using suspension crystallization techniques thus presenting the likelihood of the occurrence of particle breakage within the crystallization vessel (Gerstlauer, 2001). Recent designs for hardness testers have featured new units capable of measuring single crystals down to hundreds of microns. Using the Vicker's indentation test, hardness values for several substances are recorded in the literature (Gahn, 1999a). Harder substances require less work to form cracks (Bravi, 2003). As shown in Table 5.1, potash alum has the highest hardness value; therefore, more work is required to deform potash alum crystals than NaCl and KCl crystals.

Table 5.1 Crystal Habit and Hardness of Select Crystals

Crystal	**Crystal Habit**[Mullin 2001]	**Hardness (H_v)**[Gahn 1999] **MPa**	**Hardness (H_v)**[Bravi 2003] **MPa**
NaCl	Cubic (FCC)	167	166
KCl	Cubic (FCC)	97	91
Potash alum	Octahedral	726	-

Particle breakage modeling is an area of interest in crystallization since breakage affects the PSD of the final product. One approach has been to design population balance equations (PBEs) that theoretically account for breakage as either a function of attrition, fragmentation, or both (Gahn, 1997; Hill, 2004; Gahn, 1999a). One study created model equations for attrition of brittle crystalline solids (Gahn, 1997; Gahn, 1999a; Gahn, 1999b). Initially, the equation included a function to determine the impact energy needed to fracture the hard surfaces of crystals (Gahn, 1997). The models were later extended to include functions for attrition as well (Gahn, 1999a; Gahn, 1999b). However, the models were based solely on single crystal breakage analysis. Other researchers utilized mass or mass fraction analysis to create mass-based breakage distribution functions (Austin, 1976; Mazzarotta, 1992; Mazzarotta, 1996); however, the results of the previous chapter showed that mass analysis in the form of child particle mass recovered and number analysis should be conducted to accurately represent the breakage occurring in a stirred vessel.

In this chapter, the goals are to quantify the breakage of KCl and potash alum crystals in a nonsolvent based on adjusted agitation rates and to compare the results to the equivalent Mesh 40 NaCl crystal agitation at 1500 rpm for 30 and 60 minutes presented in Chapter 4. From the resulting PSDs, particle breakage will be modeled based on number fraction and major axis using the Austin (1976) equation and the power law form of the product function (Hill, 1995). Modeling parameters will be based on the number fraction and major axis of the crystals. Further modeling of the NaCl agitation rate in acetonitrile at 30 and 60 minutes is also presented in this chapter.

5.2 Methodology

Potassium chloride (KCl) and potassium aluminum sulfate dodecahydrate (potash alum, $KAl(SO4)_2 \cdot 12H2O$) were acquired from Fisher Scientific in crystalline form. Anhydrous (see Appendix I) sodium chloride (NaCl) crystals were obtained from a commercial source. All crystals were classified by size using the commercial NaCl crystal sieving method presented in the last paragraph of Section 4.2.1.

Potash alum is insoluble in acetone which will serve as its nonsolvent (Liley, 1997). Since the solubility of KCl in acetonitrile is 0.0024g/100g (Burgess, 1978), acetonitrile is used as the nonsolvent for KCl. Due to the different particle size ranges, crystals, and suspension fluids used in each case, adjustments are needed to provide conditions that are as hydrodynamically similar as possible. Since agitation can produce turbulent conditions, adjusting the agitation rate based on Reynolds number is considered. For stirred vessels, the Reynolds number as a function of agitation rate, N, is given by

$$Re = \frac{\rho N D^2}{\mu}. \tag{5.1}$$

For select agitation rates, the Reynolds number for agitation in acetone (ACTE), acetonitrile (ACTL), and aqueous NaCl saturated solution (SS) is compared in Table 5.2. More turbulence is calculated to occur in acetone which had a range of Reynold's numbers between 10.0 - 20.0 x 10^4. Adjusting agitation rates for ACTE and SS based on a Reynold's number identical to that of ACTL (Table 5.3) reveals agitation rates over 3 times higher in SS and slightly lower in ACTE. However, Chapter 4 results show more breakage occurred in SS; thus, increasing the agitation rate based on Reynold's number in SS will not produce an PSD equivalent to ACTL. A second method is to adjust rates

Table 5.2 Reynold's Number Calculation for ACTL, SS, ACTE

Agitation Rate		**ACTL**		**SS**		**ACTE**	
rpm	rps	Re	$Re/10^4$	Re	$Re/10^4$	Re	$Re/10^4$
1000	16.7	88398	8.8	25806	2.6	100190	10.0
1250	20.8	110498	11.0	32258	3.2	125237	12.5
1500	25.0	132597	13.3	38710	3.9	150284	15.0
1750	29.2	154697	15.5	45161	4.5	175332	17.5
2000	33.3	176796	17.7	51613	5.2	200379	20.0

Table 5.3 Adjusted Agitation Rate Using Reynold's Number

Re	**ACTL**		**Equivalent SS**		**Equivalent ACTE**	
	rpm	**rps**	**rpm**	**rps**	**rpm**	**rps**
88398	1000	16.7	3425	57.1	882	14.7
110498	1250	20.8	4282	71.4	1103	18.4
132597	1500	25.0	5138	85.6	1323	22.1
154697	1750	29.2	5995	99.9	1544	25.7
176796	2000	33.3	6851	114.2	1765	29.4

using Zwietering's correlation. The adjusted agitation rates are based on NaCl crystals suspended in acetonitrile at 1500 rpm. Results are shown in Table 5.4 with individual calculations shown in Appendix C.

Breakage experiments in this chapter follow the same breakage, filtration, separation, and analysis procedures presented in Section 4.2 with the exception that all particles were investigated using only the Olympus microscope. Each run was performed at 30 and 60 minutes. After breakage, the PSD is compared to that of an unbroken sample of each material based on the initial size.

Table 5.4 Adjusted Agitation Rates Based on NaCl at 1500 rpm Using Zwietering's Correlation

Crystal	Suspension Fluid	Particle size, µm	Agitation Rate, rps	Agitation rate, rpm
NaCl	Acetonitrile	425	25.0	1500
KCl	Acetonitrile	250	29.7	1760
		425	26.7	1600
Potash Alum	Acetone	600	27.9	1680
		850	26.1	1560

5.3 Results

5.3.1 Mass, Number, and Shape Analysis

Images of unbroken and broken crystal are presented in Appendix F. In Table 5.5, no significant change is seen in the mass fraction of the recovered child particles for NaCl, KCl, and potash alum. This finding suggests that adjusting for the agitation rate using Zwietering's (1958) correlation will produce similar mass fractions for particles of various crystalline material and crystal sizes. In Figure 5.1, the breakage of Mesh 40 KCl particles is presented while Figure 5.2 shows Mesh 60 KCl particles. Significant breakage occurs after 30 minutes for each size with no significant change between 30 and 60 minutes. A decrease by number of around 30% is seen in the dominant major axis. Potash alum breakage PSDs are shown in Figures 5.3-5.4. Significant quantities of fines were produced for both Mesh 20 and 30 potash alum particles that reduced the peak of the dominant major axis. Over 50% of all child particles by number are less than 100 microns in length for each potash alum crystal size range.

5.4 Effect of Crystal and Suspension Fluid Properties

The PSDs of potash alum presented in the previous section are significantly different from the PSDs of NaCl and KCl as it pertains to the amount of child particles produced which brings into question the cause of this discrepancy. Three possible explanations exist: 1) the difference in fluid properties, 2) the initial size of the crystals, and 3) the characteristics of the crystalline material - crystal habit or geometric shape, bonding, and hardness.

Table 5.5 Agitation Rates and Mass Fractions of Adjusted NaCl, KCl, and Potash Alum

Crystal	Mesh (Size)	time, min	Rate, rps	Rate, rpm	x_p	x_c
NaCl	40 (425 µm)	30	25.0	1500	0.94	0.06
		60			0.93	0.07
KCl	40 (425 µm)	30	26.7	1600	0.98	0.02
		60			0.97	0.03
	60 (250 µm)	30	29.6	1780	0.995	0.005
		60			0.992	0.008
Potash Alum	20 (800 µm)	30	26.1	1560	0.96	0.04
		60			0.95	0.05
	30 (650 µm)	30	27.9	1680	0.98	0.02
		60			0.98	0.02

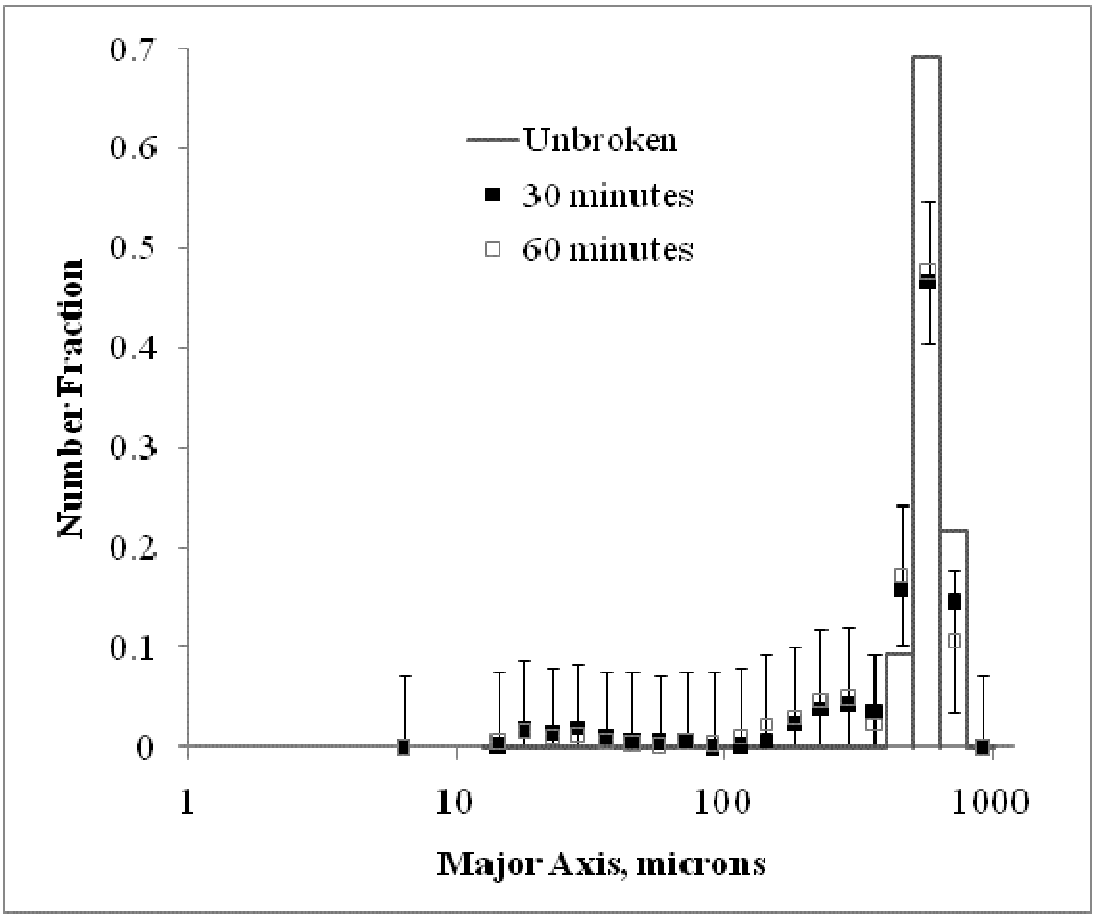

Figure 5.1 PSD for KCl Crystal Breakage in ACTL for 30 and 60 minutes at 1600 rpm

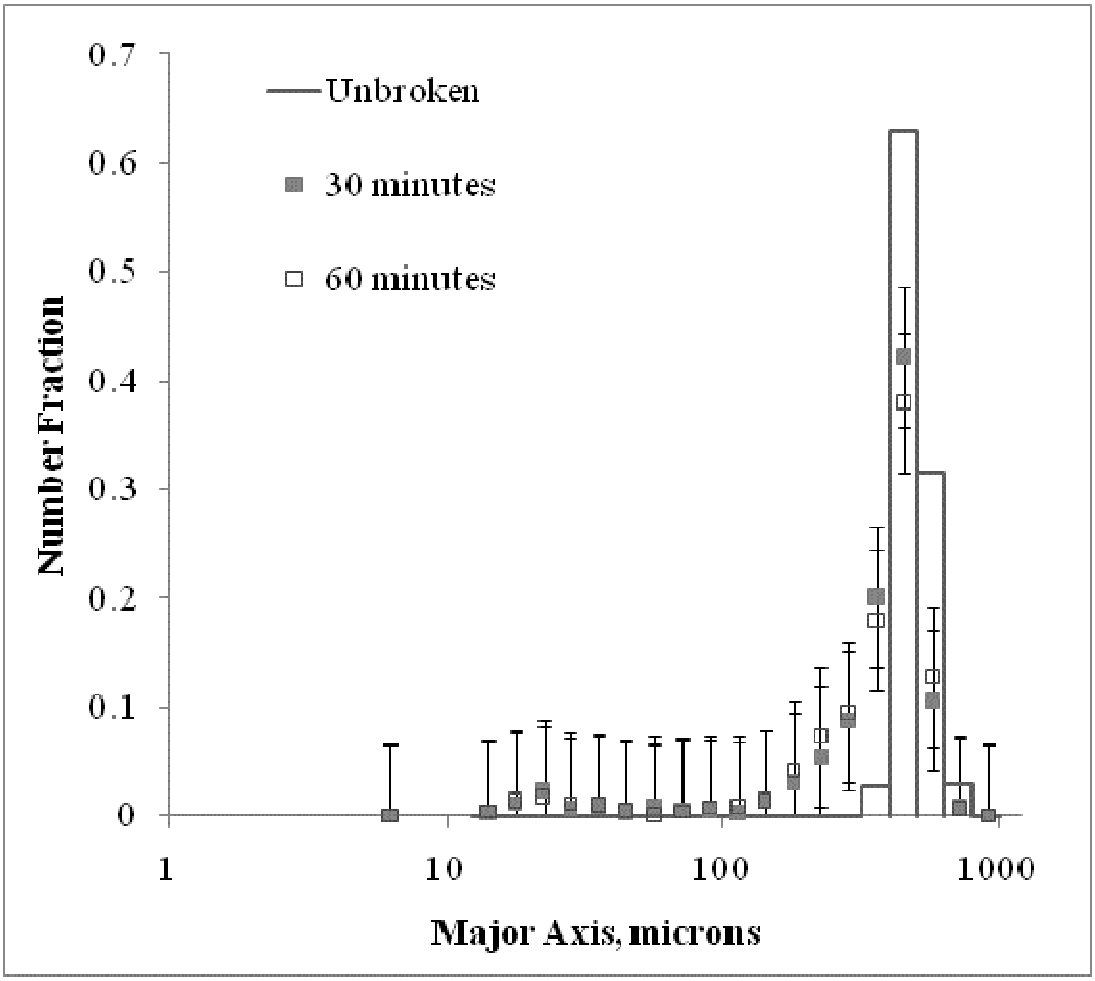

Figure 5.2 PSD for KCl Crystal Breakage in ACTL for 30 and 60 Minutes at 1780 rpm

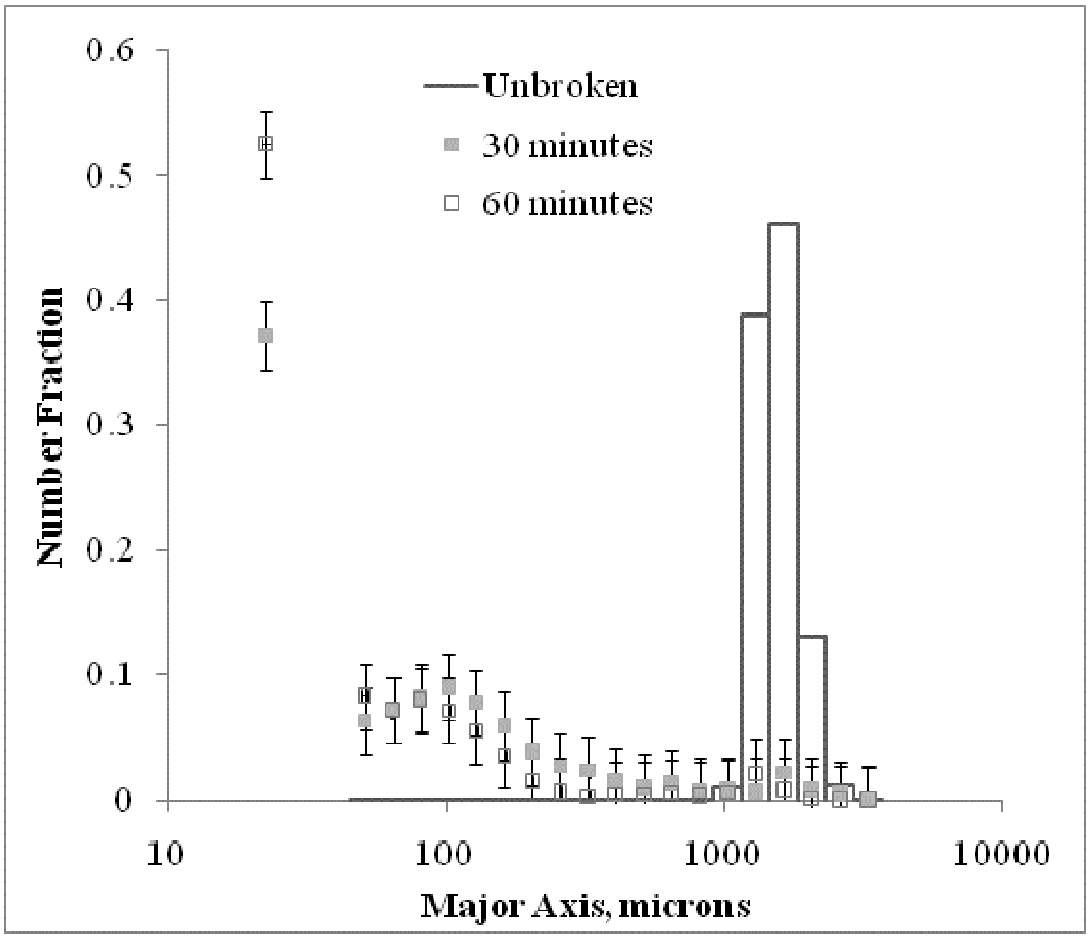

Figure 5.3 PSD for Potash Alum Crystal Breakage in Acetone for 30 and 60 Minutes at 1560 rpm

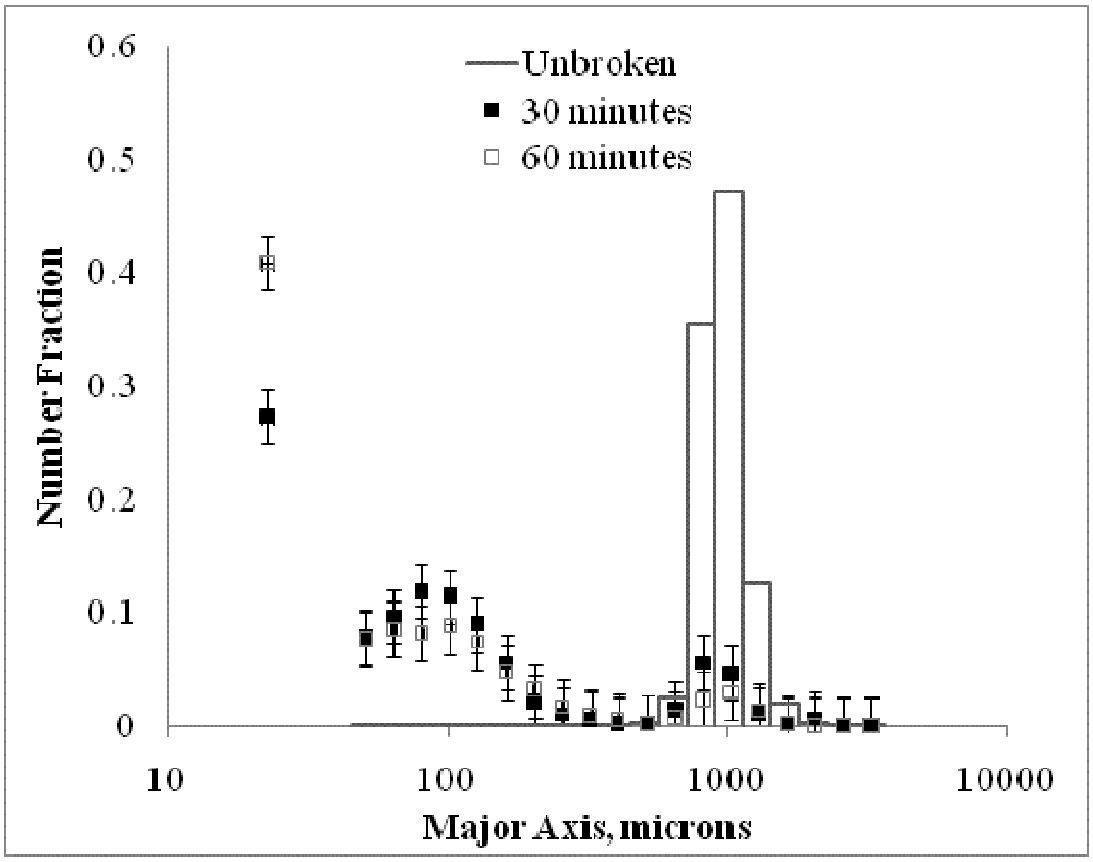

Figure 5.4 PSD for Potash Alum Crystal Breakage in Acetone for 30 and 60 Minutes at 1680 rpm

5.4.1 Fluid Properties

While NaCl and KCl breakage experiments were conducted in acetonitrile, potash alum experiments were conducted in acetone with differences in density and viscosity accounted for using Zwietering's correlation. However, KCl experiments were repeated in acetone (ACTE) based on the adjusted agitation rates presented in Table 5.6 to determine if nonsolvent properties will alter the PSD. Figures 5.5 and 5.6 show the resulting PSDs for Mesh 40 and Mesh 60 KCl crystal breakage in ACTL and ACTE respectively. For the Mesh 40 particles, no significant difference was found based on PSD for 30 or 60 minutes. In terms of Mesh 60 KCl crystals, only a slight change in breakage production was noticed. Furthermore, a comparison of parent and child particle mass fraction in

Table 5.6 Adjusted Agitation Rate Using Zwietering's Correlation for Acetone Trial

Crystal	Suspension Fluid	Particle size, µm	Agitation Rate, rps	Agitation rate, rpm
NaCl	Acetonitrile	425	25.0	1500
KCl	Acetonitrile	250	29.6	1780
		425	26.7	1600
	Acetone	250	30.4	1820
		425	27.3	1640
Potash Alum	Acetone	425	29.9	1800
		600	27.9	1680
		850	26.1	1560

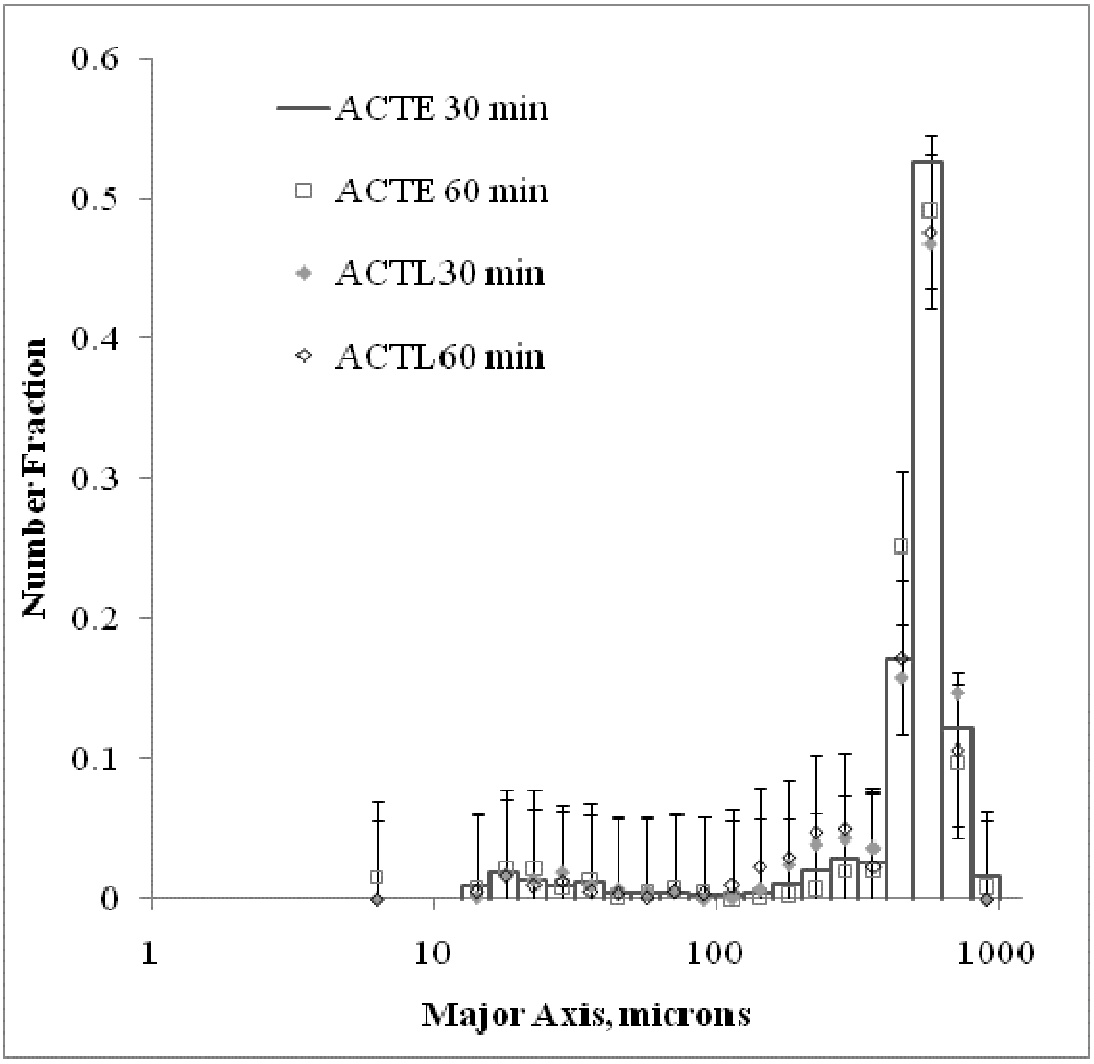

Figure 5.5 PSD of Mesh 40 KCl Crystal Breakage in ACTL and ACTE for 30 and 60 Minutes

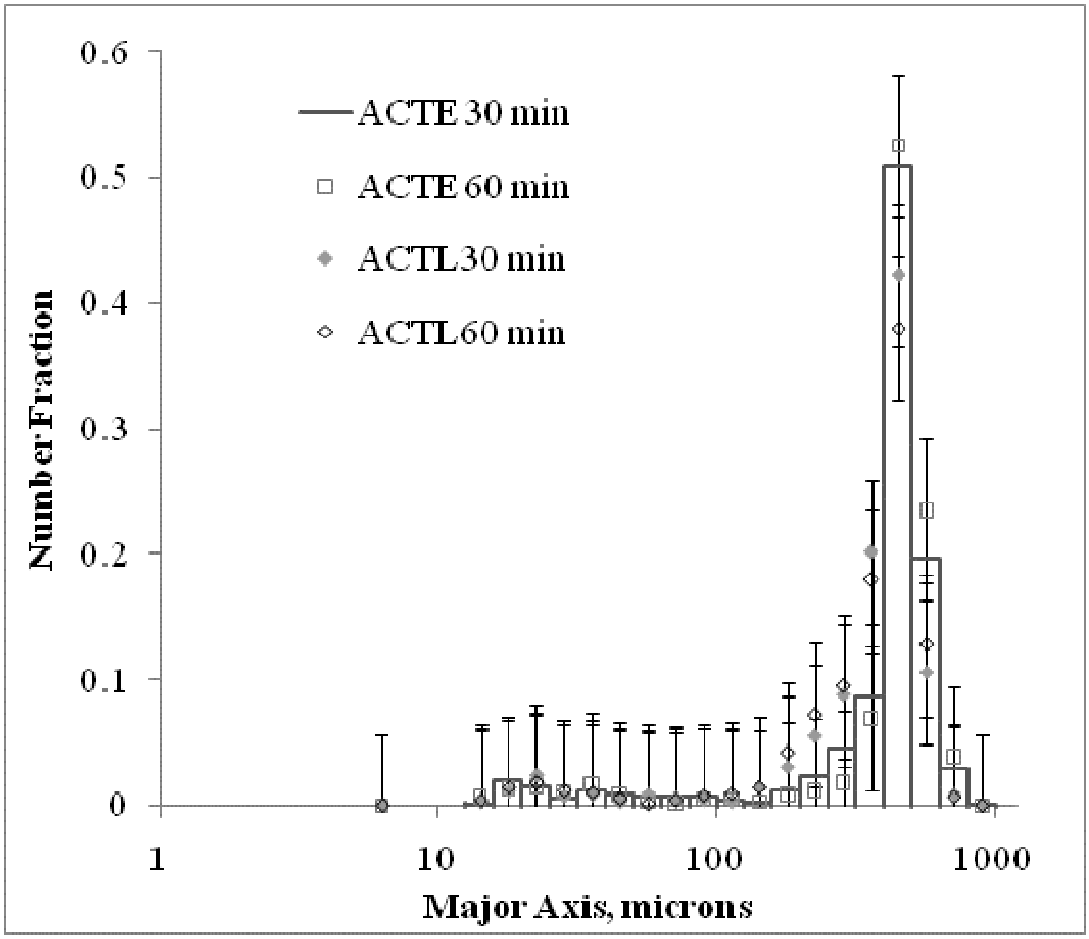

Figure 5.6 PSD of Mesh 60 KCl Crystal Breakage in ACTL and ACTE for 30 and 60 Minutes

Table 5.7 also shows no significant change in the fraction of particles recovered after breakage. These findings suggest that a change in nonsolvent will not produce a significant change in PSD if agitation rates are adjusted using Zwietering's correlation.

Table 5.7 KCl Mass Fractions in ACTL and ACTE

Fluid	Mesh	time, min	x_p	x_c
ACTL	40	30	0.98	0.02
		60	0.97	0.03
	60	30	0.995	0.005
		60	0.992	0.008
ACTE	40	30	0.98	0.02
		60	0.98	0.02
	60	30	0.998	0.002
		60	0.998	0.002

5.4.2 Initial Crystal Size

The second factor under consideration is the initial particle size utilized for potash alum crystals. The initial size of the NaCl crystals was the Mesh 40 (~425 microns) range while KCl crystals were Mesh 40 and the smaller Mesh 60 (~250 micron) range. To determine whether initial particle size adjustments are sufficient using Zwietering's correlation, Mesh 40 (used for NaCl and KCl) potash alum crystals were agitated at 30 and 60 minutes to compare with Mesh 40 breakage of NaCl and KCl. Figure 5.7 presents the PSD of the broken Mesh 40 potash alum crystals. The graph does not resemble the curves seen in the PSDs in Figures 5.3 and 5.4 for Mesh 20 and Mesh 30 potash alum breakage. For example in Figure 5.7, the dominant peak of the unbroken material ~700 μm remains dominant after 30 and 60 minutes of breakage whereas in Figures 5.3 and 5.4 the dominant peak shifted to the smallest bin of particles ~30 μm in length. Moreover,

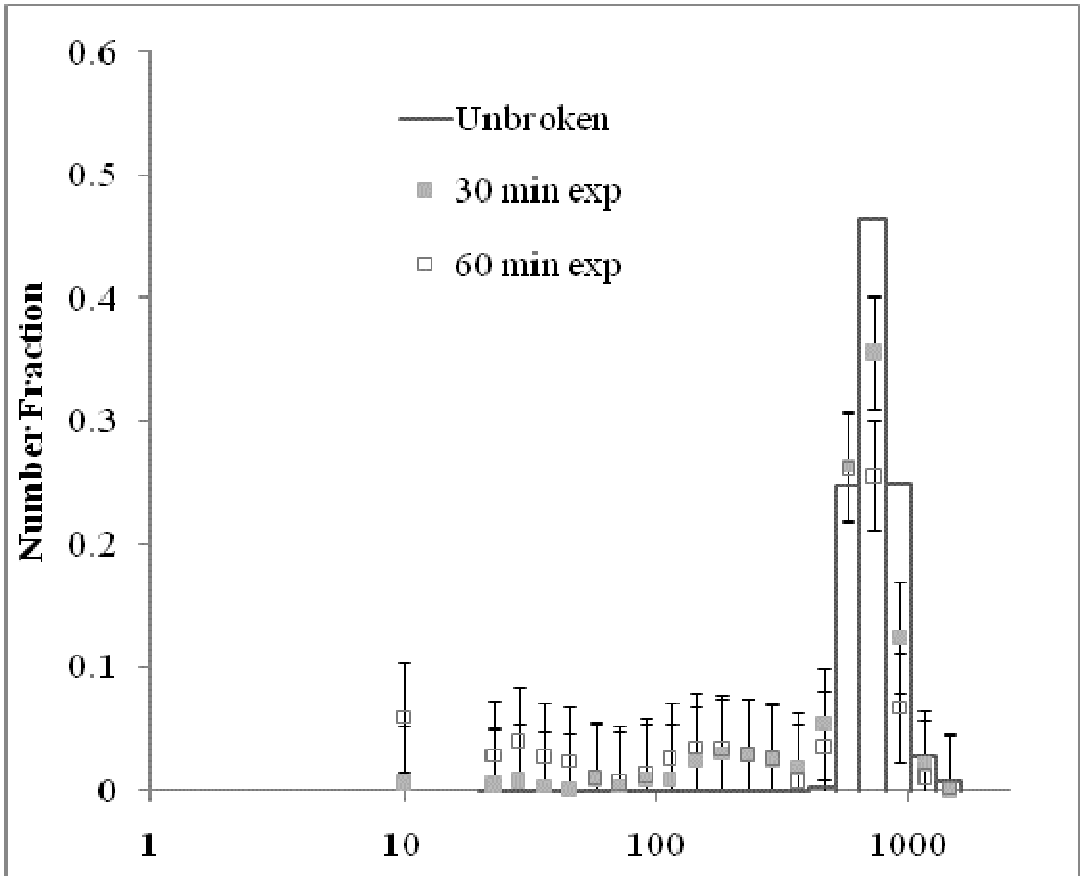

Figure 5.7 PSD of Mesh 40 Potash Alum Crystals Agitated in Acetone for 30 and 60 Minutes at 1640 rpm

100 µm crystals in Figure 5.3 and 5.4 have a number fraction between 0.08 and 0.10 while the number fraction is less than 0.01 in Figure 5.7. In Figure 5.8, Mesh 40 breakage of KCl and potash alum was compared. Overall dominant peaks for potash alum (~700 µm) are larger than those of KCl (~600 µm) for 30 minutes. However, potash's largest peaks only represent 30-40% of the total number of particles while KCl's dominant peaks represent about half of all particles which brings into question the meaning of such a difference in distribution between the materials. Although the results have a much closer fit than the Mesh 20 or Mesh 30 potash alum, the curves are not identical. These findings

further suggest the Zwietering correlation does not account for all the differences in material properties. This is reasonable since the Zwietering correlation does not account for properties such as particle shape or hardness.

5.4.3 Crystal Size and Other Characteristics

In Figure 5.8, it is observed that the range of particle sizes between the KCl and potash alum crystals are different with potash alum having the widest initial size range of the two materials. The reason for this discrepancy in range is largely due to the differences in geometric shape of the particles. Figure 5.9 shows images of an octahedral crystal representing the crystal habit of potash alum and a cubic crystal representing the crystal habit of potassium chloride. The octahedral shape is that of two pyramids connected at the base. In comparison, the octahedral crystal has four faces that meet at each corner, while the cube has three faces that meet at each corner. In terms of hardness, potash alum has a Vicker's hardness value that is 4 times greater than that of NaCl and 7 times greater than that of KCl. Based on this parameter, less work should be required to fracture the alkali halides. However, both NaCl and KCl are noted in the literature for their ductility, or ability to deform under tensile stress (Gahn, 1995).

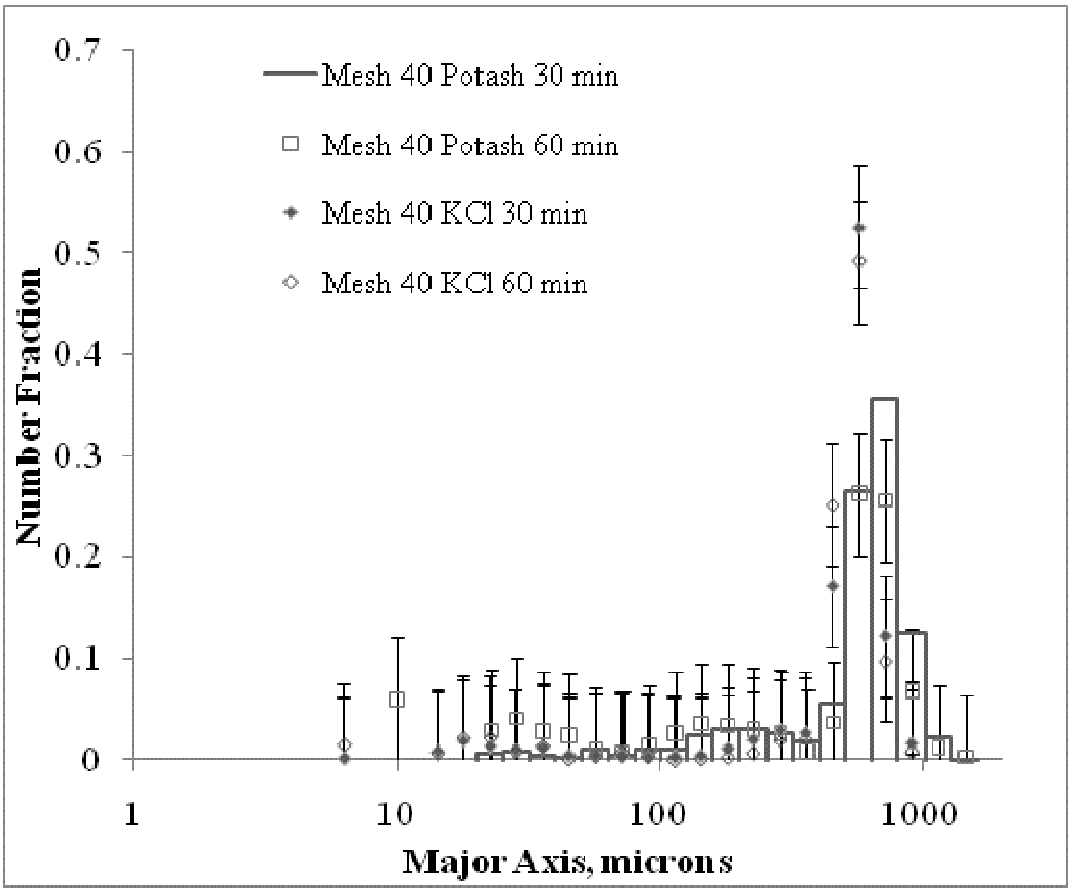

Figure 5.8 PSD of Mesh 40 KCl and Potash Alum Crystals Agitated in Acetone for 30 and 60 Minutes

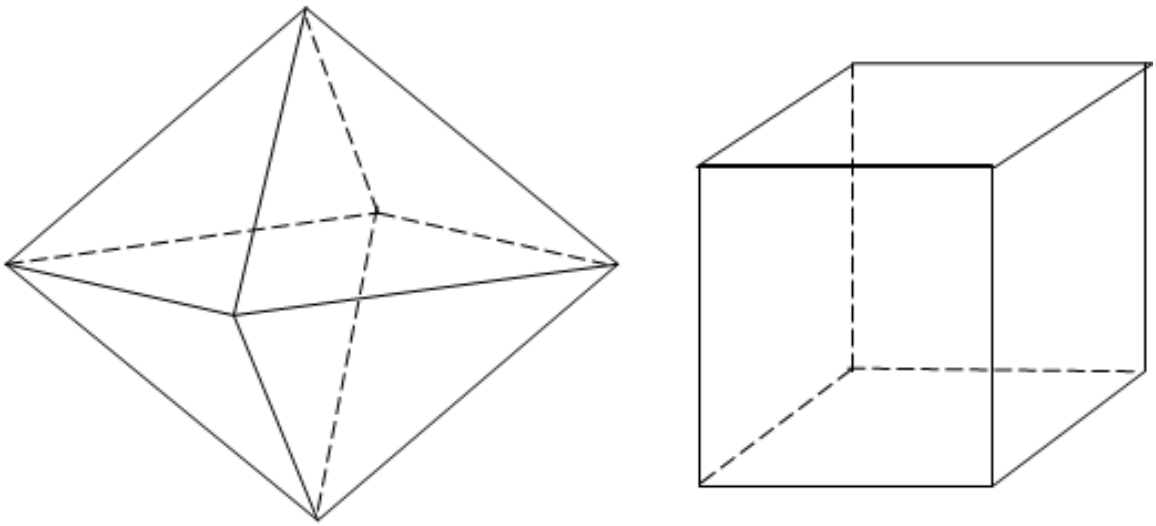

Figure 5.9 Comparison of Octahedral and Cubic Crystal Habits

Since particles size ranges are based on sieving in mass analysis, two dimensions of each particle will determine whether the particle will become captured on the screen of the sieve. In the case of cubic material, all sides of the crystals are identical. In Figure 5.10 and 5.11, the sieve diameters of cubic and octahedral particles are shown. For a cubic particle, only two lengths are possible. The first length is the edge where two faces meet; the second is the distance between two corners in the crystal. Both lengths are highlighted in gray in Figure 5.10. For an octahedral crystal, Figure 5.11 highlights three possible sieve diameters. Along with the edges and the distance between each corner, the distance between each edge is another length measurement.

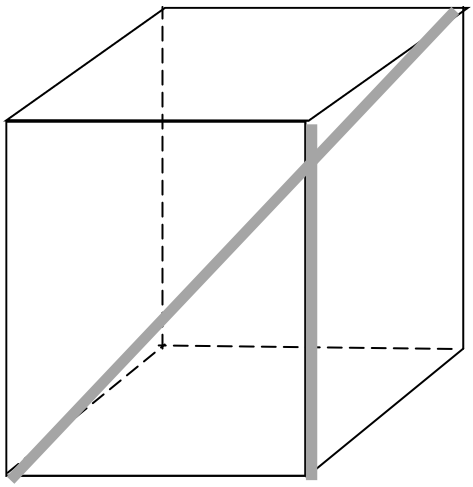

Figure 5.10 Sieve Diameters of Cubic Crystal (gray marks represent sieve diameters)

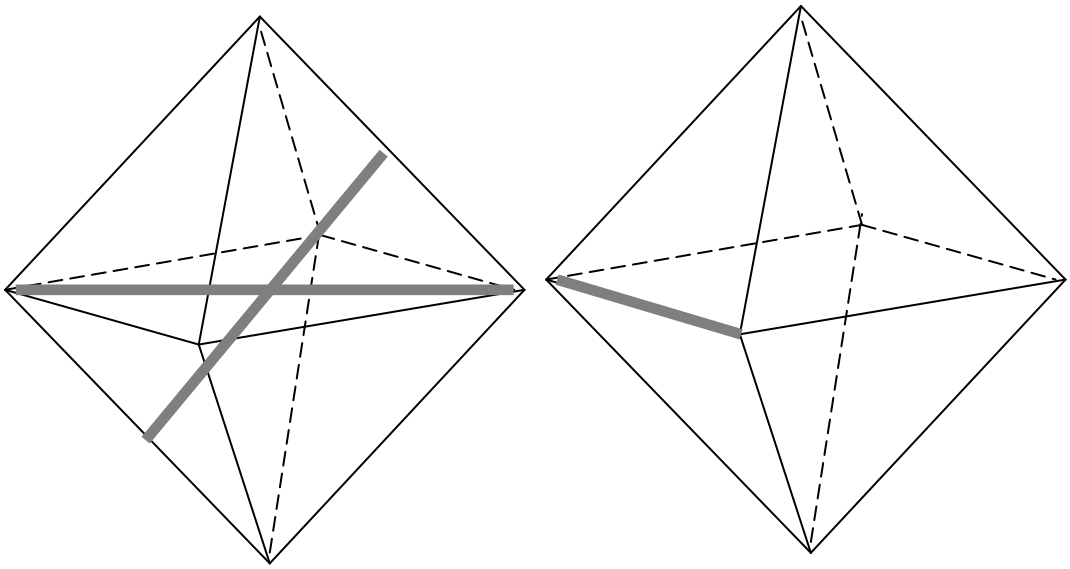

Figure 5.11 Sieve Diameters of Octahedral Crystal (gray marks represent sieve diameters)

Another difference in material to consider is the bonding of the material. Alum is an isomorphous double salt that possesses a univalent and trivalent cation (Alum, 2008). In the case of potash alum, potassium (K) represents the univalent cation and aluminum (Al) represents the trivalent cation. NaCl and KCl contain only an individual cation and

anion and share a common anion in Cl^-. Thus, the bonding for NaCl and KCl is ionic bonding. Moreover, potash alum has both ionic and covalent bonds and is a dodecahydrate (containing $12H_2O$) compound thus voids may exist in the crystal due to water evaporation. More analysis is needed to determine this effect.

5.5 Modeling Particle Breakage

As shown in this research, both fragmentation and attrition should be modeled to represent the PSD of particle breakage in an agitated vessel. Therefore, for population balance modeling the following is used in Equation 2.26

$$\frac{dn(t)}{dt} = \left(\frac{dn}{dt}\right)_{breakage} = \left(\frac{dn}{dt}\right)_{attrition} + \left(\frac{dn}{dt}\right)_{fragmentation} \tag{5.2}$$

where n(t) is the number density of particles at a given time. Austin's (1976) equation can be used to describe the attrition product that is produced during the grinding process based on the following breakage function and is presented in Chapter 2 as

$$B_{i,j} = \phi\left(\frac{x_i}{x_j}\right)^{\gamma} + (1-\phi)\left(\frac{x_i}{x_j}\right)^{\beta}, \quad (0 \le \phi \le 1). \tag{5.3}$$

In Equation 2.34, breakage modeling is performed by adjusting the values of β, γ, and ϕ in terms of parent particle size, x_j, and child particle size, x_i. An example of Austin's function, a number-based breakage distribution function, is presented in Figure 5.12 for a parent particle of 1000 microns in length where $\gamma = 2.8$, $= 3.5$, and $\phi = 0.36$. For this example, the majority of particles produced are fines less than 100 microns in length. This correlation does not support all of the findings in this investigation; however, Austin's equation is applicable to the peaks less than 100 microns in length. To model the fragmentation seen in the experimental PSDs, the product function developed by Hill (1995)

$$b'_v(v,w) = \frac{pv^m(w-v)^{m+(m+1)(p-2)}[m+(m+1)(p-1)]!}{w^{pm+p-1}m![m+(m+1)(p-2)]!} \quad (5.4)$$

is used. A sample product function curve is presented in Figure 5.13 where p = 5 and m = 2. It is noted that this distribution yields very few particles smaller than 100 μm with most particles at ~500 μm. Breakage function determinations are based on the discretized number-based equation (Hill 1995)

$$\frac{d}{dt}N_i = \sum_{j=i+1}^{\infty} \beta_j b_{ij} S_j N_j - \delta_i S_i N_i \quad (5.5)$$

where b_{ij} is the breakage distribution function(attrition equation or product function). These breakage functions can be combined using

$$\frac{dN_i}{dt} = \left(\frac{dN_i}{dt}\right)_{attrition} + \left(\frac{dN_i}{dt}\right)_{fragmentation} \quad (5.6)$$

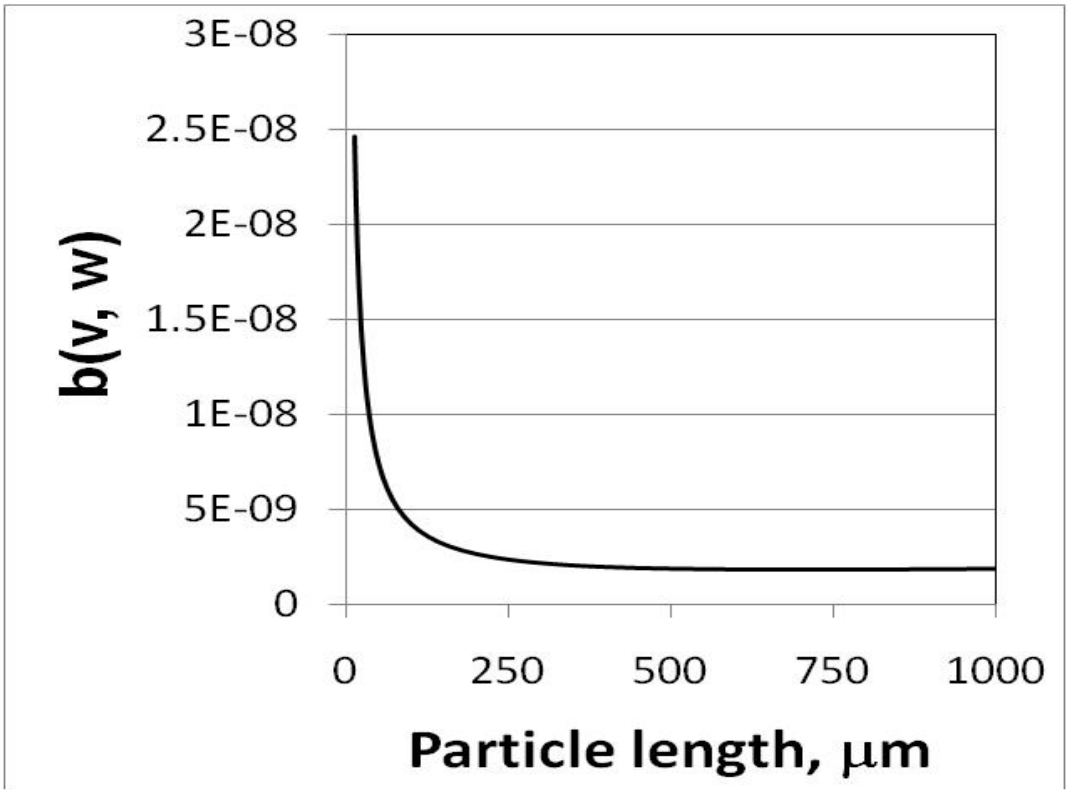

Figure 5.12 Simulation of Austin Attrition Function with β = 3.5, γ = 2.8, and ϕ = 0.36

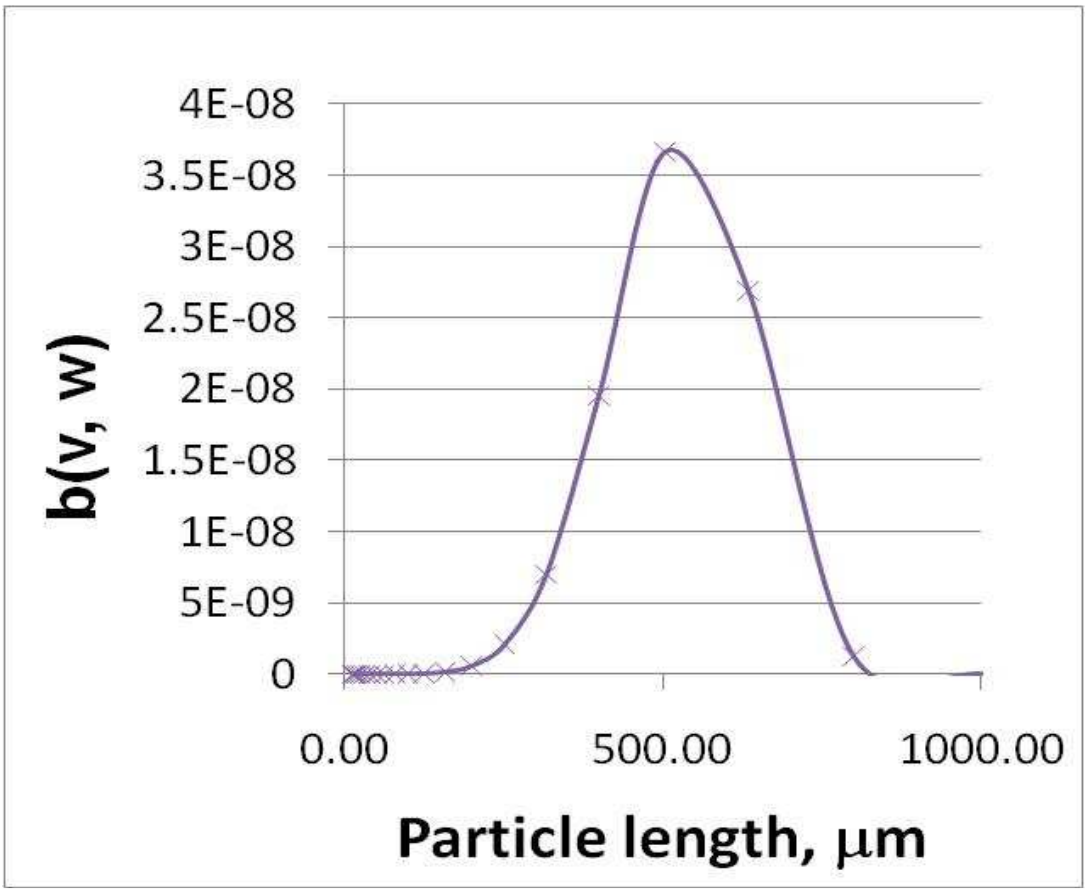

Figure 5.13 Simulation of Power Law Form of the Product Function with p = 5 and m =2

where $N_i(t)$ is the number of particles. The simulation parameters should match the experimental data at multiple residence times. While many sets of simulation parameters can produce the desired results at a single residence time, few sets can match the experimental data at multiple residence times.

To determine the error in the simulation results, the difference between the simulation number fraction, $n_{f_{i,sim}}$, and the experimental number fractions, $n_{f_{i,exp}}$, for each interval, z_i, was calculated.

$$z_i = n_{f_{i,sim}} - n_{f_{exp}} \tag{5.7}$$

The total error, z, was calculated for each experiment as

$$z = \sum_{i=1}^{n} (z_i{}^2) \tag{5.8}$$

where n is the total number of intervals, *i,* and interval errors are squared to eliminate negative differences in number fraction differences.

Modeling results for NaCl, potash alum, and KCl (in acetone) at 30 and 60 minutes was achieved with results presented in Figures 5.14 - 5.16. Modeling parameters are listed in Table 5.8. The results are a well shaped fit with few discrepancies. In Figure 5.15, modeling of potash alum crystals shows more significant error than NaCl modeling. KCl results are similar to those for NaCl. Overall, the proposed model represents a good fit of the experimental data although curves are not exact.

Agitation rate modeling was also conducted for the NaCl crystals. Agitation rates of 1000 rpm, 1500 rpm, and 2000 rpm are shown in Figures 5.17-5.19. Breakage rates, S_c ($v^{-\alpha}min^{-1}$), based on attrition and fragmentation are listed in Table 5.9 for each experiment and are graphed in Figure 5.20. As the agitation rate increases, an almost linear increase is seen in the fragmentation or product breakage rate while the attrition breakage shows positive curvature. The attrition rate of breakage is greater than the fragmentation rate of breakage as expected from experimental data.

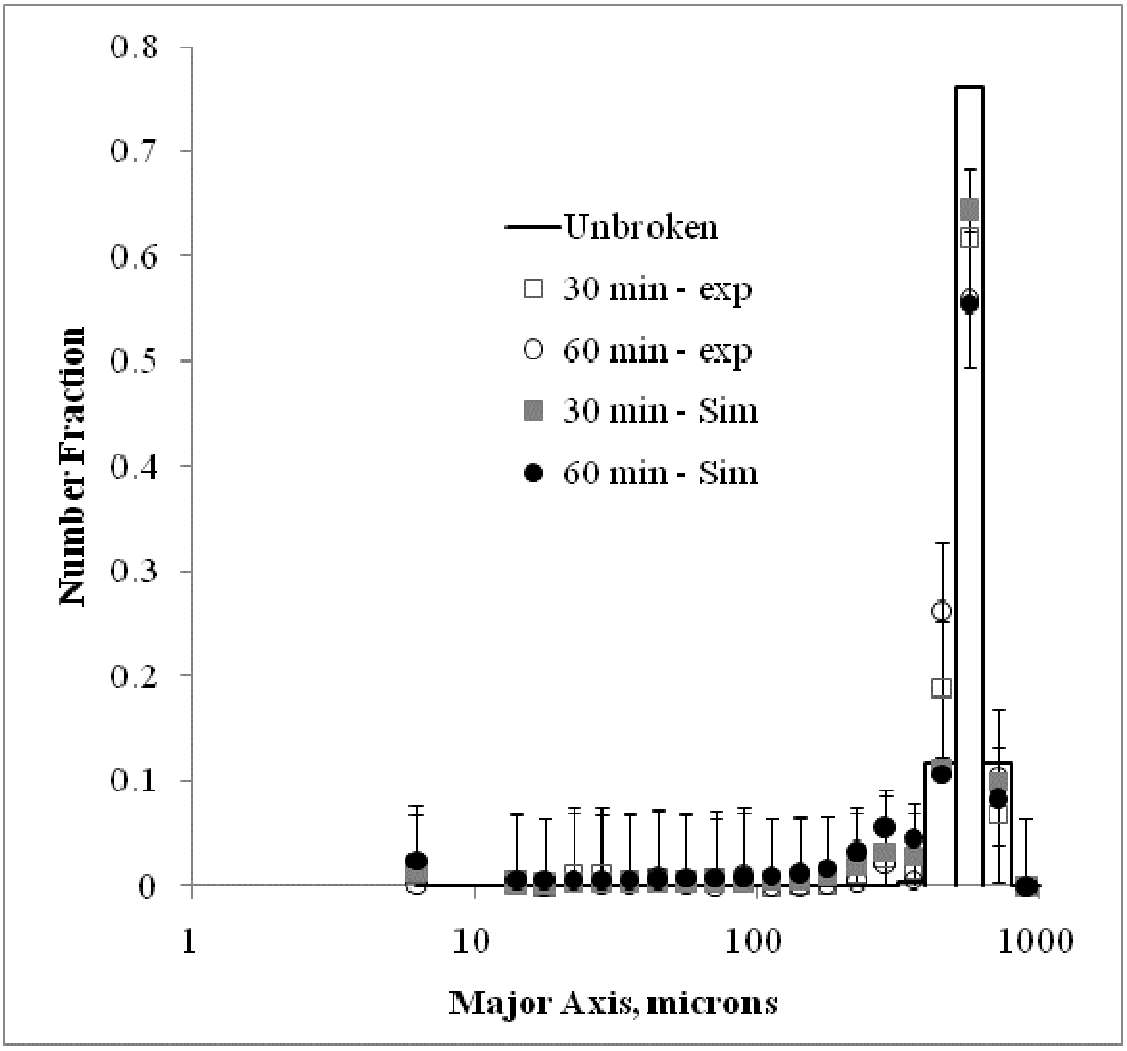

Figure 5.14 Modeling of Mesh 40 NaCl Crystal Breakage Agitated in Acetonitrile for 30 and 60 Minutes

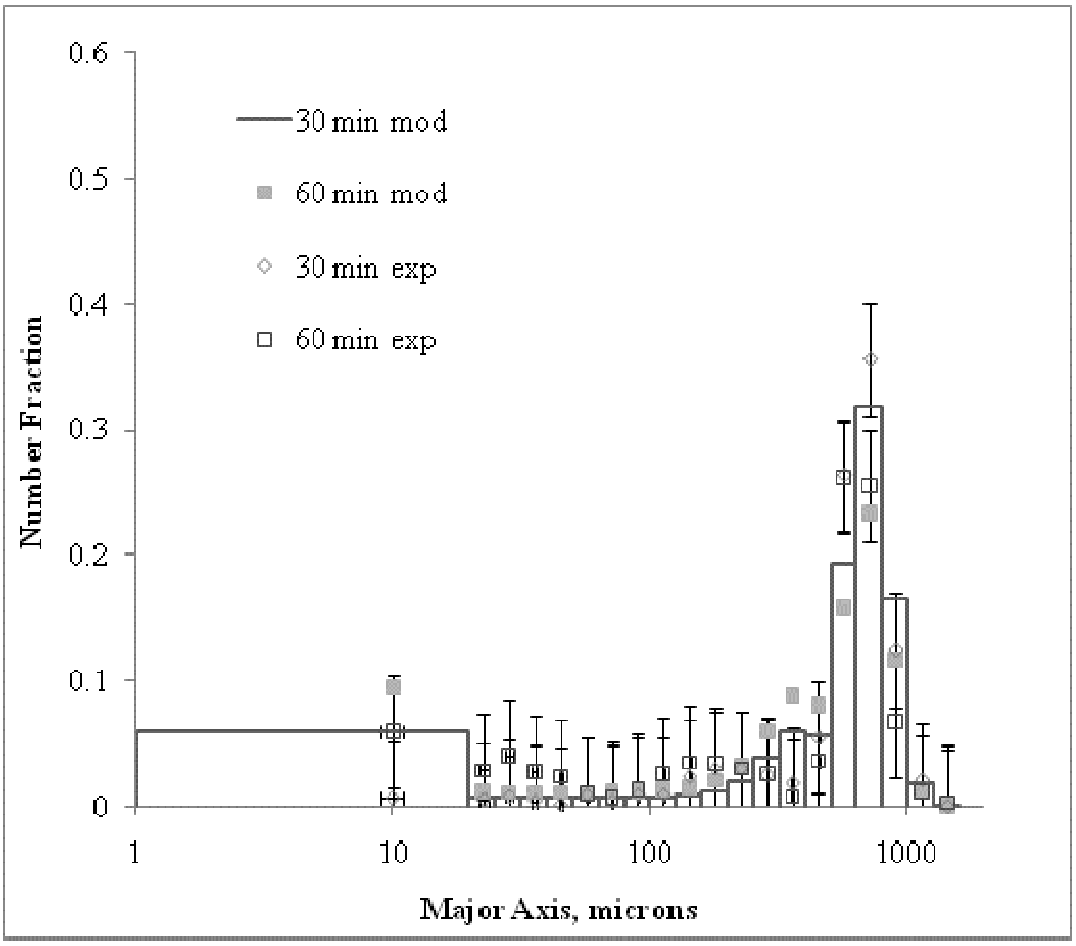

Figure 5.15 Modeling of Mesh 40 Potash Alum Crystal Breakage Agitated in Acetone for 30 and 60 Minutes

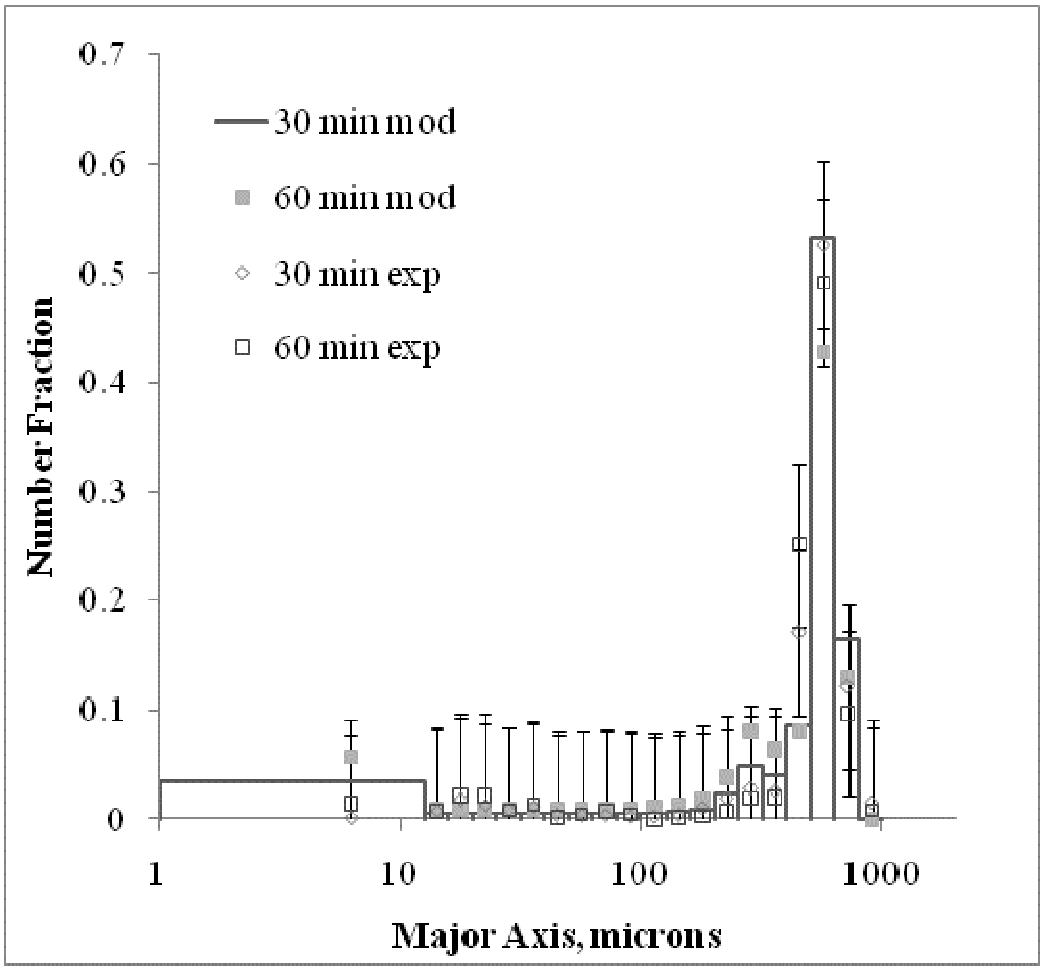

Figure 5.16 Modeling of Mesh 40 KCl Crystal Breakage Agitated in Acetone for 30 and 60 Minutes

Table 5.8 Breakage Function Parameters for NaCl, KCl, and Potash Alum

	Product Function				Attrition Function				
Crystal	$S_{c,10^7}$	α	p	m	□	γ	β	α	$S_{c,10^7}$
NaCl	0.8	0.5	5	2	0.36	3.1	3.8	0.35	5.0
KCl	0.9	0.5	5	3	0.36	2.8	3.5	0.33	6.0
Potash Alum	1.1	0.5	5	2	0.36	2.8	3.5	0.35	5.0

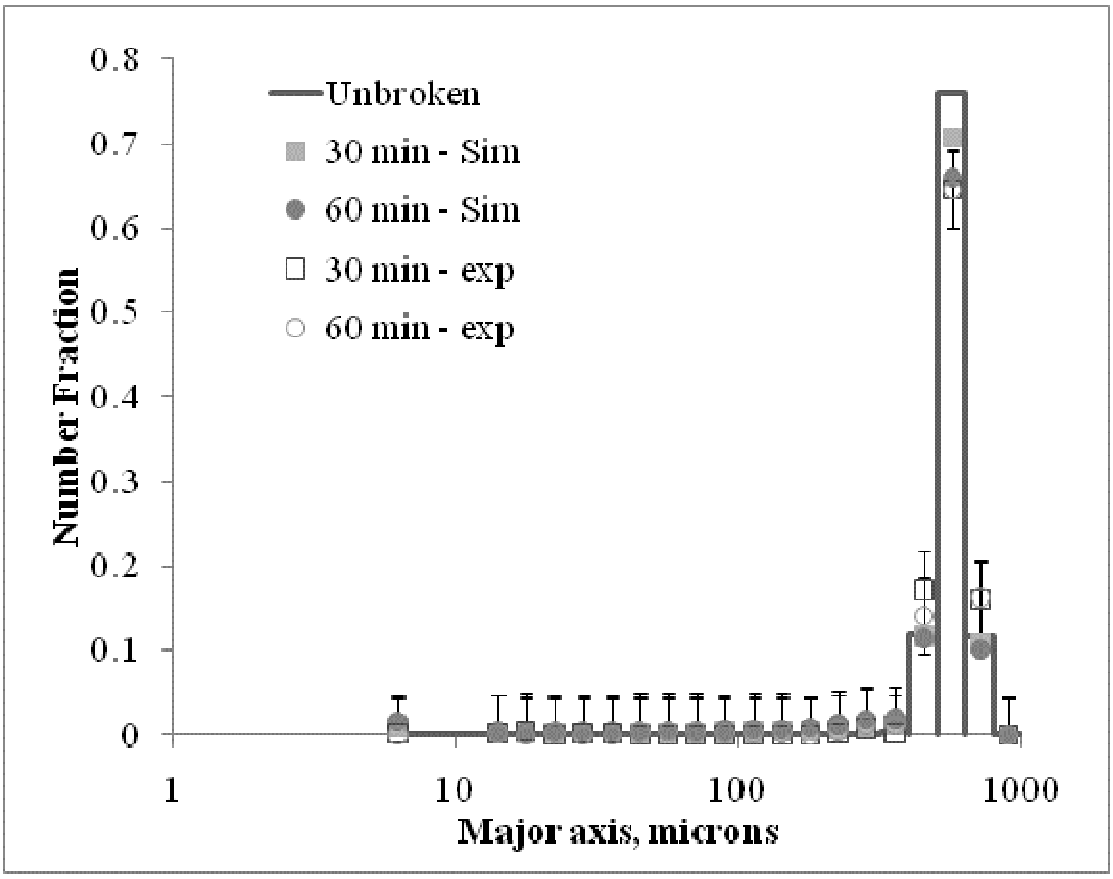

Figure 5.17 Modeling Results for NaCl Crystal Breakage in Acetonitrile at 1000 rpm for 30 and 60 Minutes

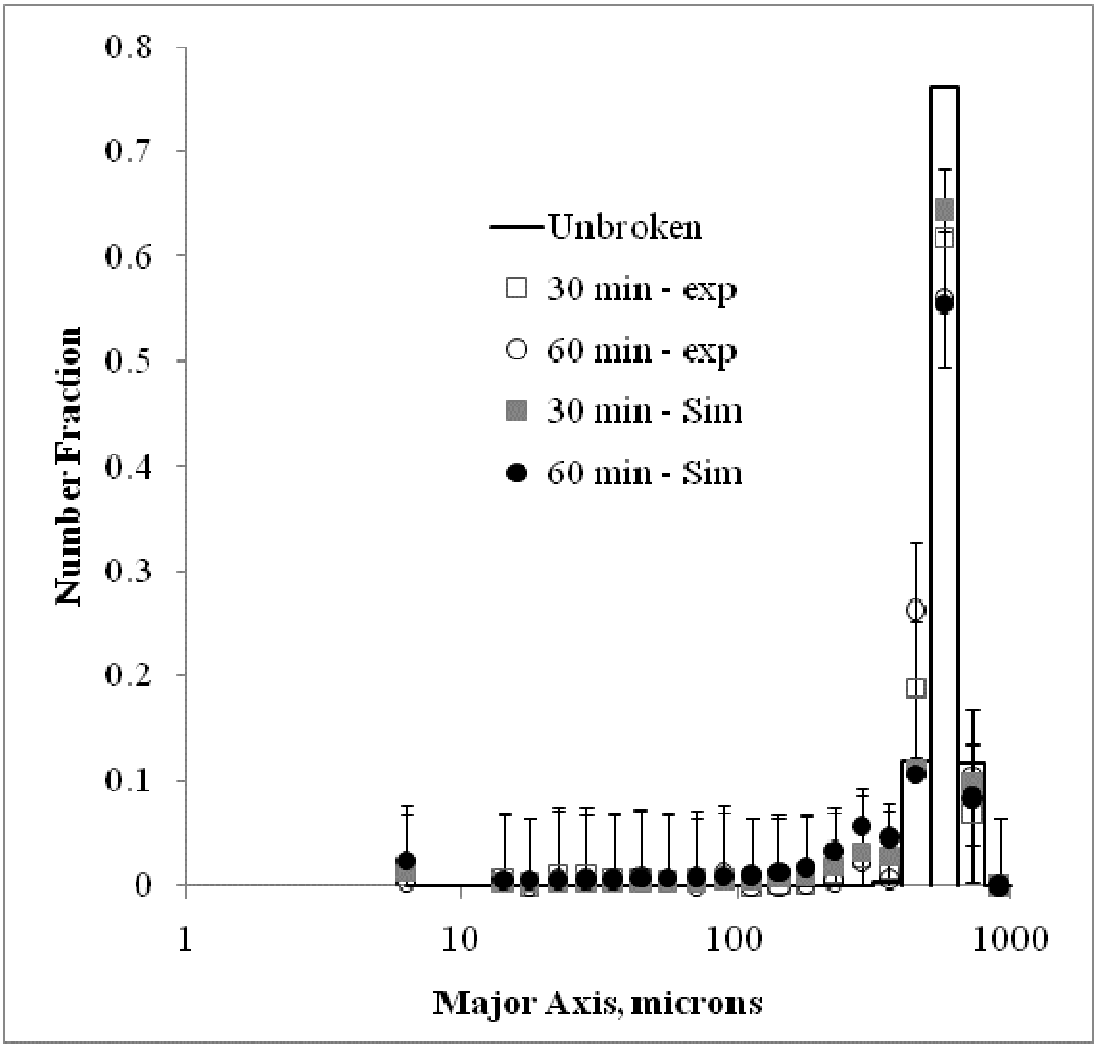

Figure 5.18 Modeling Results for NaCl Crystal Breakage in Acetonitrile at 1500 rpm for 30 and 60 Minutes

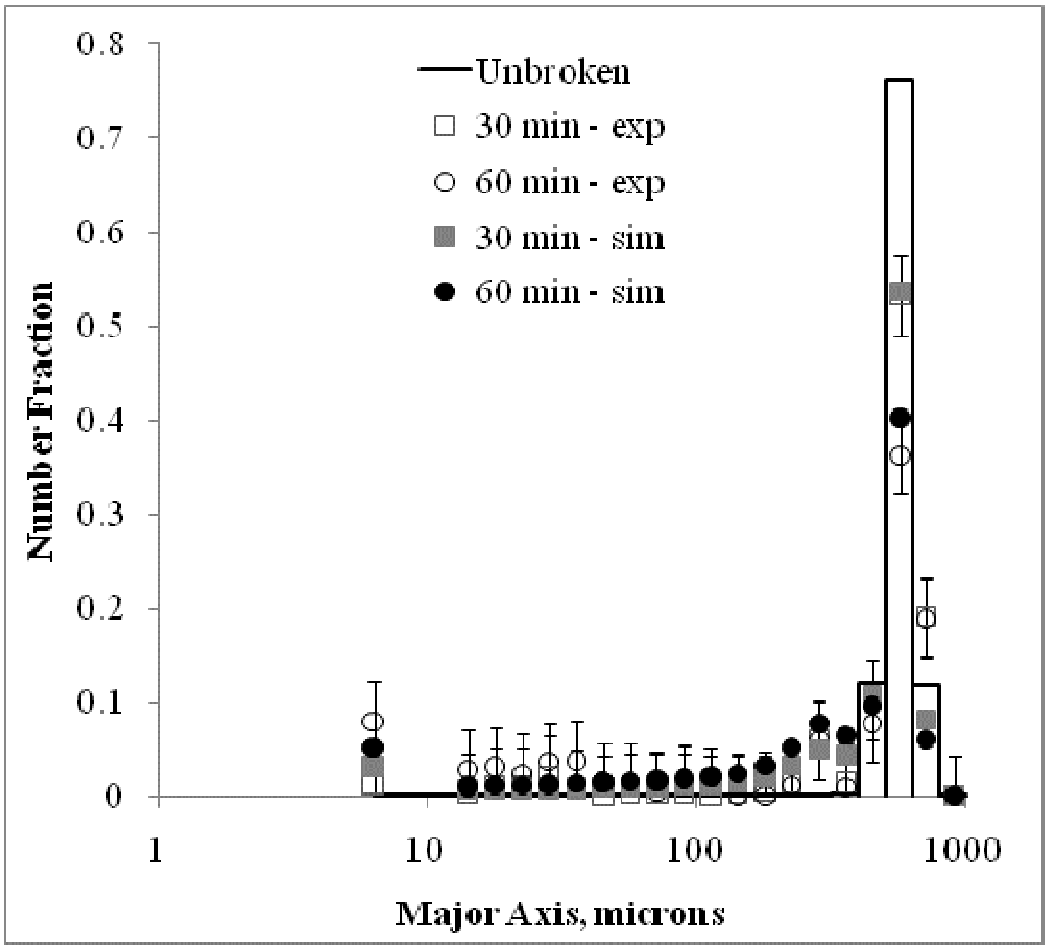

Figure 5.19 Modeling Results for NaCl Crystal Breakage in Acetonitrile at 2000 rpm for 30 and 60 Minutes

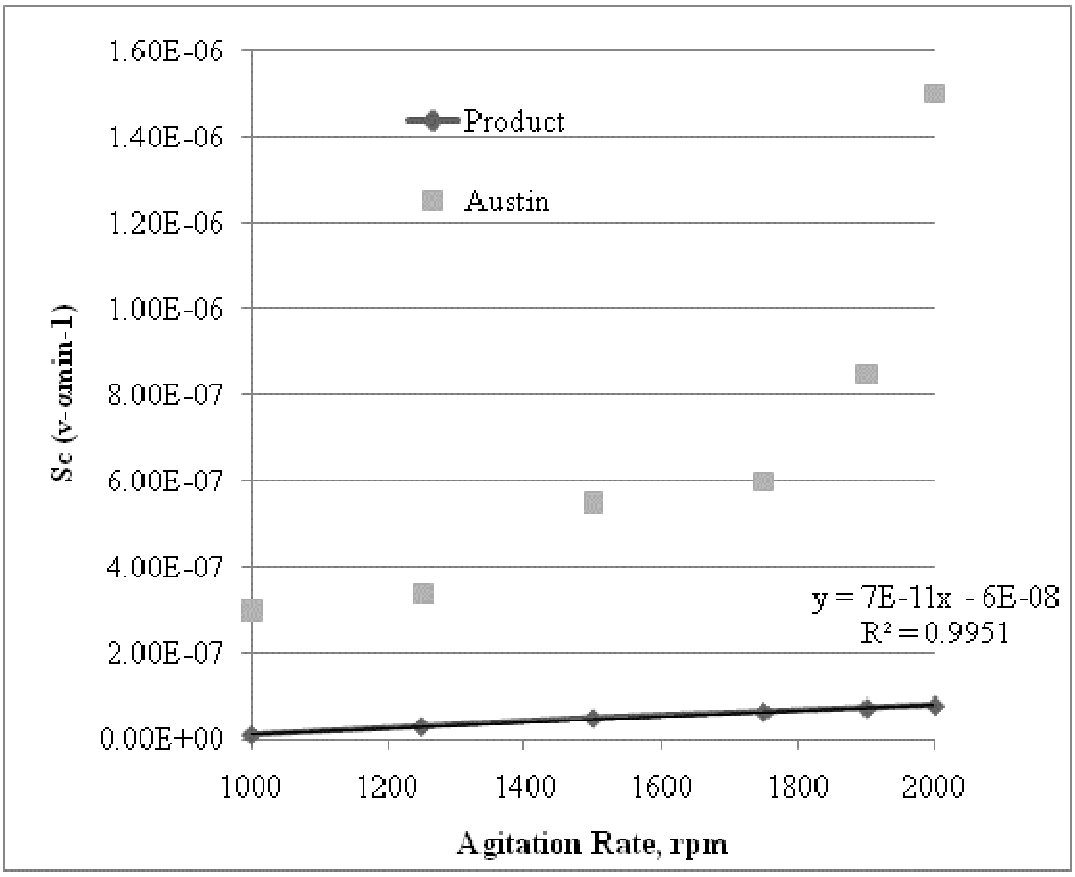

Figure 5.20 Attrition and Fragmentation Breakage Rates for NaCl Crystal Breakage Agitation Rate Investigation

Table 5.9 Attrition and Fragmentation Rate of Breakage Table for NaCl Crystal Breakage Agitation Experiments in Acetonitrile

RPM	Product	Austin
1000	1.00E-08	3.00E-07
1250	3.00E-08	3.40E-07
1500	5.00E-08	5.50E-07
1750	6.50E-08	6.00E-07
1900	7.40E-08	8.50E-07
2000	8.00E-08	1.50E-06

The difference between simulation and experimental values were calculated as error values, z_i, for each experiment. To achieve accuracy with the model, error should be minimized. Values for Σz_i^2 are presented in Table 5.10 for each NaCl attrition rate investigated in Chapter 4 and in Table 5.11 for the Mesh 40 NaCl, KCl (acetone), and potash alum comparison. The combined total error calculated for each NaCl agitation rate investigation was less than 0.043±0.003 and less than 0.055±0.002 for each material investigated. This value shows that each number fraction for each investigation is not exact; however, the resulting values are within 5.5% of simulation error. Based on the calculated error, significant differences exist in the modeling of each Mesh 40 crystal with the most significance existing for the 60 minute results. Only the 1500 rpm agitation rate simulation had a significant difference based on calculated error.

Table 5.10 Number Fraction Error Deviation Table for NaCl Crystal Breakage Agitation Experiments in Acetonitrile

Rate	30 min	60 min	Average	**Total**	Standard Deviation
1000 rpm	0.010	0.005	0.008	**0.015**	0.001
1250 rpm	0.001	0.030	0.015	**0.030**	0.002
1500 rpm	0.008	0.030	0.019	**0.038**	0.003
1750 rpm	0.003	0.013	0.008	**0.016**	0.001
1900 rpm	0.016	0.007	0.012	**0.023**	0.002
2000 rpm	0.015	0.028	0.022	**0.043**	0.003

Table 5.11 Number Fraction Error Deviation Table for Mesh 40 NaCl in ACTL, KCl in ACTE, and Potash Alum in ACTE

Crystal	30 min	60 min	Average	**Total**	Standard Deviation
NaCl	0.008	0.030	0.019	**0.038**	0.003
KCl (acetone)	0.011	0.044	0.028	**0.055**	0.004
Potash Alum	0.014	0.027	0.020	**0.040**	0.002

5.6 Conclusions

Adjusted agitation rates are commonly used to provide similar conditions for particle suspended in a vessel for various materials. Adjusting for material properties using Zwietering's correlation produced similar PSDs for KCl in acetone and KCl in acetonitrile. KCl crystals of the same parent particle size were tested in two nonsolvents, and the agitation rate was adjusted using the Zwietering correlation. Within experimental error, the results were the same. This finding showed that the Zwietering correlation did correct for differences in fluid properties. Other experiments with KCl and potash alum crystals with the same parent particle size showed definite differences. Since properties such as density and viscosity are accounted for by the Zwietering correlation, this demonstrates that the resulting PSD differences are due to a material's response to impact and is a function of a crystal's hardness and morphology. Furthermore, characteristics of the materials such as crystal geometry or number of sieve diameters may provide a reasonable justification for the differences in the particle size distributions. More research is needed to determine the relevance of multiple crystal characteristics on particle breakage.

Furthermore, the overall rate of breakage increased with agitation rate for NaCl. The fragmentation rate increased almost linearly while the attrition rate increase showed positive curvature. Lastly, modeling of crystal breakage is possible using a combination of Austin's attrition equation and the power law form of the product law form; however, such modeling is not precise.

5.7 References

Alum. *The Columbia Encyclopedia.* New York: Columbia UP, 2008. *Credo Reference*. 7 Nov. 2008. Web. 15 Jan. 2010. <http://www.credoreference.com/entry/columency/alum>.

Austin, L., Shoji, K., Bhatia, V., Jindal, V., and K. Savage (1976). Some Results on the Description of Size Reduction as a Rate Process in Various Mills. *Ind. Eng. Chem., Process Des. Dev., Vol. 15(1)*, 187-196.

Bravi, M., Di Cave, S., Mazzarotta, B., and N. Verdone (2003). Relating the attrition behavior of crystals in a stirred vessel to their mechanical properties. *Chem. Eng. J. Vol. 94*, 223-229.

Burgess, J. (1978). *Metal Ions in Solution*. Halsted Press, Horwood, NY.

Gahn, C., and A. Mersmann (1995). The brittleness of substances crystallized in industrial processes. *Powder Tech. Vol. 85*, 71-81.

Gahn, C. and A. Mersmann (1997). Theoretical Prediction and Experimental Determination of Attrition Rates. *Chem. Eng. Res. Design Vol. 75(2)*, 125-131.

Gahn, C., and A. Mersmann (1999a). Brittle fracture in crystallization processes Part A. Attrition and abrasion of brittle solids. *Chem. Eng. Sci. Vol.54,* 1273-1282.

Gahn, C., and A. Mersmann (1999b). Brittle fracture in crystallization processes Part B. Growth of fragments and scale-up of suspension crystallizers. *Chem. Eng. Sci. Vol. 54,* 1283-1292.

Gerstlauer, A., Mitrovic, A., Motz, S., and E.-D. Gilles (2001). A population model of crystallization processes using two independent particle properties. *Chem. Eng. Sci. Vol. 56*, 2553-2565.

Hill, P.J. and K.M. Ng (1995). New Discretization Procedure for the Breakage Equation. *AIChE J. Vol. 41(5)*, 1204-1216.

Hill, P. (2004), Statistics of Multiple Particle Breakage Accounting for Particle Shape. *AIChE J. Vol. 50(5)* 937-952.

Liley, P.E., Thomson, G.H., Friend, D.G., Daubert, T.E., and E. Buck. (1997). Physical and Chemical Data. In R.H. Perry and D.W. Green (Eds). *Perry's Chemical Engineers' Handbook 7th Ed.*, McGraw-Hill, New York, 2.1-2.144.

Mazzarotta, B. (1992). Abrasion and Breakage Phenomena in Agitated Crystal Suspensions. *Chem. Eng. Sci. Vol. 47(12)*, 3105-3111.

Mazzarotta, B., Di Cave, S., and G. Bonifazi (1996). Influence of Time on Crystal Attrition in a Stirred Vessel. *AIChE J. Vol. 42 (12)*, 3354-3558.

Mullin, J. W. (2001). *Crystallization 4th Ed*., Butterworth-Heinemann, Boston.

Potassium Chloride. *The Columbia Encyclopedia.* New York: Columbia UP, 2008. *Credo Reference*. 7 Nov. 2008. Web. 15 Jan. 2010. <http://www.credoreference.com/entry/columency/potassium_chloride>.

Tabor, D. (1956). The physical meaning of indentation and scratch hardness. *Br. J. Appl. Phys. Vol. 7*, 159-166.

Ulrich, J. and M. Kruse (1990). Hardness of Salts Used in Industrial Crystallization. In A.S. Myerson and K. Toyokura (Eds.). *Crystallization as a Separation Process*, *ACS Symposium Series Vol. 438*, 43-54.

Zwietering, T. N. (1958). Suspending Solid Particles in Liquids by Agitators. *Chem. Eng. Sci. Vol. 8*, 244-253.

CHAPTER VI

RESEARCH CONCLUSIONS

Although crystal breakage in stirred vessels has been previously studied, much is still unknown in the experimentation, analysis, and modeling of particle breakage. This work sought to 1) study aging effects on breakage experiments in saturated solutions, and 2) quantify crystal attribute effects on particle breakage in a stirred vessel. Comparison of parameters for previous research and this work are presented in Table 6.1-6.2.

The first focus of this research was to determine whether a saturated solution or a nonsolvent was optimal for breakage research. Using an NaCl aqueous saturated solution and acetonitrile as a nonsolvent, magma density and agitation rate were varied, and the two suspension fluids were compared. The particle size distribution of the saturated solution breakage was significantly different than that of the nonsolvent breakage in terms of magma density and agitation rate. The distributions have shown more fines production in saturated solution. Based on magma density values between 1 and 7 g/100 mL suspension fluid, the average child particle major axis was 60% larger in acetonitrile than in saturated solution. In both suspension fluids, the average child particle major axis decreased with increasing agitation rate for 60 minutes of agitation as expected. The mass fraction analysis of the child particles recovered has shown various number fraction production. Overall, the particle size distributions produced in saturated solutions

Table 6.1 Crystal Breakage in the Literature with this Work

Source	Crystals Examined	Crystal Habit	Size Range, microns	Laboratory Grown
Nienow and Conti, 1978	Copper Sulfate Nickel Ammonium Sulfate	Octahedral* Monoclinic*	1200-1800	Yes
Conti and Nienow, 1980	Nickel Ammonium Sulfate Hexahydrate	Monoclinic*	~1060	Yes
Offermann and Ulrich, 1982	Sodium Chloride	Cubic*	300-400	NR
Shamlou et. al, 1990	Potassium Sulfate	Orthorhombic*	Varied (600-1000)	Yes
Mazzarotta, 1992	Potassium Sulfate	Orthorhombic*	500-600, 1000-1180	Yes
Chianese et. al, 1993	Potassium Sulfate	Orthorhombic*	1000-1180	Yes
Synowiec et. al, 1993	Potassium Sulfate Potassium Aluminum Sulfate	Orthorhombic* Octahedral*	Varied (100-1000)	Yes
Mazzarotta, 1996	Sucrose	Monoclinic*	1180-1400	No
Bravi et al., 2003	Citric Acid Pentaerythritol Potassium Chloride Potassium Sulfate Sodium Chloride Sodium Perborate Sodium Sulphate Sucrose	Monoclinic Tetragonal Cubic Orthorhombic Cubic Dendritic Monoclinic Monoclinic	500-600 500-600 250-300 355-425 355-425 425-500 710-850 355-425	No
This Research (Part 1)	**Sodium Chloride**	**Cubic**	**Varied (250-3350)**	**No, Yes**
This Research (Part 2)	**Sodium Chloride**	**Cubic**	**425-600**	**No**
	Potassium Chloride	**Cubic**	**(250-425, 425-600)**	**No**
	Potassium Aluminum Sulfate Dodecahydrate	**Octahedral**	**Varied (425-2000)**	**No**

NOTE: * Obtained from Mullin, 2001. NR = Not recorded.

Table 6.2 Operating Conditions of Literature Breakage Research with this Work

Source	Agitation Rate, rpm	Suspension Density, kg/m3	Fluid	Time
Nienow and Conti, 1978	Varied (500-900)	Varied (88.5-265.5)	saturated solution (50/50 wt % water/methanol), nonsolvent (acetone)	Varied (0-24 hr.)
Conti and Nienow, 1980	420	88.5	saturated solution	Varied (0-48 hr.)
Offermann and Ulrich, 1982	Varied (0-1600)	Varied (0-510)	nonsolvent (acetone), aqueous saturated solution	5 sec.
Shamlou et. al, 1990	Varied (0-2000)	363	methanol (low solubility)	Varied (0-60 min.)
Mazzarotta, 1992	950, 1100	Varied (13.33-30.00)	saturated hydroalcoholic solution	Varied (0.5-10 hr.)
Chianese et. al, 1993	650	Varied (5-60)	saturated (methanol-water) solution, pure water	2 hr.
Synowiec et. al, 1993	NR	Varied (0-88)	saturated ethanol solution	2 hr.
Mazzarotta, 1996	1100	100	nonsolvent (xylene)	Varied (0-8 hr.)
Bravi et al., 2003	700* 600 800 1000 900 800 700 700	100	nonsolvent (xylene)	1 hr.
This Research (Part 1)	**Varied (0-2000)**	**Varied (10-100)**	**aqueous saturated solution, nonsolvent (acetonitrile)**	**Varied (0, 0.5, 1 hr.)**
This Research (Part 2)	**1500 (Adjusted**)**	**50**	**nonsolvent (acetonitrile)** **nonsolvent (acetonitrile, acetone)** **nonsolvent (acetone)**	**Varied (0, 0.5, 1 hr.)** **Varied (0, 0.5, 1 hr.)**

NOTE: * Agitation rates in this study are adjusted for off bottom clearance for each individual crystal presented in Table 2.4.**Rates adjusted based on 1500 rpm NaCl in acetonitrile.

differed significantly from the particle size distributions produced in nonsolvents. Although the Zwietering correlation was used to adjust the agitation rates to account for viscosity and density differences, the experiments in saturated solutions and acetonitrile still produced significantly different particle size distributions. Therefore, mechanisms such as aging or nucleation cannot be ignored in saturated solutions, which makes nonsolvents optimal for particle breakage research.

The second focus of this research was to study the effects of crystal attributes on breakage. The first part of this focus was to study a single material, NaCl. Based on optical observations, both attrition and fragmentation were determined to occur due to agitation in a stirred vessel. The degree of attrition or fragmentation is largely based on the initial size range of the particles and material properties. As the parent particle size decreased, fragmentation decreased. Furthermore, it is necessary to consider particle size distributions when analyzing the mass of child particles smaller than the original parent size since the size of the child particles can affect the mass of child particles recovered. Based on shape factor analysis, child particles smaller than the original unbroken size range did not become more rounded in any investigation. Instead, more irregularly shaped particles were noted in image analysis which could explain the filter plugging observed in industry.

The second part of the crystal attributes studies was to compare the breakage of the NaCl crystals with the breakage of other crystal compounds. Hydrodynamically similar conditions were needed to make comparisons between different materials and suspension fluids. Zwietering's correlation was given as a plausible method of adjustment since the correlation accounted for the properties of the solid, liquid, and vessel geometry as well. With adjusted agitation rates for differences in density and viscosity, similar

particle size distributions were seen for KCl in two nonsolvents, acetone and acetonitrile, which proved that a change in nonsolvent had no significant effect on the particle size distribution. However, a comparison of KCl and potash alum crystal breakage of similar parent particle size revealed significantly different particle size distributions. The differences suggest that a crystal's properties, such as morphology and hardness, will alter the particle size distribution after agitation adjustment. Zwietering's correlation provided a basis for adjusting agitation rates to produce similar PSDs; however, this method requires modifications that account for the initial particle size or the geometry of the crystal such as shape factors.

The final part of the crystal attributes study was modeling the particle breakage that occurred due to agitation in a stirred vessel. Since attrition and fragmentation occur in a stirred vessel, each mechanism was represented in the population balance equation with Austin's equation for attrition and the power law form of the product function for fragmentation. Overall, the rate of breakage increased with agitation rate for NaCl as was expected. Both the attrition and fragmentation rates increased with increasing agitation; however, the fragmentation rate increase was almost linear while the attrition rate increase had positive curvature. The proposed equation with Austin's equation for attrition and the power law function for fragmentation proved applicable with an error of 4.3% for the agitation rate model and up to a maximum error of 5.5% for each individual crystal compound investigation; however, simulations were not exact. More experimentation is needed to validate proposed model of a combination of Austin's equation and the power law form of the product function.

Based on this research, several areas of investigation remain in the area of particle breakage and modeling. These possible areas for future researchers include:

- Breakage experiments with crystals of various geometric shapes including plates and needles. Experimentation in this area should focus more on shape factor modeling.
- Breakage experiments based on the number of corners and the maximum sieve diameters presented by a single crystal form.
- Breakage experiments that improve Zwietering's correlation as it pertains to the representation of particle suspension in stirred vessels by adjusting agitation rates.
- Comprehensive breakage study of KCl to compare with the breakage results of NaCl.

6.1 References

Bravi, M., Di Cave, S., Mazzarotta, B., and N. Verdone (2003). Relating the attrition behavior of crystals in a stirred vessel to their mechanical properties. *Chem. Eng. J. Vol. 94*, 223-229.

Chianese, A., Di Berardino, F., and A.G. Jones (1993). On the Effect of Secondary Nucleation on the Crystal Size Distribution from a Seeded Batch Crystallizer. *Chem. Eng. Sci. Vol. 48(3)*, 551-560.

Conti, R. and A.W. Nienow (1980). Particle abrasion at high solids concentration in stirred vessels-II. *Chem. Eng. Sci. Vol. 35*, 543-547.

Mazzarotta, B. (1992). Abrasion and Breakage Phenomena in Agitated Crystal Suspensions. *Chem. Eng. Sci. Vol. 47(12)*, 3105-3111.

Mazzarotta, B., Di Cave, S., and G. Bonifazi (1996). Influence of Time on Crystal Attrition in a Stirred Vessel. *AIChE J. Vol. 42 (12)*, 3354-3558.

Mullin, J. W. (2001). *Crystallization 4th Ed*., Butterworth-Heinemann, Boston.

Nienow, A. W., and R. Conti (1978). Particle abrasion at high solids concentration in stirred vessels. *Chem. Eng. Sci. Vol. 33*, 1077-1086.

Offermann, H. and J. Ulrich (1982). On the Mechanical Attrition of Crystals. In S.J. Jancic and E.J. de Jong (Eds.). *Industrial Crystallization 81*, North-Holland, New York, 313-314.

Shamlou, P.A., Jones, A. G., and K. Djamarani (1990). Hydrodynamics of Secondary Nucleation in Suspension Crystallization. *Chem. Eng. Sci. Vol. 45(5)*, 1405-1416.

Synowiec, P., Jones, A.G., and P. Ayazi Shamlou (1993). Crystal Break-Up in Dilute Turbently Agitated Suspensions. *Chem. Eng. Sci. Vol. 48(20)*, 3485-3495.

APPENDIX A

MATERIAL PROPERTIES

A.1 Suspension Fluid Properties

Table A.1 Properties of Suspension Fluids

Liquids	Formula	MW	ρ, g/cm^3	μ, cP
Aqueous NaCl Saturated Solution	$NaCl/H_2O$		1.200	2.00
Acetone	CH_3COCH_3	58.08	0.792	0.34
Acetonitrile	CH3CN	41.05	0.781	0.38
Water	H_2O	18.02	0.998	1.00

NOTE: Molecular weight (MW) values were obtained from Smith et. al (2001). Density and viscosity values were obtained from Liley (1997). Saturated solution density is recorded in Mullin (2001). Kinematic viscosities in Table A.2 were calculated using the following equation.

$$\nu\left(\frac{m^2}{s}\right) = \mu\left(\frac{kg}{m*s}\right)/\rho\left(\frac{kg}{m^3}\right) \quad \text{(A.1)}$$

Table A.2 Kinematic Viscosity Table

Liquids	ρ, g/cm^3	ρ, kg/m^3	μ, cP	μ, kg/(m*s)	ν, m^2/s
Aqueous NaCl Saturated Solution	1.200	1200	2.00	0.002	1.667E-06
Acetone	0.792	792	0.34	0.00034	4.293E-07
Acetonitrile	0.781	781	0.38	0.00038	4.866E-07
Water	0.998	998	1.00	0.001002	1.004E-06

Suspension fluid testing results are presented in Table A.3 for water, saturated solution, and acetonitrile. All values were relatively similar to those reported in the literature (Liley, 1997). It is important that density readings remain constant to ensure a fully saturated product. The average density reading for all saturated solution (SS) runs was 1.20 ± 0.001 g/cm^3 before and after experimentation.

Table A.3 Density Measurements of Suspension Fluids

Suspension Fluid	Injection #	ρ_{exp}	ρ_{lit}
Water (Reference)	1	0.9983	0.99823
	2	0.9983	
	3	0.9983	
	4	0.9983	
Aqueous Saturated Solution (NaCl)	1	1.2008	1.200
	2	1.2009	
	3	1.2009	
	4	1.2009	
Acetonitrile	1	0.7821	0.781
	2	0.782	
	3	0.7821	
	4	0.7822	

A.2 Solid Properties

Table A.4 Properties of Crystals

Solids	Formula	MW	ρ, g/cm^3	ρ, kg/m^3	Crystal Habit
Sodium Chloride	NaCl	56.45	2.168	2168	Face Centered Cubic
Potassium Chloride	KCl	74.55	1.980	1980	Face Centered Cubic
Potassium Aluminum Sulfate	$KAl(SO_4)_2 \cdot 12(H_2O)$	258.2	1.760	1760	Octahedral

NOTE: Molecular weight (MW), density values, and crystal structures were obtained from Mullin (2001).

Table A.5 Solubility Table of Crystals (T = 20°C)

Solids	Solubility, g crystals/100g solvent	Solvent
Sodium Chloride	35.8	Water
	0.0003	Acetonitrile
	0.000042	Acetone
Potassium Chloride	36.0	Water
	0.0024	Acetonitrile
	0.000091	Acetone

References

Liley, P.E., Thomson, G.H., Friend, D.G., Daubert, T.E., and E. Buck. (1997). Physical and Chemical Data. In R.H. Perry and D.W. Green (Eds). *Perry's Chemical Engineers' Handbook 7th Ed.*, McGraw-Hill, New York, 2.1-2.144.

Mullin, J. W. (2001). *Crystallization 4th Ed*., Butterworth-Heinemann, Boston.

Smith, J.M., Van Ness, H.C., and M.M. Abbot (2001). *Introduction to Chemical Engineering Thermodynamics 6th Ed.* McGraw-Hill, Boston, 654-655.

APPENDIX B

VESSEL PROPERTIES

B.1 Vessel Dimensions and Schematic

Vessel and Stirrer Dimensions:

C = 1.5 cm = 0.015 meters

T = 4.0 inches = 0.1016 meters

D = 2.0 inches = 0.0508 meters

Vessel: One Liter Open Beaker

Covering: Parafilm

Motor: Min. Speed - 50 rpm

Max Speed - 2000 rpm

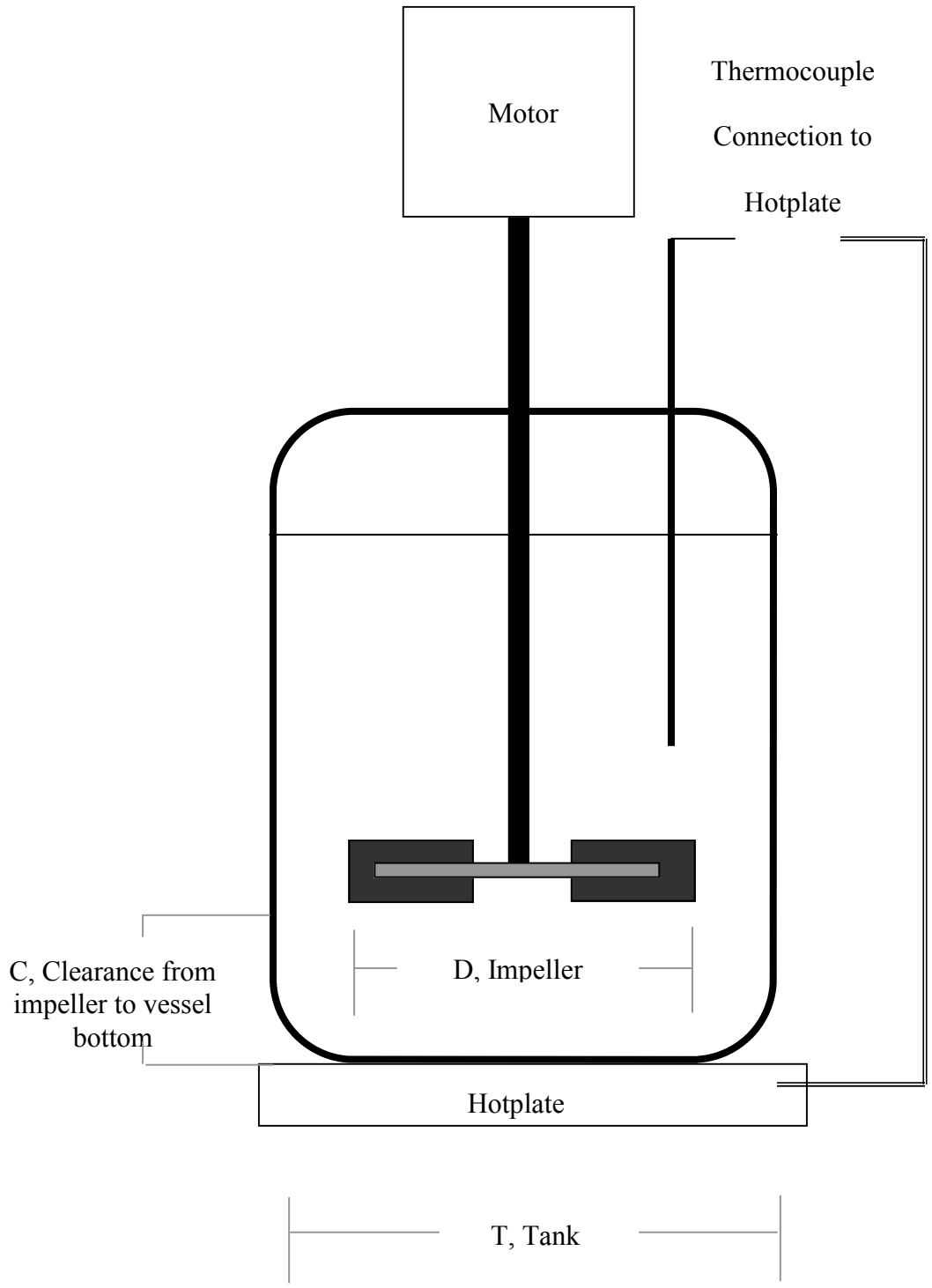

Figure B.1 Schematic of Breakage System

APPENDIX C

SUSPENSION CALCULATIONS

C.1 Suspension Calculations

C.1.1 System Constants

In all of the following cases,

T = 20°C

g = 9.81 m/s^2

S = 5.2 (Mersmann 2001)

Magma Density (MD) = 5 g crystals / 100 mL liquid

Suspension Equations (Zwietering 1958, Mersmann 2001):

$$N_{js} = S\frac{v^{0.1}\mathrm{d_p}^{0.2}\left(\frac{g*\Delta\rho}{\rho_L}\right)^{0.45}\chi^{0.13}}{D^{0.85}} \quad \text{(C. 1)}$$

$$S\ (\mathrm{T}, \mathrm{C}, \mathrm{D}) = 5.2$$

$$\chi = \frac{grams\ of\ solid\ particles}{grams\ of\ mother\ liquor} \times 100 \quad \text{(C. 2)}$$

References

Mersmann, A. (2001). *Crystallization Technology Handbook 2nd Ed*., Marcel Dekker, Inc., New York.

Zwietering, T. N. (1958). Suspending Solid Particles in Liquids by Agitators. *Chem. Eng. Sci. Vol. 8*, 244-253.

C.1.2 Just Suspended NaCl Mesh 40 Particles Calculation

For Mesh 40 NaCl particles,

$$d_p = 425\ \mu m = 4.25 \times 10^{-4}\ m$$

for this example. Therefore,

$$\chi = \frac{25\ g\ NaCl}{393.5\text{g acetonitrile}} \times 100 = 6.353$$

and Zwietering equations becomes

$$N = (5.2)\frac{\left(4.866 \times 10^{-7}\frac{m^2}{s}\right)^{0.1}(4.25 \times 10^{-4}\text{m})^{0.2}\left(\frac{9.81\frac{\text{m}}{\text{s}^2} * (2.168 - 0.781)\frac{\text{g}}{\text{cm}^3}}{(0.781)\frac{\text{g}}{\text{cm}^3}}\right)^{0.45}(6.353)^{0.13}}{(0.0508m)^{0.85}}$$

$$N = \frac{(5.2)(0.000425\ m)^{0.02}\left(4.866 \times \frac{10^{-7}m^2}{\text{s}}\right)^{0.1}\left[\left(9.81\frac{m}{s^2}\right)(1.769)\right]^{0.45}(1.272)}{(0.0508m)^{0.85}}$$

$$N = (5.2)\frac{(0.2117m^{0.2})\left(0.2336\frac{m^{0.2}}{s^{0.1}}\right)\left(3.593\frac{m^{0.45}}{s^{0.9}}\right)(1.272)}{(0.0794)\ m^{0.85}}$$

$$N = 14.79\ rps = 888\ rpm$$

C.1.3 Adjusted Agitation Rate Calculations

The reference for calculations is Mesh 40 NaCl crystals suspended in acetonitrile agitated at 1500 rpm or 25 rps.

C.1.3.1 Mesh 40 KCL Particles in Acetonitrile

$$N_{KCl} = N_{NaCl} \frac{v_{ACTL} d_{40}^{0.2} \left(\frac{\rho_{NaCl} - \rho_{ACTL}}{\rho_{ACTL}}\right)^{0.45} \chi_{ACTL}^{0.13}}{v_{ACTL}\, d_{40}^{0.2} \left(\frac{\rho_{KCl} - \rho_{ACTL}}{\rho_{ACTL}}\right)^{0.45} \chi_{ACTL}^{0.13}} \quad \text{(C. 3)}$$

Since the viscosity and the volume (grams) of acetonitrile do not change and the size of the particles under analysis are the same, the viscosity, particle diameter, and particle loading terms in Eq. C.3 are constants are cancelled out in Eq. C.4 producing the following relationship.

$$N_{KCl} = N_{NaCl} \frac{\left(\frac{\rho_{NaCl} - \rho_{ACTL}}{\rho_{ACTL}}\right)^{0.45}}{\left(\frac{\rho_{KCl} - \rho_{ACTL}}{\rho_{ACTL}}\right)^{0.45}} \quad \text{(C. 4)}$$

Since density units cancel and inserting the agitation rate and material densities, the Eq. C.4 becomes

$$N_{KCl} = 25\ rps \frac{\left(\frac{2.168-0.781}{0.781}\right)^{0.45}}{\left(\frac{1.98-0.781}{0.781}\right)^{0.45}}.$$

Thus, the agitation rate for KCl particles in acetonitrile is

$$N_{KCl} = 25\ rps \left(\frac{1.294}{1.213}\right)$$

$$N_{KCl_{40}} = 26.67\ rps \approx 1600\ rpm.$$

C.1.3.2 Mesh 60 KCl Particles in Acetonitrile

For a different particle size, the particle diameter term is replaced in the Eq. C.5.

$$N_{KCl} = N_{NaCl} \frac{d_{p40}^{0.2} \left(\frac{\rho_{NaCl} - \rho_{ACTL}}{\rho_{ACTL}}\right)^{0.45}}{d_{p60}^{0.2} \left(\frac{\rho_{KCl} - \rho_{ACTL}}{\rho_{ACTL}}\right)^{0.45}} \tag{C. 5}$$

$$N_{KCl} = 25\, rps \frac{(4.25 \times 10^{-4} m)^{0.2} \left(\frac{2.168 - 0.781}{0.781}\right)^{0.45}}{(2.50 \times 10^{-4} m)^{0.2} \left(\frac{1.98 - 0.781}{0.781}\right)^{0.45}}$$

$$N_{KCl} = 25\, rps \left(\frac{0.2117}{0.1904}\right)\left(\frac{1.294}{1.213}\right)$$

The agitation rate for Mesh 60 KCL particles in acetonitrile is

$$N_{KCl_{60}} = 29.65\, rps \approx 1780\, rpm.$$

C.1.3.3 Mesh 30 Potash Alum Particles in Acetone

For potash alum crystals, the suspension fluid was acetone; therefore, the terms for particle loading and viscosity are reintroduced to in the following equation.

$$N_{PA_{30}} = N_{NaCl_{40}} \frac{v_{ACTL}^{0.1} d_{p40}^{0.2} \left(\frac{\rho_{NaCl}-\rho_{ACTL}}{\rho_{ACTL}}\right)^{0.45} \chi_{ACTL}^{0.13}}{v_{ACTE}^{0.1} d_{p30}^{0.2} \left(\frac{\rho_{PA}-\rho_{ACTE}}{\rho_{ACTE}}\right)^{0.45} \chi_{ACTE}^{0.13}} \quad \text{(C. 6)}$$

To account for acetone properties, the particle loading for 25g crystals was determined as follows.

$$\chi_{\text{ACTE}} = \frac{25\ g\ crystals}{396\text{g ACTE}} \times 100 = 6.313$$

$$N_{PA_{30}} = 25\ rps \frac{\left(4.866 \times 10^{-7} \frac{m^2}{s}\right)^{0.1} (4.25 \times 10^{-4} m)^{0.2} \left(\frac{2.168-0.781}{0.781}\right)^{0.45} (6.353)^{0.13}}{\left(4.293 \times 10^{-7} \frac{m^2}{s}\right)^{0.1} (6.00 \times 10^{-4} m)^{0.2} \left(\frac{1.76-0.792}{0.792}\right)^{0.45} (6.313)^{0.13}}$$

$$N_{PA_{30}} = 25\ \text{rps} \frac{(0.2336)(0.2117)(1.294)(1.272)}{(0.2308)(0.2268)(1.095)(1.271)}$$

$$N_{PA_{30}} = 25\,rps\,\left(\frac{0.0814}{0.0729}\right)$$

$$N_{PA_{30}} = 27.93\,rps\;\approx 1680\,rpm$$

C.1.3.4 For Mesh 20 Potash Alum Particles in Acetone

$$N_{PA_{20}} = N_{NaCl_{40}} \frac{v_{ACTL}^{0.1} d_{p_{40}}^{0.2} \left(\frac{\rho_{NaCl} - \rho_{ACTL}}{\rho_{ACTL}}\right)^{0.45} \chi_{ACTL}^{0.13}}{v_{ACTE}^{0.1} d_{p_{20}}^{0.2} \left(\frac{\rho_{PA} - \rho_{ACTE}}{\rho_{ACTE}}\right)^{0.45} \chi_{ACTE}^{0.13}}$$

$$N_{PA_{20}} = 25\ rps \frac{\left(4.866 \times 10^{-7} \frac{m^2}{s}\right)^{0.1} (4.25 \times 10^{-4} m)^{0.2} \left(\frac{2.168 - 0.781}{0.781}\right)^{0.45} (6.353)^{0.13}}{\left(4.293 \times 10^{-7} \frac{m^2}{s}\right)^{0.1} (8.5 \times 10^{-4} m)^{0.2} \left(\frac{1.76 - 0.792}{0.792}\right)^{0.45} (6.313)^{0.13}}$$

$$N_{PA_{20}} = 25\ \text{rps} \frac{(0.2336)(0.2117)(1.294)(1.272)}{(0.2308)(0.2432\ )(1.095)(1.271)}$$

$$N_{PA_{20}} = 25\ rps\ \left(\frac{0.0814}{0.0781}\right)$$

$$N_{PA_{20}} = 26.06\ rps\ \approx 1560\ rpm$$

C.1.3.5 Mesh 40 KCl Particles in Acetone

$$N_{KCl_{40}} = N_{NaCl_{40}} \frac{v_{ACTL}^{0.1} \left(\frac{\rho_{NaCl} - \rho_{ACTL}}{\rho_{ACTL}}\right)^{0.45} \chi_{ACTL}^{0.13}}{v_{ACTE}^{0.1} \left(\frac{\rho_{KCl} - \rho_{ACTE}}{\rho_{ACTE}}\right)^{0.45} \chi_{ACTE}^{0.13}}$$

$$N_{KCl_{40}} = 25\ rps \frac{\left(4.866 \times 10^{-7} \frac{m^2}{s}\right)^{0.1} \left(\frac{2.168 - 0.781}{0.781}\right)^{0.45} (6.353)^{0.13}}{\left(4.293 \times 10^{-7} \frac{m^2}{s}\right)^{0.1} \left(\frac{1.98 - 0.792}{0.792}\right)^{0.45} (6.313)^{0.13}}$$

$$N_{KCl_{40}} = 25\ \text{rps} \frac{(0.2336)(1.294)(1.272)}{(0.2308)(1.200)(1.271)}$$

$$N_{KCl_{40}} = 25\ rps\ \left(\frac{0.3845}{0.3520}\right)$$

$$N_{KCl_{40}} = 27.31\ rps\ \approx 1640\ rpm$$

C.1.3.6 Mesh 60 KCl Particles in Acetone

$$N_{KCl_{60}} = N_{NaCl_{40}} \frac{v_{ACTL}^{0.1} d_{p_{40}}^{0.2} \left(\frac{\rho_{NaCl} - \rho_{ACTL}}{\rho_{ACTL}}\right)^{0.45} \chi_{ACTL}^{0.13}}{v_{ACTE}^{0.1} d_{p_{60}}^{0.2} \left(\frac{\rho_{KCl} - \rho_{ACTE}}{\rho_{ACTE}}\right)^{0.45} \chi_{ACTE}^{0.13}}$$

$$N_{KCl_{60}} = 25\ rps \frac{\left(4.866 \times 10^{-7} \frac{m^2}{s}\right)^{0.1} (4.25 \times 10^{-4} m)^{0.2} \left(\frac{2.168 - 0.781}{0.781}\right)^{0.45} (6.353)^{0.13}}{\left(4.293 \times 10^{-7} \frac{m^2}{s}\right)^{0.1} (2.5 \times 10^{-4} m)^{0.2} \left(\frac{1.98 - 0.792}{0.792}\right)^{0.45} (6.313)^{0.13}}$$

$$N_{KCl_{60}} = 25\ \text{rps} \frac{(0.2336)(0.2117)(1.294)(1.272)}{(0.2308)(0.1904\ )(1.200)(1.271)}$$

$$N_{KCl_{60}} = 25\ rps\ \left(\frac{0.0814}{0.0670}\right)$$

$$N_{KCl_{60}} = 30.37\ rps\ \approx 1820\ rpm$$

APPENDIX D

IMAGE ACQUISITON AND ANALYSIS PROCEDURE

D.1 Image Acquisition

- Begin by turning on camera and/or microscope and opening Image-Pro Plus or DINOlite software on the computer.
- Place slide with sample on the microscope stand.
- To capture an image using Image-Pro Plus, click on the camera icon on the toolbar. A new window will open with image acquisition tools. Click PREVIEW in the top left hand corner of the new window. A live view of the sample will appear in a new window. Position slide and adjust microscope if necessary.
- Before taking image, click MORE in the bottom right corner. This button reveals more of the window. In the middle of the right side, click on the IMAGE tab. Under the tab, select whether a new ACTIVE IMAGE or SAVE IMAGE AS in this section. If SAVE IMAGE AS is selected, choose where to save by clicking the BROWSE button. Once a prefix and file location are chosen, click OK. When ready, click SNAP in the top left corner to take the image.
- To capture an image using DINOlite, simply click on the screen showing the preview of the sample. To save images, go to MY DOCUMENTS on the computer and select PICTURES. Next, double click on DIGITAL MICROSCOPE. Select the images and move to the appropriate file.

D.2 Image-Pro Plus Analysis Directions

- To begin, click on the OPEN FOLDER icon on the toolbar. From the folder containing the images, select 15 images to analyze (Note: Do not attempt to open more than 15 images or the software will crash. The 15 images are normally already aligned in the window. Just select the first column of images by clicking on the first image, holding down SHIFT key, and selecting the last file in the first column.). Click OPEN. All images will open simultaneously.
- Next, click PROCESS on the toolbar and select TILE IMAGES. A pop-up window will appear. (NOTE: During analysis DO NOT close any pop-up windows to save time of analysis.) Click the ALL>> button and select a grid of 1 x 15. (Selection of other grid types is not advised. All grids should be in the form of 1 x L with L being a number between 1 - 15.) Click APPLY. A new image will appear with the previously opened 15 images in one long image. The previous images are closed at this time.
- It is extremely important to select the calibration of the lenses used to take the image. (Calibration should be performed at least once a month on both apparatus to ensure accuracy of results and consistency between each device.) To select calibration, move mouse to the bottom right corner of the home screen and double click on the image specifications listed in black font. Select the appropriate calibration. (NOTE: In most cases, it is easier to name calibrations with lens type, i.e. 2x, 4x, 10x.)
- To select which parameters to measure, click on MEASURE on the toolbar of the home page. Select COUNT/SIZE in the new pop-up window. In the new window,

click on MEASUREMENTS. Highlight the need measurements: AREA, ASPECT, AXIS (MAJOR), AXIS (MINOR), PERIMETER, and ROUNDNESS. (NOTE: It is important to choose measurements prior to the following steps to ensure measurements will not reset after analyzing one set of images.) Click OK.

- In the measure window, click COUNT. Particles will be highlight and counted. Particles on the boundaries of the image are rejected in the count since the full particle is not in the image. If a noticeable error has occurred in particle counting, such as the particle is not highlight or an unknown artifact is highlighted, corrections are made in two methods: 1) Under EDIT in the measure window, select either SPLIT IMAGE or DRAW/MERGE IMAGE as needed or 2) Hide an item by double click that item and checking HIDE at the bottom left of the new pop-up window. This action removes the item from the measurement data.
- In the measure window, click VIEW and select MEASUREMENT DATA. In the new window, click on FILE and select EXPORT DATA. An Excel spreadsheet will open containing data from the analysis.
- For next set of experiments simply repeat the previous steps. To ensure that previous data is not overwritten in the spreadsheet, in the MEASUREMENT DATA window click FILE and select EXPORT OPTIONS. Select append to bottom circle and click OK.
- Once analysis is complete, save spreadsheet in appropriate folder.

APPENDIX E

ADDITIONAL PARTICLE SIZE DISTRIBUTIONS

E.1 Initial Particle Size Investigation PSDs

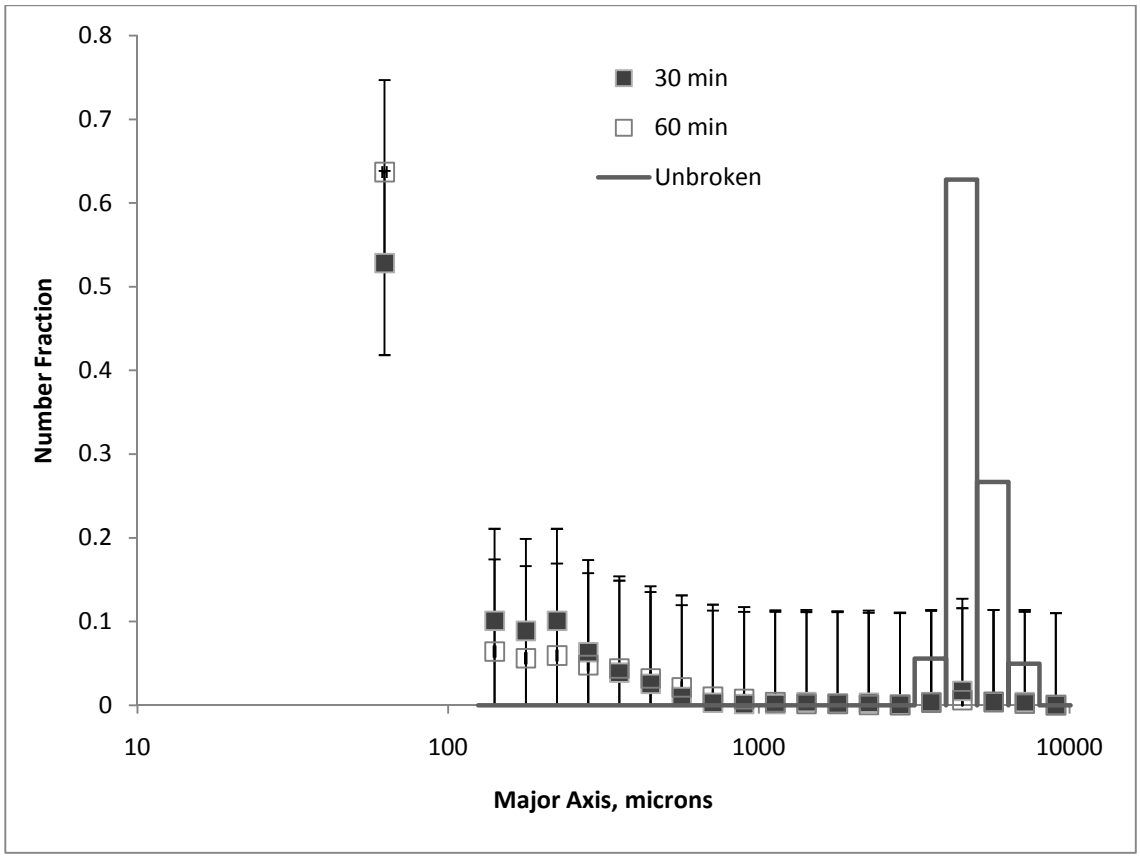

Figure E.1 Mesh 6 NaCl Crystal Breakage Results

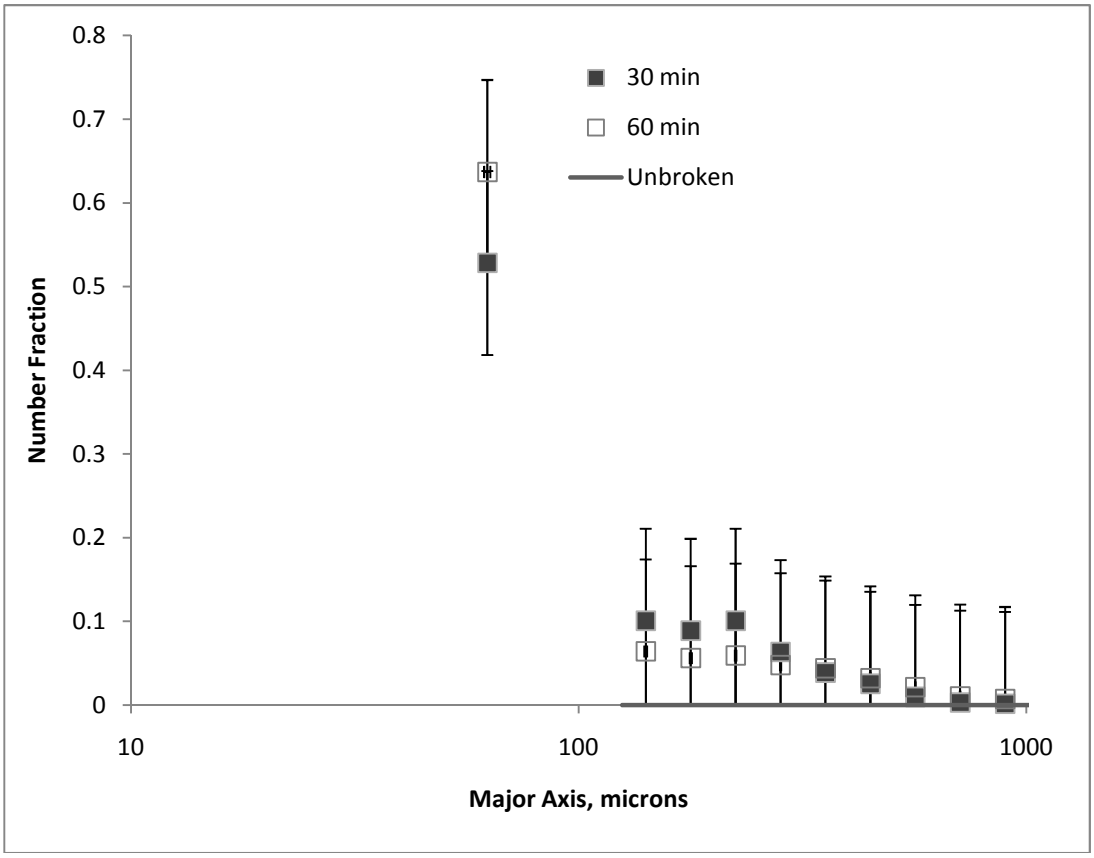

Figure E.2 Mesh 6 NaCl Crystal Breakage Results <1000 Microns without Adjustments

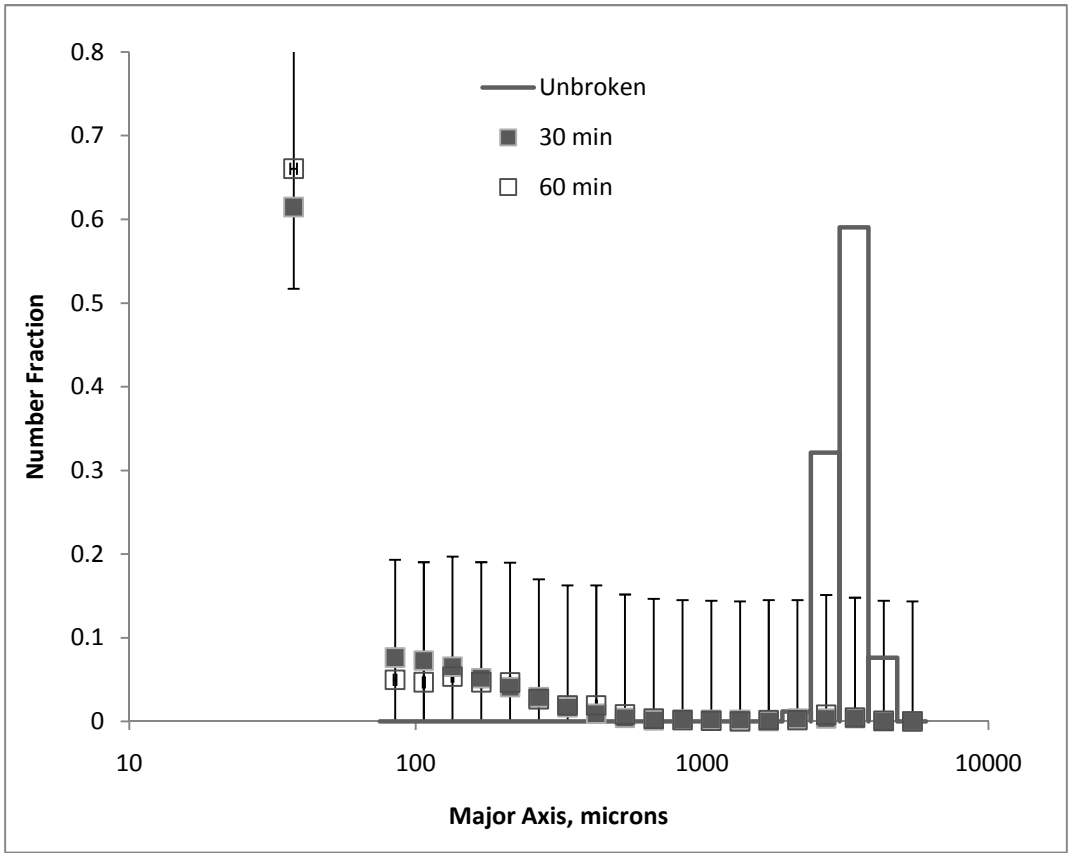

Figure E.3 Mesh 10 NaCl Crystal Breakage Results

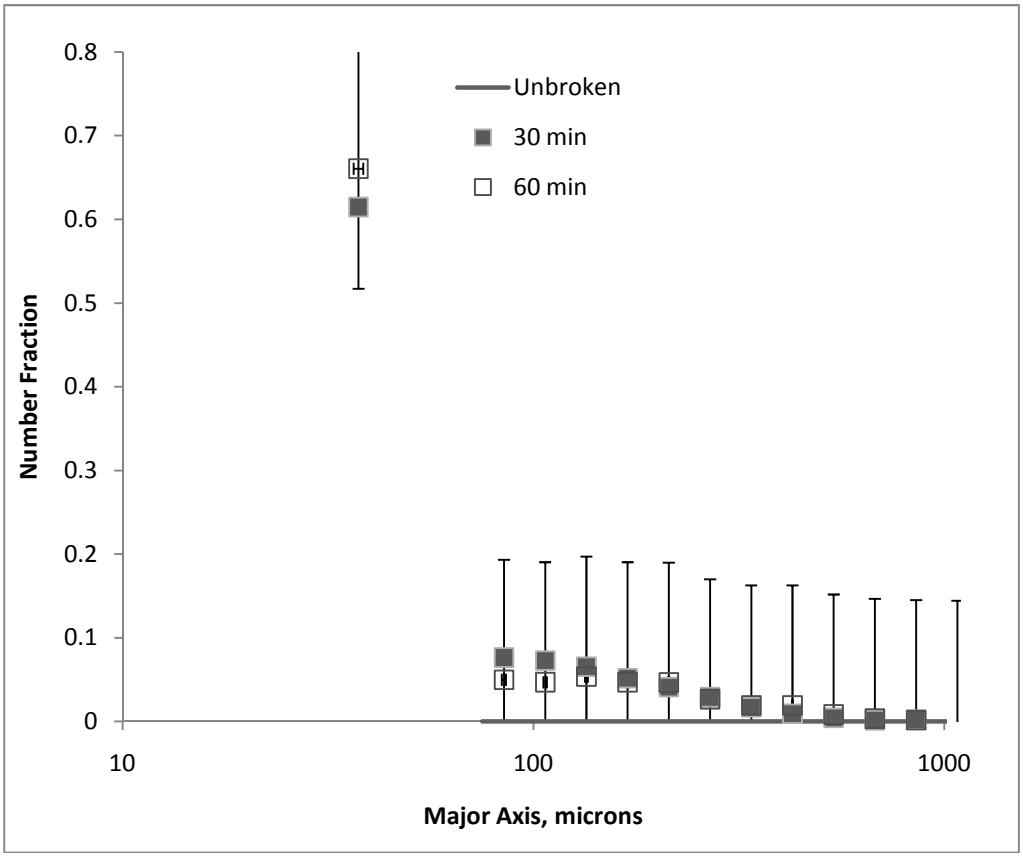

Figure E.4 Mesh 10 NaCl Crystal Breakage <600 microns without Adjustment

APPENDIX F

PARTICLE BREAKAGE IMAGES

F.1 NaCl Breakage

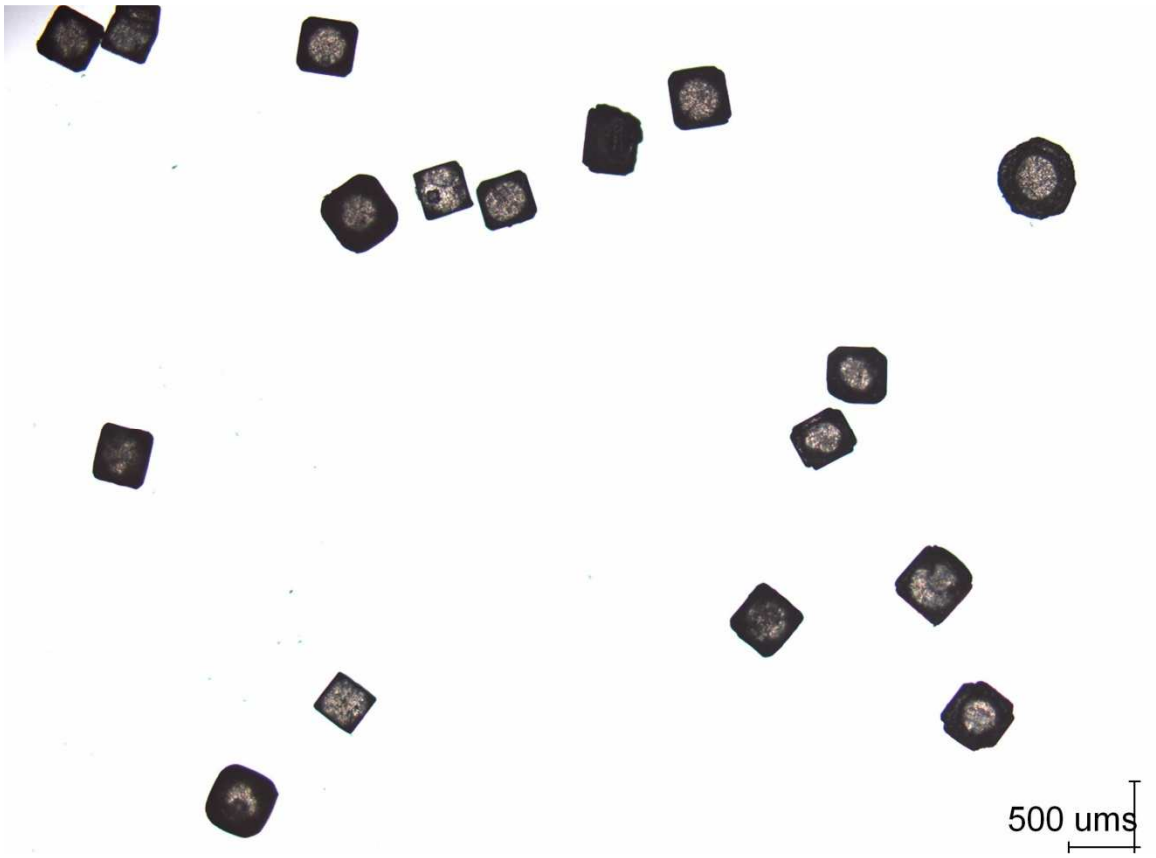

Figure F.1 Unbroken Mesh 40 NaCl Crystals

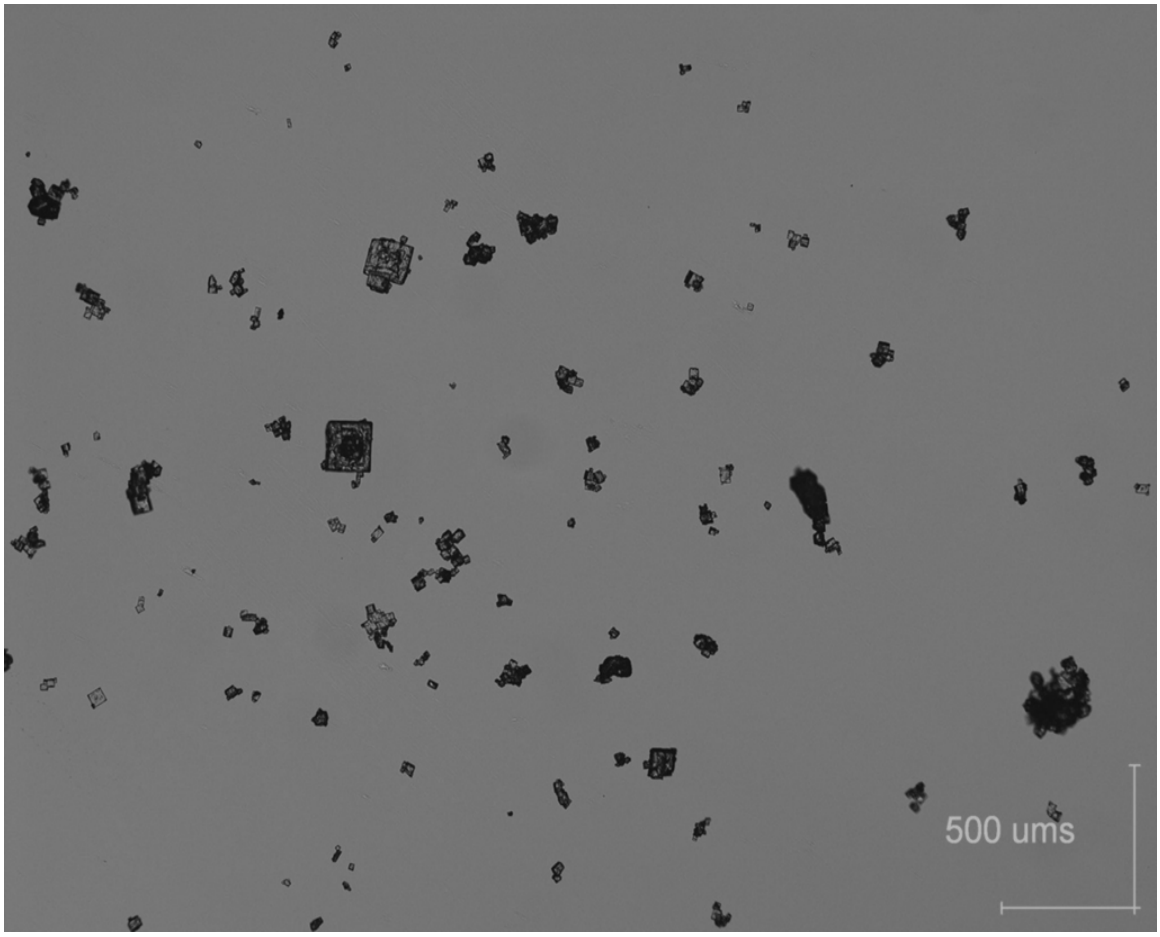

Figure F.2 SS Broken NaCl Crystals

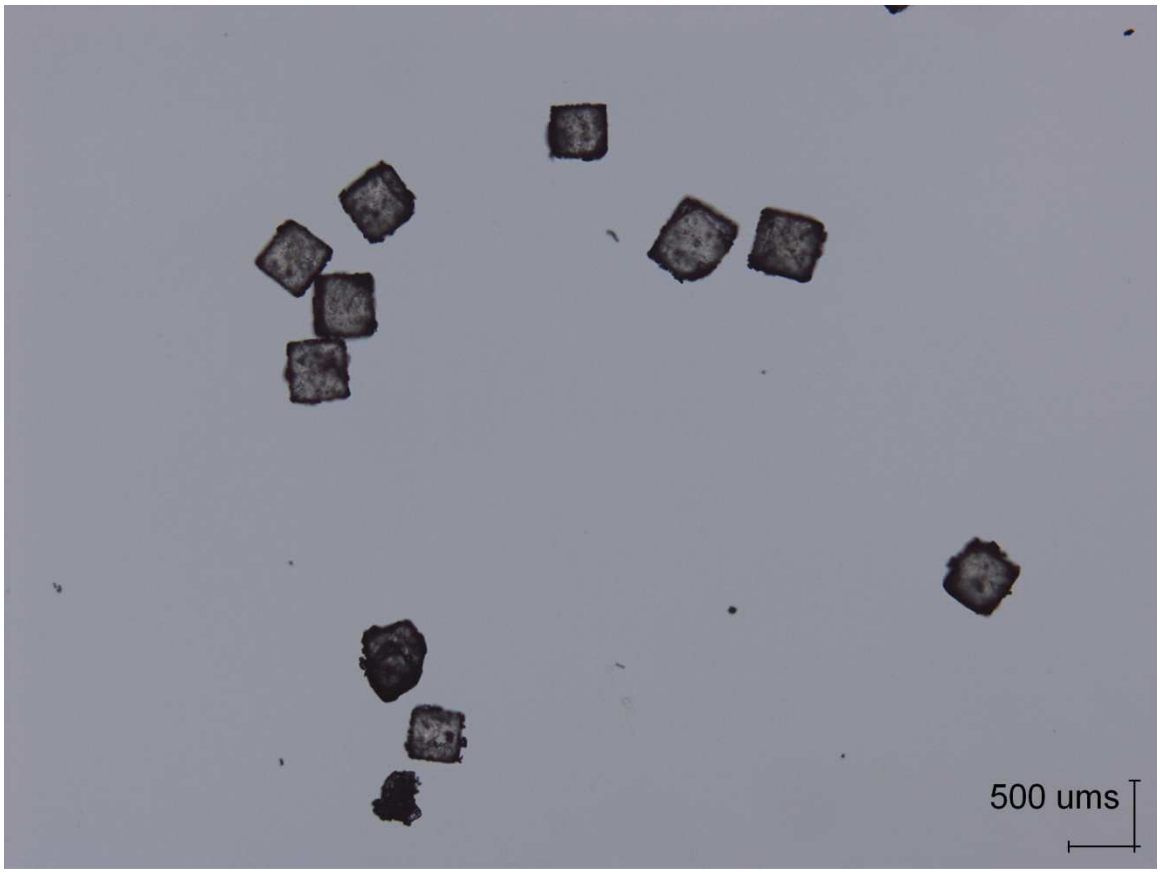

Figure F.3 ACTL Broken NaCl Crystals

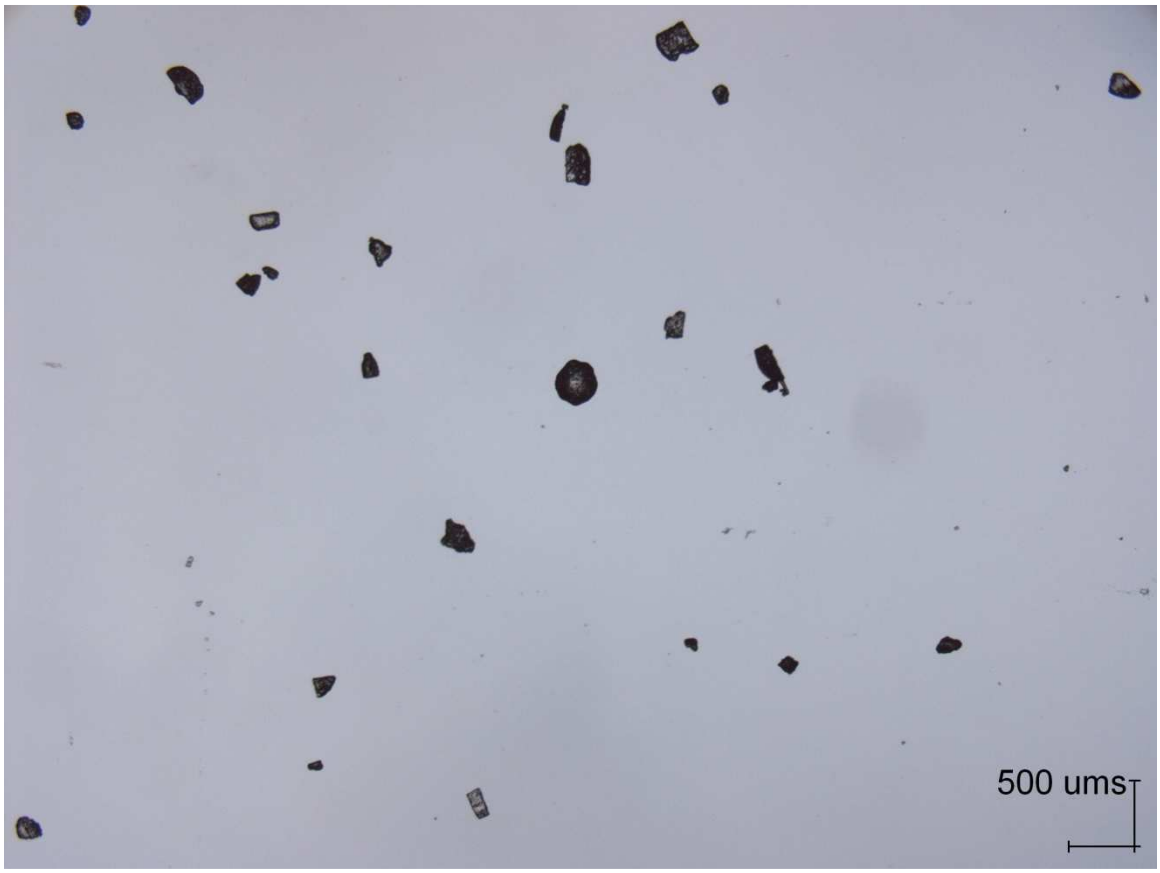

Figure F.4 Mesh 40 KCl Crystal Breakage

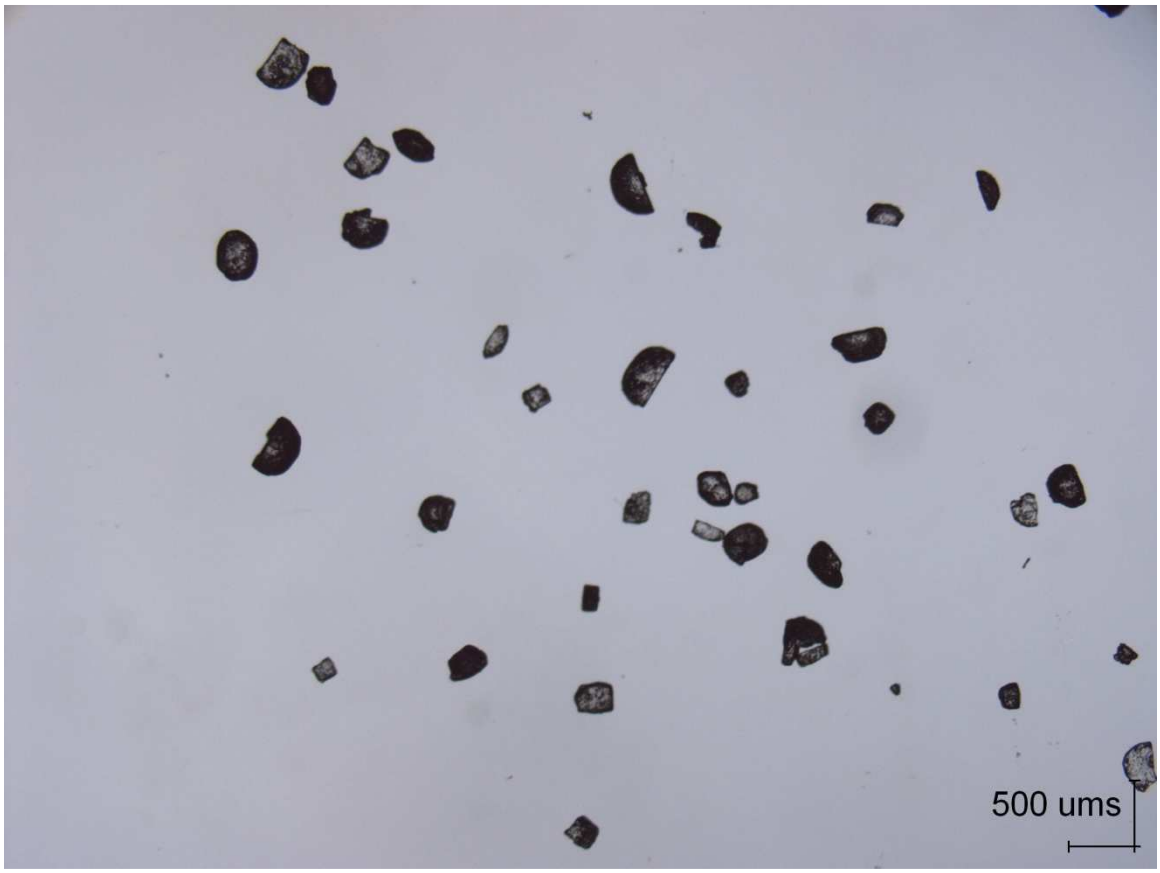

Figure F.5 Mesh 60 KCl Crystal Breakage

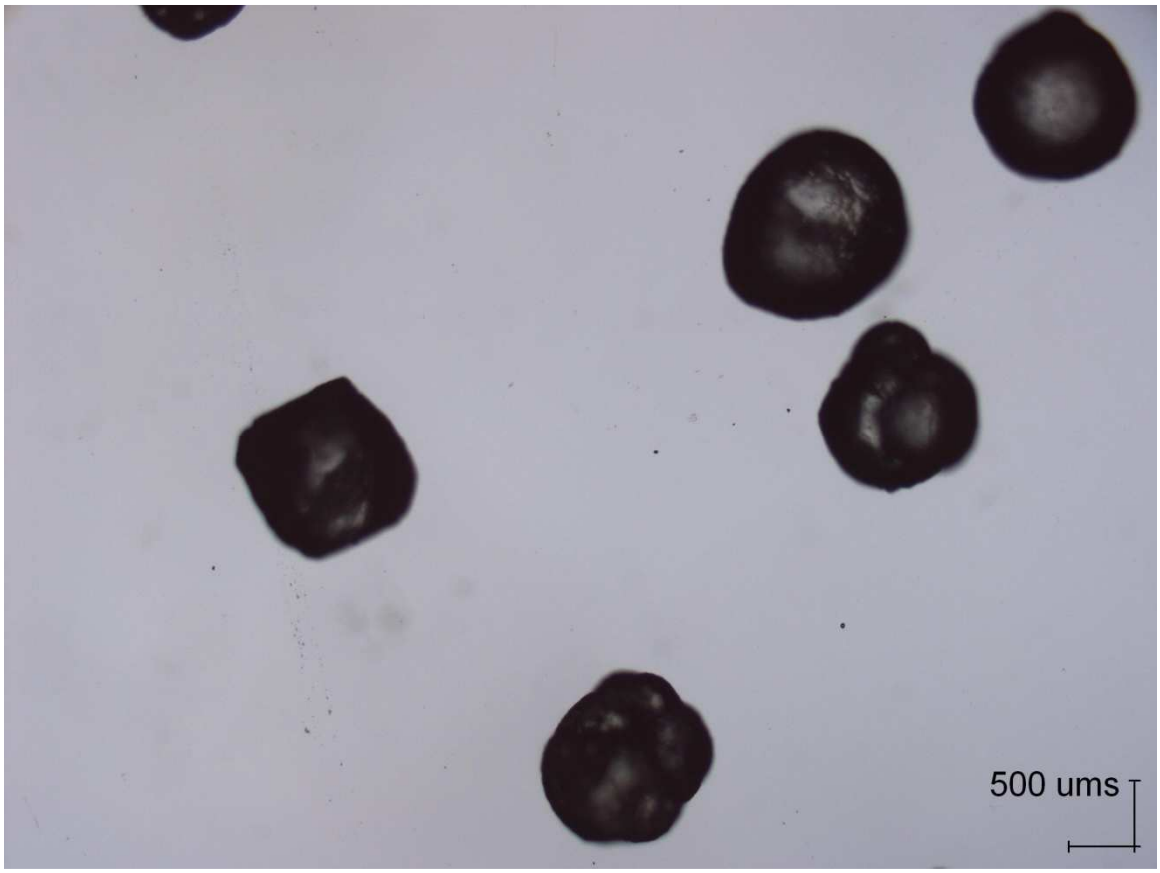

Figure F.6 Unbroken Mesh 20 Potash Alum Crystals

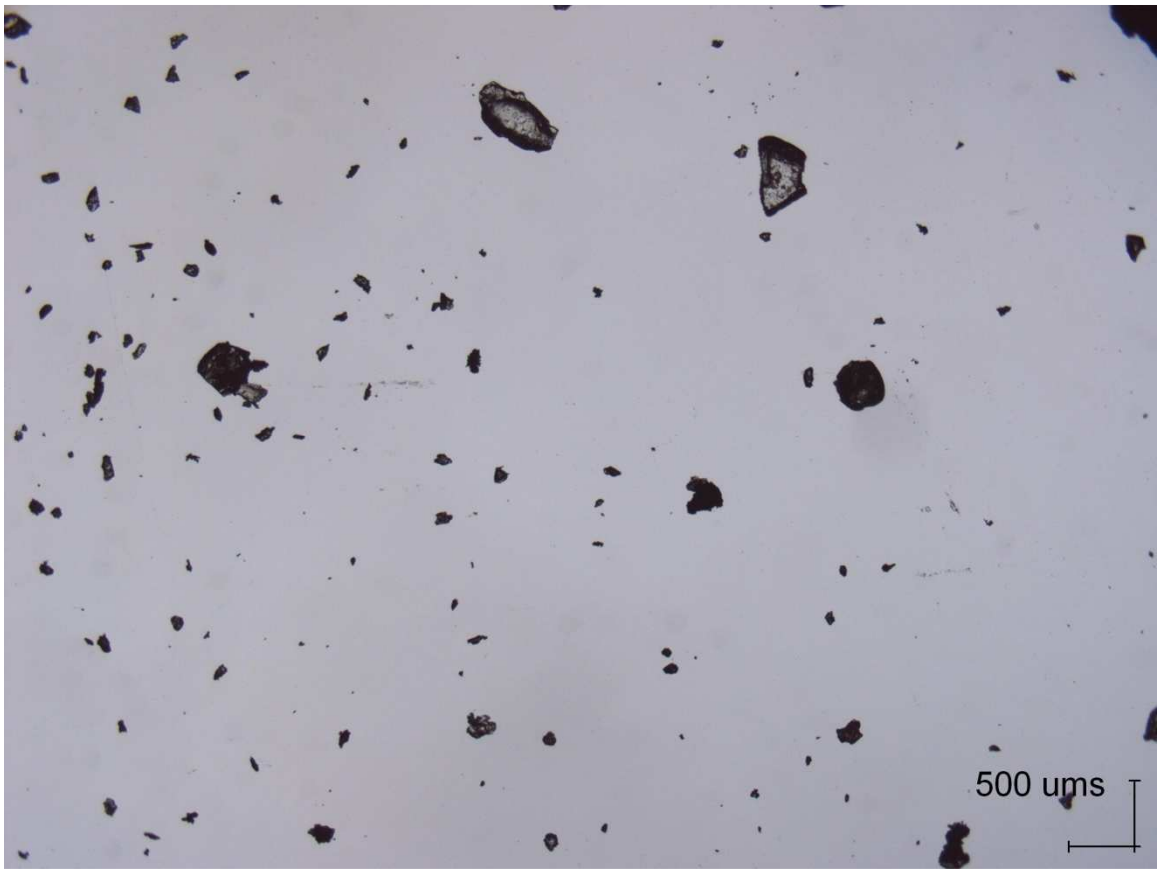

Figure F.7 Mesh 20 Potash Alum Crystal Breakage

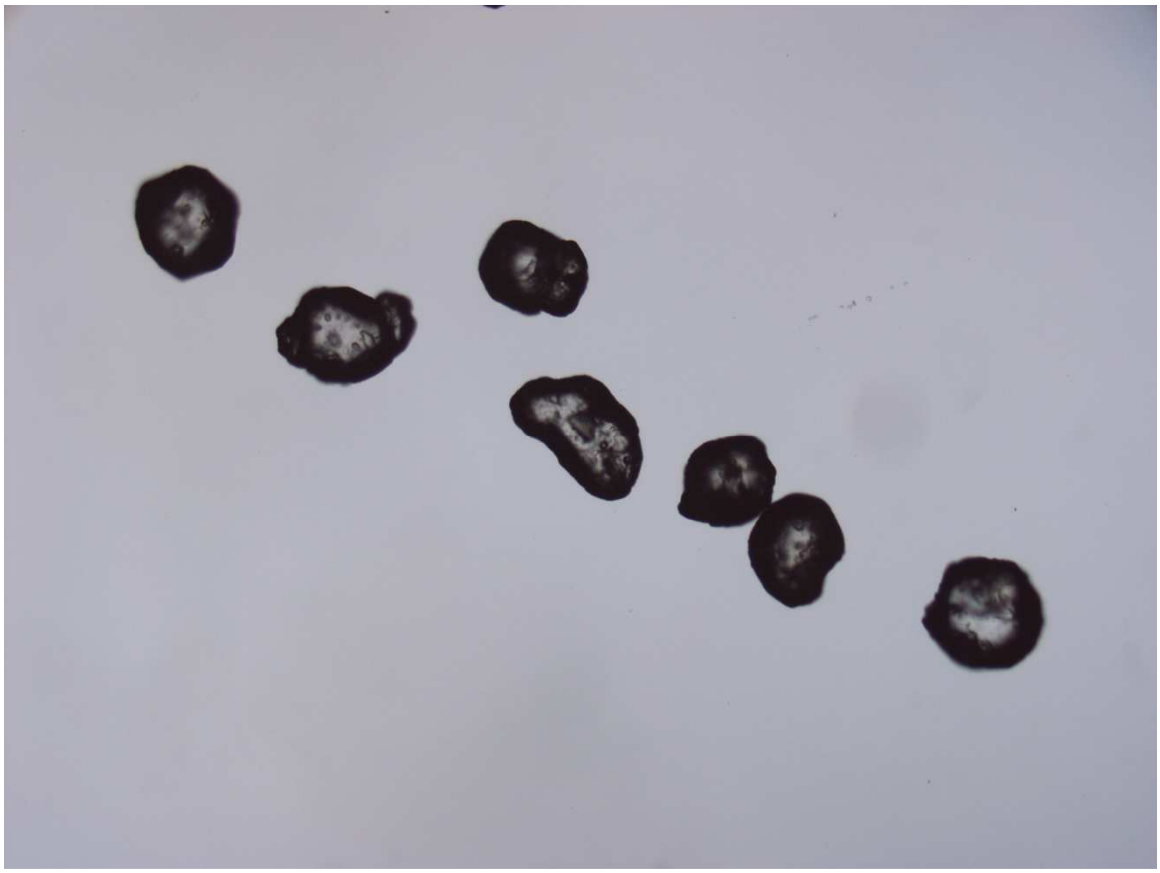

Figure F.8 Unbroken Mesh 30 Potash Alum Crystals

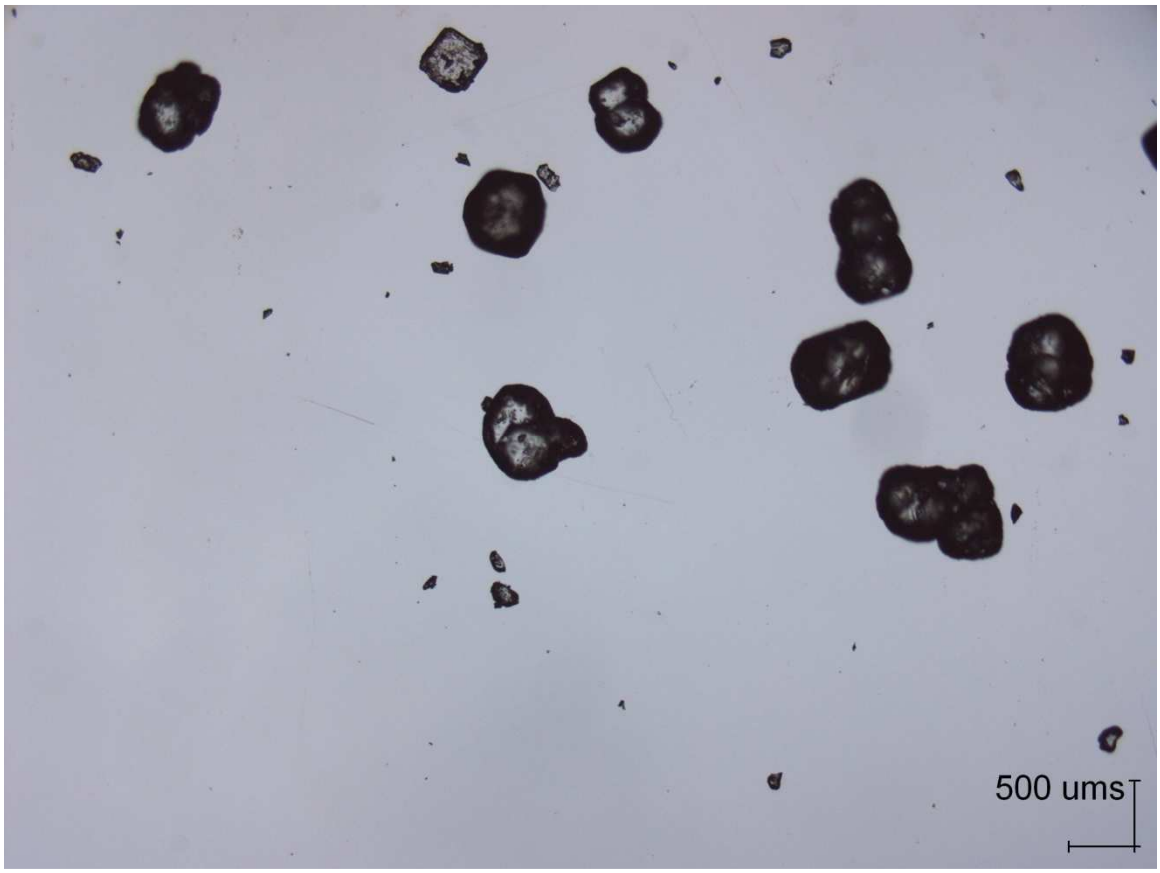

Figure F.9 Mesh 30 Potash Alum Crystal Breakage

APPENDIX G

STATISTICAL DATA

G.1 NaCl Confidence Intervals

Confidence intervals were determined using Design Expert (version 8.0.1, StatEase, Inc., Minneapolis, MN, 2010) software. Single agitation rates and single initial particle sizes were evaluated for 0, 30, and 60 minutes. Agitation rate and magma density confidence intervals were evaluated for the rates and densities under consideration. In the following tables, the response measured in each case was the number fraction. **SE Mean** is the standard deviation associated with the prediction of an average value under the specific conditions. **CI** represents the confidence interval. For $\alpha = 0.05$, the CI has **low** and **high** values that are calculated to contain the true mean **95%** of the time. Finally, **SE Pred** is the standard deviation associated with the prediction of an individual observation.

Table G.1 Aqueous Saturated Solution Confidence Intervals

	Prediction	**SE Mean**	**95% CI low**	**95% CI high**	**SE Pred**
Agitation Rate	0.165	0.021	0.123	0.207	0.096
Magma Density	0.101	0.015	0.072	0.131	0.055

Table G.2 Acetonitrile NaCl Confidence Intervals

		Prediction	SE Mean	95% CI low	95% CI high	SE Pred
Single Agitation Rates	1000rpm	0.184	0.041	0.101	0.267	0.138
	1500rpm	0.181	0.040	0.101	0.260	0.132
	2000rpm	0.109	0.022	0.066	0.153	0.117
Factors	Agitation Rates	0.171	0.026	0.121	0.222	0.117
	Magma Density	0.215	0.022	0.172	0.258	0.081
Mesh	6	0.220	0.055	0.111	0.330	0.131
	10	0.227	0.072	0.083	0.371	0.143
	30	0.136	0.024	0.088	0.184	0.131
	40	0.181	0.040	0.101	0.260	0.132
	60	0.176	0.031	0.113	0.239	0.105

G.2 KCl and Potash Alum Confidence Intervals

Table G.3 KCl Confidence Intervals

		Prediction	SE Mean	95% CI low	95% CI high	SE Pred
Mesh	40 acte	0.164	0.038	0.089	0.240	0.117
	40 actl	0.159	0.035	0.088	0.230	0.109
	40 combo	0.158	0.029	0.101	0.215	0.101
	60 acte	0.129	0.037	0.056	0.203	0.114
	60 actl	0.114	0.031	0.051	0.177	0.097
	60 combo	0.124	0.029	0.066	0.183	0.104

Table G.4 Potash Alum Confidence Intervals

		Prediction	SE Mean	95% CI low	95% CI high	SE Pred
Mesh	20	0.048	0.013	0.021	0.074	0.106
	30	0.048	0.012	0.024	0.072	0.095
	40	0.158	0.023	0.111	0.205	0.078

G.3 Confidence Intervals of Comparisons

Table G.5 Comparison of Materials Confidence Intervals

		Prediction	SE Mean	95% CI low	95% CI high	SE Pred
SS vs. ACTL	Magma Density	0.124	0.018	0.089	0.159	0.071
	Agitation Rate	0.124	0.018	0.089	0.159	0.071
	Agitation Rate (30 min)	0.208	0.021	0.167	0.250	0.087
	Agitation Rate (60 min)	0.186	0.019	0.148	0.223	0.079
Potash Alum vs. KCl	Mesh 40	0.159	0.030	0.099	0.219	0.088

APPENDIX H

SAMPLE ANALYSIS PROCEDURE

Table H.1 Sample Raw Data of Crystals From Image Pro Analysis

Obj.#	Area	Aspect Ratio	Perimeter	Axis (major)	Axis (minor)	Roundness
1	336386	1.213	2147.16	722.54	595.44	1.091
2	318388	1.043	2088.81	652.60	625.95	1.091
3	278251	1.074	1871.41	617.30	574.69	1.002
4	225850	1.128	1716.79	570.53	505.69	1.038
5	182050	1.059	1578.65	498.04	470.39	1.089
6	125030	1.138	1405.00	429.05	377.05	1.256
7	127897	1.049	1338.16	415.93	396.39	1.114
8	115951	1.075	1366.14	401.67	373.61	1.281
9	63904	1.367	1111.29	336.89	246.42	1.538
10	67493	1.150	1039.77	316.91	275.53	1.275
11	52713	1.147	865.01	278.98	243.17	1.130
12	32633	1.066	721.54	212.01	198.92	1.270
13	25209	1.199	631.85	197.37	164.55	1.260
14	26592	1.120	641.73	196.59	175.54	1.232
15	9130	2.460	504.87	174.88	71.10	2.222
16	6733	1.808	485.93	132.99	73.55	2.791
17	3963	2.528	267.50	115.12	45.53	1.437
18	3425	2.125	224.34	96.53	45.43	1.169
19	2502	1.610	186.98	72.13	44.80	1.112
20	1384	2.131	156.21	61.76	28.98	1.403
21	914	2.057	180.03	52.08	25.32	2.821
22	1792	1.158	151.25	51.70	44.66	1.016
23	676	2.445	103.72	46.13	18.87	1.266
24	923	1.417	108.66	41.08	28.99	1.018
25	1020	1.164	114.06	39.13	33.61	1.014
26	364	1.869	76.64	30.35	16.24	1.284
27	319	1.331	63.70	23.41	17.58	1.012
28	338	1.075	66.58	21.86	20.33	1.044
29	123	2.195	41.52	18.90	8.61	1.113
30	189	1.417	45.36	18.52	13.07	1.000
31	42	5.720	30.97	17.76	3.11	1.818
32	161	1.408	41.38	17.15	12.18	1.000
33	69	3.063	32.81	16.53	5.40	1.242
34	107	1.963	37.05	16.38	8.34	1.021
35	152	1.273	41.30	15.75	12.37	1.000

Table H.2 Number of Particles per Major Axis L_i Range and Aspect Ratio Chart of Particles in Each Sample Range

		Aspect Ratio										
L_i	N_i	1	1.5	2	2.5	3	3.5	4	4.5	5	5.5	6
0	0	0	0	0	0	0	0	0	0	0	0	0
12.5	0	0	0	0	0	0	0	0	0	0	0	0
15.749	0	0	0	0	0	0	0	0	0	0	0	0
19.8425	7	0	3	1	1	0	1	0	0	0	0	1
25	2	0	2	0	0	0	0	0	0	0	0	0
31.498	1	0	0	1	0	0	0	0	0	0	0	0
39.685	1	0	1	0	0	0	0	0	0	0	0	0
50	2	0	1	0	1	0	0	0	0	0	0	0
62.9961	3	0	1	0	2	0	0	0	0	0	0	0
79.3701	1	0	0	1	0	0	0	0	0	0	0	0
100	1	0	0	0	1	0	0	0	0	0	0	0
125.992	1	0	0	0	0	1	0	0	0	0	0	0
158.74	1	0	0	1	0	0	0	0	0	0	0	0
200	3	0	2	0	1	0	0	0	0	0	0	0
251.984	1	0	1	0	0	0	0	0	0	0	0	0
317.48	2	0	2	0	0	0	0	0	0	0	0	0
400	1	0	1	0	0	0	0	0	0	0	0	0
503.968	4	0	4	0	0	0	0	0	0	0	0	0
634.96	2	0	2	0	0	0	0	0	0	0	0	0
800	2	0	2	0	0	0	0	0	0	0	0	0
1007.94	0	0	0	0	0	0	0	0	0	0	0	0
	35											

Table H.3 Major Axis L_i and Number Fraction n_i of Particle in each Sample Range

$\mathbf{L_i}$	$\boldsymbol{n_i}$
0	0
12.5	0
15.75	0
19.84	0.200
25	0.057
31.50	0.029
39.69	0.029
50	0.057
63.00	0.086
79.37	0.029
100	0.029
125.99	0.029
158.74	0.029
200	0.086
251.98	0.029
317.48	0.057
400	0.029
503.97	0.114
634.96	0.057
800	0.057
1007.94	0

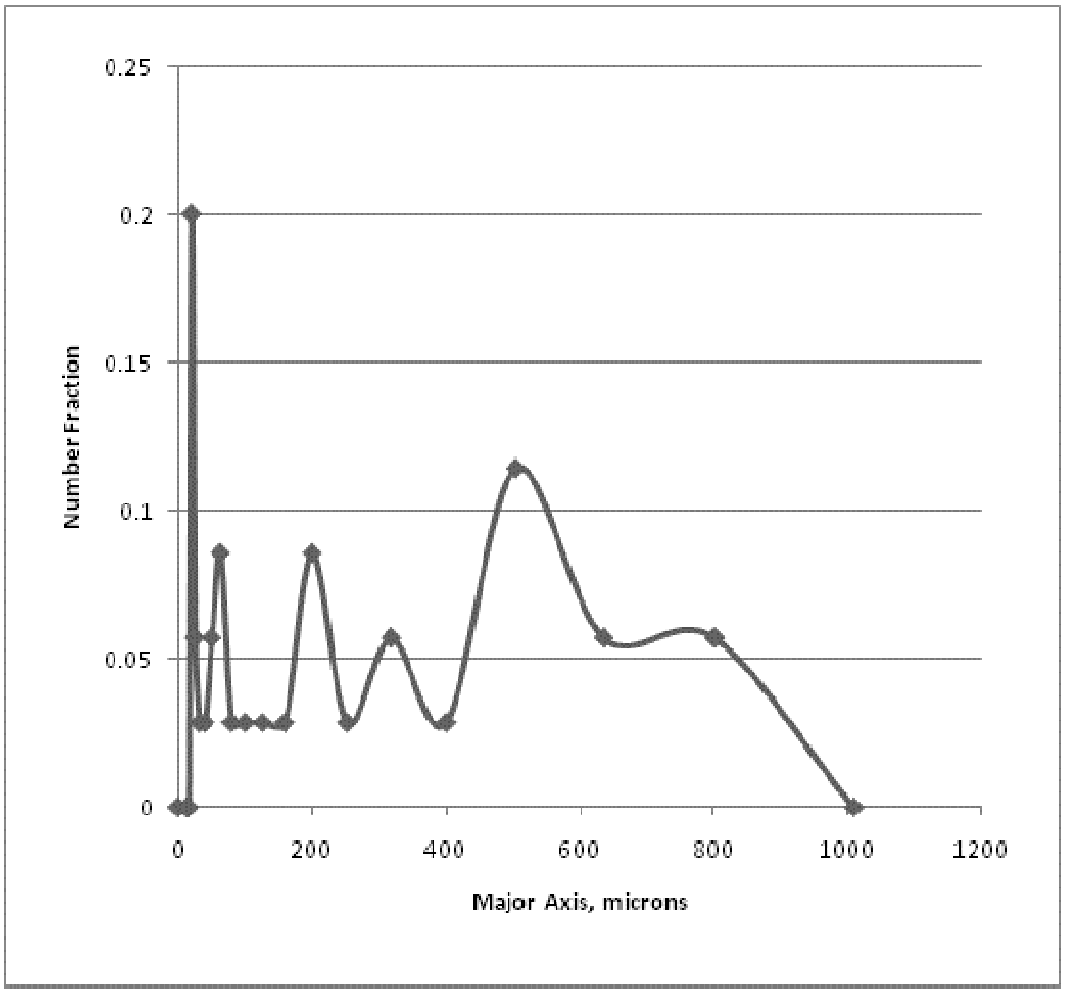

Figure H.1 Graph of Number Fraction and Major Axis for Particles in the Sample

APPENDIX I

SIMULTANEOUS DIFFERENTIAL SCANNING CALORIMETER AND THERMO GRAVIMETRIC ANALYSIS (SDT) RESULTS

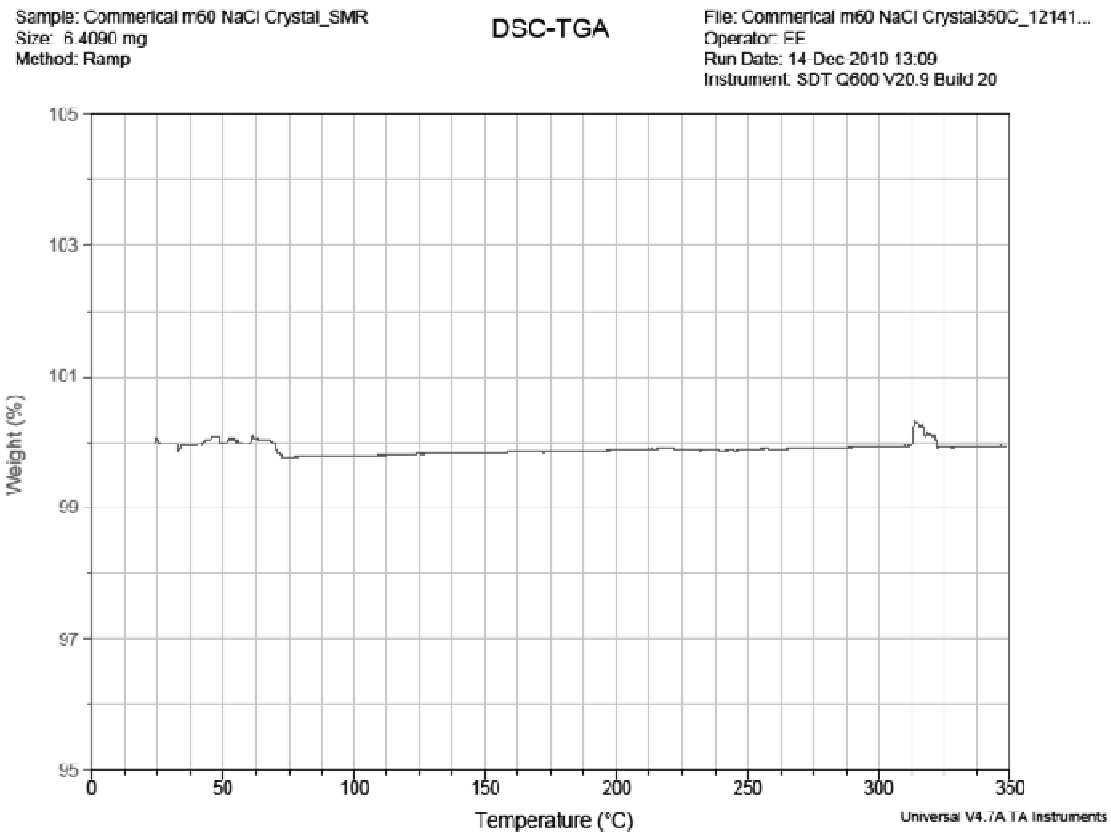

Figure I.1 Simultaneous Differential Scanning Calorimeter and Thermo Gravimetric Analyzer (SDT) or DSC-TGA Results of Commercial Sodium Chloride Crystals

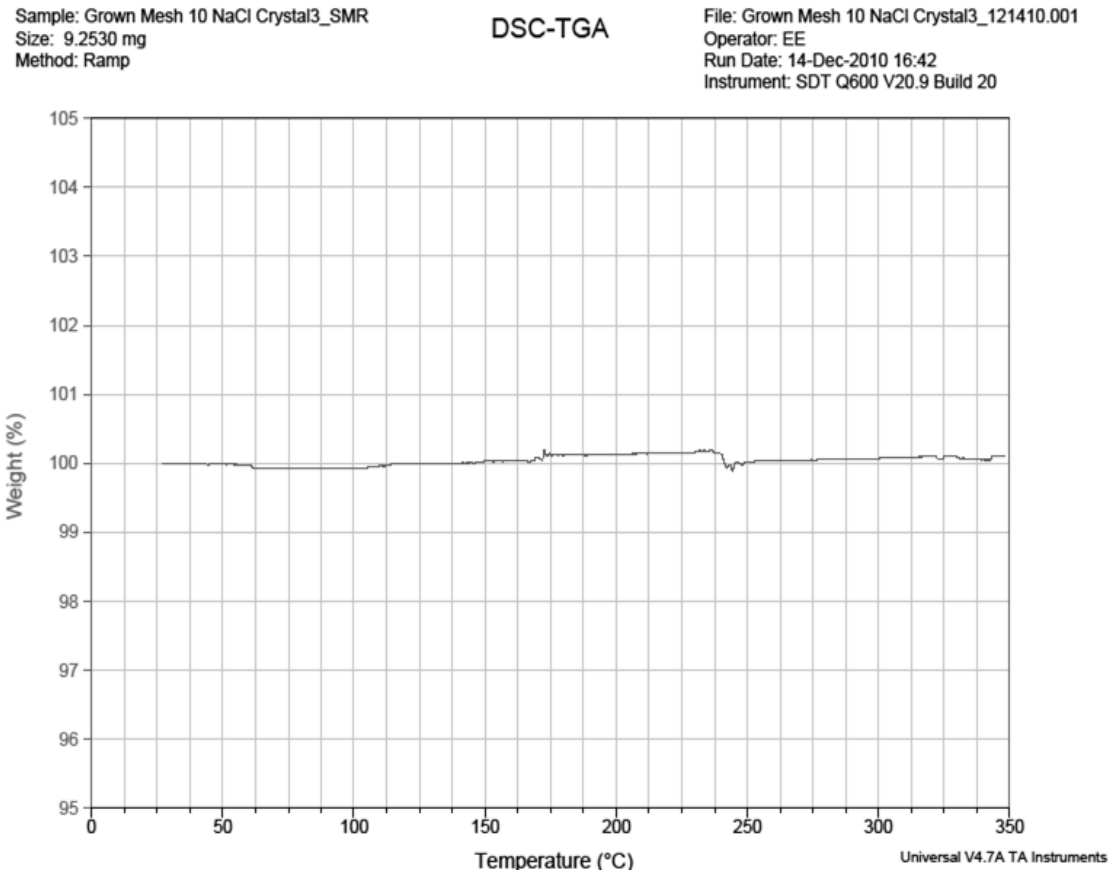

Figure I.3 Simultaneous Differential Scanning Calorimeter and Thermo Gravimetric Analyzer (SDT) or DSC-TGA Results of a Mesh 10 Laboratory Grown Sodium Chloride Crystal